

Cover: The front cover is an artist's impression of the female thorax (blue), representing breast cancer patients. Radiotherapy (yellow triangle) is widely used for the treatment of breast cancer. However, surrounding normal tissue – such as the heart and the vasculature – may also lie to some extent in the field of radiation (yellow lines within the yellow triangle). The vasculature of the heart is very sensitive to radiation and can thus be injured by radiotherapy. The folded paper hearts symbolize radiation-induced heart damage of individual patients.

The work described in this thesis was carried out at the department of Biological Stress Response of the Netherlands Cancer Institute in Amsterdam, the Netherlands and were financially supported by the Dutch Cancer Society (KWF grant 2008 – 3993).

Financial support by the Dutch Heart Foundation for the publication of this thesis is grateful acknowledged.

The printing of this thesis was friendly sponsored by:

Dutch Cancer Society



Cover design: Esther Ris, www.proefschriftomslag.nl

Lay out: Esther Ris, www.proefschriftomslag.nl & Eva Bakker, www.nietiedereenkenteva.com

Printing: proefschriften.nl

ISBN:978-90-6464-848-9

Copyright 2015 © Ingar Seemann

Amsterdam, The Netherlands. All rights reserved. No part of this publication may be reproduced, stored in a retrieval system, or transmitted in any form or by any means, electronic, mechanical, photocopying, recording or otherwise, without the prior permission of the copyright owner.

VRIJE UNIVERSITEIT

Radiation and anthracycline induced cardiovascular damage

Late side effects of thoracic cancer treatment

ACADEMISCH PROEFSCHRIFT

ter verkrijging van de graad Doctor aan
de Vrije Universiteit Amsterdam,
op gezag van de rector magnificus
prof.dr. F.A. van der Duyn Schouten,
in het openbaar te verdedigen
ten overstaan van de promotiecommissie
van de Faculteit der Geneeskunde
op donderdag 23 april 2015 om 13.45 uur
in de aula van de universiteit,
De Boelelaan 1105

door

Ingar Seemann

geboren te Henstedt-Ulzburg, Duitsland

promotor: prof.dr. M. Verheij

copromotor: dr. F.A. Stewart

promotiecommissie:

prof. dr. F. E. van Leeuwen

prof. dr. H. te Riele

prof. dr. R. P. Coppes

prof. dr. J. H. A. M. Kaanders

dr. B. M. P. Aleman

Table of contents

| | | |
|-----------|---|----|
| Chapter 1 | Introduction | 9 |
| | Preface | 10 |
| 1.1 | Understanding radiation-induced cardiovascular damage and strategies for intervention | 11 |
| 1.2 | General introduction | 22 |
| 1.3 | Aim and outline of the thesis | 29 |

Part I Underlying mechanisms of radiation and anthracycline-induced cardiovascular damage

| | | |
|-----------|---|-----|
| Chapter 2 | Irradiation induced modest changes in murine cardiac function despite progressive structural damage to the myocardium and microvasculature | 43 |
| Chapter 3 | Local heart irradiation of ApoE ^(-/-) mice induces microvascular and endocardial damage and accelerates coronary atherosclerosis | 65 |
| Chapter 4 | Radiation- and anthracycline-induced cardiac toxicity and the influence of ErbB2 blocking agents | 87 |
| Chapter 5 | Endoglin haplo-insufficiency modifies the inflammatory response in irradiated mouse hearts without affecting structural and microvascular changes | 111 |

Part II Intervention and strategies to overcome radiation-induced cardiovascular damage

| | | |
|-----------|--|------------|
| Chapter 6 | Thalidomide is not able to inhibit radiation-induced heart disease | 135 |
| Chapter 7 | Mouse bone marrow-derived endothelial progenitor cells do not restore radiation-induced microvascular damage | 153 |
| Chapter 8 | Discussion and concluding remarks | 169 |
| | Future Perspectives | 178 |
| | Summary | 185 |
| | Samenvatting | 189 |
| | List of abbreviations | 193 |
| | List of publications | 199 |
| | Acknowledgment | 203 |
| | Curriculum Vitae | 211 |



Chapter 1

Introduction

Preface

Radiotherapy is an effective treatment of cancer, although it contributes to late toxicity in surrounding normal (non-cancer) tissue. Nearly half of all thoracic and chest wall cancer patients receive radiotherapy alone or in combination with chemotherapy or specific tyrosine kinase receptor inhibitors. Much work has been done to improve early detection, treatment schedules and techniques, which increased the life expectancy of cancer survivors. Yet, increased life expectancy also augmented the number of late toxicity events in surrounding normal tissue. Little is known about the underlying mechanisms and the contribution of microvascular damage to late cardiac toxicity after radiotherapy alone or in combination with chemotherapy or tyrosine kinase receptor inhibitors. In this thesis, we therefore investigated the molecular players and pathways involved in radiation induced cardiovascular damage in order to be able to improve existing therapies and to apply new strategies for intervention.

1.1 Understanding radiation-induced cardiovascular damage and strategies for intervention

F.A. Stewart, I. Seemann, S. Hoving, N.S. Russell

Clinical Oncology October 2013

Abstract

There is a clear association between therapeutic doses of thoracic irradiation and increased risk of cardiovascular disease (CVD) in cancer survivors, although these effects may take decades to become symptomatic. Long-term survivors of Hodgkin lymphoma and childhood cancers have 2 to >7-fold increased risks for late cardiac deaths after total tumor doses of 30-40 Gy, given in 2-Gy fractions, where large volumes of heart were included in the field. Increased cardiac mortality is also seen in women irradiated for breast cancer. Breast doses are generally 40-50 Gy in 2-Gy fractions but only a small part of the heart is included in the treatment fields and mean heart doses rarely exceeded 10-15 Gy, even with older techniques. The relative risks (RR) of cardiac mortality (1.1-1.4) are consequently lower than for Hodgkin lymphoma survivors. Some epidemiological studies show increased risks of cardiac death after accidental or environmental total body exposures to much lower radiation doses. The mechanisms whereby these cardiac effects occur are not fully understood and it is likely that different mechanisms are involved after high therapeutic doses to the heart, or part of the heart, than after low total body exposures. It is also likely that these various mechanisms result in different cardiac pathologies, e.g. coronary artery atherosclerosis leading to myocardial infarct, versus microvascular damage and fibrosis leading to congestive heart failure. Experimental studies can help to unravel some of these mechanisms and may identify suitable strategies for managing or inhibiting CVD. In this overview, the main epidemiological and clinical evidence for radiation-induced CVD is summarized. Experimental data shedding light on some of the underlying pathologies and possible targets for intervention is also discussed.

Introduction

Cancer patients who received therapeutic doses (30-50 Gy in 2 Gy fractions) of thoracic radiotherapy prior 2000 have increased risk of cardiac mortality at >10 years after treatment. Modern radiotherapy techniques reduce the average and maximum dose to the heart, but techniques such as IMRT (intensity modulated radiotherapy) can be associated with total body exposures of 2-3 Gy. There is epidemiological evidence that such doses may also increase the risk of cardiovascular damage. Although there are still many unanswered questions, it is clear that radiation can induce a wide spectrum of cardiac and vascular pathologies, which may have different underlying mechanisms (1-6).

This overview aims to summarize the most important epidemiological studies contributing to our understanding of the relationship between radiation dose and risk of cardiac morbidity. We then review the experimental data that has provided information on pathological changes in the irradiated heart and possible mechanisms of damage. Finally, we examine the evidence (so far rather limited) for pharmacological inhibition of radiation-induced cardiovascular disease (CVD).

Cardiac damage after therapeutic radiotherapy to cancer patients

Hodgkin lymphoma patients treated with older radiotherapy techniques (including the entire heart and aortic arch in the irradiation fields) have a risk of late cardiac mortality 2 to >7-fold greater than the general population (7-10). For example, significantly increased standardized incidence ratios (SIR) of myocardial infarct (2.4, 95% CI 1.1-5.2), angina (4.9, 2.0-12.0), valve disease (7.0, 2.6-18.5) and congestive heart failure (7.4, 1.8-30.0) were observed in >1,400 patients treated for Hodgkinlymphoma, with a median follow-up of >18 years (8). This study also demonstrated that the risk was significantly greater for patients irradiated at young age (SIR for myocardial infarction 2.6 for irradiation at age 36 to 40, compared with 5.4 for those irradiated at age <20 years), and that the use of anthracycline chemotherapy further increased the risk of congestive heart failure and valve disease. Prospective screening studies have identified cardiovascular abnormalities, such as diastolic dysfunction, valvular and conduction defects, in a high percentage of asymptomatic Hodgkinlymphoma survivors (7, 11). This indicates that occult radiation-induced cardiac damage is very common in this patient population, which could lead to cardiac mortality at a later stage.

Two recent publications demonstrated a relationship between cardiovascular morbidity or mortality and cardiac dose in long-term survivors of various childhood cancers (12, 13). In

the Tukenova study, the relative risk (RR) cardiovascular death due to radiotherapy was 5.0 (CI 1.2-21.4). Risk was significantly correlated with total mean heart dose: RR 25.1 for doses of >15 Gy, RR 12.5 for 5-14.9 Gy, no significant increased risk for doses <5 Gy. Mulrooney reported on the long-term cardiac outcomes of >14,000 survivors of childhood cancer. Cardiac doses of 15-35 Gy significantly increased the hazard rate (HR) of congestive heart failure (2.2, 1.4-3.5), myocardial infarction (2.4, 1.2-4.9), pericardial disease (2.2, 1.3-3.9) and valve abnormalities (3.3, 2.1-5.1), with respect to non-irradiated cancer survivors. Doses >35 Gy were associated with even higher HR and doses <5 Gy were not associated with significantly increased risks.

Increased cardiac morbidity and mortality are well documented after post-operative irradiation for breast cancer (1, 3, 14-16). For these patients the breast is irradiated to about 50 Gy in 2 Gy fractions, although only a small part of the heart is exposed to high doses and dose distributions vary considerably depending on tumor location and radiotherapy technique used. Mean cardiac doses and doses to specific heart structures were estimated for breast cancer patients treated with common radiotherapy techniques up to the early 1990s (17). These calculations showed that total doses averaged over the whole heart were 3-17 Gy for women with left-sided breast cancer and irradiation of the internal mammary chain, with even higher doses to the left anterior descending coronary artery (LADCA). In a population of >4000 10-year survivors of breast cancer treated in the Netherlands between 1970 and 1986, radiation to the internal mammary chain was associated with significantly increased risk of cardiovascular disease (estimated mean heart dose 6-15 Gy), while for breast irradiation alone no increased risk was observed (estimated mean heart dose <7 Gy) (18). Modern radiotherapy, especially with deep inspiration breath hold techniques, can reduce the mean dose to the heart to <2 Gy, even for left-sided breast cancer, although parts of the LADCA may still be exposed to >20 Gy (19).

The Early Breast Cancer Trialists' Collaborative Group (EBCTCG) carried out meta-analyses of mortality from randomized trials of radiotherapy versus no radiotherapy (20). This study showed a significant excess of CVD in women who received radiotherapy (RR 1.27; SE 0.07). A preliminary analysis of updated EBCTCG data demonstrated that the RR of cardiac death was related to the estimated mean cardiac dose, increasing by 3% per Gy (3). The risk for cardiac death was greater for women with left-sided cancer (mean cardiac doses 12 Gy, RR 1.44) than right-sided cancer (mean cardiac dose 5 Gy, RR 1.18). This analysis also showed

that the RR increased with time from irradiation.

A recent study analyzed the incidence of heart disease in 35,000 women treated with radiotherapy for breast cancer in Denmark and Sweden from 1976-2006 (21). Radiation-related risk was studied by comparing women with left-sided and right-sided tumors, with estimated mean total heart doses of 6.3 Gy and 2.7 Gy, respectively. Cardiac mortality was not significantly influenced by tumour laterality, but left versus right incidence ratios were raised for acute myocardial infarction (1.22, CI 1.06-1.42), angina (1.25, 1.05-1.49), pericarditis (1.61, 1.06-2.43) and valvular heart disease (1.54, 1.11-2.13). Darby and colleagues have just published a population based case-control study of >2000 women irradiated for breast cancer in Sweden and Denmark between 1958 and 2001, for whom individual doses to the heart were estimated from radiotherapy charts (22). This analysis showed that the rate of major coronary events increased linearly with mean dose to the heart, by 7.4% per Gy (CI 2.9-14.5).

Although it takes more than 10 years for clinical cardiac failure to develop after irradiation, several studies using functional imaging have shown myocardial perfusion changes at ≥ 6 months after irradiation for breast cancer (22-24). Perfusion defects followed the radiotherapy field rather than bifurcations of the major coronary arteries and the incidence of perfusion defects was related to the volume of the left ventricle included in the field (23). A relationship between these perfusion defects and subsequent clinical heart disease may be expected but has not yet been demonstrated.

Cardiac damage after total body exposures <2.5 Gy

With advances in modern radiotherapy techniques, the volume of critical normal tissues exposed to high doses is considerably reduced. However, techniques such as IMRT can result in total body exposures of 2-3 Gy over the entire treatment (25). It is therefore relevant to examine the evidence for radiation-induced CVD after such doses. The life span study of A-bomb survivors provides convincing evidence for increased risks after total body exposures < 2.5 Gy (26-28). In the latest analysis the excess relative risk (ERR) for all heart disease was 14% per Gy (CI 6-23%), although analysis restricted to doses < 0.5 Gy did not show significantly elevated risks (27). Analysis of risk according to type of heart disease showed that ischemic heart disease and myocardial infarct were not significantly associated with radiation, whereas hypertensive heart failure, rheumatic heart disease and congestive heart failure were

all significantly associated with radiation (ERR/Gy 37%, 88% and 22%, respectively). In other words, cardiac diseases caused by coronary atherosclerosis (angina and myocardial infarct) were not increased by low doses of radiation, whereas cardiac diseases associated with capillary perfusion defects, inflammation and fibrosis (congestive heart failure and rheumatic heart disease) were increased.

In addition to direct cardiac effects, there is likely to be a contribution of systemic effects (non-targeted) after total body exposure. Clinical laboratory data from the adult health study (a subset of the A-bomb survivors) demonstrated significant increases in serum cholesterol, blood pressure, inflammatory markers (c-reactive protein, IL6, TNF α), as well as impairment of cell-mediated immunity (29-31). Recent evidence has also suggested an association between renal failure and radiation dose in the A-bomb survivors (32). These systemic effects could have contributed to the increased cardiac damage seen after total body exposures of low doses in A-bomb survivors, and they may also play a role in cancer patients treated with IMRT.

There are other epidemiological studies of circulatory disease in relation to radiation dose after medical, occupational or environmental total body exposures < 2.5 Gy (3, 33-39). A meta-analysis of these studies suggested an aggregate ERR of 0.08 per Gy (95% CI 0.05- 0.11) (36), and a follow-up meta-analysis reported ERR per Gy of 0.10 (0.04-0.15) for ischemic heart disease and 0.12 (0.01-0.25) for non-ischemic heart disease (34).

Experimental evidence for radiation-induced atherosclerosis

Atherosclerosis is an important factor in cardiac diseases such as myocardial infarction. Damage or senescence of endothelial cells lining the major arteries is pivotal in the initiation of atherosclerosis (83). Damaged endothelial cells have increased capacity for monocyte attachment (via inflammatory molecules E-selectin, VCAM1 and ICAM1) and recruitment into the intima (via MCP-1). After trans-migration, monocytes take up low-density lipoprotein (LDL), forming aggregates of lipid laden macrophages (the early atherosclerotic lesion).

Endothelial cells are sensitive to radiation and doses ≥ 2 Gy induce expression of inflammatory adhesion molecules and promotes leukocyte adhesion (12, 13, 23, 78). Radiation also triggers cells into senescence via damage to telomeres (84).

Radiation combined with excess LDL initiates and enhances atherosclerotic development (85-87). Inflammation and oxidative damage play a role in this process, which can be inhibited by over-expression of superoxide dismutase (88). Radiation doses of 2-8 Gy to

hypercholesterolemic animals increase the number and size of atherosclerotic lesions in major arteries and predispose to the formation of macrophage rich, unstable plaque with thrombotic features, rather than stable collagenous plaque (88-94). Such lesions are more likely to rupture and cause a fatal heart attack. After local irradiation of the thorax or neck regions, no systemic changes in inflammatory markers or increased cholesterol levels occur (92, 95). This contrasts with the situation after total body exposures, where elevated inflammatory markers (72) and cholesterol (74, 95, 96) are seen, even after low doses.

In contrast to inflammatory responses after high doses, doses <1 Gy decrease leukocyte adhesion to endothelial cells via decreased liberation of E-selectin (97) and stimulated release of TGF- β (98). One study has also demonstrated that whole body doses <0.5 Gy actually decreased the number and size of atherosclerotic lesions in hypercholesterolemic mice (96). These experimental studies suggest that radiation-induced atherosclerosis plays a role in the increased risk for myocardial infarct after high therapeutic doses of radiotherapy to the thorax, especially where the LADCA is within the high dose region. However, it seems unlikely that radiation-induced atherosclerosis is responsible for the cardiac mortalities seen after low dose total body exposures.

Experimental evidence for microvascular damage and fibrosis after cardiac irradiation

Radiation injury to the myocardium is primarily caused by damage to the microvasculature, leading to inflammatory and thrombotic changes, capillary loss, focal ischemia and interstitial fibrosis (12, 13, 50). These pathological changes can cause congestive heart failure.

The earliest morphological changes are lymphocyte adhesion and extravasation from irradiated capillaries. This is followed by loss of alkaline phosphatase in capillary endothelial cells, thrombi formation and obstruction of microvessels, vascular leakage and decreased capillary density (11, 99-102). Loss of alkaline phosphatase is a particularly sensitive marker of endothelial cell damage that occurs after doses of ≥ 2 Gy to the mouse heart (102). Although the remaining capillary endothelial cells may respond to damage by transient increase in proliferation (103), this is inadequate to maintain proper microvascular function. Recent studies have shown that endothelial cells isolated from irradiated mouse hearts have reduced ability to respond to angiogenic stimuli, and that this impairment is progressive in time (104). Reduction in the number of patent capillaries eventually leads to ischemia, myocardial cell death and fibrosis.

Myocardial degeneration coincides with the first signs of decreased cardiac function in rats.

However, further decreases in function do not occur until shortly before the onset of fatal congestive heart failure, despite increasing degeneration of myocardial mass (101). This is probably explained by compensatory mechanisms masking the extent of functional damage. Gene expression profiles of irradiated mouse hearts suggest that genes involved in survival pathways (heat shock proteins and metalloproteinases) are activated in parallel with the inflammatory pathways. At later times, especially after higher doses, the expression profile switched to a fibrotic one, with many genes involved in heart failure over-expressed (89). Experimental studies indicate that radiation injury to the capillary network is an important contributor to myocardial degeneration and heart failure after irradiation. This is supported by clinical studies that demonstrate regional perfusion defects in non-symptomatic breast cancer patients at ≥ 6 months after radiotherapy (65-67).

Damage to other cardiac structures

After high doses to the heart (≥ 36 Gy fractionated), acute pericarditis (protein rich exudate in the pericardial sac) is the first clinical sign of damage 3-6 months after irradiation (57, 64, 65). This can progress to fibrin deposition and chronic constrictive pericarditis. Similar changes are seen in mouse models of cardiac irradiation. For example, single doses of 2-16 Gy led to edematous thickening of the pericardium, with inflammatory cell deposits and hemorrhage after 16 Gy (61). Pericarditis used to be common after thoracic radiotherapy, but modern techniques restrict the heart dose and pericarditis is now rarely seen (5).

Radiation-induced fibrosis can be a consequential effect of the inflammatory response discussed above. There is experimental evidence that mast cells mediate collagen deposition in irradiated rat hearts (66). Radiation also precipitates senescent changes in fibroblasts at doses as low as 1 Gy (67, 68). Senescent fibroblasts are metabolically active and produce excessive collagen, leading to fibrosis (67, 69). In the heart, fibrosis causes functional disturbances by impairing myocardial relaxation (70), which may also contribute to cardiac rhythm disturbances.

Radiation-induced senescence and collagen production in post-mitotic fibroblasts are mediated by increased levels of TGF- β and downstream Smad proteins (71, 72). One report has described a correlation between TGF- $\beta 1$ single nucleotide polymorphism and incidence of CVD after irradiation for breast cancer. The T/T polymorphism was associated with hazard ratios of 1.79 (0.99–3.26) compared to the C/C + C/T genotype, (73). Radiation-induced cardiac fibrosis has also been shown to be mediated by Smad and Rho/ROCK signaling (74). Calcific valve disease is an important late complication of therapeutic radiation (75),

characterized by fibrotic thickening and macroscopic deposits of calcium phosphate that disturb the structure and function of the valve. Radiation induces osteogenic transformation and an increased production of osteogenic enzymes and cytokines by aortic valve interstitial cells (76).

Systemic effects

After low-dose environmental or occupational exposures, or even after therapeutic radiotherapy with IMRT, one has to consider the effects of whole body exposure and how this may impact on CVD. For example, microvascular damage to the kidney or atherosclerosis of the renal artery could lead to reno-vascular hypertension, further increasing the risk of atherosclerosis, and heart failure. Myocardial infarction may also have a worse prognosis if the microvasculature of the myocardium is already damaged. Microvascular damage in the lungs has been demonstrated, even in shielded areas, after thoracic irradiation; this can lead to pulmonary hypertension and put additional strain on the heart (77). Chronic low grade inflammatory reactions and cellular senescence caused by radiation may also accelerate the progression of cardiovascular disease.

Possible targets and strategies for intervention

As outlined above, radiation is an independent risk factor for induction and progression of atherosclerosis, including in mid-sized coronary arteries (47). Controlling other known risk factors, such as smoking, arterial hypertension, obesity and diabetes, is therefore especially important in irradiated cancer survivors. Radiation predisposes to the development of inflammatory, thrombotic lesions (48-50, 78), therefore the use of anti-inflammatory and anti-thrombotic drugs could have potential for combating radiation-induced coronary artery disease. Unfortunately, in the few experimental models where this approach has been tested, it has not proved effective. Anti-inflammatory nitric oxide releasing aspirin and, to a lesser extent, aspirin were able to inhibit or stabilize age-related atherosclerosis in hypercholesterolemic mice (79-82), but they had no effect on radiation-induced atherosclerosis (79). Similarly, the anti-platelet drug clopidogrel inhibited atherosclerosis in balloon injured arteries of hypercholesterolemic rabbits (83, 84), but not radiation-induced atherosclerosis (84, 85). This suggests that the anti-inflammatory properties of drugs used in these studies were insufficient to overcome the strong inflammatory phenotype of the irradiated lesions.

Rather more success has been reported with the use of anti-oxidant strategies. Anti-oxidant diets fed to hypercholesterolemic rabbits inhibited atherosclerosis after balloon injury and

irradiation. The macrophage and oxidized LDL content of the lesions was also reduced in both irradiated and control arteries (86). Peroxisome proliferator-activated receptor (PPAR)- γ activation upregulates anti-oxidants and this has been shown to inhibit both cholesterol-mediated and radiation-induced atherosclerosis in animal models (87, 88).

Microvascular damage is induced by modest radiation doses ≤ 2 Gy and this can lead to perfusion defects, diffuse ischemia and myocardial fibrosis, resulting in congestive heart failure. Stabilizing endothelial function and inhibition of fibrosis therefore have potential for inhibition of radiation-induced cardiac damage. Statins are good candidates for such intervention since they exert a wide range of anti-inflammatory, anti-thrombotic and anti-fibrotic effects (in addition to their cholesterol lowering properties). Statins improve vascular status (decrease coagulation and vasoconstriction) via upregulation of thrombomodulin and increased bioavailability of nitric oxide (89, 90), as well as inhibiting fibrotic pathways via inhibition of small G-proteins Rho and Rac (91). One experimental study showed that statins and a Rho/ROCK inhibitor (Y-27632) were able to reduce pulmonary and cardiac fibrosis after thoracic irradiation (74).

Stem cell technology to stimulate recovery in damaged tissue is a rapidly expanding field of research. Vascular progenitor cells, including bone marrow derived cells (BMDC) migrate to sites of ischemic damage in the heart and participate in tissue regeneration (92, 93). Preclinical studies have shown that BMDC transplantation improves microvasculature and cardiac function after acute myocardial infarct and chronic cardiac fibrosis (94, 95). This technology may also have potential for treating radiation-induced CVD, although this has not yet been tested.

Pentoxifylline (PTX) inhibits fibroblast proliferation and intracellular signaling in response to TGF- β and CTGF. Two experimental studies have shown that combined PTX and vitamin E (anti-oxidant) have some beneficial effects on radiation-induced myocardial fibrosis and left ventricular function (96, 97). The subsequent withdrawal of drugs was, however, associated with a rebound effect and development of fibrosis. Similar approaches have been used in clinical trials for inhibition of fibrosis in breast cancer patients (98, 99) but there is no information on clinical benefits regarding cardiac damage.

The rennin-angiotensin system plays a key role in regulation of hemodynamics in the circulatory system. In a rat model of radiation heart disease, the ACE inhibitor captopril was able to reduce myocardial fibrosis and capillary loss, but this did not prevent functional damage (100). There is no clinical evidence of a beneficial effect of ACE inhibitors on radiation-induced cardiotoxicity, although there are indications of a beneficial effect after chemotherapy. In a randomized trial including women treated with high dose chemotherapy, enalapril prevented

the development of late cardiotoxicity in a selected group of high risk patients (101).

Conclusions

Although modern radiotherapy protocols have led to a reduction in radiation exposure of non-target cardiovascular structures, radiation-induced CVD will remain a relevant issue for cancer survivors. Firstly, cohorts of patients treated in previous decades remain at risk for radiation induced CVD in the future. Secondly, the use of techniques such as IMRT, while reducing the volume of normal tissue exposed to high doses, actually expose large body volumes to doses of 1-3 Gy. Thirdly, adjuvant cardiotoxic drugs used in cancer treatment may compound CVD risks for patients treated with current techniques. There is now solid epidemiological evidence for increased risk of CVD in cancer patients exposed to total fractionated cardiac doses >5 Gy. There is also solid evidence for increased risk after total body exposures >1 Gy, with suggestive evidence for increased risks at lower doses.

Experimental evidence shows that doses >2 Gy, in combination with elevated cholesterol levels, initiates atherosclerosis and predisposes to an inflammatory plaque phenotype. This is a likely mechanism for radiation-induced coronary artery disease, especially where the LADCA is included in the high dose field. There is no evidence for radiation-induced atherosclerosis at doses <2Gy. After lower doses, microvascular damage is the underlying cause of subsequent myocardial ischemia, perfusion defects and fibrosis. These pathologies can eventually lead to congestive heart failure. After total body exposure to low doses, systemic effects, such as elevated cholesterol, persistent low grade inflammation, renal damage and hypertension, are likely to contribute to the increased cardiovascular risk.

Acknowledgements

The authors would like to thank members of the CARDIORISK Euratom 7th Framework Program (FP7) for many stimulating discussions on the subject of radiation-induced cardiovascular damage.

Conflict of interest statement

There were no conflicts of interest

Search strategies used and sources of information

Pubmed was used to search for original articles and reviews, with key words: cardiovascular damage and radiation, atherosclerosis and radiation.

1.2 General introduction

Radiotherapy and normal tissue damage

The German Wilhelm Conrad Roentgen presented X-rays as therapy against cancer. This soon became a standard treatment for different sorts of cancers worldwide, e.g. for Hodgkin lymphoma. However, early radiotherapy treatment schedules for Hodgkin lymphoma patients often included a large volume of heart tissue, which resulted in significant delayed toxicity. Modern radiotherapy techniques have improved, especially dose sculpting techniques, which allow the physician to irradiate the tumor more precisely and to spare more surrounding normal tissue and decrease the overall dose to the heart.

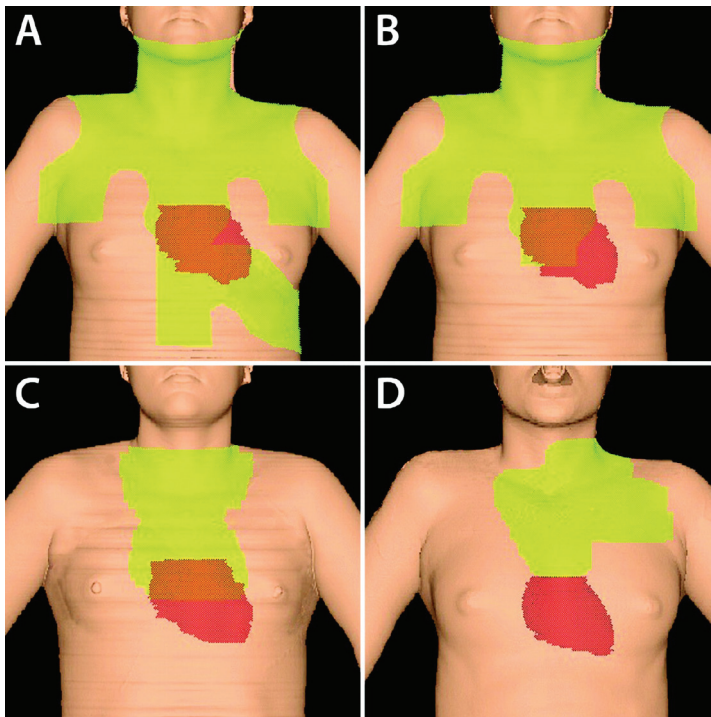


FIGURE 1 Changes in types of treatment plans and radiotherapy (RT) fields for Hodgkinlymphoma patients over time. (A) Mantle and upper abdomen field with the heart, carotid arteries, left breast and part of the lung in the field of radiation. (B) Mantle field; typical RT fields that were used with high radiation doses (36-45 Gy). (C) Contemporary involved-field RT (IFRT) treats only initially involved lymph node regions with a lower prescribed radiation dose compared to (A) and (B) and includes less normal tissue in the field of radiation. (D) Involved-node RT (INRT) allows further reduction in normal tissue dose. Light green illustrates the irradiated field. The true heart position (red) is shown. (Adapted from Hogsdon et al. (102))

However, although new techniques have the advantage of reducing the volume of normal tissue exposed to high dose irradiation, critical areas of the heart such as the left anterior descending coronary artery may still be exposed to substantial irradiation doses (17, 19, 103). Thus, it has been the long-term follow-up studies of Hodgkin lymphoma patients treated with mantle field radiotherapy, which indicated that the heart is a radiosensitive tissue. The sensitivity to radiation has been shown to cause pericarditis, cardiomyopathy, valvular disorders, coronary artery disease, chronic impairment of myocardial function, myocardial fibrosis and sudden death, although most of these disorders are only manifest many years after radiotherapy (2, 104-107). In vivo models revealed focal degeneration and necrosis of the myocardium that was primarily caused by damage to the microvasculature (64). Moreover, it has been shown that long before radiation-induced myocardial injury is manifest, decrease in microvasculature density becomes measurable (5, 6, 59, 104).

For clinical purpose but also to some extent for research purpose, it is important to make distinction between early and late side-effects.

Early side-effects of radiotherapy become apparent days after treatment in tissue with high proliferative activity, whereas late side-effects appear months to many years later (108). The primary early effect of radiotherapy on normal tissue is the sterilization of the proliferating cells. Thus, the early effects of radiotherapy are based on impairment of cell production in the face of ongoing cell loss (109). This leads eventually to progressive cell depletion, supplemented by either direct or indirect inflammatory changes. In rapidly proliferating tissues, like oral or intestinal mucosa, the surviving stem cells are able to repopulate the tissue, providing that cell depletion was not too severe. Late side-effects, however, seem to be more complex and are often irreversible and progressive.

Tissue proliferation and response to radiation has been defined in terms of tissue organization models: H-type (hierarchical-type) and F-type (flexible-type) (110). H-type tissues are rapid turnover tissues comprising stem cells, which are not functional themselves but from which intermediate "transit cells" are produced, which in turn proliferate to produce functional, post-mitotic "mature cells". Proliferating stem cells can restore the tissue integrity and structure after radiation and are maintained by self-replication. Stem cells are radiosensitive and reduction of the stem cell compartment results in an overall decline of cell production, which leads to hypoplasia (111). The heart is, however, an F-type tissue, which comprises many types of functional cells that rarely undergo proliferation, although some cell types are capable of proliferation if the occasion requires it (109). Clinical manifestation of damage in slow turnover F-type tissues is delayed, as there is no early critical depletion of post-mitotic

functional cells. When damaged cells eventually attempt mitosis they die and the ensuing cell loss stimulates a compensatory proliferation response in other damaged cells, thus creating a wave of mitotic death and accelerating further cell loss and loss of organ function (111). Although cell loss after irradiation in an F-type tissue may be delayed for many months, early inflammatory and thrombotic changes do take place (112).

One well-known cardiac late side effect induced by radiation is fibrosis. Radiation-induced fibrosis, defined by excessive fibroblast proliferation, myofibroblast differentiation and overproduction of extracellular matrix, is probably the most extensively studied late side effect due to its importance in clinical radiotherapy (2, 3, 5, 67, 69). Cardiac fibrosis is manifest in reduced tissue flexibility, reduced strength or restricted motions resulting in functional impairment (113). In the early phase of fibrogenesis, proinflammatory cytokines, interleukins and growth factors are upregulated in the irradiated tissue (5, 6, 41, 113). One of the most important inflammatory cytokines in the development of fibrosis is transforming growth factor β 1 (TGF- β 1) (114). It is defined as the master switch in the fibrotic program and is involved in proliferation and differentiation of cells; inhibition of endothelial proliferation; regulation of extracellular matrix component deposition, stimulation of myofibroblast differentiation and induct of type I collagen production (115). Radiation can activate TGF- β 1 and, by binding to transmembrane receptors, activate the TGF- β 1 signaling (116-118). Radiation-induced fibrosis is different to normal wound healing where a complex balance exists between pro-fibrotic proteins, such as TGF- β 1 and its downstream effector connective tissue growth factor (CTGF), counterbalanced by anti-fibrotic proteins e.g. tumor-necrosis factor- α (TNF- α). In the final remodeling phase of normal wound healing, new capillaries are formed and collagen degradation takes place (119). Unlike normal wound healing, radiation-induced fibrosis demonstrates continuously production of TGF- β 1 and lacks the balance between pro-fibrotic proteins and anti-fibrotic proteins. Thus, radiation-induced fibrosis is progressive over the years and can lead to organ failure.

they die and the ensuing cell loss stimulates a compensatory proliferation response in other damaged cells, thus creating a wave of mitotic death and accelerating further cell loss and loss of organ function (111). Although cell loss after irradiation in an F-type tissue may be delayed for many months, early inflammatory and thrombotic changes do take place (112). One well-known cardiac late side effect induced by radiation is fibrosis. Radiation-induced fibrosis, defined by excessive fibroblast proliferation, myofibroblast differentiation and overproduction of extracellular matrix, is probably the most extensively studied late side effect

due to its importance in clinical radiotherapy (2, 3, 5, 67, 69). Cardiac fibrosis is manifest in reduced tissue flexibility, reduced strength or restricted motions resulting in functional impairment (113). In the early phase of fibrogenesis, proinflammatory cytokines, interleukins and growth factors are upregulated in the irradiated tissue (5, 6, 41, 113). One of the most important inflammatory cytokines in the development of fibrosis is transforming growth factor β 1 (TGF- β 1) (114). It is defined as the master switch in the fibrotic program and is involved in proliferation and differentiation of cells; inhibition of endothelial proliferation; regulation of extracellular matrix component deposition, stimulation of myofibroblast differentiation and induction of type I collagen production (115). Radiation can activate TGF- β 1 and, by binding to transmembrane receptors, activate the TGF- β 1 signaling (116-118). Radiation-induced fibrosis is different to normal wound healing where a complex balance exists between pro-fibrotic proteins, such as TGF- β 1 and its downstream effector connective tissue growth factor (CTGF), counterbalanced by anti-fibrotic proteins e.g. tumor-necrosis factor- α (TNF- α). In the final remodeling phase of normal wound healing, new capillaries are formed and collagen degradation takes place (119). Unlike normal wound healing, radiation-induced fibrosis demonstrates continuous production of TGF- β 1 and lacks the balance between pro-fibrotic proteins and anti-fibrotic proteins. Thus, radiation-induced fibrosis is progressive over the years and can lead to organ failure.

Endoglin

Endoglin is a co-receptor for TGF- β 1. It is expressed at low levels in resting endothelial cells but highly expressed in proliferating vascular endothelial cells during embryogenesis and in inflamed tissue and healing wounds (120, 121). TGF- β 1, however, is a multifunctional cytokine that evokes cellular responses via specific type I and II receptors and their downstream nuclear effectors, called Smads. In endothelial cells, TGF- β 1 activates two type I receptor pathways, activin receptor-like kinase 5 (ALK5) -inducing Smad2/3 phosphorylation and activin receptor-like kinase 1 (ALK1) -promoting Smad1/5 phosphorylation (122). Activation of ALK5 inhibits cell proliferation and migration, whereas activation of ALK1 stimulates processes associated with angiogenesis (123, 124). Moreover, endoglin has been shown to be a crucial component for ALK1 signaling, thus stimulating endothelial cell proliferation, while in the absence of endoglin, ALK5 signaling is stimulated leading to inhibition of endothelial cell proliferation (124). Endoglin therefore plays an important role in the balance of ALK1 and ALK5 signaling that regulated vascular maintenance and repair (125). *In vivo* studies revealed the importance of endoglin when mice deficient in endoglin died in mid-gestation due defective angiogenesis

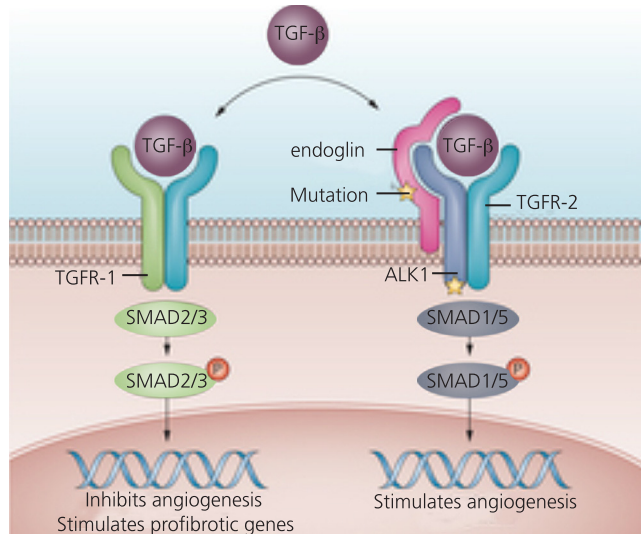


FIGURE 2 TGF- β signaling mediated by TGFR-1 and ALK1. TGF- β signaling is complex and consists of stimulated angiogenesis through ALK1, SMAD1 and SMAD5 but blocking angiogenesis through ALK5, SMAD 2 and SMAD3. Endoglin shifts binding of TGF- β to ALK1 and thus stimulating endothelial cell proliferation. Mutation (yellow stars) in ENG or ALK1 develop HHT. (Adapted from Lafyatis et al. 36)

(127). Moreover, most mice carrying a single copy of the endoglin gene develop clinical signs of hereditary hemorrhagic telangiectasia (HHT) phenotype, with extensive dilated and weak-walled vessels (127, 128). HHT is an autosomal-dominant disorder in humans, with a mutation in ENG or ACVRL1 gene (coding for endoglin and ALK1) characterized by frequent episodes of epistaxis, telangiectases, and multiorgan vascular dysplasia (129).

This phenotype is similar to radiation-induced microvascular damage, which raises the question of whether endoglin may also play a crucial role in radiation-induced cardiac injury.

Chemotherapy and Her-inhibitors

Thoracic cancer patients often receive anthracycline chemotherapy combined with radiotherapy. For breast cancer patients this may be given as adjuvant therapy post mastectomy or lumpectomy. One of the most effective anthracyclines in anti-cancer treatment is doxorubicin, a drug that is also known to increase the risk of cardiac toxicity. Cancer survivors treated with both doxorubicin and radiotherapy have a higher risk of heart failure than those treated by either therapy alone (130).

Doxorubicin induces cell killing by targeting topoisomerase II and DNA to inhibit replication and by creating iron-mediated free oxygen radicals that damage the DNA. The most cited and accepted mechanism is the formation of reactive oxygen species (ROS), which leads to

oxidative stress and causes lethal injury to the cardiac myocytes (131-133). Cardiac myocytes are postreplicative and thus unable to regenerate, therefore cell loss eventually leads to myocardial damage. Endothelial cells, however, have the ability to maintain cardiomyocyte metabolism and survival by activating prosurvival signaling pathways e.g. by releasing neuregulin-1 β (134). Neuregulin-1 β binds to epidermal growth factor receptor 4 (ErbB4) and leads to heterodimerization with ErbB2 or homodimerization with ErbB4 and therefore stimulates the intracellular signal transduction pathways (Figure 3) (135).

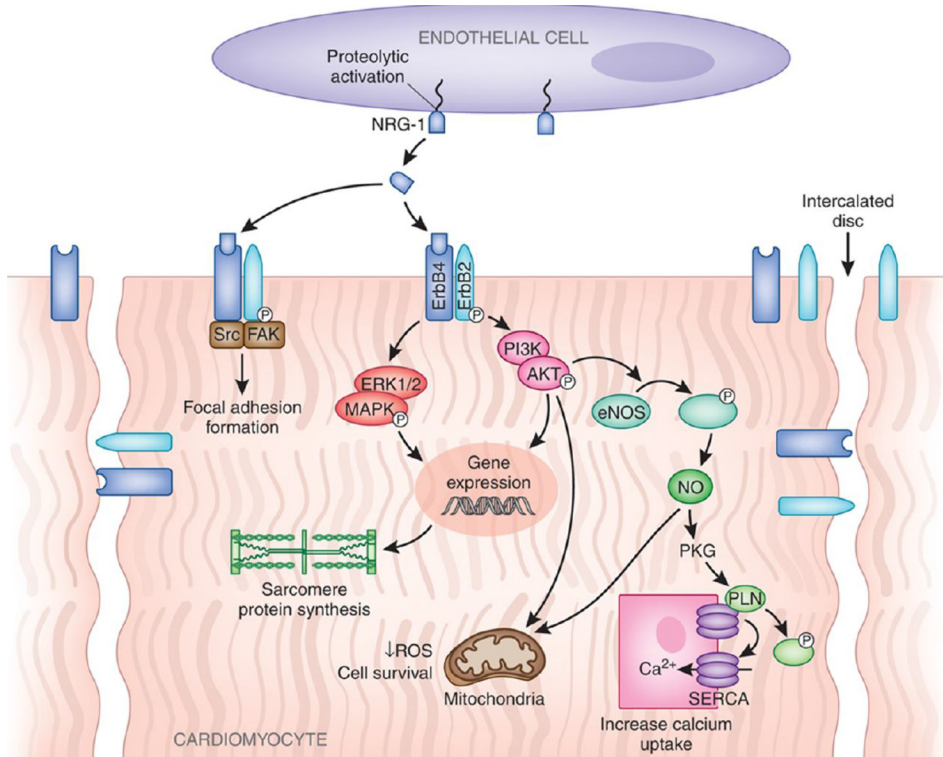


FIGURE 3 Prosurvival pathways in cardiomyocytes. Neuregulin-1 released by endothelial cells can bind to ErbB4 and activates intracellular signal transduction pathways. Adapted from Odiete et al. (46)

Approximately 20-30% of breast cancers show a highly aggressive subtype, characterized by ErbB2 overexpression. This type of breast cancer shows resistance to chemotherapy and radiotherapy, and is therefore associated with poor clinical outcome and higher risk for recurrence (137, 138). Therapeutic ErbB2-inhibitor agents have a clinical benefit in ErbB2-overexpressing breast cancers. One promising small molecule inhibitor is lapatinib, which reversibly inhibits the tyrosine kinase activities of ErbB1 and ErbB2 at equal potency. Lapatinib

blocks the signal transduction to Ras/Raf MAPKs and the PI3K/Akt pathway, which leads to increased apoptosis and decreased cellular proliferation (139). However, questions arise whether blocking of ErbB2, and thus blocking cardiomyocyte pro-survival pathways, would lead to an additional cardiac damage when combined with chemotherapy or radiotherapy.

1.3 Aim and outlines of the thesis

The underlying mechanisms of late cardiac damage, and the contribution of the cardiac microvasculature to cardiovascular disease are still poorly understood.

We therefore set up different experimental approaches that will be discussed in detail in the following chapters of this thesis.

Chapter 2: Our first aim was to develop a mouse model for characterization of the severity and rate of progression of cardiac damage after irradiation. This chapter describes the sequence of events in the irradiated mouse heart after low, intermediate and high (2, 8, 16 Gy) single doses. The histological and functional effects were investigated at early (20 weeks) and late (40 and 60 weeks) time points.

Chapter 3: Wild type mice have very low levels of low density lipoprotein (LDL) and are extremely resistant to the development of atherosclerosis. Cardiac damage identified after irradiation of wild type mice therefore does not include any component of atherosclerosis. ApoE^{-/-} mice, however, have elevated cholesterol levels, develop spontaneous atherosclerosis with age and can be used to mimic the human situation. To investigate whether the presence of elevated cholesterol would influence the development of radiation induced damage, ApoE^{-/-} mouse hearts were irradiated with single low, intermediate and high doses (2, 8, 16 Gy). Thus, this results shown in this chapter may allow us to evaluate the contribution of atherosclerosis (macrovascular damage) in the pathology of radiation induced cardiac damage.

Chapter 4: In Her2-positive breast cancer patients inhibition of epidermal growth factor receptor 2 (ErbB2)-signaling is often combined with chemotherapy and radiotherapy. The risk of cardiac toxicity after anthracyclines and radiotherapy is recognized, but little is known about increased risk when combined with ErbB2 inhibition. We designed an experimental set-up that mimicked clinical treatment protocols by administrating lapatinib together with radiation or anthracycline, or delayed until 20 weeks. These results allow us to evaluate the impact on cardiac structure and function of inhibition ErbB2 signaling during thoracic cancer treatment.

Chapter 5: Endoglin is highly expressed in damaged endothelial cells and may therefore play a crucial role in cell proliferation and revascularization. To examine the role of endoglin in radiation-induced cardiac damage and repair, thus revascularization, we exposed endoglin deficient mice (Eng^{+/-}) to cardiac irradiation with a single dose of 8 or 16 Gy.

Chapter 6: A better understanding of the underlying mechanisms of radiation-induced cardiac damage allows for the development of intervention strategies. Since inflammatory and fibrotic events are dominant features in radiation induced heart damage, we hypothesize

that thalidomide might prevent or reduce this damage. To address this hypothesis, we fed thalidomide containing chow to irradiated and unirradiated mice and measured histological and functional cardiac effects at 40 weeks after treatment.

Chapter 7: It has been described in animal models of ischemia that *in vitro* differentiated endothelial cells transplanted after ischemic injury lead to improved perfusion and prevent organ (cardiac) damage. In this study we investigated whether radiation induced cardiovascular damage can be diminished by revascularization of Bone-marrow derived endothelial cells (BM-EPCs) and whether endoglin plays a role in this process. BM-EPCs from either endoglin haplo-insufficient ($Eng^{+/-}$) or endoglin proficient ($Eng^{+/+}$) mice were transplanted into wild type mice after irradiation with 16 Gy.

Reference List

1. Borst GR, Sonke JJ, den Hollander S, Betgen A, Remeijer P, van Giersbergen A, et al. Clinical results of image-guided deep inspiration breath hold breast irradiation. *International journal of radiation oncology, biology, physics*. 2010;78(5):1345-51.
2. Taylor CW, McGale P, Povall JM, Thomas E, Kumar S, Dodwell D, et al. Estimating cardiac exposure from breast cancer radiotherapy in clinical practice. *International journal of radiation oncology, biology, physics*. 2009;73(4):1061-8.
3. Taylor CW, Nisbet A, McGale P, Darby SC. Cardiac exposures in breast cancer radiotherapy: 1950s-1990s. *International journal of radiation oncology, biology, physics*. 2007;69(5):1484-95.
4. Hodgson DC. Late effects in the era of modern therapy for Hodgkin lymphoma. *Hematology / the Education Program of the American Society of Hematology American Society of Hematology Education Program*. 2011;2011:323-9.
5. Adams MJ, Lipshultz SE, Schwartz C, Fajardo LF, Coen V, Constine LS. Radiation-associated cardiovascular disease: manifestations and management. *Seminars in radiation oncology*. 2003;13(3):346-56.
6. Andratschke N, Maurer J, Molls M, Trott KR. Late radiation-induced heart disease after radiotherapy. Clinical importance, radiobiological mechanisms and strategies of prevention. *Radiotherapy and oncology : journal of the European Society for Therapeutic Radiology and Oncology*. 2011;100(2):160-6.
7. Burns RJ, Bar-Shlomo BZ, Druck MN, Herman JG, Gilbert BW, Perrault DJ, et al. Detection of radiation cardiomyopathy by gated radionuclide angiography. *The American journal of medicine*. 1983;74(2):297-302.
8. Pohjola-Sintonen S, Totterman KJ, Salmo M, Siltanen P. Late cardiac effects of mediastinal radiotherapy in patients with Hodgkin's disease. *Cancer*. 1987;60(1):31-7.
9. Yusuf SW, Sami S, Daher IN. Radiation-induced heart disease: a clinical update. *Cardiology research and practice*. 2011;2011:317659.
10. Lauk S, Kizsel Z, Buschmann J, Trott KR. Radiation-induced heart disease in rats. *International journal of radiation oncology, biology, physics*. 1985;11(4):801-8.
11. Lauk S. Endothelial alkaline phosphatase activity loss as an early stage in the development of radiation-induced heart disease in rats. *Radiation research*. 1987;110(1):118-28.
12. Schultz-Hector S, Trott KR. Radiation-induced cardiovascular diseases: is the epidemiologic evidence compatible with the radiobiologic data? *Int J Radiat Oncol Biol Phys*. 2007;67(1):10-8.

13. Stewart FA, Hoving S, Russell NS. Vascular damage as an underlying mechanism of cardiac and cerebral toxicity in irradiated cancer patients. *Radiation research*. 2010;174(6):865-9.
14. Stone HB, Coleman CN, Anscher MS, McBride WH. Effects of radiation on normal tissue: consequences and mechanisms. *The Lancet Oncology*. 2003;4(9):529-36.
15. Wheldon TE, Michalowski AS, Kirk J. The effect of irradiation on function in self-renewing normal tissues with differing proliferative organisation. *The British journal of radiology*. 1982;55(658):759-66.
16. Michalowski A. Effects of radiation on normal tissues: hypothetical mechanisms and limitations of in situ assays of clonogenicity. *Radiation and environmental biophysics*. 1981;19(3):157-72.
17. Michael Joiner AvdK. *Basic Clinical Radiobiology*. 4th ed. Great Britain: Hodder Arnold; 2009 2009.
18. Stewart FA, Dorr W. Milestones in normal tissue radiation biology over the past 50 years: from clonogenic cell survival to cytokine networks and back to stem cell recovery. *International journal of radiation biology*. 2009;85(7):574-86.
19. Darby SC, Cutter DJ, Boerma M, Constine LS, Fajardo LF, Kodama K, et al. Radiation-related heart disease: current knowledge and future prospects. *International journal of radiation oncology, biology, physics*. 2010;76(3):656-65.
20. Lara PC, Russell NS, Smolders IJ, Bartelink H, Begg AC, Coco-Martin JM. Radiation-induced differentiation of human skin fibroblasts: relationship with cell survival and collagen production. *International journal of radiation biology*. 1996;70(6):683-92.
21. Russell NS, Lara PC, Grummels A, Hart AA, Coco-Martin JM, Bartelink H, et al. In vitro differentiation characteristics of human skin fibroblasts: correlations with radiotherapy-induced breast fibrosis in patients. *International journal of radiation biology*. 2000;76(2):231-40.
22. Bentzen SM. Preventing or reducing late side effects of radiation therapy: radiobiology meets molecular pathology. *Nature reviews Cancer*. 2006;6(9):702-13.
23. Khaled S, Gupta KB, Kucik DF. Ionizing radiation increases adhesiveness of human aortic endothelial cells via a chemokine-dependent mechanism. *Radiation research*. 2012;177(5):594-601.
24. Martin M, Lefaix J, Delanian S. TGF-beta1 and radiation fibrosis: a master switch and a specific therapeutic target? *International journal of radiation oncology, biology, physics*. 2000;47(2):277-90.
25. Arancibia R, Oyarzun A, Silva D, Tobar N, Martinez J, Smith PC. Tumor necrosis factor-alpha inhibits transforming growth factor-beta-stimulated myofibroblastic differentiation and extracellular matrix production in human gingival fibroblasts. *Journal of periodontology*. 2013;84(5):683-93.
26. Anscher MS. Targeting the TGF-beta1 pathway to prevent normal tissue injury after cancer therapy. *The oncologist*. 2010;15(4):350-9.

27. Barcellos-Hoff MH, Derynck R, Tsang ML, Weatherbee JA. Transforming growth factor-beta activation in irradiated murine mammary gland. *The Journal of clinical investigation*. 1994;93(2):892-9.
28. Scharpfenecker M, Kruse JJ, Sprong D, Russell NS, Ten Dijke P, Stewart FA. Ionizing radiation shifts the PAI-1/ID-1 balance and activates notch signaling in endothelial cells. *International journal of radiation oncology, biology, physics*. 2009;73(2):506-13.
29. Guo S, Dipietro LA. Factors affecting wound healing. *Journal of dental research*. 2010;89(3):219-29.
30. Torsney E, Charlton R, Parums D, Collis M, Arthur HM. Inducible expression of human endoglin during inflammation and wound healing in vivo. *Inflammation research : official journal of the European Histamine Research Society (et al)*. 2002;51(9):464-70.
31. Gougos A, Letarte M. Identification of a human endothelial cell antigen with monoclonal antibody 44G4 produced against a pre-B leukemic cell line. *Journal of immunology*. 1988;141(6):1925-33.
32. van Meeteren LA, Goumans MJ, ten Dijke P. TGF-beta receptor signaling pathways in angiogenesis; emerging targets for anti-angiogenesis therapy. *Current pharmaceutical biotechnology*. 2011;12(12):2108-20.
33. Akhurst RJ. Taking thalidomide out of rehab. *Nature medicine*. 2010;16(4):370-2.
34. Lebrin F, Goumans MJ, Jonker L, Carvalho RL, Valdimarsdottir G, Thorikay M, et al. Endoglin promotes endothelial cell proliferation and TGF-beta/ALK1 signal transduction. *The EMBO journal*. 2004;23(20):4018-28.
35. Gore B, Izikki M, Mercier O, Dewachter L, Fadel E, Humbert M, et al. Key role of the endothelial TGF-beta/ALK1/endoglin signaling pathway in humans and rodents pulmonary hypertension. *PloS one*. 2014;9(6):e100310.
36. Lafyatis R. Transforming growth factor beta-at the centre of systemic sclerosis. *Nature reviews Rheumatology*. 2014.
37. Bourdeau A, Dumont DJ, Letarte M. A murine model of hereditary hemorrhagic telangiectasia. *The Journal of clinical investigation*. 1999;104(10):1343-51.
38. Arthur HM, Ure J, Smith AJ, Renforth G, Wilson DI, Torsney E, et al. Endoglin, an ancillary TGFbeta receptor, is required for extraembryonic angiogenesis and plays a key role in heart development. *Developmental biology*. 2000;217(1):42-53.
39. Lopez-Novoa JM, Bernabeu C. The physiological role of endoglin in the cardiovascular system. *American journal of physiology Heart and circulatory physiology*. 2010;299(4):H959-74.
40. Bovelli D, Plataniotis G, Roila F, Group EGW. Cardiotoxicity of chemotherapeutic agents and radiotherapy-related heart disease: ESMO Clinical Practice Guidelines. *Annals of oncology : official journal of the European Society for Medical Oncology / ESMO*. 2010;21 Suppl 5:v277-82.
41. Bird BR, Swain SM. Cardiac toxicity in breast cancer survivors: review of potential cardiac problems.

- Clinical cancer research : an official journal of the American Association for Cancer Research. 2008;14(1):14-24.
42. Minotti G, Menna P, Salvatorelli E, Cairo G, Gianni L. Anthracyclines: molecular advances and pharmacologic developments in antitumor activity and cardiotoxicity. *Pharmacological reviews*. 2004;56(2):185-229.
 43. L'Ecuyer T, Sanjeev S, Thomas R, Novak R, Das L, Campbell W, et al. DNA damage is an early event in doxorubicin-induced cardiac myocyte death. *American journal of physiology Heart and circulatory physiology*. 2006;291(3):H1273-80.
 44. Davidson SM, Duchon MR. Endothelial mitochondria: contributing to vascular function and disease. *Circulation research*. 2007;100(8):1128-41.
 45. Hynes NE, Horsch K, Olayioye MA, Badache A. The ErbB receptor tyrosine family as signal integrators. *Endocrine-related cancer*. 2001;8(3):151-9.
 46. Odiete O, Hill MF, Sawyer DB. Neuregulin in cardiovascular development and disease. *Circulation research*. 2012;111(10):1376-85.
 47. Allred DC, Clark GM, Tandon AK, Molina R, Tormey DC, Osborne CK, et al. HER-2/neu in node-negative breast cancer: prognostic significance of overexpression influenced by the presence of in situ carcinoma. *Journal of clinical oncology : official journal of the American Society of Clinical Oncology*. 1992;10(4):599-605.
 48. Nahta R, Hortobagyi GN, Esteva FJ. Growth factor receptors in breast cancer: potential for therapeutic intervention. *The oncologist*. 2003;8(1):5-17.
 49. Perez EA, Suman VJ, Davidson NE, Sledge GW, Kaufman PA, Hudis CA, et al. Cardiac safety analysis of doxorubicin and cyclophosphamide followed by paclitaxel with or without trastuzumab in the North Central Cancer Treatment Group N9831 adjuvant breast cancer trial. *Journal of clinical oncology : official journal of the American Society of Clinical Oncology*. 2008;26(8):1231-8.
 50. Adams MJ, Hardenbergh PH, Constine LS, Lipshultz SE. Radiation-associated cardiovascular disease. *Crit Rev Oncol Hematol*. 2003;45(1):55-75.
 51. Filopei J, Frishman W. Radiation-induced heart disease. *Cardiol Rev*. 2012;20(4):184-8.
 52. Adams MJ, Lipsitz SR, Colan SD, Tarbell NJ, Treves ST, Diller L, et al. Cardiovascular status in long-term survivors of Hodgkin's disease treated with chest radiotherapy. *J Clin Oncol*. 2004;22(15):3139-48.
 53. Aleman BM, van den Belt-Dusebout AW, De Bruin ML, van 't Veer MB, Baaijens MH, de Boer JP, et al. Late cardiotoxicity after treatment for Hodgkin lymphoma. *Blood*. 2007;109(5):1878-86.
 54. Hancock SL, Donaldson SS, Hoppe RT. Cardiac disease following treatment of Hodgkin's disease in children and adolescents. *J Clin Oncol*. 1993;11(7):1208-15.
 55. Swerdlow AJ, Higgins CD, Smith P, Cunningham D, Hancock BW, Horwich A, et al. Myocardial

- infarction mortality risk after treatment for Hodgkin disease: a collaborative British cohort study. *J Natl Cancer Inst.* 2007;99(3):206-14.
56. Heidenreich PA, Hancock SL, Vagelos RH, Lee BK, Schnittger I. Diastolic dysfunction after mediastinal irradiation. *Am Heart J.* 2005;150(5):977-82.
57. Mulrooney DA, Yeazel MW, Kawashima T, Mertens AC, Mitby P, Stovall M, et al. Cardiac outcomes in a cohort of adult survivors of childhood and adolescent cancer: retrospective analysis of the Childhood Cancer Survivor Study cohort. *BMJ.* 2009;339:b4606.
58. Tukenova M, Guibout C, Oberlin O, Doyon F, Mousannif A, Haddy N, et al. Role of cancer treatment in long-term overall and cardiovascular mortality after childhood cancer. *J Clin Oncol.* 2010;28(8):1308-15.
59. Darby SC, McGale P, Taylor CW, Peto R. Long-term mortality from heart disease and lung cancer after radiotherapy for early breast cancer: prospective cohort study of about 300,000 women in US SEER cancer registries. *Lancet Oncol.* 2005;6(8):557-65.
60. Gaya AM, Ashford RF. Cardiac complications of radiation therapy. *Clin Oncol (R Coll Radiol).* 2005;17(3):153-9.
61. Senkus-Konefka E, Jassem J. Cardiovascular effects of breast cancer radiotherapy. *Cancer Treat Rev.* 2007;33(6):578-93.
62. Hoening MJ, Botma A, Aleman BM, Baaijens MH, Bartelink H, Klijn JG, et al. Long-term risk of cardiovascular disease in 10-year survivors of breast cancer. *J Natl Cancer Inst.* 2007;99(5):365-75.
63. Clarke M, Collins R, Darby S, Davies C, Elphinstone P, Evans E, et al. Effects of radiotherapy and of differences in the extent of surgery for early breast cancer on local recurrence and 15-year survival: an overview of the randomised trials. *Lancet.* 2005;366(9503):2087-106.
64. McGale P, Darby SC, Hall P, Adolphsson J, Bengtsson NO, Bennet AM, et al. Incidence of heart disease in 35,000 women treated with radiotherapy for breast cancer in Denmark and Sweden. *Radiother Oncol.* 2011;100(2):167-75.
65. Gyenes G, Fornander T, Carlens P, Glas U, Rutqvist LE. Myocardial damage in breast cancer patients treated with adjuvant radiotherapy: a prospective study. *Int J Radiat Oncol Biol Phys.* 1996;36(4):899-905.
66. Marks LB, Yu X, Prosnitz RG, Zhou SM, Hardenbergh PH, Blazing M, et al. The incidence and functional consequences of RT-associated cardiac perfusion defects. *Int J Radiat Oncol Biol Phys.* 2005;63(1):214-23.
67. Seddon B, Cook A, Gothard L, Salmon E, Latus K, Underwood SR, et al. Detection of defects in myocardial perfusion imaging in patients with early breast cancer treated with radiotherapy. *Radiother Oncol.* 2002;64(1):53-63.

68. Chera BS, Rodriguez C, Morris CG, Louis D, Yeung D, Li Z, et al. Dosimetric comparison of three different involved nodal irradiation techniques for stage II Hodgkin's lymphoma patients: conventional radiotherapy, intensity-modulated radiotherapy, and three-dimensional proton radiotherapy. *Int J Radiat Oncol Biol Phys.* 2009;75(4):1173-80.
69. Preston DL, Shimizu Y, Pierce DA, Suyama A, Mabuchi K. Studies of mortality of atomic bomb survivors. Report 13: Solid cancer and noncancer disease mortality: 1950-1997. *Radiat Res.* 2003;160(4):381-407.
70. Shimizu Y, Kodama K, Nishi N, Kasagi F, Suyama A, Soda M, et al. Radiation exposure and circulatory disease risk: Hiroshima and Nagasaki atomic bomb survivor data, 1950-2003. *BMJ.* 2010;340:b5349.
71. Shimizu Y, Pierce DA, Preston DL, Mabuchi K. Studies of the mortality of atomic bomb survivors. Report 12, part II. Noncancer mortality: 1950-1990. *Radiat Res.* 1999;152(4):374-89.
72. Hayashi T, Kusunoki Y, Hakoda M, Morishita Y, Kubo Y, Maki M, et al. Radiation dose-dependent increases in inflammatory response markers in A-bomb survivors. *Int J Radiat Biol.* 2003;79(2):129-36.
73. Sasaki H, Wong FL, Yamada M, Kodama K. The effects of aging and radiation exposure on blood pressure levels of atomic bomb survivors. *J Clin Epidemiol.* 2002;55(10):974-81.
74. Wong FL, Yamada M, Sasaki H, Kodama K, Hosoda Y. Effects of radiation on the longitudinal trends of total serum cholesterol levels in the atomic bomb survivors. *Radiat Res.* 1999;151(6):736-46.
75. Adams MJ, Grant EJ, Kodama K, Shimizu Y, Kasagi F, Suyama A, et al. Radiation dose associated with renal failure mortality: a potential pathway to partially explain increased cardiovascular disease mortality observed after whole-body irradiation. *Radiat Res.* 2012;177(2):220-8.
76. UNSCEAR 2008. Effects of ionizing radiation, Report to the General Assembly, Scientific Annexes A and B. In: Radiation UNSCotEoA, editor. New York: United Nations; 2006.
77. Little MP, Azizova TV, Bazyka D, Bouffler SD, Cardis E, Chekin S, et al. Systematic review and meta-analysis of circulatory disease from exposure to low-level ionizing radiation and estimates of potential population mortality risks. *Environ Health Perspect.* 2012;120(11):1503-11.
78. Little MP, Tawn EJ, Tzoulaki I, Wakeford R, Hildebrandt G, Paris F, et al. A systematic review of epidemiological associations between low and moderate doses of ionizing radiation and late cardiovascular effects, and their possible mechanisms. *Radiation research.* 2008;169(1):99-109.
79. Little MP, Tawn EJ, Tzoulaki I, Wakeford R, Hildebrandt G, Paris F, et al. Review and meta-analysis of epidemiological associations between low/moderate doses of ionizing radiation and circulatory disease risks, and their possible mechanisms. *Radiat Environ Biophys.* 2010;49(2):139-53.
80. McGale P, Darby SC. Low doses of ionizing radiation and circulatory diseases: a systematic review of the published epidemiological evidence. *Radiat Res.* 2005;163(3):247-57.

81. McGale P, Darby SC. Commentary: A dose-response relationship for radiation-induced heart disease-current issues and future prospects. *Int J Epidemiol.* 2008;37(3):518-23.
82. Metz-Flamant C, Bonaventure A, Milliat F, Tirmarche M, Laurier D, Bernier MO. (Low doses of ionizing radiation and risk of cardiovascular disease: A review of epidemiological studies). *Rev Epidemiol Sante Publique.* 2009;57(5):347-59.
83. Lusis AJ. Atherosclerosis. *Nature.* 2000;407(6801):233-41.
84. Hewitt G, Jurk D, Marques FD, Correia-Melo C, Hardy T, Gackowska A, et al. Telomeres are favoured targets of a persistent DNA damage response in ageing and stress-induced senescence. *Nat Commun.* 2012;3:708.
85. Konings AW, Smit Sibinga CT, Aarnoudse MW, de Wit SS, Lamberts HB. Initial events in radiation-induced atheromatosis. II. Damage to intimal cells. *Strahlentherapie.* 1978;154(11):795-800.
86. Stewart JR, Fajardo LF, Gillette SM, Constine LS. Radiation injury to the heart. *Int J Radiat Oncol Biol Phys.* 1995;31(5):1205-11.
87. Veinot JP, Edwards WD. Pathology of radiation-induced heart disease: a surgical and autopsy study of 27 cases. *Hum Pathol.* 1996;27(8):766-73.
88. Tribble DL, Barcellos-Hoff MH, Chu BM, Gong EL. Ionizing radiation accelerates aortic lesion formation in fat-fed mice via SOD-inhibitable processes. *Arterioscler Thromb Vasc Biol.* 1999;19(6):1387-92.
89. Gabriels K, Hoving S, Seemann I, Visser NL, Gijbels MJ, Pol JF, et al. Local heart irradiation of ApoE(-/-) mice induces microvascular and endocardial damage and accelerates coronary atherosclerosis. *Radiother Oncol.* 2012;105(3):358-64.
90. Hoving S, Heeneman S, Gijbels MJ, te Poele JA, Russell NS, Daemen MJ, et al. Single-dose and fractionated irradiation promote initiation and progression of atherosclerosis and induce an inflammatory plaque phenotype in ApoE(-/-) mice. *Int J Radiat Oncol Biol Phys.* 2008;71(3):848-57.
91. Pakala R, Leborgne L, Cheneau E, Chan RC, Yazdi H, Fournadjiev J, et al. Radiation-induced atherosclerotic plaque progression in a hypercholesterolemic rabbit: a prospective vulnerable plaque model? *Cardiovasc Radiat Med.* 2003;4(3):146-51.
92. Stewart FA, Heeneman S, Te Poele J, Kruse J, Russell NS, Gijbels M, et al. Ionizing radiation accelerates the development of atherosclerotic lesions in ApoE(-/-) mice and predisposes to an inflammatory plaque phenotype prone to hemorrhage. *Am J Pathol.* 2006;168(2):649-58.
93. Vos J, Aarnoudse MW, Dijk F, Lamberts HB. On the cellular origin and development of atheromatous plaques. A light and electron microscopic study of combined X-ray and hypercholesterolemia-induced atheromatosis in the carotid artery of the rabbit. *Virchows Arch B Cell Pathol Incl Mol Pathol.* 1983;43(1):1-16.
94. Yu T, Parks BW, Yu S, Srivastava R, Gupta K, Wu X, et al. Iron-ion radiation accelerates atherosclerosis

- in apolipoprotein E-deficient mice. *Radiat Res.* 2011;175(6):766-73.
95. Baker JE, Fish BL, Su J, Haworth ST, Strande JL, Komorowski RA, et al. 10 Gy total body irradiation increases risk of coronary sclerosis, degeneration of heart structure and function in a rat model. *Int J Radiat Biol.* 2009;85(12):1089-100.
96. Mitchel RE, Hasu M, Bugden M, Wyatt H, Little MP, Gola A, et al. Low-dose radiation exposure and atherosclerosis in ApoE(-)/(-) mice. *Radiat Res.* 2011;175(5):665-76.
97. Hildebrandt G, Maggiorella L, Rodel F, Rodel V, Willis D, Trott KR. Mononuclear cell adhesion and cell adhesion molecule liberation after X-irradiation of activated endothelial cells in vitro. *Int J Radiat Biol.* 2002;78(4):315-25.
98. Arenas M, Gil F, Gironella M, Hernandez V, Jorcano S, Biete A, et al. Anti-inflammatory effects of low-dose radiotherapy in an experimental model of systemic inflammation in mice. *Int J Radiat Oncol Biol Phys.* 2006;66(2):560-7.
99. Fajardo LF, Stewart JR. Experimental radiation-induced heart disease. I. Light microscopic studies. *Am J Pathol.* 1970;59(2):299-316.
100. Fajardo LF, Berthrong M, Anderson RE. *Radiation pathology.* New York: Oxford University Press; 2001.
101. Schultz-Hector S. Radiation-induced heart disease: review of experimental data on dose response and pathogenesis. *Int J Radiat Biol.* 1992;61(2):149-60.
102. Seemann I, Gabriels K, Visser NL, Hoving S, te Poele JA, Pol JF, et al. Irradiation induced modest changes in murine cardiac function despite progressive structural damage to the myocardium and microvasculature. *Radiother Oncol.* 2012;103(2):143-50.
103. Lauk S, Trott KR. Endothelial cell proliferation in the rat heart following local heart irradiation. *Int J Radiat Biol.* 1990;57(5):1017-30.
104. Kanthou C, Gharaei Z, Haagen J, Lunt SJ, Reyes-Aldasoro C, Doerr W, et al. Inhibition of angiogenesis in the mouse heart by ionizing radiation. AACR 103rd Annual Meeting. Chicago: Cancer Research; 2012.
105. McChesney SL, Gillette EL, Orton EC. Canine cardiomyopathy after whole heart and partial lung irradiation. *Int J Radiat Oncol Biol Phys.* 1988;14(6):1169-74.
106. Boerma M, Wang J, Wondergem J, Joseph J, Qiu X, Kennedy RH, et al. Influence of mast cells on structural and functional manifestations of radiation-induced heart disease. *Cancer Res.* 2005;65(8):3100-7.
107. Rodemann HP, Peterson HP, Schwenke K, von Wangenheim KH. Terminal differentiation of human fibroblasts is induced by radiation. *Scanning Microsc.* 1991/12/01 ed1991. p. 1135-42; discussion 42-3.
108. Kruse JJ, Zurcher C, Strootman EG, Bart CI, Schlagwein N, Leer JW, et al. Structural changes in the

- auricles of the rat heart after local ionizing irradiation. *Radiother Oncol.* 2001;58(3):303-11.
109. Burger A, Loffler H, Bamberg M, Rodemann HP. Molecular and cellular basis of radiation fibrosis. *Int J Radiat Biol.* 1998;73(4):401-8.
110. Evans RA, Tian YC, Steadman R, Phillips AO. TGF-beta1-mediated fibroblast-myofibroblast terminal differentiation-the role of Smad proteins. *Exp Cell Res.* 2003;282(2):90-100.
111. Hilbers FS, Boekel NB, van den Broek AJ, van Hien R, Cornelissen S, Aleman BM, et al. Genetic variants in TGFbeta-1 and PAI-1 as possible risk factors for cardiovascular disease after radiotherapy for breast cancer. *Radiother Oncol.* 2012;102(1):115-21.
112. Monceau V, Pasinetti N, Schupp C, Pouzoulet F, Opolon P, Vozenin MC. Modulation of the Rho/ROCK pathway in heart and lung after thorax irradiation reveals targets to improve normal tissue toxicity. *Curr Drug Targets.* 2010;11(11):1395-404.
113. Heidenreich PA, Schnittger I, Strauss HW, Vagelos RH, Lee BK, Mariscal CS, et al. Screening for coronary artery disease after mediastinal irradiation for Hodgkin's disease. *J Clin Oncol.* 2007;25(1):43-9.
114. Nadlonek NA, Weyant MJ, Yu JA, Cleveland JC, Jr., Reece TB, Meng X, et al. Radiation induces osteogenesis in human aortic valve interstitial cells. *J Thorac Cardiovasc Surg.* 2012;144(6):1466-70.
115. Ghobadi G, Bartelds B, van der Veen SJ, Dickinson MG, Brandenburg S, Berger RM, et al. Lung irradiation induces pulmonary vascular remodelling resembling pulmonary arterial hypertension. *Thorax.* 2012;67(4):334-41.
116. Schiller NK, Kubo N, Boisvert WA, Curtiss LK. Effect of gamma-irradiation and bone marrow transplantation on atherosclerosis in LDL receptor-deficient mice. *Arterioscler Thromb Vasc Biol.* 2001;21(10):1674-80.
117. Hoving S, Heeneman S, Gijbels MJ, te Poele JA, Bolla M, Pol JF, et al. NO-donating aspirin and aspirin partially inhibit age-related atherosclerosis but not radiation-induced atherosclerosis in ApoE null mice. *PLoS One.* 2010;5(9):e12874.
118. Momi S, Pitchford SC, Alberti PF, Minuz P, Del Soldato P, Gresele P. Nitroaspirin plus clopidogrel versus aspirin plus clopidogrel against platelet thromboembolism and intimal thickening in mice. *Thromb Haemost.* 2005;93(3):535-43.
119. Napoli C. Nitric oxide and atherosclerotic lesion progression: an overview. *J Card Surg.* 2002;17(4):355-62.
120. Yu H, Kumar SR, Tang L, Terramani TT, Rowe VL, Wang Y, et al. Injury induced neointima formation and its inhibition by retrovirus-mediated transfer of nitride oxide synthase gene in an in-vitro human saphenous vein culture model. *Atherosclerosis.* 2002;161(1):113-22.
121. Li M, Zhang Y, Ren H, Zhu X. Effect of clopidogrel on the inflammatory progression of early atherosclerosis in rabbits model. *Atherosclerosis.* 2007;194(2):348-56.

122. Waksman R, Pakala R, Roy P, Baffour R, Hellinga D, Seabron R, et al. Effect of clopidogrel on neointimal formation and inflammation in balloon-denuded and radiated hypercholesterolemic rabbit iliac arteries. *J Interv Cardiol.* 2008;21(2):122-8.
123. Hoving S, Heeneman S, Gijbels MJ, te Poele JA, Pol JF, Gabriels K, et al. Anti-inflammatory and anti-thrombotic intervention strategies using atorvastatin, clopidogrel and knock-down of CD40L do not modify radiation-induced atherosclerosis in ApoE null mice. *Radiother Oncol.* 2011;101(1):100-8.
124. Leborgne L, Pakala R, Dilcher C, Hellinga D, Seabron R, Tio FO, et al. Effect of antioxidants on atherosclerotic plaque formation in balloon-denuded and irradiated hypercholesterolemic rabbits. *J Cardiovasc Pharmacol.* 2005;46(4):540-7.
125. Pakala R, Dilcher C, Baffour R, Hellinga D, Seabron R, Joner M, et al. Peroxisome proliferator-activated receptor gamma ligand pioglitazone alters neointimal composition in a balloon-denuded and radiated hypercholesterolemic rabbit. *J Cardiovasc Pharmacol.* 2006;48(6):299-305.
126. van der Hoorn JW, Jukema JW, Havekes LM, Lundholm E, Camejo G, Rensen PC, et al. The dual PPARalpha/gamma agonist tesaglitazar blocks progression of pre-existing atherosclerosis in APOE*3Leiden.CETP transgenic mice. *Br J Pharmacol.* 2009;156(7):1067-75.
127. Shi J, Wang J, Zheng H, Ling W, Joseph J, Li D, et al. Statins increase thrombomodulin expression and function in human endothelial cells by a nitric oxide-dependent mechanism and counteract tumor necrosis factor alpha-induced thrombomodulin downregulation. *Blood Coagul Fibrinolysis.* 2003;14(6):575-85.
128. Trochu JN, Mital S, Zhang X, Xu X, Ochoa M, Liao JK, et al. Preservation of NO production by statins in the treatment of heart failure. *Cardiovasc Res.* 2003;60(2):250-8.
129. Haydont V, Mathe D, Bourquier C, Abdelali J, Aigueperse J, Bourhis J, et al. Induction of CTGF by TGF-beta1 in normal and radiation enteritis human smooth muscle cells: Smad/Rho balance and therapeutic perspectives. *Radiother Oncol.* 2005;76(2):219-25.
130. Dai W, Kloner RA. Bone marrow-derived cell transplantation therapy for myocardial infarction: lessons learned and future questions. *Am J Transplant.* 2011;11(11):2297-301.
131. Kumar AH, Caplice NM. Clinical potential of adult vascular progenitor cells. *Arterioscler Thromb Vasc Biol.* 2010;30(6):1080-7.
132. Yuen DA, Connelly KA, Advani A, Liao C, Kuliszewski MA, Trogadis J, et al. Culture-modified bone marrow cells attenuate cardiac and renal injury in a chronic kidney disease rat model via a novel antifibrotic mechanism. *PLoS One.* 2010;5(3):e9543.
133. Jujo K, li M, Losordo DW. Endothelial progenitor cells in neovascularization of infarcted myocardium. *J Mol Cell Cardiol.* 2008;45(4):530-44.
134. Boerma M, Roberto KA, Hauer-Jensen M. Prevention and treatment of functional and structural

- radiation injury in the rat heart by pentoxifylline and alpha-tocopherol. *Int J Radiat Oncol Biol Phys.* 2008;72(1):170-7.
135. Liu H, Xiong M, Xia YF, Cui NJ, Lu RB, Deng L, et al. Studies on pentoxifylline and tocopherol combination for radiation-induced heart disease in rats. *Int J Radiat Oncol Biol Phys.* 2009;73(5):1552-9.
136. Delanian S, Porcher R, Rudant J, Lefaix JL. Kinetics of response to long-term treatment combining pentoxifylline and tocopherol in patients with superficial radiation-induced fibrosis. *J Clin Oncol.* 2005;23(34):8570-9.
137. Magnusson M, Hoglund P, Johansson K, Jonsson C, Killander F, Malmstrom P, et al. Pentoxifylline and vitamin E treatment for prevention of radiation-induced side-effects in women with breast cancer: a phase two, double-blind, placebo-controlled randomised clinical trial (Ptx-5). *Eur J Cancer.* 2009;45(14):2488-95.
138. Yarom R, Harper IS, Wynchank S, van Schalkwyk D, Madhoo J, Williams K, et al. Effect of captopril on changes in rats' hearts induced by long-term irradiation. *Radiat Res.* 1993;133(2):187-97.
139. Cardinale D, Colombo A, Sandri MT, Lamantia G, Colombo N, Civelli M, et al. Prevention of high-dose chemotherapy-induced cardiotoxicity in high-risk patients by angiotensin-converting enzyme inhibition. *Circulation.* 2006;114(23):2474-81.



Chapter 2

Irradiation induced modest changes in murine cardiac function despite progressive structural damage to the myocardium and microvasculature

.....
I. Seemann¹, K. Gabriels¹, N.L. Visser, S. Hoving, J.A. te Poele, J.F. Pol, M.J. Gijbels, B.J. Janssen, F.W. van Leeuwen, M.J. Daemen, S. Heeneman², F.A. Stewart.²

¹ Those authors contributed equally

² Those authors contributed equally

Radiotherapy and Oncology May 2012

Abstract

Background: Radiotherapy of thoracic and chest wall tumors increases the long-term risk of cardiotoxicity, but the underlying mechanisms are unclear.

Materials and Methods: Single doses of 2-16 Gy were delivered to the hearts of mice and damage was evaluated at 20, 40 and 60 weeks, relative to age-matched controls. Single photon emission computed tomography (SPECT/CT) and ultrasound were used to measure cardiac geometry and function, which was related to histo-morphology and microvascular damage.

Results: Gated SPECT/CT and ultrasound demonstrated decreases in end diastolic and systolic volumes, while the ejection fraction was increased at 20 and 40 weeks after 2-16 Gy. Cardiac blood volume was decreased at 20 and 60 weeks after irradiation. Histological examination revealed inflammatory changes at 20 and 40 weeks after 8-16 Gy. Microvascular density in the left ventricle was decreased at 40 and 60 weeks after 8-16 Gy, with functional damage to remaining microvasculature manifest as decreased alkaline phosphatase (2-16 Gy), increased von Willebrand Factor and albumin leakage from vessels (8-16 Gy), and amyloidosis (16 Gy). 16 Gy lead to sudden death at 30-40 weeks in 38% of mice.

Conclusions: Irradiation with 2 to 8 Gy induced modest changes in murine cardiac function within 20 weeks but this did not deteriorate further, despite progressive structural and microvascular damage. This indicates that heart function can compensate for significant structural damage, although higher doses, eventually lead to sudden death.

Introduction

Radiation-induced heart disease (RIHD) can be a severe late side effect in cancer patients irradiated to their thorax (1). This has relevance for long-term survivors of cancer (2). Cancers with a good long-term prognosis that are treated with thoracic irradiation include childhood cancers, breast cancer and Hodgkin lymphoma. RIHD was first described in the 1960's, after mantle field radiotherapy for Hodgkin lymphoma (3). Since then treatment options and techniques, especially the development of dose-sculpting radiation techniques, have improved and the relative 5-year survival rates for childhood cancer, including Hodgkin lymphoma, have increased from 30% in 1960 to 79% in 2010 (4). However, longer survival in Hodgkin lymphoma patients is associated with increased risks (relative to age-matched unirradiated populations) of late cardiac morbidity and mortality; from 2% after 5 years to 23% after 20 years (5). Epidemiological studies also demonstrate increased risks for cardiac mortality and morbidity for breast cancer patients that received radiotherapy (2,6). Although the relative risk is lower than for Hodgkin lymphoma patients, the large number of women irradiated for breast cancer makes this a significant health problem. For both patient groups, the risk of RIHD becomes significant 10 years after treatment and increases with time (6,7).

RIHD includes a wide spectrum of cardiac pathologies, like pericarditis, cardiomyopathy, valvular disorders, myocardial fibrosis, coronary artery disease, conduction abnormalities and sudden death (8-10). In the early stages, before the onset of functional impairment, some experimental studies have shown evidence of inflammation in the myocardium, endothelial cell damage and decreased myocardial capillary density (11-13). Regional cardiac perfusion defects have also been identified in non-symptomatic breast cancer patients from 6 months after radiotherapy (14,15). This suggests that early microvascular damage may precede severe cardiac functional impairment.

The risk of RIHD is now well recognized but the underlying mechanisms of its initiation and progression, and the roles played by microvascular damage, fibrosis and atherosclerosis remain unclear. In this study, local cardiac irradiation of mice was used, with different doses and prolonged follow-up, to shed light on the dose dependence of the severity, latency and rate of progression of structural and functional cardiovascular damage. This is the first study that characterizes in detail both the functional and structural cardiac damages after local heart irradiation in mice.

Materials and Methods

Mice and irradiation procedure

Male C57BL/6J mice aged 8-12 weeks (from Charles River Laboratories, France) were randomly allocated to different treatment groups and housed in a temperature-controlled room with 12 hour light-dark cycle. Standard mouse chow and water were provided ad libitum. During irradiation or sham treatment (0 Gy) mice were held unanaesthetized in a prone position, in restraining jigs with the thorax fixed using adjustable hinges. Single doses of 2, 8 or 16 Gy were given to the heart using 250 kV X rays, operating at 12 mA and filtered with 0.6 mm of copper. The dose rate was 0.94 Gy/min. The field size (10.6 x 15.0 mm) and position was determined in pilot studies using mammograms to visualize the hearts of mice of the same sex and weight. In order to ensure that the whole heart was irradiated in all mice, up to 30% of the lung volume was included in the field. The rest of the body was shielded with a 3 mm thick lead plate.

Separate cohorts of animals were irradiated for functional imaging and harvesting of hearts for analyses at 20, 40 and 60 weeks after irradiation. Each dose and time point typically comprised 10 to 15 mice (n=165 in total). Age-matched controls (sham irradiated) were always included and these provide the appropriate comparison for irradiated groups at that time point.

Experiments were in agreement with the Dutch law on animal experiments and welfare, and in line with the international *Guide for the Care and Use of Laboratory Animals* (Eighth edition).

SPECT/CT

Single photon emission computed tomography (SPECT) acquisitions were made with the dedicated small-animal NanoSPECT/CT (Bioscan Europe, Ltd., Paris, France). Animals were anesthetized with Hypnorm (Fentanyl 0.26 mg/kg/Fluanisone 8.33 mg/kg, VetaPharma, Ltd., Leeds, UK) and Dormicum (Midazolam, 4.17 mg/kg, Roche, Woerden, the Netherlands) via intraperitoneal (i.p.) injection (1:2:1 Hypnorm:H₂O:Dormicum; 120 µl/mouse), placed on the animal bed in the prone position and scanned in the tail-first direction. Human Serum Albumin (HSA) (Vasculosis, IBA Molecular, Gif-sur-Yvette, France) was labeled with 1-1.5 ml ^{99m}Tc-pertechnetate. The radiotracer (150 µl) was injected intravenously (i.v.), at a total activity of about 50 MBq per mouse. X-ray topogram and SPECT acquisition were initiated directly after tracer administration. A total body scan was used to calculate the ratio between the total radioactivity (MBq) in the mouse and in the heart, and hence calculate the blood volume of the heart chambers.

Gated SPECT/CT

Three-lead electrodes (3M red Dot 2282E, 3M, St.Paul, USA) were attached to both hind paws and right front paw of the mouse and connected to the integrated electrocardiography (ECG) monitor to measure heart rate (HR). ECG-gated data were recorded in 8 time-bins per cardiac cycle. The tracer tetrofosmin (Myoview, GE-healthcare, Hoevelaken, the Netherlands) was labeled with ^{99m}Tc -pertechnetate according to the manufacturer's protocol. The radiotracer (150 μl) was injected i.v. with a total activity of about 65 MBq per mouse. Acquisitions were started one hour after tracer incubation. Once a stable HR was established, a short X-ray topogram was made to set the field of view (FOV) and so focus on the thorax to reduce scan time. After the FOV was set, gated SPECT acquisition was started using a quadruple-head gamma camera high precision gantry, equipped with 4 pyramid collimators and 9 pinhole apertures (diameter 1.2 mm). The axial FOV was 16 mm. A 20% window centered on the 140 keV photoelectric peak of ^{99m}Tc was used to acquire 20 projections with uniform angular sampling over a 360° radius into a 128×128 matrix. ECG-gated data were recorded in 8 time-bins per cardiac cycle, with an accepted frame time of 180 seconds. HiSPECT NG software (InVivoScope, Bioscan) was used to perform iterative reconstruction into 3D-datasets. Quantitative analysis of the reconstructed datasets was performed on a clinical e.soft (*syngo*-based) workstation (Siemens Medical Solutions, Siemens AG, Erlangen, Germany), using algorithms to automatically reconstruct a count based 3D model of the dimensions of the left ventricular (LV) end diastolic and systolic volumes (EDV, ESV), as well as the thickness of the LV wall in diastole and systole. The ejection fraction (EF) was calculated based on the difference between EDV and ESV divided by EDV.

2D- ultrasound

Mice were lightly sedated with 2% isoflurane (Forane, Abbott, Hoofddorp, the Netherlands). Echocardiography images were acquired using a Vevo 770 system (VisualSonics, Toronto, Canada). Images were obtained using a 30 MHz transducer with a focal depth range of 13 mm. Acquisitions were made in B-mode in the long-axis view as well as in the short view, at the papillary muscle level, at a frame rate of about 90 MHz. Measurements of LV dimensions were obtained by visual determination in three respective cardiac cycles in long-axis mode. Calculations were based on the measurement of left ventricular length and left ventricular surface area during diastole and systole and the EF was calculated as described above.

Tissue preparation

At termination of the experiment, the heart was perfused via the aortic arch (retro-grade),

under lethal sodium pentobarbital anesthesia (18 mg i.p per mouse), with PBS (frozen sections) or PBS followed by 1% paraformaldehyde (paraffin sections). The heart was then quickly excised before freezing on dry ice or immersion in 1% paraformaldehyde.

Histology

Cross-sections were cut at the level of the mid-horizontal plane from fixed paraffin-embedded tissues (3 μ m) or frozen tissues (7 μ m).

Paraffin sections: Transverse sections were stained with hematoxylin and eosin (H&E) to measure the epicardial and myocardial thickness. To determine the extent of inflammation, sections were immuno-labeled with anti-CD45 antibody (1:5000, Becton&Dickinson, Franklin lakes, USA). Perls'-staining was performed to investigate the presence of iron-containing macrophages, indicative of previous hemorrhage. Based on a Sirius red staining, interstitial collagen was determined in the subendocardium and myocardium of the LV. Double staining for laminin (1:600) and collagen IV (1:2000, both kindly provided by Dr. J Cleutjens, Maastricht University, the Netherlands) was used to measure the cross-sectional area of cardiomyocytes. To investigate vascular leakage, paraffin sections were stained for albumin (1:2500, Abcam, Cambridge, USA) and myocardial deposition was determined. A Congo red staining was used to detect amyloid deposits in the myocardium. Within one time group all sections were processed identically, at the same time with precisely the same incubation times for the primary and secondary antibody and diaminobenzidine (DAB) solution (Sigma, Zwijndrecht, the Netherlands). Therefore, all differences between the treatments are ultimately due to DAB identification of the relevant protein.

Photographs of the LV wall (excluding the septum) were taken using a 5x objective (Leica DFC320) and 12 measurements per heart were performed to measure the epicardial and myocardial thickness. The number of CD45-positive cells per section was counted separately in the epicard and myocard to determine the extent of inflammation. Perls' stained sections were examined for evidence of iron-containing macrophages and this was recorded as positive or negative for each section. Interstitial collagen was quantified in five randomly selected areas of the subendocardium and myocardium of the LV (40x objective) and results are expressed as percentage tissue positive for Sirius red relative to myocardial area. Photographs of laminin as percentage tissue positive for Sirius red relative to myocardial area. Photographs of laminin and collagen IV stained sections were taken using a 20x objective and approximately 200 subendocardial myocytes were measured per heart. Cardiac amyloidosis was diagnosed by the apple-green birefringence of extracellular deposited amyloid fibrils, when stained with

Congo red dye and viewed under polarized light. Morphometric parameters were analyzed using a computerized morphometry system (Leica Qwin V3, Leica, Rijswijk, the Netherlands).

Frozen sections: An anti-CD31 antibody (1:50, Becton&Dickinson) was used to visualize cardiac vasculature of the central part of the heart. To quantify the percentage of perfused microvessels, FITC-lectin (Fluorescein labeled Lycopersicon Esculentum (Tomato) Lectin (LEL, TL), Vector, Burlingame, USA) (100 µl) was injected i.v. 5 minutes before a lethal injection of sodium pentobarbital. Frozen sections were then stained for CD31 (1:50, Becton&Dickinson) using a fluorescent secondary antibody labeled with Alexa Fluor 594 (Invitrogen, Breda, the Netherlands). To visualize tissue hypoxia, mice were injected i.v. with 10nM of the hypoxic cell marker and 2-nitroimidazole agent EF5 (a kind gift from Dr. C Koch, Department of Radiation Oncology, University of Pennsylvania, USA) 2 hours prior to humane killing, and hearts were stained according to published protocols (www.hypoxia-imaging.org). To check the immunohistochemical procedure, tumor tissue was included as positive hypoxic control; this showed significant areas of EF5 positivity.

To determine functional changes in the microvasculature a histochemical staining with Naphtol AS-MX / DMF and fast Blue BB salt was performed to detect endothelial cell alkaline phosphatase. Sections were also reacted with antibodies against von Willebrand Factor (vWF) (1:4000, Abcam) or thrombomodulin (TM) (1:200, American Diagnostica, Stamford, USA), as markers of thrombotic changes, and vascular cell adhesion molecule 1 (VCAM-1) (1:200, Becton&Dickinson), as a marker for vascular inflammation. Within one time group all sections were processed identically, at the same time with precisely the same incubation times for the primary and secondary antibody and DAB solution.

For quantification of microvessels, five random fields (40x objective) from transverse sections of the subendocardium were photographed with a CCD 2 - Color Microscope system, including a Zeiss AxioCam color camera (AxioCam HRc, Zeiss, Göttingen, Germany) and a computerized morphometry system (Leica Qwin V3) was used to quantify the microvascular density (MVD). Vessels beneath a size of 1.5 or above 200 µm² were automatically excluded from the measurements. Photographs of CD31/FITC-lectin were taken with a confocal microscope (Leica) and analyzed using Image J computer analysis program, to determine the percentage of microvessels that were perfused. Photographs of whole sections stained for ALP, vWF and TM were taken with an Aperio scanner (Scanscope-XT, Aperio technologies, Vista, USA) using 40x objective. Analyses of the percentage myocardium, excluding endocardium, positive for each marker were done with a computerized morphometry system (Leica Qwin V3). VCAM-1-stained sections were semi-quantitatively analyzed (without knowledge of treatment group)

according to the criteria: no, mild, or strong expression.

Statistics

Data are expressed as mean \pm SEM. Irradiated and control groups were compared using non-parametric Mann-Whitney U-tests or Fisher's exact test (table 2, supplemental table 1 and figure 5). Group differences were considered statistically significant at $p < 0.05$.

Results

Mouse survival and weight

There were very few unscheduled deaths after 2-8 Gy cardiac irradiation, although heart/body weight ratios of irradiated mice were 12-13% lower than in age-matched controls at 40 weeks and body weights were reduced by 6-13% at 60 weeks (Table 1). After 16 Gy, 38% of mice died or had to be humanely killed between 30 and 40 weeks. Because of these unscheduled deaths, all remaining animals in the 16 Gy group were killed at 40 weeks.

TABLE 1 Body and organ weights of mice at sacrifice

| Treatment | Body weight (g) | Heart weight (g) | Lung weight (g) | Heart/body weight (g) |
|-----------------|-----------------|-------------------|-------------------|-----------------------|
| <i>20 weeks</i> | | | | |
| 0 Gy | 30.6 \pm 0.7 | ND | ND | ND |
| 2 Gy | 32.4 \pm 0.4 | 0.21 \pm 0.007 | ND | 6.4 \pm 0.2 |
| 8 Gy | 31.9 \pm 0.7 | 0.19 \pm 0.005 | ND | 5.9 \pm 0.2 |
| 16 Gy | 29.4 \pm 0.6 | ND | ND | ND |
| <i>40 weeks</i> | | | | |
| 0 Gy | 32.8 \pm 0.6 | 0.19 \pm 0.005 | 0.18 \pm 0.003 | 6.0 \pm 0.1 |
| 2 Gy | 35.2* \pm 0.4 | 0.18 \pm 0.005 | 0.17* \pm 0.003 | 5.2* \pm 0.1 |
| 8 Gy | 34.0 \pm 0.5 | 0.18 \pm 0.005 | 0.17* \pm 0.002 | 5.3* \pm 0.1 |
| 16 Gy | 32.7 \pm 0.5 | 0.18* \pm 0.004 | 0.19 \pm 0.005 | 5.4* \pm 0.1 |
| <i>60 weeks</i> | | | | |
| 0 Gy | 38.9 \pm 0.7 | 0.20 \pm 0.007 | 0.18 \pm 0.005 | 5.2 \pm 0.2 |
| 2 Gy | 36.7* \pm 0.8 | 0.21 \pm 0.006 | 0.19 \pm 0.006 | 5.8* \pm 0.2 |
| 8 Gy | 34.0* \pm 0.8 | 0.20 \pm 0.007 | 0.19 \pm 0.007 | 5.9 \pm 0.3 |
| 16 Gy | ND | ND | ND | ND |

* Indicates significant differences between irradiated and age-matched control groups. ($p < 0.05$; Mann-Whitney U-test), ND = not determined.

Non-invasive cardiac imaging

SPECT/CT and ultrasound were used to examine whether irradiation influenced cardiac function; these imaging experiments were performed in separate groups of mice. Static SPECT/CT images ($^{99m}\text{Tc-HSA}$) indicated a significant reduction (18-25%) in total cardiac blood volume at 20 weeks after 2-16 Gy compared to age-matched controls. There was no further reduction in mean cardiac blood volume for remaining mice tested at 40 weeks and no significant differences were observed between irradiated and control groups at this time. By 60 weeks, cardiac blood volumes were again significantly lower after 2-8 Gy than in control animals (21-36%) (Figure 1A).

Gated SPECT/CT images ($^{99m}\text{Tc-Myoview}$) showed radiation-induced decreases in EDV (10-25%) and ESV (16-39%) and increases in EF (6-20%) at 20 weeks after 2-16 Gy (Figure 1 B-D). At 40 weeks, EDV and ESV were still similarly decreased, concomitant with a significant increase in EF (20%) after 8 Gy (Figure 1 B-D).

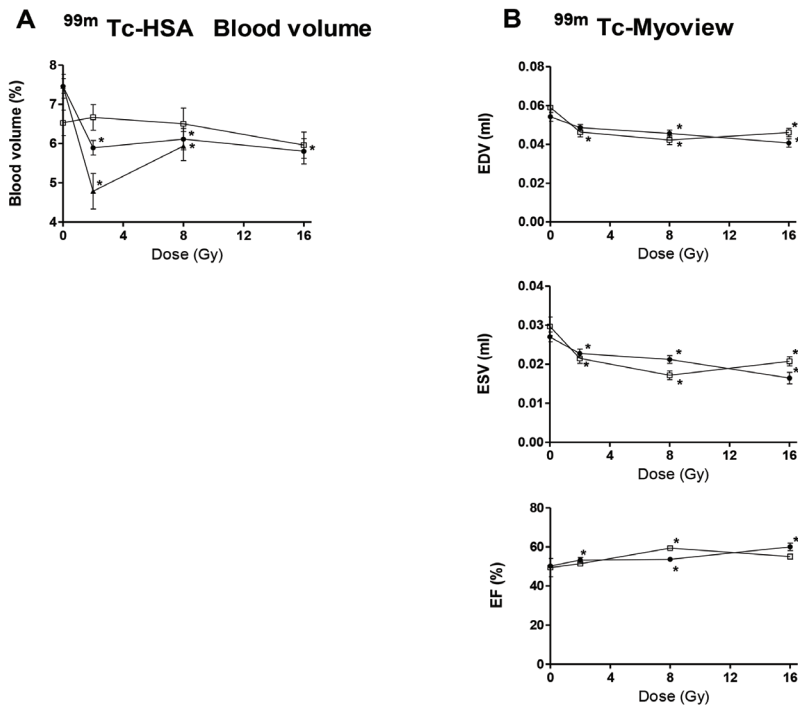


FIGURE 1 Cardiac blood volume (A) or EDV, ESV and EF (B) at 20 weeks (●), 40 weeks (□) or 60 weeks (▲) after irradiation or sham treatment. Values represent mean \pm SEM (9-18 mice in each irradiated group), * $p < 0.05$ compared to age-matched controls.

^{99m}Tc -Myoview gated SPECT/CT scans also showed increases in both anterior and posterior wall thickening (systole versus diastole) at 20 weeks after 16 Gy and in the posterior wall at 40 weeks after 8 Gy (Figure 2).

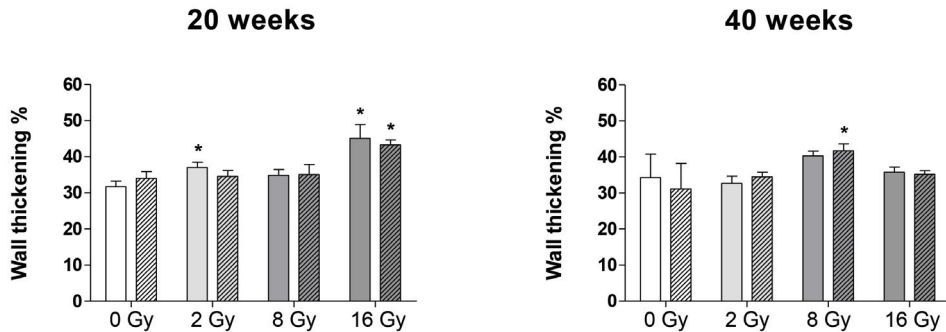


FIGURE 2 Mean LV wall thickening at anterior (solid bars) and posterior (hatched bars) positions 20 and 40 weeks after irradiation (mean \pm SEM). Values represent mean \pm SEM (9-18 mice in each irradiated group), * $p < 0.05$ compared to age-matched controls.

Ultrasound measurements showed similar decreases in EDV (20%) and ESV (33%) to those measured by gated SPECT, and an increase in EF (28%) at 20 weeks after 16 Gy. However, at 40 weeks irradiated and control groups were not significantly different when measured by ultrasound (Supplemental Figure 1).

Inflammatory and fibrotic changes in irradiated hearts

The epicardium and myocardium of irradiated and age-matched control mice were examined for evidence of inflammatory and fibrotic changes. At 20 weeks, high doses (8-16 Gy) resulted in increased epicardial thickness (Figure 3A), associated with the presence of CD45-positive inflammatory cells (Figure 3B) and iron-containing macrophages (Table 2), indicative of previous hemorrhage. At 40 weeks, epicardial thickening was seen after 2-16 Gy, but increased numbers of CD45-positive inflammatory cells (per section) were only found after 16 Gy (Figure 3A, 3B). Iron-containing macrophages were still present in the epicardium of all hearts after 8 to 16 Gy (Table 2). At 60 weeks, there was no evidence of increased epicardial thickening or inflammation after 2 to 8 Gy (Figure 3 A, B) and the incidence of hearts with iron-containing macrophages was reduced compared to 40 weeks.

The number of CD45-positive inflammatory cells (per section) in the myocardium increased

significantly at 40 weeks after 16 Gy, but not at earlier times or lower doses (Figure 3C). Iron-containing macrophages were found in the myocardium of all these hearts, as well as at 20 weeks after 8-16 Gy (Table 2). The amount of interstitial collagen in the LV myocardium was significantly increased at 40 weeks after 8 to 16 Gy and 60 weeks after 2 to 8 Gy, although this was never more than 2-5% of the tissue area (Figure 3D). Analysis of the mean size of individual myocytes showed transient increased size (indicative of swelling) at 20 weeks after 16 Gy, followed by reduced myocyte cell size in irradiated hearts at later times after all doses (Supplemental Figure 2).

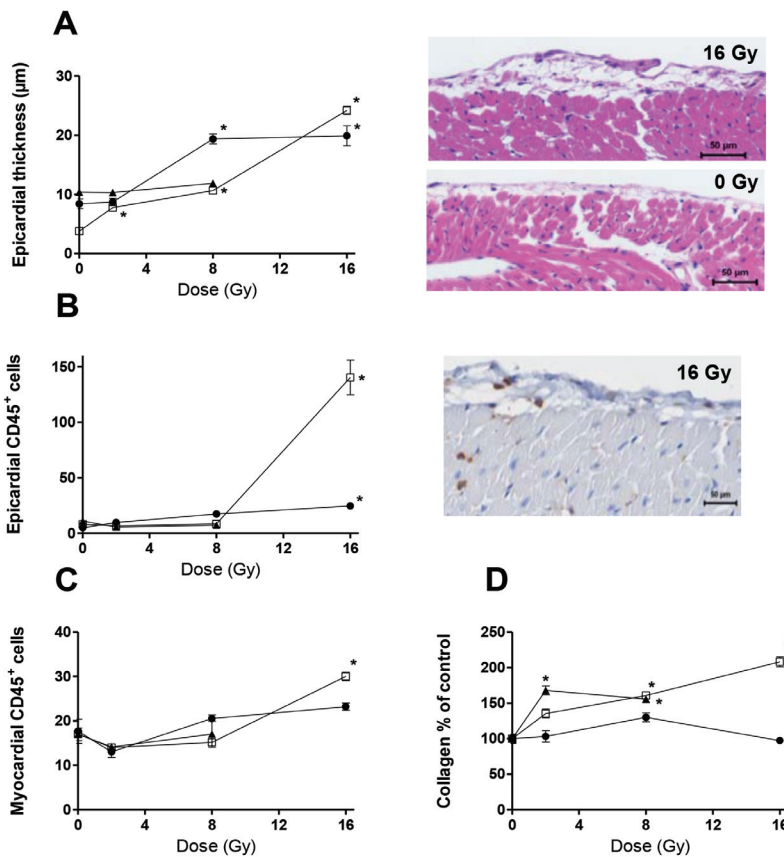


FIGURE 3 Inflammatory and fibrotic changes at 20 weeks (●), 40 weeks (□) or 60 weeks (▲) after irradiation or sham treatment. Values represent mean ± SEM (with at least 4-7 mice in each irradiated group), *p<0.05 compared to age-matched controls. (A) Epicardial thickness and H&E photographs illustrate extensive fibrous thickening (arrow) after irradiation. (B) Quantification and photographs (16 Gy, 20 weeks) of CD45+ cells per section in the epicardium and (C) myocardium. (D) Percentage interstitial collagen content of irradiated heart sections, relative to age-matched controls.

TABLE 2 Perl's staining at 20 - 60 weeks after irradiation demonstrates increased incidence of iron-containing macrophages in the epicardium and myocardium.

| | Epicard | Myocard |
|-----------------|----------------|----------------|
| <i>20 weeks</i> | | |
| 0 Gy | 0/4 | 0/4 |
| 2 Gy | 0/5 | 0/5 |
| 8 Gy | 9/9* | 9/9* |
| 16 Gy | 10/10* | 10/10* |
| <i>40 weeks</i> | | |
| 0 Gy | 0/8 | 4/8 |
| 2 Gy | 2/8 | 7/8 |
| 8 Gy | 8/8* | 7/8 |
| 16 Gy | 14/14* | 14/14* |
| <i>60 weeks</i> | | |
| 0 Gy | 0/5 | 2/5 |
| 2 Gy | 2/7 | 5/7 |
| 8 Gy | 3/5 | 2/5 |
| 16 Gy | ND | ND |

* Indicates significant differences between irradiated and age-matched control groups. (p<0.05; Mann-Whitney U-test), ND = not determined.

Microvascular density (MVD) and vascular function in irradiated hearts

Doses of 2 to 8 Gy led to a transient increase (16-24%) in MVD at 20 weeks after 2-8 Gy, relative to age-matched controls. At 40 weeks MVD was comparable between controls and 2-8 Gy, but there was a significant decrease after 16 Gy (26%). By 60 weeks MVD was significantly decreased after 8 Gy (23%), indicative of progressive loss of microvessels in a dose and time dependent way (Figure 4A). However, the loss of microvascular density did not lead to marked impairment of perfusion or tissue hypoxia. In 40-week age-matched controls, 87% of microvessels were functionally perfused (positive for CD31 and FITC-lectin), compared with 84% at 40 weeks after 16 Gy. There was a total absence of severe hypoxia in both control and irradiated hearts, since all sections were completely negative for EF5 staining, whereas positive control samples of mouse tumor sections (processed together with the heart sections) demonstrated clear areas of EF5 staining.

To further investigate functional changes in the microvasculature, the amount of endothelial cell ALP was quantified (Figure 4B). At 20 weeks after irradiation with 8-16 Gy, there was a significant decrease (30-44%) in percentage tissue stained for ALP, relative to age-matched

controls. By 40 weeks, the 2 Gy dose group also had significantly less ALP expression, indicative of further progression of endothelial damage in small blood vessel. At 60 weeks the ALP expression in irradiated groups (2 and 8 Gy) was 50% of the mean control value, but these differences were borderline significant ($p=0.05$).

Analysis of the pro-thrombotic endothelial marker vWF showed significant increases at 20 weeks after 8-16 Gy and 40 weeks after 16 Gy (Figure 4C). By 60 weeks no differences between groups were observed. Semi-quantitative analysis of VCAM-1 expression in endothelial cells showed significant increases at 20 weeks after 2 and 16 Gy and 40 weeks after 8 Gy (Supplemental data Table 1). There were no significant changes in the amount of thrombomodulin expression at 20 to 60 weeks after irradiation, relative to age-matched controls (data not shown).

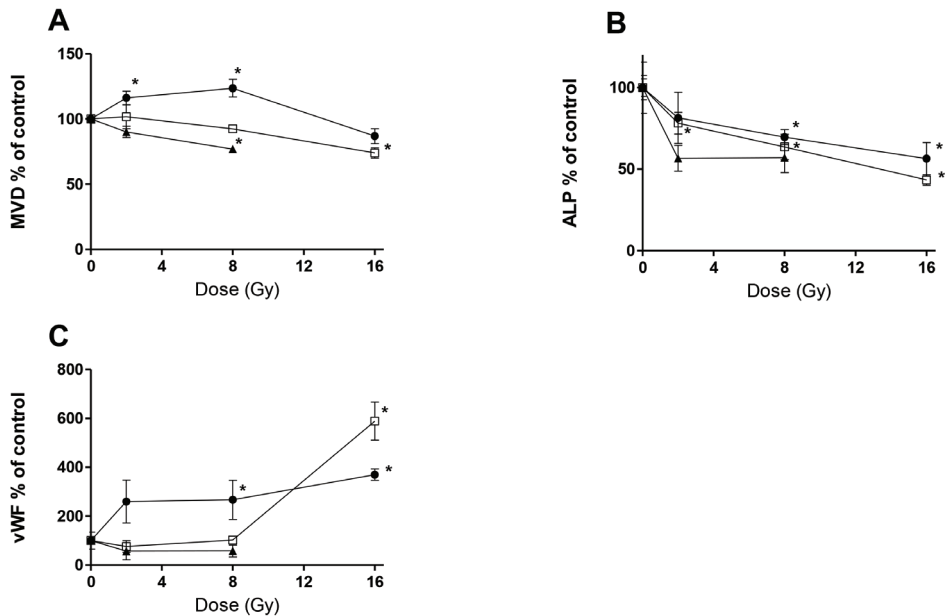


FIGURE 4 Microvascular alterations at 20 weeks (●), 40 weeks (□) or 60 weeks (▲) after irradiation or sham treatment. (Mean \pm SEM with at least 4-7 mice in almost all groups). * $p<0.05$ compared to age-matched controls. (A) MVD per unit area expresses as percentage of age-matched control values. (B) ALP positive tissue areas as % of age-matched unirradiated controls. (C) vWF positive tissue areas as % of age-matched controls.

To investigate whether these structural and functional changes in the microvasculature were associated with vascular leakage, we stained for albumin deposition in the myocardium. At 40 weeks, half of the hearts irradiated with 2 Gy and almost all hearts irradiated with 8-16 Gy

showed albumin in the myocardium (Figure 5). Only one age-matched control heart showed mild albumin deposition in controls. After 16 Gy, myocardial albumin was extensive in 5 of 11 hearts and all these animals also had diffuse amyloidosis, which was confirmed with a Congo red staining (Figure 5B, 5C). Of the remaining 6 animals from this group, 5 animals showed mild albumin deposition and all these animals also had focal amyloidosis (Figure 5A).

Incidence of hearts with albumin protein deposition in the myocardium

| | mild deposition | strong deposition | any deposition |
|-----------------|-----------------|-------------------|----------------|
| <i>20 weeks</i> | ND | ND | ND |
| <i>40 weeks</i> | | | |
| 0 Gy | 1/5 | 0/5 | 1/5 |
| 2 Gy | 4/8 | 0/8 | 4/8 |
| 8 Gy | 8/8 * | 0/8 | 8/8 * |
| 16 Gy | 5/11 | 5/11 | 10/11 * # |
| <i>60 weeks</i> | | | |
| 0 Gy | 1/5 | 2/5 | 3/5 |
| 2 Gy | 3/7 | 1/7 | 4/7 |
| 8 Gy | 2/4 | 2/4 | 4/4 |
| 16 Gy | ND | ND | ND |

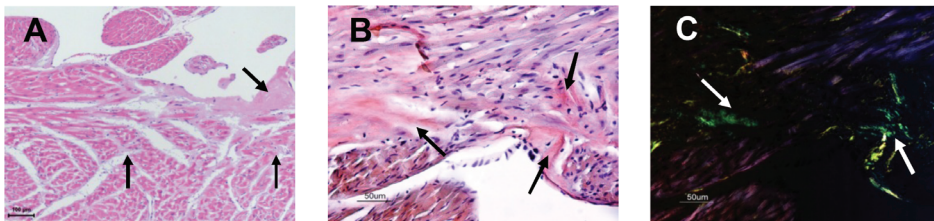


FIGURE 5 Evidence for blood vessel leakage after irradiation. (A) H&E staining showing amyloid deposition (arrows). (B) Amyloidosis was confirmed by Congo-Red staining and (C) yellow-green birefringence by polarizing microscopy at 40 weeks after 16 Gy. Incidence of hearts showing increased expression of plasma protein albumin outside blood vessels. * $p < 0.05$ compared to age-matched controls. # Hearts showing strong albumin protein deposition also had diffuse amyloidosis. ND = not determined

Discussion

This study demonstrated that irradiation affects cardiac structure and microvascular function in a dose and time-dependent manner, with substantial damage after intermediate and high dose irradiation (8-16 Gy) and minor alterations after lower doses (2 Gy). Moreover, high doses induced changes at earlier time points and these effects progressed in time.

The transient increase in MVD at 20 weeks after 2 and 8 Gy was presumably due to stimulated

proliferation in response to damage, whereas proliferation after 16 Gy was counterbalanced by endothelial cell loss. The decreased MVD at 40-60 weeks after high doses confirms earlier studies in irradiated rat hearts (16). However, this did not lead to a marked loss of vascular perfusion and no severe hypoxia was detected.

Despite the lack of hypoxia, progressive microvasculature damage was indicated by the vascular leakage, decreased amount of endothelial cell ALP and increased vWF in irradiated hearts. ALP is abundantly present in healthy cardiac microvasculature whereas loss of ALP is indicative of endothelial cell damage (16). In our studies, ALP expression was significantly reduced at 20 weeks after high doses (8-16 Gy) and after 2-16 Gy at later times. Increased deposition of vWF in irradiated rat hearts has been previously described as an indicator of thrombotic endothelial cell damage (17). In our studies, increases in vWF deposition were limited to hearts that received high doses irradiation (8-16 Gy), with the largest increase at later times after the highest dose. Myocardial deposition of albumin (indicative of vascular leakage) was seen in almost all hearts examined at 40 weeks after 8-16 Gy, and this was strongly correlated with amyloidosis. All of the hearts exhibiting strong extracellular albumin deposition at 40 weeks after 16 Gy also had diffuse amyloidosis and those with mild albumin deposition had focal amyloidosis. Amyloidosis is caused by extracellular deposition of insoluble, abnormal fibrils, derived from aggregation of misfolded proteins. A prominent clinical feature of cardiac amyloidosis is heart failure (18). The presence of amyloidosis may therefore have contributed to the sudden death seen in 38% of mice between 30 and 40 weeks after 16 Gy.

Changes in cardiac function after irradiation were modest and non-progressive, despite the progressive deterioration of microvascular structure and function. This suggests that in mice the myocardium can compensate for structural degeneration to some extent. However, 16 Gy lead to sudden death at 30-40 weeks in a significant proportion of mice. It was only possible to autopsy a few of these mice so the exact cause of death remained unclear. The cardiac function at 20 weeks, for those mice that subsequently died, was comparable to mice which completed 40 weeks follow up after 16 Gy (Supplemental Figure 3). There was also no indication of arrhythmia at 20 weeks in these mice. However, neither cardiac function nor histological analyses were done between 20 weeks and sudden death of these mice, therefore it remains possible that they subsequently developed conduction defects leading to arrhythmia and sudden cardiac death (19). We suspect that amyloidosis may be involved in the sudden deaths seen after 16 Gy, since 4 of 7 mice that died immediately after their 40 week imaging procedure did have diffuse amyloidosis. These sudden deaths imply that compensatory mechanisms seen after low to intermediate doses (2-8 Gy), especially at earlier

times, can not maintain cardiac function after high dose irradiation.

There is some evidence from *in vitro* studies that cardiomyocytes can react to stress signals directly by initiating an inflammatory response (20). This response leads to the presence of macrophages, which can interact with cardiac myocytes and lead to decreased myocyte contractility, both *in vitro* and *in vivo*, resulting in a decrease in systolic and diastolic filling (21). We also observed this effect in our mouse model after irradiation. Decreased myocyte cell area and increased collagen deposition after irradiation may also have contributed to impaired myocardial contractility (22). Sarcoplasmic reticulum Ca^{2+} ATPase (SERCA) has been described as a compensatory mechanism in failing human myocardium, by maintaining relaxation and contraction of cardiomyocytes. However, this remains speculative and further investigations are necessary to understand compensatory mechanisms in the damaged heart (20).

In conclusion, these studies demonstrated decreases in both systolic and diastolic volumes and increased ejection fractions at 20-40 weeks after irradiation. The presence of inflammatory cells and iron-containing macrophages within the thickened epicardium suggests this could be due to constrictive pericarditis. This constrictive remodeling of the heart could also lead to loss of normal blood filling and emptying during diastole and systole. However, the overall cardiac function remained within normal physiological limits, which suggests that compensatory mechanisms can initially maintain cardiac function after irradiation, despite deteriorating underlying morphology and vascular function. Ultimately, however, this compensatory mechanism fails, leading to sudden death.

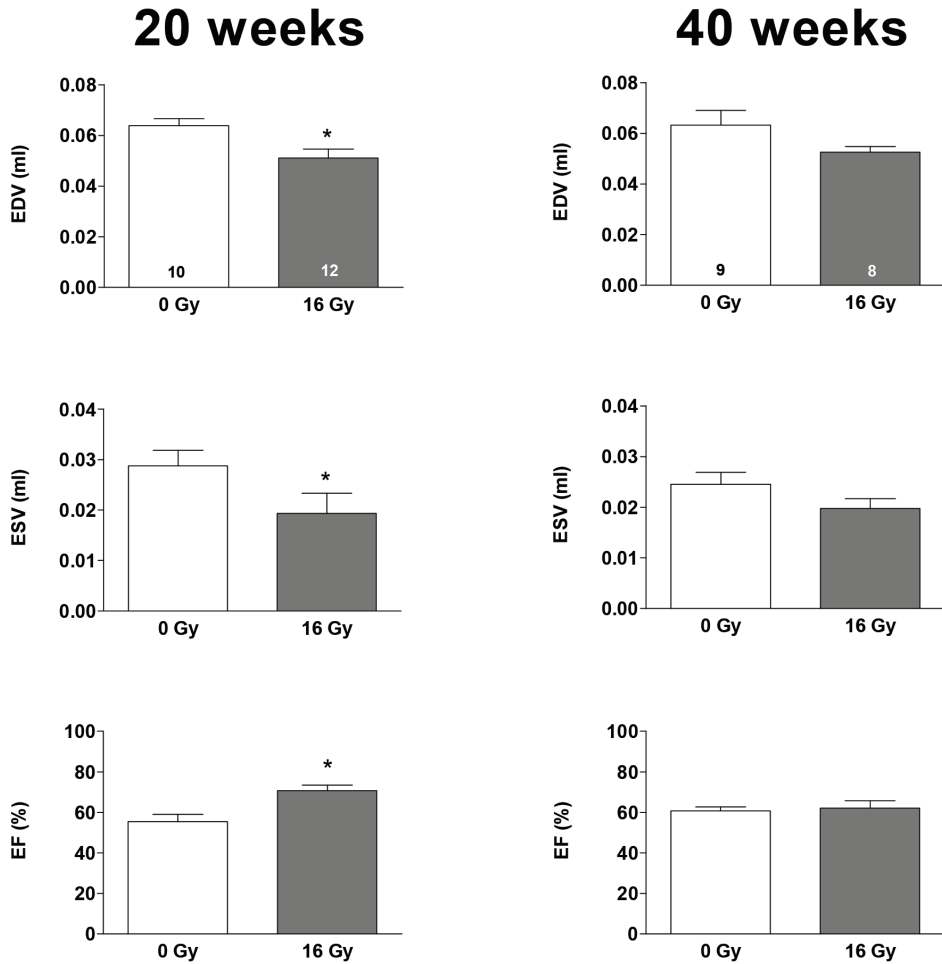
Acknowledgments

The authors thank Bert Pool, Department of Nuclear Medicine, The Netherlands Cancer Institute, for help with the NanoSPECT/CT and Dr. Jack Cleutjens, Department of Pathology, University of Maastricht, for help with the Leica Qwin morphometry system.

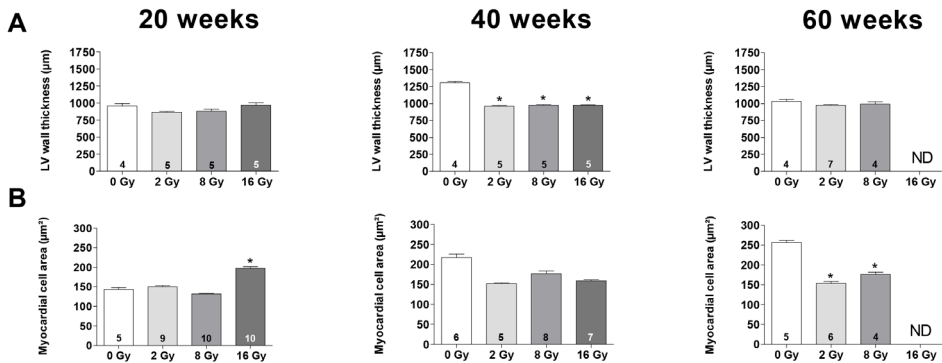
This research was funded by the European Atomic Energy Community's Seventh Framework Program, grant 211403 (Cardiorisk), and the Dutch Cancer Foundation, grant NKI 2008-3993.

There were no conflicts of interest.

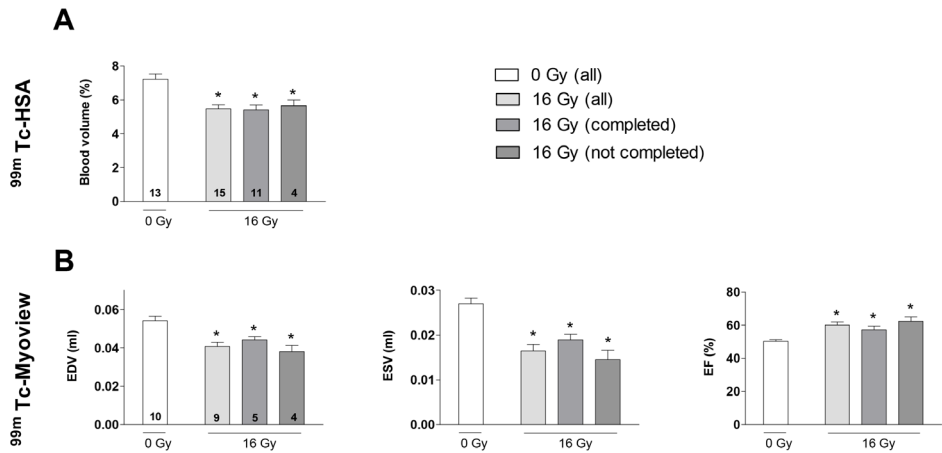
Supplemental data



SUPPLEMENTAL FIGURE 1 Ultrasound measurements (mean \pm SEM) of EDV, ESV and EF for control and 16 Gy mice at 20 and 40 weeks. Numbers of mice indicated in the bars. * $p < 0.05$ compared to age-matched controls.



SUPPLEMENTAL FIGURE 2 Myocardial alterations 20-60 weeks after irradiation (mean \pm SEM with numbers of mice per group indicated). * $p < 0.05$ compared to age-matched controls. (A) LV wall thickness. (B) Mean myocardial cell area.



SUPPLEMENTAL FIGURE 3 Non-invasive imaging for measurement of cardiac function in unirradiated and age-matched irradiated groups at 20 weeks after treatment, including 16 Gy treated mice that suddenly died between 30-40 weeks. (A) SPECT/CT, using ^{99m}Tc -HSA measurements of mean cardiac blood volume (% total) \pm SEM. (B) Gated SPECT/CT measurements with ^{99m}Tc -Myoview. Values represent mean \pm SEM, numbers of mice indicated in the bars. * $p < 0.05$ compared to age-matched controls. (all) representing total amount mice of group 0 Gy and 16 Gy. (completed) representing amount of mice that completed 40 weeks follow up (not completed) representing amount of mice that died before 40 weeks.

SUPPLEMENTAL TABLE 1 Incidence of hearts with VCAM-1 expression in the myocardium

| | mild expression | strong expression | any expression |
|-----------------|------------------------|--------------------------|-----------------------|
| <i>20 weeks</i> | | | |
| 0 Gy | 0/4 | 0/4 | 0/4 |
| 2 Gy | 3/4 | 1/4 | 4/4* |
| 8 Gy | 2/4 | 0/4 | 2/4 |
| 16 Gy | 1/4 | 3/4 | 4/4* |
| <i>40 weeks</i> | | | |
| 0 Gy | 2/10 | 0/10 | 2/10 |
| 2 Gy | 3/7 | 0/7 | 3/7 |
| 8 Gy | 5/10 | 4/10 | 9/10* |
| 16 Gy | 7/14 | 1/14 | 8/14 |
| <i>60 weeks</i> | | | |
| 0 Gy | 7/7 | 0/7 | 7/7 |
| 2 Gy | 2/5 | 3/5 | 5/5 |
| 8 Gy | 2/4 | 2/4 | 4/4 |
| 16 Gy | ND | ND | ND |

* p<0.05 compared to age-matched controls

Reference List

1. McGale P, Darby SC, Hall P et al. Incidence of heart disease in 35,000 women treated with radiotherapy for breast cancer in Denmark and Sweden. *Radiother Oncol.* 2011;100:167-175.
2. Gyenes G, Rutqvist LE, Liedberg A and Fornander T. Long-term cardiac morbidity and mortality in a randomized trial of pre- and postoperative radiation therapy versus surgery alone in primary breast cancer. *Radiother Oncol.* 1998;48:185-190.
3. Cohn KE, Stewart JR, Fajardo LF and Hancock EW. Heart disease following radiation. *Medicine (Baltimore).* 1967;46:281-298.
4. Armstrong GT, Stovall M and Robison LL. Long-term effects of radiation exposure among adult survivors of childhood cancer: results from the childhood cancer survivor study. *Radiat Res.* 2010;174:840-850.
5. Galper SL, Yu JB, Mauch PM et al. Clinically significant cardiac disease in patients with Hodgkin lymphoma treated with mediastinal irradiation. *Blood.* 2011;117:412-418.
6. Darby SC, Cutter DJ, Boerma M et al. Radiation-related heart disease: current knowledge and future prospects. *Int J Radiat Oncol Biol Phys.* 2010;76:656-665.
7. Aleman BM, van den Belt-Dusebout AW, Klokman WJ, Van't Veer MB, Bartelink H and van Leeuwen FE. Long-term cause-specific mortality of patients treated for Hodgkin disease. *J Clin Oncol.* 2003;21:3431-3439.
8. Adams MJ, Hardenbergh PH, Constine LS and Lipshultz SE. Radiation-associated cardiovascular disease. *Crit Rev Oncol Hematol.* 2003;45:55-75.
9. Yusuf SW, Sami S and Daher IN. Radiation-induced heart disease: a clinical update. *Cardiol Res Pract.* 2011;2011:317659.
10. Andratschke N, Maurer J, Molls M, Trott KR. Late radiation-induced heart disease after radiotherapy. Clinical importance, radiobiological mechanisms and strategies of prevention. *Radiother Oncol.* 2011;100:160-166.
11. Fajardo LF, Stewart JR. Capillary injury preceding radiation-induced myocardial fibrosis. *Radiology.* 1971;101:429-433.
12. Lauk S, Kizel Z, Buschmann J and Trott KR. Radiation-induced heart disease in rats. *Int J Radiat Oncol Biol Phys.* 1985;11:801-808.
13. Schultz-Hector S, Trott KR. Radiation-induced cardiovascular diseases: is the epidemiologic evidence compatible with the radiobiologic data? *Int J Radiat Oncol Biol Phys.* 2007;67:10-18.
14. Marks LB, Yu X, Prosnitz RG et al. The incidence and functional consequences of RT-associated cardiac perfusion defects. *Int J Radiat Oncol Biol Phys.* 2005;63:214-223.

15. Seddon B, Cook A, Gothard L et al. Detection of defects in myocardial perfusion imaging in patients with early breast cancer treated with radiotherapy. *Radiother Oncol.* 2002;64:53-63.
16. Schultz-Hector S, Balz K. Radiation-induced loss of endothelial alkaline phosphatase activity and development of myocardial degeneration. An ultrastructural study. *Lab Invest.* 1994;71:252-260.
17. Boerma M, Kruse JJ, van Loenen M et al. Increased deposition of von Willebrand factor in the rat heart after local ionizing irradiation. *Strahlenther Onkol.* 2004;180:109-116.
18. McCarthy RE, III, Kasper EK. A review of the amyloidoses that infiltrate the heart. *Clin Cardiol.* 1998;21:547-552.
19. Heidenreich PA, Kapoor JR. Radiation induced heart disease: systemic disorders in heart disease. *Heart.* 2009;95:252-258.
20. Boyd JH, Kan B, Roberts H, Wang Y and Walley KR. S100A8 and S100A9 mediate endotoxin-induced cardiomyocyte dysfunction via the receptor for advanced glycation end products. *Circ Res.* 2008;102:1239-1246.
21. Simms MG, Walley KR. Activated macrophages decrease rat cardiac myocyte contractility: importance of ICAM-1-dependent adhesion. *Am J Physiol.* 1999;277:H253-H260.
22. Kruse JJ, Zurcher C, Strootman EG et al. Structural changes in the auricles of the rat heart after local ionizing irradiation. *Radiother Oncol.* 2001;58:303-311.



Chapter 3

Local heart irradiation of ApoE^{-/-} mice induces microvascular and endocardial damage and accelerates coronary atherosclerosis

.....
K.Gabriels¹, S.Hoving¹, I.Seemann, N. L. Visser, M. J. Gijbels, J.F. Pol, M.J. Daemen, F. A. Stewart², S. Heeneman²

¹Authors contributed equally (performing experiments and analyses)

²Authors contributed equally (designing and supervision of the study)

Radiotherapy and Oncology december 2012

Abstract

Background: Radiotherapy of thoracic and chest-wall tumors increases the long-term risk of radiation-induced heart disease, such as a myocardial infarction. Cancer patients commonly have additional risk factors for cardiovascular disease, such as hypercholesterolemia. The goal of this study is to define the interaction of irradiation with such cardiovascular risk factors in radiation-induced damage to the heart and coronary arteries.

Materials and Methods: Hypercholesterolemic and atherosclerosis-prone *ApoE^{-/-}* mice received local heart irradiation with a single dose of 0, 2, 8 or 16 Gy. Histopathological changes, microvascular damage and functional alterations were assessed after 20 and 40 weeks.

Results: Inflammatory cells were significantly increased in the left ventricular myocardium at 20 and 40 weeks after 8 and 16 Gy. Microvascular density decreased at both follow-up time-points after 8 and 16 Gy. Remaining vessels had decreased alkaline phosphatase activity (2-16 Gy) and increased von Willebrand Factor expression (16 Gy), indicative of endothelial cell damage. The endocardium was extensively damaged after 16 Gy, with foam cell accumulations at 20 weeks, and fibrosis and protein leakage at 40 weeks.

Despite an accelerated coronary atherosclerotic lesion development at 20 weeks after 16 Gy, gated SPECT and ultrasound measurements showed only minor changes in functional cardiac parameters at 20 weeks.

Conclusions: The combination of hypercholesterolemia and local cardiac irradiation induced an inflammatory response, microvascular and endocardial damage, and accelerated the development of coronary atherosclerosis. Despite these pronounced effects, cardiac function of *ApoE^{-/-}* mice was maintained.

Introduction

Improvements in cancer therapy and earlier detection and diagnosis have lead to increasing numbers of cancer survivors. Unfortunately, this also means that more patients are at risk of developing treatment-related late tissue damage and mortality. Thoracic radiotherapy, given to Hodgkin lymphoma and breast cancer patients, is widely recognized as an independent long-term risk factor for developing heart diseases.(1-4) The pathological consequences of radiation-induced heart disease following therapeutic irradiation are pericarditis, myocardial fibrosis, coronary artery disease, valvular disorders and conduction abnormalities.(5-7)

In a previous study (8), the dose and time dependence of structural and functional cardiovascular damage after thoracic irradiation were investigated in C57BL/6J mice. Inflammation, especially in the epicardium, and micro-vascular endothelial damage leading to vascular leakage progressed with dose (2-16 Gy) and time (20-60 weeks follow-up). However, only modest and non-progressive changes in cardiac function, detected by gated SPECT, were observed in mice surviving cardiac irradiation of 2 and 8 Gy. These data indicated that the heart was able to compensate for the structural damage. Nevertheless, 16 Gy irradiation led to excessive protein leakage in the myocardium and 38% of mice failed to maintain cardiac function at 40 weeks follow-up.

C57BL/6J mice have extremely low plasma levels of cholesterol, especially low-density lipoproteins, and they are resistant to the development of atherosclerosis.(9) Cardiac damage identified after irradiation in such models therefore does not include any component of macrovascular damage as a result of accelerated atherosclerosis.

The effect of irradiation on the development of atherosclerosis has been studied in apolipoproteinE^{-/-} (ApoE^{-/-}) mice, which have elevated cholesterol levels and do develop age-related atherosclerosis. After local carotid artery irradiation with a single dose of 14 Gy or fractionated doses (20 x 2 Gy), an accelerated development of inflammatory atherosclerotic plaques was observed.(9, 10) Hu et al.(11) described the distribution of atherosclerotic lesions in the coronary arteries of 60 week old ApoE^{-/-} mice and found relatively few lesions (approximately 4 lesions per heart) after the second level of branching of the coronary arteries, that developed independently from valvular lesions. However, the effect of irradiation on this coronary lesion development is not known.

The aim of this study is to investigate the effect of local thoracic irradiation of hypercholesterolemic ApoE^{-/-} mice on cardiac structure and function, and to compare this with previous results of irradiated wild-type C57BL/6J mice in the absence of atherosclerosis (8). This should allow us to evaluate the contribution of macrovascular (atherosclerosis) and microvascular changes in the pathology of radiation-induced cardiac damage.

Materials and methods

Mice and irradiation procedure

Male *ApoE^{-/-}* mice (C57BL/6J background), aged 10-12 weeks (bred at The Netherlands Cancer Institute), were housed in a temperature-controlled room with 12 h light-dark cycle and received standardized mouse chow (3.7% fat, RMI (E) SQC, SDS, London, UK) and water ad libitum.

Irradiation procedure was performed as described previously (8). Mice were randomly allocated to receive single doses of 2, 8 or 16 Gy locally to the heart (irradiation field of 10.6 x 15.0 mm, including 30% lung volume) at a dose rate of 0.94 Gy/min using 250 kV X-rays, operating at 12 mA and filtered with 0.6 mm of copper, or sham-treatment (0 Gy) as a control. Mice were sacrificed 20 or 40 weeks after irradiation, and hearts and lungs were collected.

Experiments were in agreement with the Dutch law on animal experiments and welfare, and in line with the international Guide for the Care and Use of Laboratory Animals (eighth edition).

Tissue preparation and histology

The heart was perfused via the aortic arch (retro-grade) with phosphate-buffered saline (PBS) (frozen sections) or PBS followed by 1% paraformaldehyde (paraffin sections), under lethal sodium pentobarbital anesthesia (18 mg i.p. per mouse). Immediately after perfusion, the heart was excised, divided into three parts (base, mid and apex) and frozen on dry ice or immersed in 1% paraformaldehyde. Cross-sections were cut at the level of the mid-horizontal plane of the heart from fixed paraffin-embedded tissues (3 µm) or frozen tissues (7 µm).

Paraffin sections

Sections were immuno-labeled with anti-CD45 antibody (1:5000, Becton&Dickinson, Franklin lakes, USA) or anti-CD3 antibody (1:200, Dako, Carpinteria, USA) to determine the extent of leukocyte and T-cell infiltration, respectively. The absolute number of CD45-positive leukocytes per section was counted in the left ventricular (LV) myocardium. The number of CD3-positive T cells was counted per LV myocardial area (8 random 40x photographs). Interstitial collagen was quantified in 5 randomly selected areas of the LV myocardium based on a Sirius Red staining and results were expressed as percentage tissue positive for Sirius Red, excluding perivascular collagen, relative to myocardial area. To determine if there was a pre-mortem bleeding, a Perls' staining was performed to detect iron. Macrophages store iron

by metabolizing hemoglobin from engulfed red blood cells. An albumin staining (1:2500, Abcam, Cambridge, USA) was performed to determine myocardial deposition as a measure of vascular leakage and a Congo Red staining was used as previously described⁸ to detect amyloid deposits in the myocardium.

To investigate coronary atherosclerotic plaque development, transverse sections of the complete mid-part of the heart were cut, stained every 57 μm with hematoxylin and eosin (H&E) and analyzed for the presence and number of coronary lesions. An average of 20 slides per heart was analyzed. Results are expressed as number of coronary lesions per mouse and mean values per group are shown. Percentage necrotic core of the coronary lesions was determined by dividing the necrotic core area by total plaque area.

Frozen sections

Sections were stained with H&E to measure the myocardial thickness. Photographs of the LV wall were taken using a 5x objective and 12 measurements per heart were performed. To detect alterations in the number of macrophages after irradiation, frozen sections were stained with anti-F4/80 antibody (1:300, AbD Serotec, Dusseldorf, Germany) and counted per LV myocardial area (8 random 40x photographs).

An anti-CD31 antibody (1:50, Becton&Dickinson, Franklin lakes, USA) was used to visualize cardiac vasculature of the mid part of the heart and to quantify microvascular density (MVD). Five random areas (40x photographs) from transverse sections of the subendocardium were photographed with a CCD 2 - Color Microscope system, including a Zeiss AxioCam color camera (AxioCam HRc, Zeiss, Göttingen, Germany). Vessels beneath a size of 1.5 or above 200 μm^2 were automatically excluded from the measurements, to ensure that only microvasculature was counted. To determine functional changes in the microvasculature, a histochemical staining with Naphtol AS MX/DMF and fast Blue BB salt was performed to detect endothelial cell alkaline phosphatase (ALP) activity. Sections were also stained with an antibody against von Willebrand Factor (vWF) (1:4000, Abcam, Cambridge, USA) as a thrombotic marker. Photographs of whole sections stained for ALP and vWF were taken with an Aperio scanner (Scanscope-XT, Aperio technologies, Vista, USA) using a 40x objective. Analyses of the percentage myocardium positive for each marker were performed in 23 and 30 mice at 20 and 40 weeks FU respectively.

Morphometric parameters were analyzed using a computerized morphometry system (Leica Qwin V3, Leica, Rijswijk, The Netherlands).

Gene expression profiling and pathway analysis

Total RNA was isolated from frozen sections (30 slides of 30 μm) of the mid part of the heart of 17 mice at 20 weeks FU (5, 4 and 8 for respectively 0, 2 and 16 Gy) and 21 mice at 40 weeks FU (6, 7 and 8 for respectively 0, 2 and 16 Gy) using Trizol® Reagent (Invitrogen Corporation, Carlsbad, USA) according to the manufacturer's protocol. The quantity of total RNA was measured using a spectrophotometer (NanoDrop, Thermo scientific, Wilmington, USA) followed by a quality check measured by Agilent 2100 Bioanalyzer with the RNA Integrity Number (RIN) (Agilent technologies, Santa Clara, USA). Samples with a RIN above 7 were used for DNase treatment and amplified (350 ng per sample) using Illumina Totalprep RNA Amplification kit (Ambion, Grand Island, USA). Hybridization of aRNA to Illumina Expression Bead Chips Mouse Whole Genome (WG-6 vs. 2.0) and subsequent washing, blocking and detecting were performed according to the manufacturer's protocol (Illumina, San Diego, USA). Samples were scanned on the IlluminaR BeadArray™ 500GX Reader using IlluminaR Bead-Scan image data acquisition software (version 2.3.0.13). MouseWG-6 vs. 2.0 BeadChip contains the full set of MouseRef-8 BeadChip probes with additional 11.603 probes from RIKEN FANTOM2, NCBI RefSeq as well from the MEEBO database.

Before analyzing, the database was normalized using the robust spline normalization method within the microarray facility of The Netherlands Cancer Institute.(12) Log^2 ratio between expression of genes from control mice and expression of genes from irradiated mice was calculated using Excel version 2003, as well as the sum of the expression of genes from both, control and irradiated mice. According to the sum of both expressions, genes with sums below 6 were discarded. The threshold for standard deviation (SD) was set to 3 and mean \pm nSD was calculated to identify genes that are above expression 6 and above threshold 3 of SD. These gene numbers were further analyzed in Ingenuity Pathway Analysis (IPA) version September 2011 core analysis. IPA calculates a significant score for each associated network. This score indicates the likelihood that the assembly of a set of focus genes in a network could be explained by random chance alone. A score of 2 indicates a 1 in 100 chance that the focus genes are together in a network due to random chance. Therefore, networks with scores of 2 or higher have at least a 99% confidence of not being generated by random chance alone.

Gated single photon emission computed tomography (gSPECT)

The tracer tetrofosmin (Myoview, GE-healthcare, Hoevelaken, The Netherlands) was labeled with $^{99\text{m}}\text{Tc}$ -pertechnetate according to the manufacturer's protocol and injected i.v. (150 μl) with a total activity of 70 MBq per mouse. Three lead electrodes (3M red Dot 2282E,

3M, St. Paul, USA) were attached to both hind paws and right front paw of the mouse and connected to the integrated electrocardiography (ECG) monitor to measure heart rate (HR). Acquisitions were started 1 h after injection of the tracer as described previously (8). HiSPECT NG software (InVivoScope, Bioscan) was used to perform iterative reconstruction into 3D datasets. Quantitative analysis of the reconstructed datasets was performed on a clinical e.soft (syngo-based) workstation (Siemens Medical Solutions, Siemens AG, Erlangen, Germany), using algorithms to automatically reconstruct a count based 3D model of the dimensions of the LV end diastolic and systolic volumes (EDV, ESV). The ejection fraction (EF) was calculated based on the difference between EDV and ESV divided by EDV.

2D-Ultrasound

Mice were sedated with 2% isoflurane (Forane, Abbott, Hoofddorp, The Netherlands). Echocardiography images were acquired using a Vevo 770 system (VisualSonics, Toronto, USA) using a 30 MHz transducer with a focal depth range of 13 mm. Acquisitions were made in B-mode long-axis, as well as short-axis view, at the papillary muscle level as described previously⁸. Calculations were based on the measurement of LV length and surface area during diastole and systole and the EF was calculated as described above.

Statistics

Except where otherwise stated, data are expressed as mean \pm SEM. Irradiated and control groups were compared using nonparametric Mann-Whitney U-test. Statistical analysis on data presented in tables was performed using Fisher's exact test. Group differences were considered statistically significant at $P < 0.05$.

Results

Mouse weight

Local heart irradiation with 16 Gy induced a significant increase in heart, lung and heart/body weight at 40 weeks follow-up (FU), compared to age-matched controls (Supplemental Table I). No significant differences were observed after lower doses or at 20 weeks after 16 Gy. Histological examination of lung tissue did not reveal any abnormalities after irradiation. Premature deaths were 7% and 20% of total mice (killed before the planned 20 and 40 weeks sacrifice time respectively). This was due to non-radiation induced causes such as elephant teeth, fighting or a tumor that developed spontaneously outside the irradiation field.

Increased inflammation after 8 and 16 Gy irradiation

There were no significant differences in LV wall thickness, as measured from histological sections, at 20 or 40 weeks after irradiation (data not shown). The number of CD45-positive leukocytes was not increased at 20 weeks after irradiation, but at 40 weeks after 8 and 16 Gy there was a significant increased influx of leukocytes in the myocardium (Figure 1A). The number of CD3-positive T cells in the myocardium of *ApoE*^{-/-} mice was significantly increased at both 20 and 40 weeks after 8 and 16 Gy, compared to unirradiated mice (Figure 1B), while F4/80-positive macrophages showed no differences between irradiated hearts and controls (data not shown). The amount of interstitial collagen increased significantly at 20 and 40 weeks after 8 and 16 Gy, although not more than 2% of tissue area was affected (Figure 2).

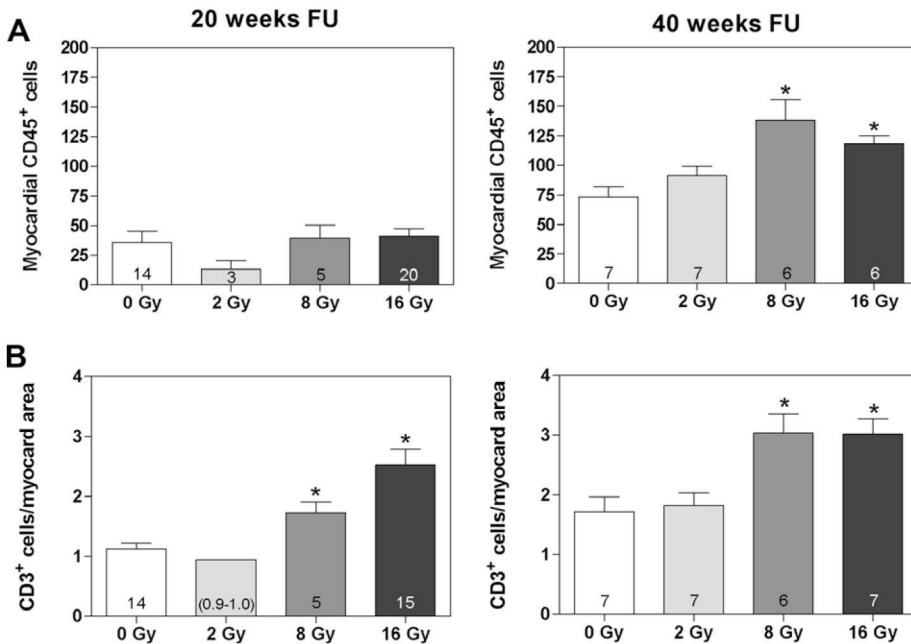


FIGURE 1 Inflammatory changes in the LV myocardium at 20 and 40 weeks after irradiation. (A) Number of CD45-positive leukocytes in the myocardium per section. (B) Quantification of CD3-positive T cells per myocardial area (40x objective). Bars represent mean \pm SEM with numbers of mice indicated per group (the total number of mice analyzed per irradiation and FU group can differ between different stainings due to bad quality of the tissue during staining procedure). Analysis of CD3-positive T cells at 20 weeks after 2 Gy was only possible on 2 mice, therefore values are presented in the bar. * $p < 0.05$ compared to age-matched controls.

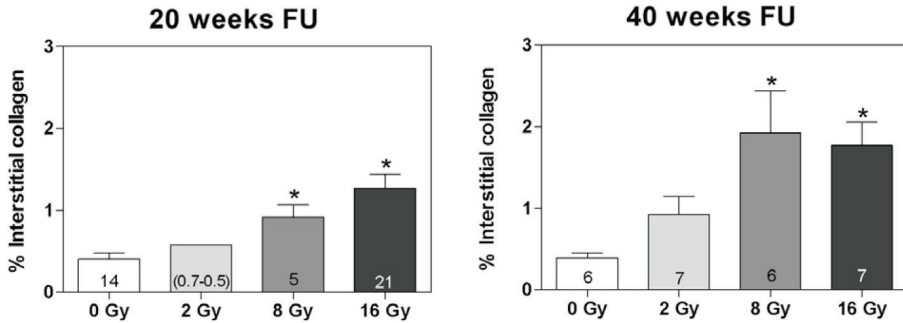


FIGURE 2 Fibrotic changes in the LV myocardium at 20 and 40 weeks after irradiation. Percentage interstitial collagen per tissue area. Bars represent mean \pm SEM with numbers of mice indicated per group. Collagen measurements at 20 weeks after 2 Gy were only possible on 2 mice, therefore values are presented in the bars. * $p < 0.05$ compared to age-matched controls.

Endothelial damage of microvasculature after irradiation

At 20 and 40 weeks after 8 and 16 Gy, there was a significant decrease in MVD compared to control mice (Figure 3A). In addition to the loss of capillaries, the remaining vessels had signs of endothelial damage, as indicated by a significant decrease in ALP activity at 20 and 40 weeks (2-16 Gy) (Figure 3B) and increased expression of the thrombotic marker vWF after 16 Gy (Figure 3C).

Perls' staining was performed to analyze the presence of iron in the myocardium, which is an indication of a previous hemorrhage. Iron-containing macrophages were observed in the myocardium of almost all 8 and 16 Gy irradiated hearts at 20 and 40 weeks (Table 1).

Analysis of myocardial albumin deposition, as an indication of vascular leakage, showed the presence of albumin in almost all hearts irradiated with 8 or 16 Gy at 40 weeks FU, but not at 20 weeks (Table 1), while amyloid deposits were not detected.

Irradiation increased the number of coronary lesions and caused endocardial damage

Irradiation with 16 Gy significantly increased the number of coronary atherosclerotic lesions in the mid part of the heart at 20 weeks FU (Figure 4A and B). There was also a trend for increased numbers of lesions at 40 weeks after 8 or 16 Gy, but this difference was no longer significant due to an increased number of age-related coronary lesions in unirradiated mice. Analysis of the necrotic core of the coronary plaques at 20 and 40 weeks FU revealed an increased level of necrosis after irradiation (an average of 33.7% and 39.7% of plaque area was necrotic at respectively 20 and 40 weeks after 16 Gy, compared to 0% and 1.8% after 0 Gy).



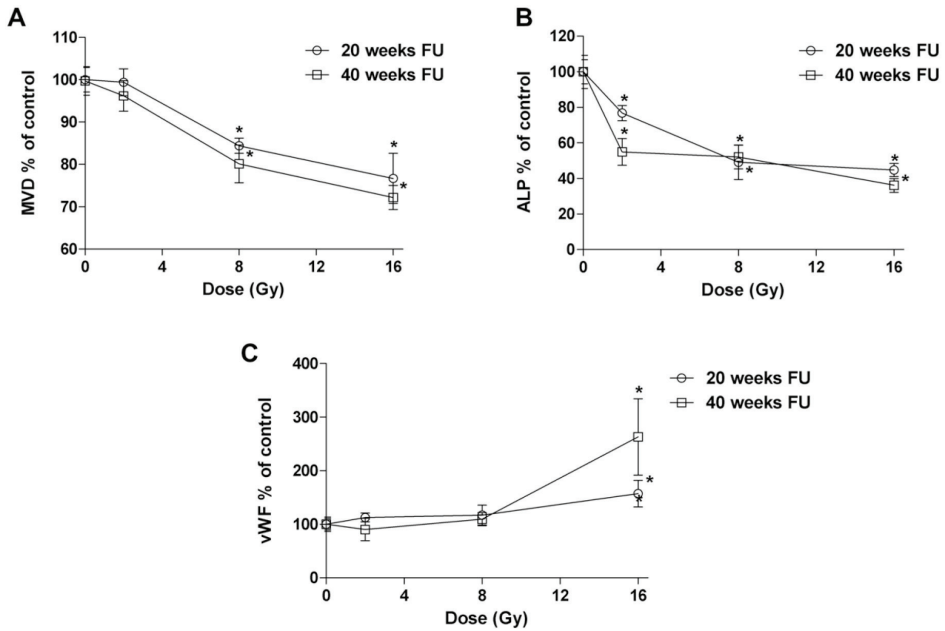


FIGURE 3 Microvascular alterations at 20 and 40 weeks after irradiation. (A) MVD per area expressed as percentage of 0 Gy values. (B) ALP-positive and (C) vWF-positive tissue per myocardial area expressed as percentage of age-matched controls. Number of mice included for analysis was 6, 5, 4 and 8, and 8, 7, 8 and 7 at respectively 20 and 40 weeks after 0, 2, 8 and 16 Gy. Values represent mean \pm SEM. * $p < 0.05$ compared to age-matched controls.

TABLE 1 Incidence of mice showing iron (Fe)-containing macrophages (Perl's staining) and albumin protein deposition in the myocardium at 20 and 40 weeks after irradiation.

| Treatment | Fe-containing macrophages | Albumin deposition |
|--------------------|---------------------------|--------------------|
| <i>20 weeks FU</i> | | |
| 0 Gy | 3/14 | 0/14 |
| 2 Gy | 0/3 | 0/3 |
| 8 Gy | 5/5* | 0/5 |
| 16 Gy | 20/21* | 0/21 |
| <i>40 weeks FU</i> | | |
| 0 Gy | 1/7 | 1/7 |
| 2 Gy | 1/7 | 2/7 |
| 8 Gy | 6/6* | 4/6 |
| 16 Gy | 5/7 | 6/7 |

* $p < 0.05$ compared to age-matched controls.

The endocardium of the 16 Gy irradiated mice showed the appearance of foam cell accumulations, as well as erythrocyte accumulations, at 20 weeks FU (Figure 4C), which was not observed after 0, 2 or 8 Gy (Table 2). At 40 weeks after 8 and 16 Gy increased endocardial collagen deposition (Table 2, Figure 4D) and fibrin deposits (confirmed by Martius Scarlet Blue staining), suggesting endocardial protein leakage (Table 2, Figure 4E and F), were observed.

Low-dose irradiation induced survival pathways, while high dose induced fibrotic pathways. In order to identify genes and pathways potentially involved in the cardiac response to irradiation, microarray and pathway analyses were performed using the software program IPA (a full list of gene expression levels after cardiac irradiation of *ApoE^{-/-}* mice can be found at <http://www.ebi.ac.uk/arrayexpress>). Radiation significantly regulated 111 (2 Gy) and 169 (16 Gy) genes at 20 weeks, and 116 (2 Gy) and 158 (16 Gy) genes at 40 weeks. Supplemental Figures I-IV show gene interaction networks of these radiation-regulated genes. Known ingenuity functional and/or canonical pathway analysis (Supplemental Table II) was used to identify overrepresentation of radiation-correlated genes within known functional assignments (such as inflammatory response) and to generate hypotheses.

The most significant pathway for 2 Gy at 20 weeks (Supplemental Figure I) was involved in cellular growth and proliferation. Matrix metalloproteinase 2 (MMP2) was identified as a central molecule. Furthermore, genes within this pathway were also involved in the first canonical pathway 'circadian rhythm' (nervous system) and in maintenance of blood pressure and heart beat (aryl hydrocarbon receptor nuclear translocator like, ARNTL). Irradiation with 16 Gy at 20 weeks (Supplemental Figure II) resulted in a significant regulation in cell-to-cell signaling and interaction pathway, with tissue inhibitor of metalloproteinase 1 (TIMP1) and heme oxygenase 1 (HMOX1) as central genes; both genes were significantly upregulated. Moreover, the classical and alternative pathway of the complement system was negatively regulated after 16 Gy. This operates within the cell-to-cell signaling and interaction pathway and was the first canonical pathway. Inflammatory response and inflammatory disease were also among the top biological functions altered after high-dose irradiation, including significant upregulation of Angiopoietin 2 (ANGPT2).

At 40 weeks after 2 Gy (Supplemental Figure III), cellular development associated network was significantly regulated. This includes cyclin dependent kinase inhibitor 1A (CDKN1A) and a number of heat shock genes, with heat shock protein 70 (Hsp70) as central molecule. P13K/Akt signaling was the prominent canonical pathway. Irradiation with 16 Gy (Supplemental Figure IV) resulted in significant regulation in cell movement pathway at 40 weeks. The most pronounced molecules within this pathway are fibronectin-1 and collagen, indicating tissue

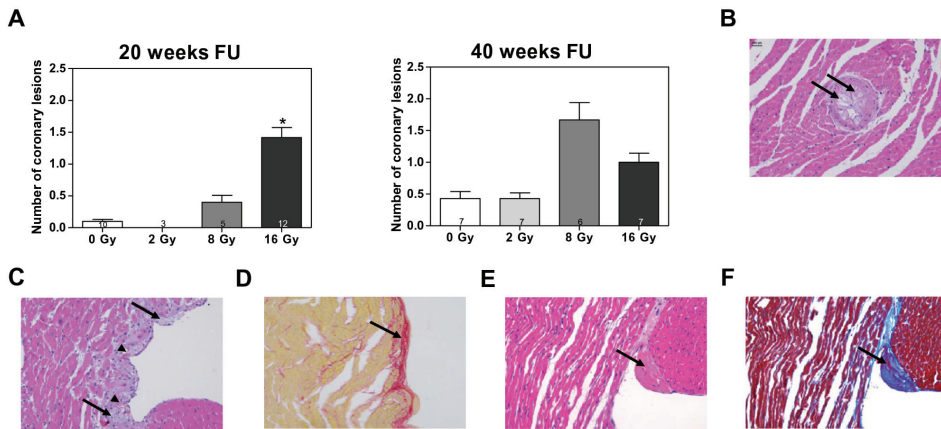


FIGURE 4 (A) Number of coronary atherosclerotic lesions examined in the mid-part of the heart at 20 and 40 weeks after irradiation. Bars represent mean \pm SEM with numbers of mice indicated per group. * $P < 0.05$ compared to age-matched controls. (B) Representative H&E photograph of a coronary atherosclerotic lesion, showing necrosis (arrows) after 16 Gy. (C) Representative H&E of subendocardial foam cell (arrows) and erythrocyte (arrowheads) accumulation observed at 20 weeks after 16 Gy. (D) Sirius Red photograph showing endocardial fibrosis (arrow) at 40 weeks after 16 Gy irradiation. (E) shows endocardial fibrin deposition on H&E-stained section (arrow), confirmed by Martius Scarlet Blue staining (F). Photographs are taken with 20x objective.

TABLE 2 Incidence of hearts showing endocardial damage with foam cell accumulation at 20 weeks, and protein leakage and collagen deposition at 40 weeks after irradiation.

| Treatment | Foam cell accumulation | Protein leakage | Collagen deposition | |
|--------------------|------------------------|-----------------|---------------------|--------|
| | | | Mild | Strong |
| <i>20 weeks FU</i> | | | | |
| 0 Gy | 0/10 | 0/10 | 0/10 | 0/10 |
| 2 Gy | 0/3 | 0/3 | 0/3 | 0/3 |
| 8 Gy | 0/5 | 0/5 | 0/5 | 0/5 |
| 16 Gy | 7/12* | 1/12 | 1/12 | 1/12 |
| <i>40 weeks FU</i> | | | | |
| 0 Gy | 0/7 | 0/7 | 5/7 | 2/7 |
| 2 Gy | 0/7 | 0/7 | 6/7 | 1/7 |
| 8 Gy | 0/6 | 2/6 | 0/5 | 5/5 |
| 16 Gy | 0/7 | 6/7* | 2/6 | 4/6 |

* $p < 0.05$ compared to age-matched controls.

injury. Moreover, fibrosis was the most upregulated canonical pathway including, connective tissue growth factor (CTGF), endothelin 1 (EDN1), fibronectin 1 (FN1) and platelet-derived growth factor (PDGF). Once again, inflammatory response and inflammatory disease were also among the top biological functions altered at 40 weeks after high-dose irradiation.

Modest changes in cardiac function after irradiation

Ultrasound measurements showed significant decreases in EDV and ESV, and an increase in EF at 20 weeks after 16 Gy (Supplemental Figure V). Gated-SPECT (^{99m}Tc-Myoview) showed similar radiation-induced decreases in EDV and ESV. However, these parameters are all within normal ranges and are not indicative of severe cardiac dysfunction.

Discussion

In this study the effect of local cardiac irradiation on heart structure and function, and the development of coronary atherosclerotic lesions, was investigated in hypercholesterolemic ApoE^{-/-} mice. Compared to previously examined C57BL/6J mice (8), which do not develop atherosclerosis, radiation-induced inflammatory changes in the myocardium of ApoE^{-/-} mice were similar, although the baseline level of inflammation in ApoE^{-/-} mice was higher, as expected (13). Pathway analyses also indicated a stimulated inflammatory response at 20 and 40 weeks after 16 Gy. This included upregulation of ANGPT2, which is increased in endothelial cells after tissue injury and stimulates an aggressive fibrotic response.(14) Furthermore, 16 Gy regulated cell-to-cell signaling and interaction pathway of which TIMP1 is a central gene. TIMP1 levels are correlated with myocardial hypertrophy, fibrosis and diastolic dysfunction.(15) Moreover, the complement system pathway was negatively regulated after 16 Gy, whereas activation of the pathway results in beneficial effects in immune defense.(16) In contrast, 2 Gy triggered a survival response, presumably in an attempt to stimulate recovery, by regulating the pathway of cellular growth and proliferation (20 weeks) and cellular development (40 weeks). Hsp and MMP2 are known to be involved in these pathways and play a crucial role in cardiomyocyte protection.(17, 18) Hsp70 can protect from stress-induced injury by inhibiting Fas-mediated apoptosis. Another central molecule of the cellular development pathway is CDKN1A, which is known to play a role in stress response and repair of DNA damage.(19)

On the other hand, high-dose irradiation induced fibrotic pathways. Diffuse interstitial fibrosis is one of the morphological hallmarks of radiation-induced myocardial injury.(20, 21) An increase in interstitial collagen content with dose was found in the myocardium of ApoE^{-/-} mice at 20 and 40 weeks after irradiation, which was not observed until 40 weeks after

irradiation of C57BL/6J mice (8). Microarray pathway analysis also showed highly upregulated collagen pathway in *ApoE*^{-/-} mice after 16 Gy, which was not observed in C57BL/6J mice (data shown at <http://www.ebi.ac.uk/arrayexpress>). This could eventually lead to a more serious increase in cardiac fibrosis at later time-points.

In previous studies (9, 10), we investigated the effect of local irradiation on the progression of atherosclerosis in the carotid arteries of *ApoE*^{-/-} mice and observed an accelerated development of inflammatory plaques. In addition, the present study shows an accelerated development, independently from valvular lesions, of atherosclerotic lesions in the coronary arteries after radiotherapy. High-dose irradiation significantly increased the number of coronary lesions at 20 weeks FU (in mice aged 30 weeks), while age-related atherosclerosis in these coronary arteries is mostly observed at 60 weeks of age in *ApoE*^{-/-} mice.(11) In addition, the coronary lesions in irradiated hearts contained much larger necrotic cores, indicative of a more advanced phenotype.

Radiation has been shown to increase the permeability of endothelial cells by induction of inflammatory and thrombotic pathways (22, 23), including increased production and release of vWF. The increase in vWF deposition in the irradiated heart observed in this study is also indicative of thrombotic endothelial cell damage.(21) This could increase vascular permeability and, combined with hypercholesterolemia, lead to lipid accumulation, thus stimulating atherogenesis. Furthermore, at 20 weeks 16 Gy irradiation regulated genes that are associated with severe and persistent endothelial damage, but prevent intravascular thrombosis (e.g. HMOX124). Irradiated *ApoE*^{-/-} hearts also showed microvascular damage, indicated by a loss of microvessels and a decreased activity of endothelial ALP in the remaining vessels. Decreased ALP activity was already observed at 20 weeks after 2 Gy in *ApoE*^{-/-} mice, whereas there was no decrease in MVD after this dose. Decreases in ALP were only found after higher doses in C57BL/6J mice (8), suggesting that hypercholesterolemia accelerated the response. An increase in the presence of iron-containing macrophages, as a sign of vascular damage and bleeding, was found in the myocardium of irradiated mice and was associated with an increased deposition of albumin at 40 weeks after high-dose irradiation. These results indicate that *ApoE*^{-/-} mice are susceptible to both macrovascular and microvascular damage. In addition, high-dose irradiation caused an increased permeability of the endocardium, leading to leakage of fibrin at 40 weeks.

Irradiation of *ApoE*^{-/-} mice modestly affected cardiac function at 20 weeks FU, similar to C57BL/6J mice (8). However, 16 Gy lead to sudden death of C57BL/6J mice before 40 weeks FU, while *ApoE*^{-/-} mice survived until 40 weeks after local high-dose irradiation. The high

mortality rate observed in C57BL/6J mice was probably due to the prominent deposition of amyloid in the myocardium caused by vascular leakage, leading to the inability to compensate for the structural damage and to maintain cardiac function. Since ApoE itself is one of the components of amyloid (25), irradiated ApoE^{-/-} mice showed no signs of cardiac amyloidosis, although there was evidence of vascular leakage. The fact that we did not observe a decreased survival in the irradiated ApoE^{-/-} mice, despite more pronounced microvascular damage and a similar reduction in cardiac function, suggests that the amyloid deposits played a detrimental role in cardiac integrity and led to the high mortality rate of the irradiated C57BL/6J mice.

In C57BL/6J mice, inflammatory changes were mainly observed in the epicardium (8), while ApoE^{-/-} mice showed endocardial damage with foam cell accumulations at 20 weeks after 16 Gy and collagen deposits at 40 weeks. Endocardial foam cell accumulation was previously described in diabetes, hyperlipidemic diseases and congenital diseases, whereby the endocardium is subjected to atherosclerotic events similar to those in lesion-prone sites such as aortic valves and bifurcations of large arteries.(26, 27) It is possible that, 20 weeks after irradiation, the underlying damaged inflammatory myocardium attracted macrophages to the endocardium, which transform into foam cells in the presence of hyperlipidemia.

In conclusion, the combination of irradiation and hypercholesterolemia led to an early and pronounced inflammatory response and microvascular leakage in the hearts of ApoE^{-/-} mice. In addition, the progression of atherosclerosis in the coronary arteries was clearly accelerated after high-dose local irradiation of the heart, combined with foam cell deposits in the endocardium. Despite these pronounced effects on cardiac structure and increased development of coronary atherosclerosis, the mice were able to maintain cardiac function up to 40 weeks after irradiation.

Supplemental data

SUPPLEMENTAL TABLE I Body and organ weights of mice at sacrifice.

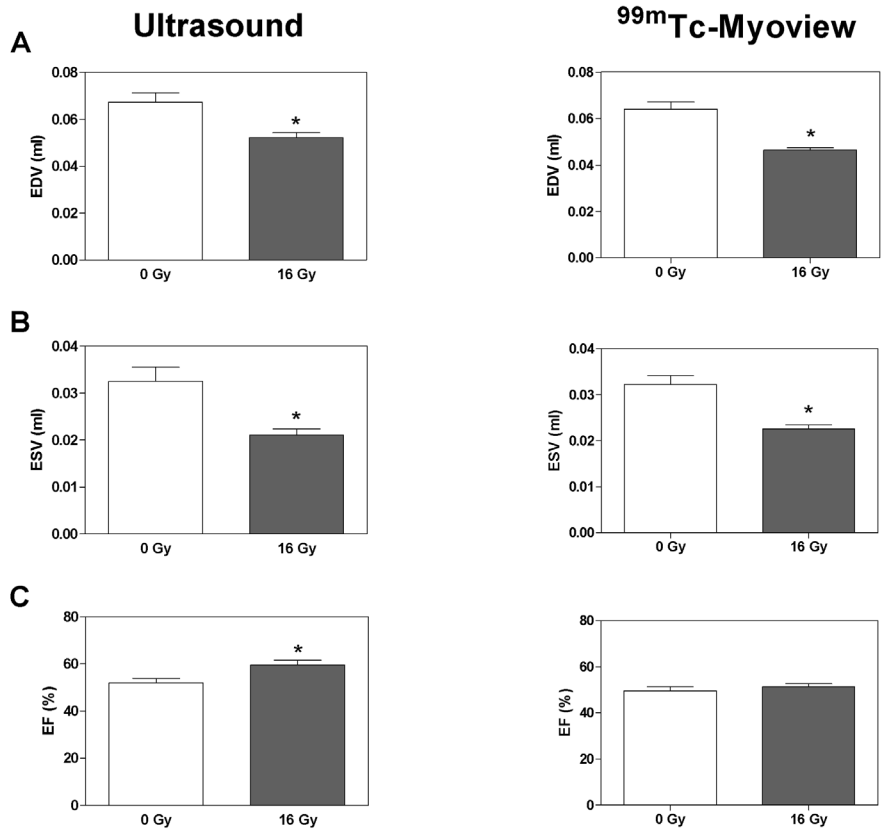
| Treatment | Body weight (g) | Heart weight (g) | Lung weight (g) | Heart/body weight% |
|--------------------|-----------------|------------------|-----------------|--------------------|
| <i>20 weeks FU</i> | | | | |
| 0 Gy | 32.3 ± 0.6 | 0.21 ± 0.006 | 0.17 ± 0.003 | 6.7 ± 0.2 |
| 2 Gy | 32.5 ± 0.3 | 0.20 ± 0.005 | 0.17 ± 0.003 | 6.0 ± 0.1 |
| 8 Gy | 32.1 ± 0.9 | 0.22 ± 0.013 | 0.17 ± 0.006 | 6.7 ± 0.4 |
| 16 Gy | 30.9 ± 0.5 | 0.21 ± 0.007 | 0.17 ± 0.002 | 6.7 ± 0.02 |
| <i>40 weeks FU</i> | | | | |
| 0 Gy | 33.2 ± 0.8 | 0.20 ± 0.006 | 0.17 ± 0.004 | 6.0 ± 0.1 |
| 2 Gy | 32.5 ± 1.0 | 0.21 ± 0.009 | 0.17 ± 0.004 | 6.3 ± 0.3 |
| 8 Gy | 34.5 ± 1.1 | 0.21 ± 0.005 | 0.18 ± 0.004 | 6.1 ± 0.2 |
| 16 Gy | 34.1 ± 0.8 | 0.23 ± 0.006 | 0.21 ± 0.011* | 6.9 ± 0.2* |

Values represent mean ± SEM. * p<0.05 compared to age-matched controls.

SUPPLEMENTAL TABLE II Top first pathway and significant canonical pathways (limited to three) analyzed in Ingenuity Pathway Analysis (IPA) at 20 and 40 weeks after 2 and 16 Gy. IPA score represents the likelihood (decreases with a score >2) that the set of focus genes in a pathway could be explained by random chance alone.

| | Pathway | IPA score | Canonical pathway |
|--------------------|--|-----------|--|
| <i>20 weeks FU</i> | | | |
| 2 Gy | Cellular growth and proliferation | 49 | 1. Circadian rhythm signaling |
| 16 Gy | Cell - to - cell signaling and interaction | 45 | 1. Complement system 2. Fibrosis 3. Acute phase response signaling |
| <i>40 weeks FU</i> | | | |
| 2 Gy | Cellular development | 46 | ND |
| 10 Gy | Cellular movement | 35 | 1. Fibrosis |

ND means not detected.



SUPPLEMENTAL FIGURE V Ultrasound and myoview (gated SPECT/CT) measurements of (A) EDV, (B) ESV and (C) EF for control and 16 Gy irradiated mice at 20 weeks FU. Bars represent mean \pm SEM. * $p < 0.05$ compared to age-matched controls.

References

1. Gyenes G, Rutqvist LE, Liedberg A, et al. Long-term cardiac morbidity and mortality in a randomized trial of pre- and postoperative radiation therapy versus surgery alone in primary breast cancer. *Radiother Oncol* 1998; 48: 185-190.
2. Aleman BM, van den Belt-Dusebout AW, Klokman WJ, et al. Long-term cause-specific mortality of patients treated for Hodgkin disease. *J Clin Oncol* 2003; 21: 3431-3439.
3. Adams MJ, Hardenbergh PH, Constine LS, et al. Radiation-associated cardiovascular disease. *Crit Rev Oncol Hematol* 2003; 45: 55-75.
4. McGale P, Darby SC, Hall P, et al. Incidence of heart disease in 35,000 women treated with radiotherapy for breast cancer in Denmark and Sweden. *Radiother Oncol* 2011; 100: 167-175.
5. Schultz-Hector S, Trott KR. Radiation-induced cardiovascular diseases: is the epidemiologic evidence compatible with the radiobiologic data? *Int J Radiat Oncol Biol Phys* 2007; 67: 10-18.
6. Darby SC, Cutter DJ, Boerma M, et al. Radiation-related heart disease: current knowledge and future prospects. *Int J Radiat Oncol Biol Phys* 2010; 76: 656-665.
7. Andratschke N, Maurer J, Molls M, et al. Late radiation-induced heart disease after radiotherapy. Clinical importance, radiobiological mechanisms and strategies of prevention. *Radiother Oncol* 2011; 100: 160-166.
8. Seemann I, Gabriels K, Visser NL, et al. Irradiation induced modest changes in murine cardiac function despite progressive structural damage to the myocardium and microvasculature. *Radiother Oncol* 2012; 103: 143-150.
9. Hoving S, Heeneman S, Gijbels MJ, et al. Single-dose and fractionated irradiation promote initiation and progression of atherosclerosis and induce an inflammatory plaque phenotype in ApoE(-/-) mice. *Int J Radiat Oncol Biol Phys* 2008; 71: 848-857.
10. Stewart FA, Heeneman S, Te Poele J, et al. Ionizing radiation accelerates the development of atherosclerotic lesions in ApoE-/- mice and predisposes to an inflammatory plaque phenotype prone to hemorrhage. *Am J Pathol* 2006; 168: 649-658.
11. Hu W, Polinsky P, Sadoun E, et al. Atherosclerotic lesions in the common coronary arteries of ApoE knockout mice. *Cardiovasc Pathol* 2005; 14: 120-125.
12. Du P, Kibbe WA, Lin SM. lumi: a pipeline for processing Illumina microarray. *Bioinformatics* 2008; 24: 1547-1548.
13. Tenger C, Zhou X. Apolipoprotein E modulates immune activation by acting on the antigen-presenting cell. *Immunology* 2003; 109: 392-397.
14. Jeansson M, Gawlik A, Anderson G, et al. Angiotensin-1 is essential in mouse vasculature during development and in response to injury. *The Journal of clinical investigation* 2011; 121: 2278-2289

15. Moore L, Fan D, Basu R, et al. Tissue inhibitor of metalloproteinases (TIMPs) in heart failure. *Heart failure reviews* 2012; 17: 693-706.
16. Yasuda M, Takeuchi K, Hiruma M, et al. The complement system in ischemic heart disease. *Circulation* 1990; 81: 156-163.
17. Zhao Y, Wang W, Qian L. Hsp70 may protect cardiomyocytes from stress-induced injury by inhibiting Fas-mediated apoptosis. *Cell stress & chaperones* 2007; 12: 83-95.
18. Matsusaka H, Ikeuchi M, Matsushima S, et al. Selective disruption of MMP-2 gene exacerbates myocardial inflammation and dysfunction in mice with cytokine-induced cardiomyopathy. *American journal of physiology Heart and circulatory physiology* 2005; 289: H1858-1864.
19. Bendjennat M, Boulaire J, Jascur T, et al. UV irradiation triggers ubiquitin-dependent degradation of p21(WAF1) to promote DNA repair. *Cell* 2003; 114: 599-610.
20. Kruse JJ, Zurcher C, Strootman EG, et al. Structural changes in the auricles of the rat heart after local ionizing irradiation. *Radiother Oncol* 2001; 58: 303-311.
21. Boerma M, Kruse JJ, van Loenen M, et al. Increased deposition of von Willebrand factor in the rat heart after local ionizing irradiation. *Strahlentherapie und Onkologie : Organ der Deutschen Rontgengesellschaft et al.* 2004; 180: 109-116.
22. Konings AW, Smit Sibinga CT, Aarnoudse MW, et al. Initial events in radiation-induced atheromatosis. II. Damage to intimal cells. *Strahlentherapie* 1978; 154: 795-800.
23. van Kleef E, Verheij M, te Poele H, et al. In vitro and In vivo expression of endothelial von Willebrand factor and leukocyte accumulation after fractionated irradiation. *Radiation research* 2000; 154: 375-381.
24. True AL, Olive M, Boehm M, et al. Heme oxygenase-1 deficiency accelerates formation of arterial thrombosis through oxidative damage to the endothelium, which is rescued by inhaled carbon monoxide. *Circulation research* 2007; 101: 893-901.
25. Sawabe M, Hamamatsu A, Ito T, et al. Early pathogenesis of cardiac amyloid deposition in senile systemic amyloidosis: close relationship between amyloid deposits and the basement membranes of myocardial cells. *Virchows Archiv : an international journal of pathology* 2003; 442: 252-257.
26. Stehbens WE, Delahunt B, Zuccollo JM. The histopathology of endocardial sclerosis. *Cardiovasc Pathol* 2000; 9: 161-173.
27. Popov D, Sima A, Stern D, et al. The pathomorphological alterations of endocardial endothelium in experimental diabetes and diabetes associated with hyperlipidemia. *Acta Diabetol* 1996; 33: 41-47.
- Moore L, Fan D, Basu R, et al. Tissue inhibitor of metalloproteinases (TIMPs) in heart failure. *Heart failure reviews* 2012; 17: 693-706.



Chapter 4

Radiation- and anthracycline-induced cardiac toxicity and the influence of ErbB2 blocking agents

.....
I. Seemann, J.A.M. te Poele, J.Y. Song, S. Hoving, N.S. Russell, F.A. Stewart

Breast Cancer Research and Treatment October 2013

Abstract

Background: Inhibition of ErbB2-signaling in Her2-positive breast cancer patients is regularly combined with chemotherapy and radiotherapy. The risk of cardiotoxicity after anthracyclines and radiotherapy is recognized, but little is known about increased risk when these treatments are combined with ErbB2 inhibition. This study investigated whether ErbB2 inhibition increased radiation or anthracycline induced toxicity.

Materials and Methods: In an *in vitro* study, human cardiomyocytes were treated with irradiation or doxorubicin, alone or in combination with trastuzumab, and evaluated for cell survival and growth. Groups of mice received 0 or 14 Gy to the heart, alone or in combination with lapatinib, or 3x4 mg/kg doxorubicin alone or in combination with lapatinib. Mice were evaluated 40 weeks after treatment for cardiac damage. Changes in cardiac function (^{99m}Tc-myoview gated SPECT) were related to histomorphology and microvascular damage.

Results: Radiation or doxorubicin-induced cardiomyocyte toxicity (*in vitro*) were not exacerbated by trastuzumab. Cardiac irradiation of mice decreased microvascular density and increased endothelial damage in surviving capillaries (decrease alkaline phosphatase expression and increased von Willebrand factor), but these changes were not exacerbated by lapatinib. Inflammatory responses in the irradiated epicardium (CD45+ and F4/80+ cells) were significantly reduced in combination with lapatinib. Irradiation, doxorubicin and lapatinib each induced cardiac fibrosis but this was not further enhanced when treatments were combined. At the ultrastructural level, both lapatinib and doxorubicin induced mitochondrial damage, which was enhanced in combined treatments. Lapatinib alone also induced mild changes in cardiac function but this was not enhanced in the combined treatments.

Conclusion: Trastuzumab did not enhance direct radiation or anthracycline toxicity of cardiomyocytes *in vitro*. Lapatinib did not enhance the risk of radiation or anthracycline-induced cardiac toxicity in mice up to 40 weeks after treatment, but mitochondrial damage was more severe after doxorubicin combined with lapatinib.

Introduction

Cardiovascular damage has been reported as a long-term toxicity in breast cancer survivors previously treated with radiotherapy (RT) and anthracycline chemotherapy (CT) (1). Prospective functional imaging studies show that ~40 % of left-sided breast cancer patients treated with RT develop asymptomatic cardiac perfusion defects within 2 years and about 16 % eventually develop wall-motion abnormalities (2–4). Yearly, 1.5 million new breast cancer patients are diagnosed worldwide who will undergo RT, CT, surgery, and/or adjuvant hormonal therapy. Approximately 15–20 % of breast cancers show a highly aggressive subtype, characterized by epidermal growth factor receptor 2 (ErbB2) overexpression. Such cancers are fast-growing, highly invasive, resistant to CT and RT and are therefore associated with higher risk for recurrence (5, 6). Epidermal growth factor receptor 1 (ErbB1) is also expressed in several human tumors, including breast cancer, and makes significant contributions to invasion and growth of tumors (7).

The established role of ErbB1 and ErbB2 in breast cancer makes them attractive therapeutic targets. Trastuzumab, a humanized anti-ErbB2 monoclonal antibody, is the most prominent, first-line agent for ErbB2 (HER2)-overexpressing metastatic breast cancer (8). Clinical studies using trastuzumab confirmed the benefits of inhibiting ErbB2 signaling, including inhibition of p27Kip1, activation of PTEN tumor suppressor gene and induction of G1 cell cycle arrest (9). Adjuvant treatment with trastuzumab for operable breast cancer improves overall survival rate in Her2-positive breast cancer patients by ~30 % and reduces the risk of recurrence by ~50 % (10,11). However, heart failure occurs in 1.7–4.1 % of patients treated with trastuzumab and cardiac toxicity lead to discontinuation of the adjuvant treatment in 19 % of the patients (10–12).

ErbB2 is an orphan receptor that has no ligand binding site but dimerizes with other ligand-bound EGRF receptors (HER3, HER4). One of the most common ligands of the EGFR pathway in the heart is neuregulin-1. Targeting both ErbB1 and ErbB2 is hypothesized to have superior therapeutic effects relative to single-agent treatment. Dual inhibitor lapatinib (GW572016) is a small molecule, reversible inhibitor of the tyrosine kinase activities of ErbB1 and ErbB2 at equal potency. Lapatinib works by blocking the signaling transduction to Ras/Raf MAPKs and the PI3K/Akt pathway, which leads to increased apoptosis and decreased cellular proliferation. Perez and colleagues reviewed 44 studies in which lapatinib (as monotherapy or in combination with previously given anthracyclines or trastuzumab) induced low levels of cardiac toxicity, as detected by reversible decreased left ventricle ejection fraction (LVEF) (13). The mechanisms whereby cardiac toxicity occurs after ErbB2 inhibition is not fully understood,

since non- malignant cells do not over-express ErbB2. However, ErbB2 signaling and the ligand Neuregulin-1 are known to play a crucial role in survival and growth of cardiac myocytes (14, 15). Moreover, a recent study demonstrated that irradiation inhibited ErbB2 signaling in rat hearts until the onset of fibrosis after 10 weeks. As fibrosis progressed, ErbB2 and the EGFR ligand neuregulin were significantly upregulated, presumably as an attempt to regenerate the myocardium (16). This raises the question whether delayed inhibition of ErbB2 after CT or RT could lead to increased cardiac toxicity.

Little is known about the long-term cardiac outcome of lapatinib in combination with anthracycline CT or irradiation. In this study, we first investigated whether blocking of ErbB2 enhanced the toxicity of radiation- or doxorubicin (Dox)-treated cardiomyocytes in vitro. We subsequently investigated the influence of combined ErbB1/2 inhibition in mice treated with cardiac irradiation or systemic Dox. For these studies lapatinib was given for 20 weeks in the chow, either at the time of irradiation or Dox (direct), or delayed until 20 weeks after irradiation or Dox. This was designed to mimic clinical treatment protocols and to investigate the influence of lapatinib on the short- and long- term damage repair process following irradiation or anthracyclines. Structural and functional changes were monitored at 40 weeks after treatment to determine whether ErbB1/2 inhibition caused increased cardiac damage or inhibited recovery after radiation or anthracycline treatment.

As far as we are aware, this is the first study that characterizes in detail long-term cardiac toxicity after lapatinib in combination with irradiation or Dox.

Materials and Methods

Cell culture conditions and treatment

Human cardiac myocytes (HCM) from Promocell (Heidelberg, Germany) were cultured in DMEM (Gibco®, Invitrogen) supplemented with 10 % fetal calf serum, 1 % penicillin, and 1 % streptomycin at 37 °C with 5 % CO₂. The HCM express markers of early stage differentiation such as GATA-4 and sarcomeric alpha-actin and act more like progenitor cells with capacity for proliferation. For irradiation experiments, cells were seeded in 96-well plates (1,000 per well) and irradiated with 0, 2.5, 5, or 10 Gy (137Cs irradiation, with a dose rate of 0.66 Gy/min) before exposure to 0, 0.1, 1, or 10 µg/ml trastuzumab (Roche, from the Netherlands Cancer Institute pharmacy) for 14 or 21 days. Cells were then washed (39 with PBS) to remove drugs and evaluated for cell viability. For Dox experiments, 4,000 cells per well were seeded and treated with 0, 0.0025, 0.025, 0.25, 2.5, 25, and 250 µg/ml Dox

(Doxorubicin hydrochloride 2 mg/ml PCH, from the Netherlands Cancer Institute pharmacy) and trastuzumab (0–10 µg/ml) for 3 days, washed and evaluated for cell viability directly or re-incubated with trastuzumab until evaluation at 14 days. Cell viability was detected by cell counting kit-8 (CCK-8, Sigma, Zwijndrecht, the Netherlands) following the manufacturer's protocol.

Mice and treatments groups

Male C57BL/6 mice, aged 8–12 weeks (Charles River Laboratories, France) were randomly allocated to receive 0 Gy or 14 Gy to the heart, or 4 mg/kg Dox intraperitoneal (i.p.) weekly for 3 weeks. Separate cohorts of animals were included for irradiation or anthracycline combined with lapatinib, as well as age-matched controls. Lapatinib (from the Netherlands Cancer Institute pharmacy) was mixed with standard mouse chow to a final concentration of 0.48 g/kg. Assuming consumption of 5 g chow/mouse/day, this is equivalent to 100 mg/kg/day. A pilot study with 100 mg/kg/day given in chow or by oral gavages resulted in the same plasma concentration (mean 946 ng/ml and 909 ng/ml lapatinib after chow diet and oral gavages). Lapatinib diet was either started 7 days before irradiation or Dox (direct schedule) to achieve steady state plasma levels, or delayed until 20 weeks after treatment (Figure 1).

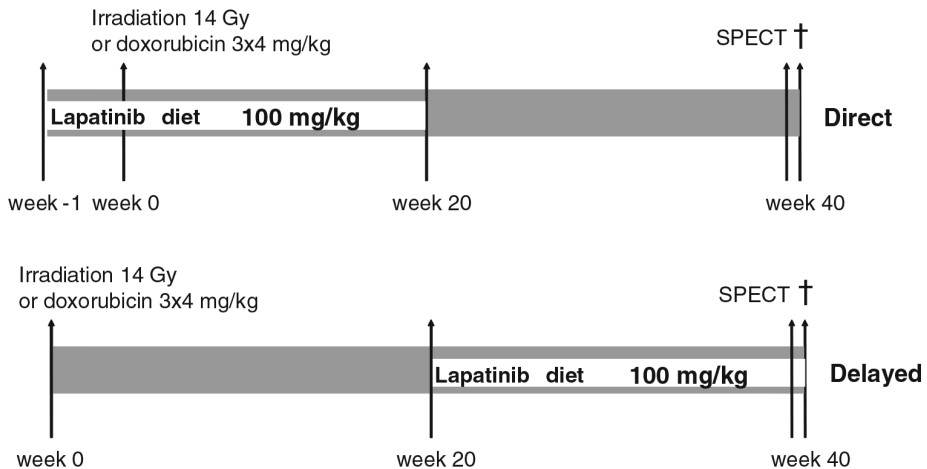


FIGURE 1 Schedule overview. Schematic representation of schedules for lapatinib given for 20 weeks in the chow, starting at the time of irradiation or doxorubicin (direct), or starting 20 weeks after irradiation or doxorubicin (delayed).

Irradiation was with 250 kV X-rays, operating at 12 mA and filtered with 0.6-mm Copper. The dose rate was 0.94 Gy/min, with a field size of 10.6 × 9.15 mm (including the whole heart and up to 30 % lung volume); the rest of the mouse was shielded with lead. For irradiation, unanesthetized mice were immobilized in a prone position in acrylic perspex jigs. Each treatment group comprised 10–15 mice (n = 125 in total). Experiments were in agreement with the Dutch law on animal experiments and welfare, and in line with the international Guide for the Care and Use of Laboratory Animals (Eighth edition).

Tissue preparation for histology

At termination of the experiment, the heart was perfused via the aortic arch (retro-grade), under lethal sodium pentobarbital anesthesia (18 mg per mouse, i.p.), with PBS (frozen sections) or PBS followed by 1 % paraformaldehyde (paraffin sections). The heart was then quickly excised before freezing on dry ice or immersion in 1 % paraformaldehyde.

Cross-sections were cut at the level of the mid-horizontal plane from fixed paraffin-embedded tissues (4 µm) or frozen tissues (7 µm).

Frozen sections

An anti-CD31 antibody (1:50, Becton&Dickinson) was used to visualize cardiac vasculature. To determine functional changes in the microvasculature, a histochemical staining with Naphthol AS-MX/DMF and fast Blue BB salt was performed to detect endothelial cell alkaline phosphatase. Sections were also reacted with antibodies against von Willebrand Factor (vWF) (1:4000, Abcam, Cambridge, USA) as a marker of thrombotic changes. All sections were processed identically, with precisely the same incubation times for the primary and secondary antibody and diaminobenzidine (DAB) solution (Sigma, Zwijndrecht, the Netherlands).

For quantification of microvascular changes, five random fields (40x objective) of the heart were photographed with a CCD 2 Color Microscope system, including a Zeiss Axio-Cam color camera (AxioCam HRc, Zeiss, Göttingen, Germany). A computerized morphometry system (Leica Qwin V3, Leica, Rijswijk, the Netherlands) was used to quantify the MVD of CD31 positive structures. Vessels <1.5 or >200 µm² were automatically excluded from the measurements. Photographs of whole sections stained for ALP and vWF were taken with an Aperio scanner (Scanscope-XT, Aperio technologies, Vista, USA) using 40x objective. Analyses of the percentage myocardium, excluding endocardium, positive for each marker were done with a computerized morphometry system (Leica Qwin V3).

Paraffin sections

To determine the extent of inflammation, sections were immuno-labeled with anti-CD45 antibody (1:400, Becton & Dickinson, Franklin lakes, USA). To detect alterations in the number of macrophages sections were stained with anti-F4/80 (1:300, AbD Serotec, Düsseldorf, Germany) and counted per left ventricle (LV) myocardial area.

All sections were processed identically; therefore, differences between the treatments are due to DAB identification of the relevant protein. Interstitial collagen was determined in the myocardium based on Sirius red staining.

Photographs of the LV wall, excluding the septum, were taken using a 40x objective (Leica DFC320). Interstitial collagen was quantified in five randomly selected areas of the subendocardium and myocardium of the LV (40x objective) and results were expressed as percentage tissue positive for Sirius red relative to myocardial area. The number of CD45+ cells per section was counted separately in the epicard and myocard to determine the extent of inflammation. Morphometric parameters were analyzed using a computerized morphometry system (Leica Qwin V3). Transverse sections were stained with hematoxylin and eosin (H&E) to check for alterations in the myocardium and blood vessels. A semi-quantitative scoring system was used, whereby for the blood vessels 1 indicates one mild/severe morphological event (degeneration of the coronary arterioles, dilation of capillaries in myocardium accompanied by edema in stroma or clotting-like materials in coronary vessels), 2 indicates two morphological events, and 3 indicates >2 severe morphological events. For the myocardium, a score of 1 indicated atrophy, 2 indicated degeneration or hypertrophy, and 3 indicated more than two events.

Electron microscopy (EM)

Tissues were fixed in Karnovsky's fixative, followed by 1 % osmiumtetroxide in 0.1 M cacodylate-buffer. After washing, pellets were stained with Ultrastain 1 (Leica, Vienna, Austria), followed by ethanol dehydration. Finally the cells were embedded in a mixture of DDSA/NMA/ Embed-812 (EMS, Hatfield, U.S.A), sectioned and stained with Ultrastain 2 (Leica, Vienna, Austria) and analyzed with a CM10 electron microscope (FEI, Eindhoven, the Netherlands).

Gated SPECT/CT

Gated single photon emission computed tomography (gSPECT) acquisitions were made with a small-animal NanoSPECT/CT (Bioscan Europe, Ltd., Paris, France). Animals were anesthetized

with Hypnorm (Fentanyl 0.26 mg/kg/Fluanisone 8.33 mg/kg, VetaPharma, Ltd., Leeds, UK) and Dormicum (Midazolam, 4.17 mg/kg, Roche, Woerden, the Netherlands) via i.p. injection (1:2:1 Hypnorm:H₂O:Dormicum; 120 µl/mouse). Myoview (GE- healthcare, Hoevelaken, the Netherlands) was labeled with 1–1.5 ml ^{99m}Tc-pertechnetate. For detailed information see Seemann et al. (17). Quantitative analysis of the reconstructed datasets was performed on a clinical e.soft (*syngo*-based) workstation (Siemens Medical Solutions, Siemens AG, Erlangen, Germany), using algorithms to automatically reconstruct a count based 3D model of the dimensions of the left ventricular (LV) end-diastolic and systolic volumes (EDV, ESV). Subsequently, a LV time volume curve and its first derivative were generated. The ejection fraction (EF) was calculated based on the difference between EDV and ESV divided by EDV and peak filling rate (PFR) (EDV/s) was calculated from the Fourier-fitted curves.

Statistics

Data are expressed as mean ± SEM and groups were compared using non-parametric Mann–Whitney exact U-tests. Group differences were considered statistically significant at p<0.05. Statistical analyses were performed using SPSS version 20.

Results

HER2 inhibition did not decrease myocyte cell viability in vitro

Exposure of human cardiomyocytes for 3 days to Dox induced a dose-dependent decrease in cell viability. However, combination of Dox with trastuzumab did not further decrease myocyte cell viability (Figure 2A). When Dox was removed after 3 days and cells were evaluated at 14 days after treatment, cell proliferation was not affected by the presence of trastuzumab. Prior exposure to (0.025 µg/ml Dox inhibited cardiomyocyte growth, but this was independent of trastuzumab exposure (Figure 2B).

Cardiomyocyte cell viability decreased after radiation doses of 2.5–10 Gy, when assessed at 14 or 21 days after treatment, but there was no further decrease in cell viability in combination with trastuzumab (Figure 2C, D).

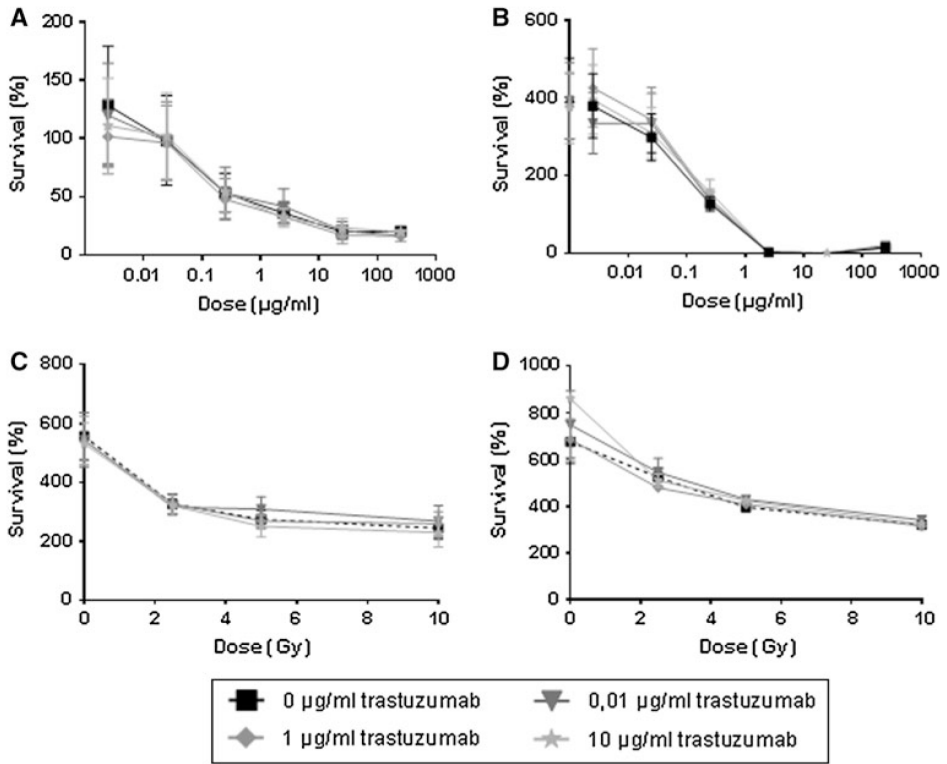


FIGURE 2 Cardiomyocyte viability after ErbB2 inhibition. Fig A/B: Human cardiomyocytes were treated with doxorubicin (0–250 µg/ml) and trastuzumab (0–10 µg/ml) for 3 days. Cells were then washed (3x with PBS) to remove drugs and evaluated for cell viability directly (2A) or re-incubated with trastuzumab only until evaluation at 14 days (2b). Each symbol represents the mean (\pm SEM) of three experiments and results are expressed as percentage cell survival. Figure C/D: Human cardiomyocytes were irradiated (0, 2.5, 5, or 10 Gy) and then exposed to trastuzumab (0–10 µg/ml) for 14 days (C) or 21 days (D) before evaluation of cell viability. Each symbol represents the mean (\pm SEM) of three experiments and results are expressed as percentage cell survival.

Mouse survival and weight

Irradiation with 14 Gy alone caused no premature deaths and few deaths occurred in combination with direct (7 %) or delayed lapatinib (12 %). Heart and body weights were slightly lower after irradiation (Figure 3A and Table S1). There were more unscheduled deaths after treatment with Dox (27 %), especially when combined with lapatinib (36 and 33 % deaths for direct and delayed lapatinib) (Figure 3B; Table S2). Since the group analyses were done on material from surviving animals only, this probably represents an underestimate of the total toxic effects of Dox. Both heart and body weights were also lower after Dox alone or in combination with lapatinib compared to age-matched control.

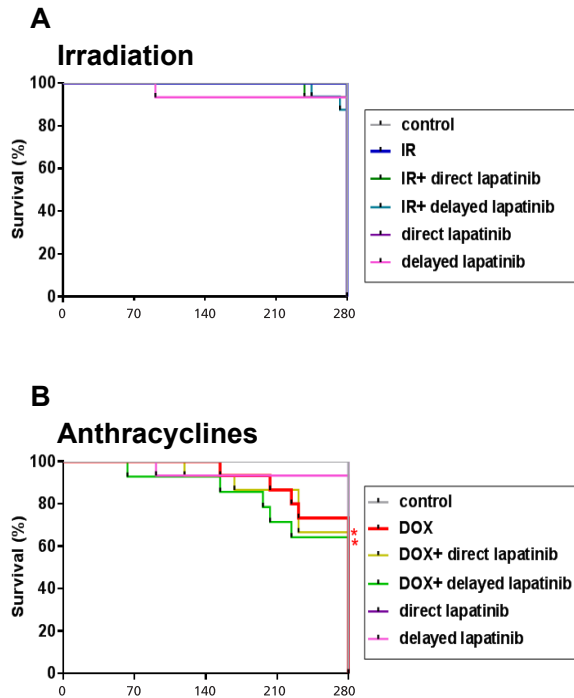


FIGURE 3 Kaplan-Meier estimated of overall survival shown for mice treated with lapatinib alone or in combination with radiation or doxorubicin. Survival data are shown for mice treated with radiation (A) or doxorubicin (B) alone or in combination with direct or delayed with lapatinib. Treatment groups were compared with age-matched controls. *Indicates significant differences between treated mice and age-matched control groups (p < 0.05; Mann-Whitney U-test).

Radiation-induced microvascular damage

MVD decreased significantly after 14 Gy radiation alone but the decline was not further enhanced by combination with either direct or delayed lapatinib treatment (Figure 4A). There were no changes in MVD after Dox treatment alone or in combination with lapatinib (data not shown). Radiation-induced changes in MVD were accompanied by endothelial damage, as shown by a marked decrease in ALP activity (Figure 4B) and an increased expression of the thrombotic endothelial marker vWF after irradiation alone (Figure 4C). None of these endothelial changes were more severe after combined treatments with lapatinib than after irradiation alone (Figure 4B, C). Endothelial damage (ALP) or thrombotic changes in the microvascular (vWF) were not detected in Dox-treated mice (data not shown).

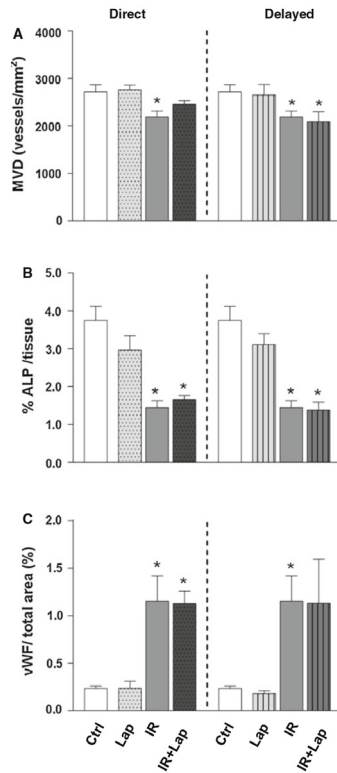


FIGURE 4 Microvascular alterations after ErbB2 inhibition alone or in combination with irradiation. (A) MVD per unit area expressed as number of microvessels per mm². (B) ALP positive tissue areas as % of total tissue. (C) vWF positive tissue areas as % of total tissue *p<0.05 compared to age-matched untreated controls. Each value represents the mean (\pm SEM) for minimal five mice per group. Ctrl control; Lap lapatinib; IR irradiation; IR+lap irradiation combined with lapatinib.

Radiation-induced inflammation

Irradiation alone led to a significant increase in CD45+ cells and F4/80+ cells in the epicardium (Figure 5) but not in the myocardium (data not shown). Strikingly, direct or delayed lapatinib decreased CD45+ and F4/80+ cells in the irradiated epicardium, compared to irradiation alone (Figure 5A, B). There were no significant inflammatory responses seen in Dox-treated mice (data not shown).

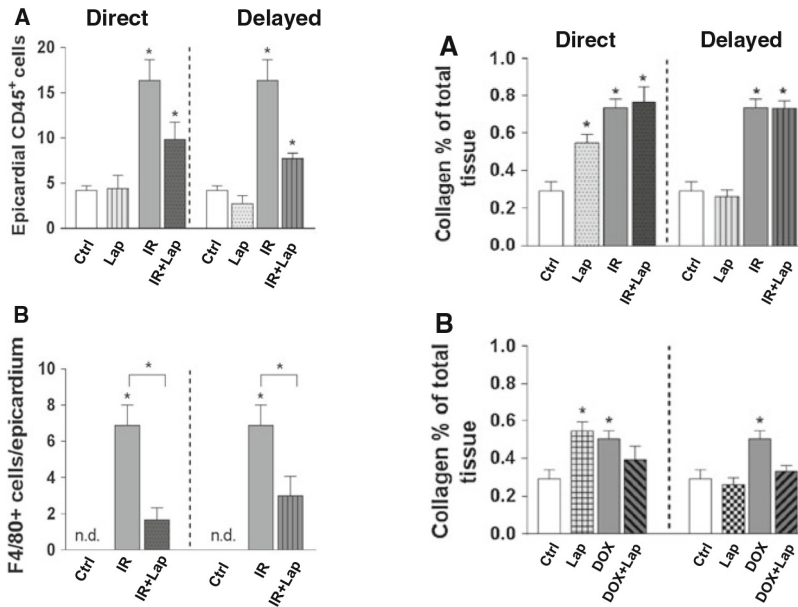


FIGURE 5 (LEFT) Inflammatory changes after ErbB2 inhibition alone or in combination with irradiation. (A) Quantification of CD45+cells (B) and of F4/80+cells per section in the epicardium. Each value represents the mean (\pm SEM) for minimal five mice per group. * $p < 0.05$ compared to age-matched untreated controls. n.d. not determined. Ctrl control; Lap lapatinib; IR irradiation; IR+Lap irradiation combined with lapatinib.

FIGURE 6 (RIGHT) Fibrotic changes after ErbB2 inhibition alone or in combination with irradiation or doxorubicin. (A) Collagen per unit area expressed as percentage of total tissue for animals treated with irradiation. (B) Collagen per unit area expressed as percentage of total tissue for animals treated with doxorubicin * $p < 0.05$ compared to age-matched untreated controls. Each value represents the mean (\pm SEM) for minimal five mice per group. n.d. not determined. Ctrl control; Lap lapatinib; DOX doxorubicin; DOX+Lap doxorubicin combined with lapatinib; IR irradiation; IR+Lap irradiation combined with lapatinib.

Irradiation- and doxorubicin-induced cardiac fibrosis

Cardiac fibrosis was significantly increased by irradiation or lapatinib alone, when administered directly (Figure 6A). Lapatinib (either direct or delayed) did not further enhance the fibrosis induced by irradiation. There was also a significant increase in cardiac fibrosis after Dox alone, but this was not further enhanced by either direct or delayed lapatinib (Figure 6B).

Structural and morphological alterations

H&E stained sections were semi-quantitatively analyzed for changes in the myocardium and blood vessels. There were only minor changes in the vasculature after irradiation alone or in combination with direct lapatinib. However, when delayed lapatinib was given to irradiated mice there was a trend for increased myocardial and blood vessel damage, including dilation of capillaries, degeneration of coronary arteries, degeneration of the myocardium, and hypertrophy of the myocardium (Figure 7). No severe changes were detected in Dox-treated mice that survived until 40 weeks. Examination of prematurely sacrificed, sick animals did demonstrate damage but this group comprised only a few mice, sacrificed at various times after treatment, so no semi-quantitative analysis was done.

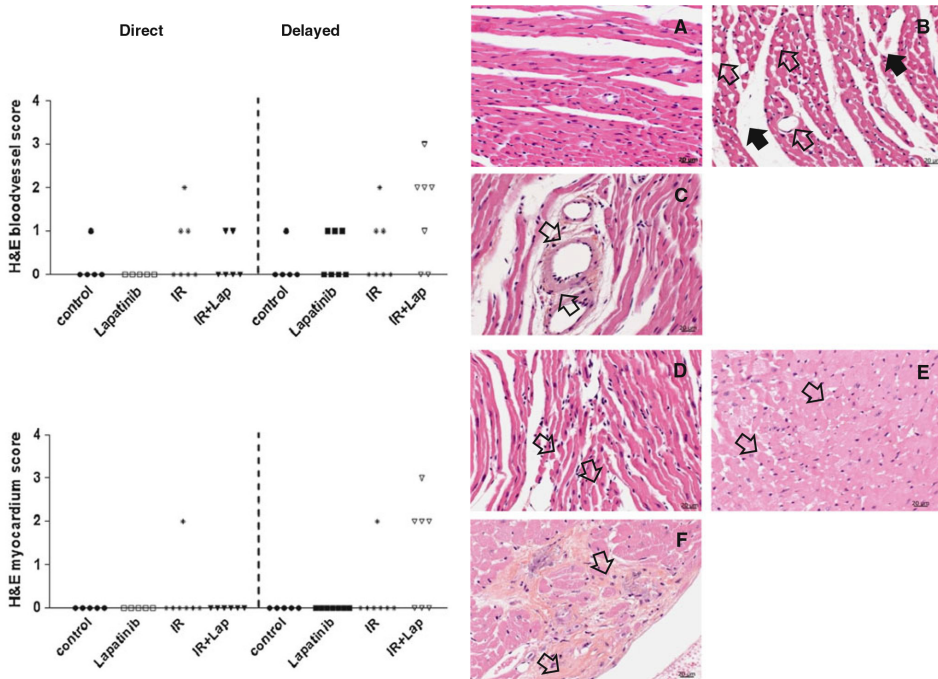


FIGURE 7 Histological changes in the myocardium and blood vessels at 40 weeks after treatment with irradiation or doxorubicin alone or in combination with lapatinib. H&E sections of the heart of mice that survived treatment with irradiation alone or in combination with lapatinib. Blood vessel and myocardium were scored for cardiac events at 40 weeks after treatment. Each symbol represents the score of one mouse (minimal five mice per group). (A) Age-matched control heart. (B) Dilated capillaries (open arrow) and edema in the stroma (dark arrow) of an irradiated heart. (C) Hyaline-like degeneration of the coronary arterioles (open arrows). (D) Atrophy of the myocardium (small, misshapen myocytes, and separated from each other, open arrows). (E) Degeneration of the myocardium. (F) Focal fibrosis (open arrows) and degeneration of endocardium

Electron microscopy (EM) analysis indicated small changes in myocyte morphology, like local vacuolization, after Dox or lapatinib treatment alone. Changes were enhanced when Dox was combined with lapatinib, either direct or delayed. Focal damage was seen with degenerative changes in the mitochondria, cloudy-swollen phenotype and disorganized, disrupted Z-bands in some cardiomyocytes, but normal looking mitochondria and Z-bands in adjacent cells (Figure 8).

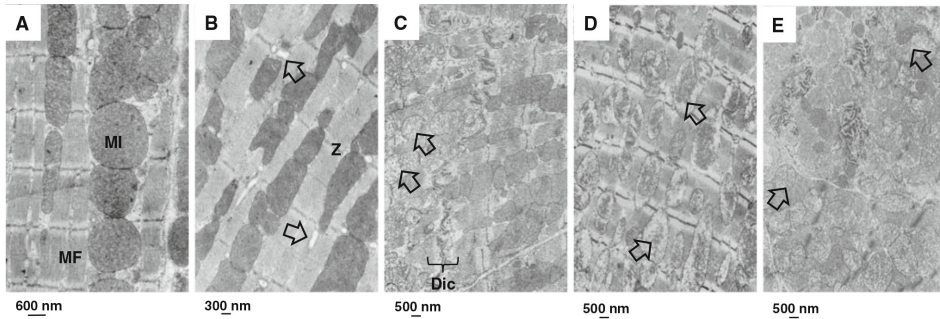


FIGURE 8 Mitochondrial changes in the myocardium after ErbB2 inhibition. Electron microscopic images of the myocardium of mice treated with lapatinib alone or in combination with doxorubicin at 40 weeks after treatment. (A) Age-matched control (n = 3); cardiomyocytes show organized sarcomeres characterized by parallel myofilaments anchored to Z bands and mitochondria were perfectly aligned and packed. (B) Doxorubicin treatment alone (n = 3); myofilament arranged regularly and mitochondria were aligned with focal vacuolization (arrow). (C) Lapatinib treatment alone (n = 3); focal damage per cardiomyocyte. Mitochondrial volume increased, mitochondrial cristae were fuzzy and had a cloudy swollen phenotype (arrow). (D) Direct lapatinib set up combined with doxorubicin (n = 3); (E) delayed lapatinib set up combined with doxorubicin (n = 3); disorganized mitochondria, mitochondrial cristae were fuzzy and had a cloudy swollen phenotype (arrow), increased volume of mitochondria. MI mitochondria; MF myofibril; Z z-bands; Dic Discus intercalatis

Lapatinib decreased left ventricle function

Cardiac function tests, determined by gated SPECT/CT, showed increases in ESV after lapatinib alone (34 and 16 % increase for direct and delayed schedules) (Figure 9). Similar increases in EDV were seen (11 and 9 % for direct and delayed schedules) (data not shown). This resulted in decreased EF (22 and 9 % decreases after direct and delayed lapatinib) (Figure 9). PFR, maximum down slope of left-ventricular volume, also showed significant decrease after lapatinib treatment (20 and 21 % after direct and delayed lapatinib) (Figure 9). Neither 14 Gy nor 3x4 mg/kg Dox induced significant changes in cardiac function, either given alone or in combination with lapatinib.

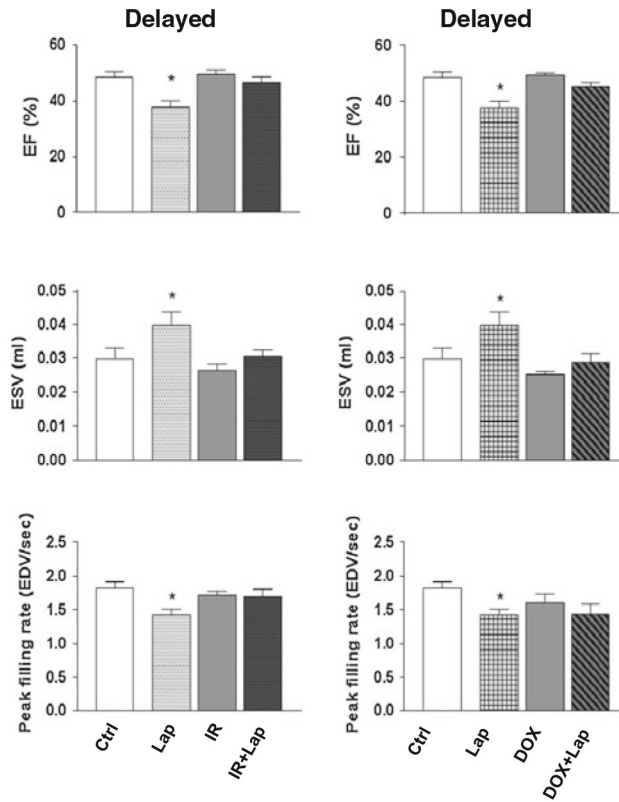


FIGURE 9 Cardiac function (EF, ESV, and PFR) measured by gated SPECT at 40 weeks after treatment with irradiation or doxorubicin alone or in combination with lapatinib or sham treatment. Values represent mean \pm SEM (8–14 mice in each treatment group), * $p < 0.05$ compared to age-matched untreated controls. Ctrl control; Lap lapatinib; DOX doxorubicin; DOX+Lap doxorubicin combined with lapatinib; IR irradiation; IR+Lap irradiation combined with lapatinib

Discussion

In this study, we investigated the effect of direct and delayed inhibition of EGFR signaling combined with irradiation or Dox on cardiomyocyte survival, morphological damage, and heart function. We demonstrated that inhibiting ErbB2 in combination with irradiation or anthracyclines did not further decrease myocyte cell viability *in vitro*. Combined inhibition of ErbB1 and ErbB2 also did not enhance radiation or Dox induced cardiac damage in mice. Indeed, the radiation-induced inflammatory responses were inhibited by lapatinib.

Inhibition of ErbB2 in HER2-overexpressing breast cancers became a standard (adjuvant) treatment as it results in improvement of outcome (18). Often this is combined with anthracycline CT (19). In addition, most patients receive adjuvant RT, either after breast conserving surgery or mastectomy (20). Previous studies have shown an increase in cardiac events after combining RT with anthracyclines, such as decline in LVEF or congestive heart failure (11, 13, 21). Long term follow up studies with ErbB2 inhibiting agents combined with these modalities are ongoing to determine both efficacy and safety, especially with regard to cardiac toxicity (ALTO study; BIG 2-06/N063D).

EGFR signaling, including ligand NRG-1, plays an important role in adult cardiomyocyte survival, since it activates the pro-survival PI3K/pathway and stimulates cardiomyocyte maintenance and function (22). Previous studies in our lab, demonstrated the ability of the mouse heart to compensate functionally for significant structural damage after previous irradiation (17). Compensatory mechanisms and pro-survival pathways might play a role in maintaining cardiomyocyte function in a damaged heart, at least until the extent of damage overwhelms the potential for stimulated survival. Sridharan et al. (16) recently demonstrated upregulation of ErbB signaling in the irradiated rat heart in parallel with developing cardiac fibrosis, leading to the suggestion that ErbB signaling and pro-survival pathways are activated in an attempt to regenerate the myocardium. Moreover, inactivation of ErbB4 in ventricular muscle cells led to a severe dilated cardiomyopathy, demonstrating the important role of ErbB signaling in the myocardium (23).

This raises the question of whether inhibition of these pathways could impair attempts of the damaged heart to regenerate. Similar to the findings of Sridharan et al. (16), we found increased expression of both ErbB2 and ErbB4 in mouse hearts at 40 weeks after irradiation, in parallel with developing fibrosis. However, this upregulation was not inhibited in the presence of lapatinib. Our data also do not indicate cardiac dysfunction after radiation alone or in combination with lapatinib, in contrast to the mild but significant changes in cardiac function after lapatinib alone (Figure 9). These data are consistent with the important role of ErbB signaling to maintain myocardium functionality and imply that that this compensatory mechanisms initiated by irradiation still operate in the presence of lapatinib.

Treatment of adult human cardiomyocytes, which have low expression of HER2, with trastuzumab, did not alter cell viability, nor did it enhance toxicity induced by either radiation or Dox (Figure 2). This is consistent with the knowledge that anthracyclines cause acute irreversible damage to the cardiomyocytes through generation of free radicals and

cardiomyocyte apoptosis (24), whereas trastuzumab-induced cardiac toxicity is dose-dependent and largely reversible (25). The doses of trastuzumab we used were sufficient to cause significant reduction in viability in HER2-overexpressing tumor cells (data not shown), but the cardiomyocytes were less sensitive to ErbB2 inhibition. Some studies, using HER2-overexpressing breast cancer cells, have shown that inhibition of PI3K -pathway may be bypassed by lateral activation of other members of the HER family (Her3) (26, 27). This raises the possibility, that activation of this compensatory feedback loop could thereby stimulate survival of cardiomyocytes.

Our in vitro results contrast somewhat with a recently published study by Hasinoff et al., in which pretreatment of isolated neonatal rat cardiac myocytes with HER1/HER2 inhibitor lapatinib potentiated doxorubicin-induced myocyte damage, assessed by LDH release and disrupted sarcomeres, although there was no enhancement of doxorubicin-induced apoptosis. A major difference between our study and that of Hasinoff is that they used neonatal cardiomyocytes and neuregulin is essential for the developing heart, which probably increases cardiomyocyte sensitivity to ErbB2 inhibition. In our study, we investigated the effects of trastuzumab (ErbB2 inhibitor) on adult cardiomyocyte survival after Dox or irradiation. We did not look at changes in cardiomyocyte function or morphology in vitro. However, our EM study from In vivo experiments would suggest enhanced cardiomyocyte damage from the combination of lapatinib and Dox, consistent with the data of Hasinoff.

Our findings suggest that trastuzumab or lapatinib induced cardiac toxicity acts by different mechanisms than anthracyclines or radiation. This raises the possibility that the cardiac toxicity seen in clinical studies where ErbB2 inhibition is combined with anthracyclines could be due to indirect effects, for example endothelial cell dysfunction and loss, with secondary damage to the cardiomyocytes.

We have previously shown (17) that local cardiac irradiation induces microvascular loss and damage. The current study shows that irradiation-induced endothelial dysfunction and loss was not further enhanced by lapatinib, either when given at the time of irradiation (direct) or delayed for 20 weeks. Mechanisms of radiation-induced cardiac toxicity include activation of TGF β and production of chemokines and pro-inflammatory cytokines, which are largely independent of the PI3K-pathway determining cardiomyocyte survival. However, the MAPK pathway has been implicated in regulation of permeability in endothelial cells (28), something we found to be increased by irradiation. These observations are consistent with the concept that mechanisms of radiation-induced cardiac damage do not involve ErbB signaling.

Slow turnover tissues, like the myocardium, have a low proliferative capacity and a small

stem-cell component, and therefore have a limited ability to repair damage. Radiation-induced cardiac toxicity is initiated by an acute inflammatory response, which progresses to fibrosis without proper tissue regeneration (29). We found that the inflammatory response initially activated by irradiation was decreased by lapatinib. We can speculate that, since the MAPK pathway mediates myocardial pro-inflammatory cytokine production, inhibiting MAPK pathway with lapatinib may decrease the pro-inflammatory cytokine production (30, 31). However, we have no data to support this hypothesis.

A further consequence of irradiation is the development of fibrosis. Similar to previous studies, our study showed increased cardiac fibrosis after irradiation or Dox alone. However, this was not further enhanced by lapatinib. On the other hand, 20 weeks of lapatinib alone in the direct set up induced fibrosis in mice sacrificed at 40 weeks. This is in contrast to no increase in fibrosis when lapatinib was delayed until 20 weeks and continued until sacrifice at 40 weeks. This might be explained by the delayed fibrotic response of the myocardium, which required time to develop after cessation of the lapatinib. We did not evaluate mice at later follow-up times than 40 weeks.

Changes in the microvasculature after Dox alone or with lapatinib were not seen. Nevertheless, fibrosis and degenerated cardiomyocytes (EM study) and 27–36 % animal lethality, as well as decreased cell viability in vitro, do indicate doxorubicin-induced damage to the myocardium via cardiomyocytes. Although anthracyclines induce acute damage, clinical symptoms are mostly detectable months or years after treatment (32). Therefore, besides acute myocardial damage, late and indirect microvascular damage may occur at later times.

We conclude that ErbB2 inhibition did not enhance direct radiation or anthracyclines toxicity of cardiomyocytes in vitro. Radiation-induced microvascular damage was not further enhanced by ErbB2 inhibition and the inflammatory response was decreased. Myocardial damage was induced by anthracyclines but not further enhanced by ErbB2 inhibition. Treatment of mice with the ErbB 1/2- blocking agent lapatinib did not further enhance the risk of radiation or anthracycline-induced cardiac toxicity up to 40 weeks after treatment.

Acknowledgments

The authors would like to thank Bert Pool, Department of Nuclear Medicine, The Netherlands Cancer Institute, for help with the NanoSPECT/CT and Dr. Jack Cleutjens, Department of Pathology, University of Maastricht, for help with the Leica Qwin morphometry system. Our thanks go to Hans Janssen and Nico Ong, Division of Cell Biology, The Netherlands Cancer Institute, for their expertise in electron microscopy. Moreover, we would like to thank Antsje

Nolles and Sjoers van der Horst for their technical assistance regarding in vitro experiments and real-time PCR analysis.

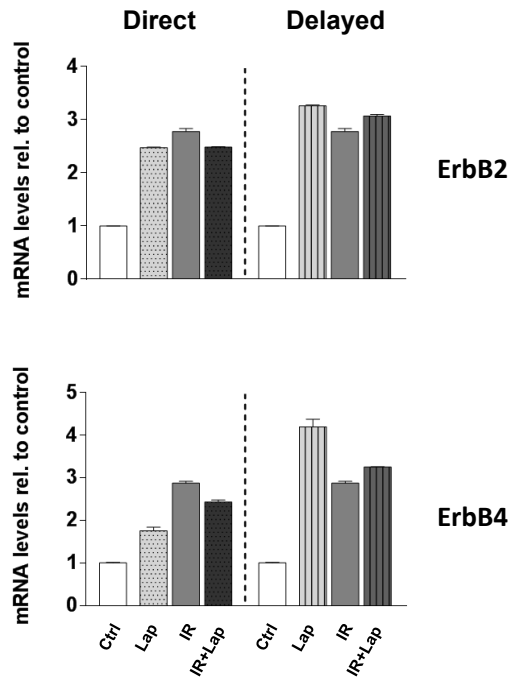
Conflict of interest

The authors declare that they have no conflict of interest.

Open Access

This article is distributed under the terms of the Creative Commons Attribution Noncommercial License which permits any noncommercial use, distribution, and reproduction in any medium, provided the original author(s) and the source are credited.

Supplemental data



Supplemental Figure 1 Expression of genes involved in ErbB2 signaling measured by RT PCR. Each bar represents the average expression per group \pm SEM. Values of sham-treated animals were set to 1. The graph show the fold-change in gene expression in treated mice relative to respective controls at 40 (n = 8) weeks after treatment.

Table S1 Body and organ weights of mice at sacrifice.

| Treatment | Body weight (g) | Heart weight (g) | Heart/body weight (g) |
|------------------------|------------------------|-------------------------|------------------------------|
| Control | 35.53 ± 1.8 | 0.19 ± 0.02 | 5.64 ± 0.7 |
| IR | 33.83 ± 2.2* | 0.17 ± 0.01* | 5.05 ± 0.5 |
| IR + direct lapatinib | 34.7 ± 1.0 | 0.19 ± 0.02 | 5.13 ± 0.4 |
| IR + delayed lapatinib | 34.9 ± 2.6 | 0.18 ± 0.01 | 5.15 ± 0.5 |
| Direct lapatinib | 33.8 ± 3.0 | 0.18 ± 0.02 | 5.39 ± 0.8 |
| Delayed lapatinib | 35.9 ± 2.0 | 0.2 ± 0.04 | 5.7 ± 1.5 |

* indicates significant differences between irradiated and age-matched control groups ($p > 0.05$; Mann-Whitney U-test).

Table S2 Body and organ weights of mice at sacrifice.

| Treatment | Body weight (g) | Heart weight (g) | Heart/body weight (g) |
|-------------------------|------------------------|-------------------------|------------------------------|
| Control | 35.53 ± 1.8 | 0.19 ± 0.02 | 5.64 ± 0.7 |
| DOX | 31.2 ± 2.5* | 0.17 ± 0.01* | 5.4 ± 0.3 |
| DOX + direct lapatinib | 30.7 ± 1.9* | 0.16 ± 0.01* | 5.3 ± 0.3 |
| DOX + delayed lapatinib | 29.3 ± 1.7* | 0.16 ± 0.01* | 5.7 ± 0.5 |
| Direct lapatinib | 33.8 ± 3.0 | 0.18 ± 0.02 | 5.39 ± 0.8 |
| Delayed lapatinib | 35.9 ± 2.0 | 0.2 ± 0.04 | 5.7 ± 1.5 |

* indicates significant differences between irradiated and age-matched control groups ($p < 0.05$; Mann-Whitney U-test).

References

1. Bovelli D, Plataniotis G, Roila F (2010) Cardiotoxicity of chemotherapeutic agents and radiotherapy-related heart disease: ESMO clinical practice guidelines. *Ann Oncol* 21(Suppl 5):v277–v282
2. Marks LB, Yu X, Prosnitz RG, Zhou SM, Hardenbergh PH et al (2005) The incidence and functional consequences of radiotherapy-associated cardiac perfusion defects. *Int J Radiat Oncol Biol Phys* 63:214–223
3. Prosnitz RG, Hubbs JL, Evans ES, Zhou SM, Yu X et al (2007) Prospective assessment of radiotherapy-associated cardiac toxicity in breast cancer patients: analysis of data 3 to 6 years after treatment. *Cancer* 110:1840–1850
4. Lind PA, Pagnanelli R, Marks LB, Borges-Neto S, Hu C et al (2003) Myocardial perfusion changes in patients irradiated for left-sided breast cancer and correlation with coronary artery distribution. *Int J Radiat Oncol Biol Phys* 55:914–920
5. Nahta R, Hortobagyi GN, Esteva FJ (2003) Growth factor receptors in breast cancer: potential for therapeutic intervention. *Oncologist* 8:5–17
6. Allred DC, Clark GM, Tandon AK, Molina R, Tormey DC et al (1992) HER-2/neu in node-negative breast cancer: prognostic significance of overexpression influenced by the presence of in situ carcinoma. *J Clin Oncol* 10:599–605
7. Xue C, Wyckoff J, Liang F, Sidani M, Violini S et al (2006) Epidermal growth factor receptor overexpression results in increased tumor cell motility *In vivo* coordinately with enhanced intravasation and metastasis. *Cancer Res* 66:192–197
8. Vogel CL, Cobleigh MA, Tripathy D, Gutheil JC, Harris LN et al (2002) Efficacy and safety of trastuzumab as a single agent in first-line treatment of HER2-overexpressing metastatic breast cancer. *J Clin Oncol* 20:719–726
9. Tan M, Yu D (2007) Molecular mechanisms of erbB2-mediated breast cancer chemoresistance. *Adv Exp Med Biol* 608:119–129
10. Joensuu H, Kellokumpu-Lehtinen PL, Bono P, Alanko T, Kataja V et al (2006) Adjuvant docetaxel or vinorelbine with or without trastuzumab for breast cancer. *N Engl J Med* 354:809–820
11. Romond EH, Perez EA, Bryant J, Suman VJ, Geyer CE Jr et al (2005) Trastuzumab plus adjuvant chemotherapy for operable HER2-positive breast cancer. *N Engl J Med* 353:1673–1684
12. Feldman AM, Lorell BH, Reis SE (2000) Trastuzumab in the treatment of metastatic breast cancer: anticancer therapy versus cardiotoxicity. *Circulation* 102:272–274
13. Perez EA, Koehler M, Byrne J, Preston AJ, Rappold E et al (2008) Cardiac safety of lapatinib: pooled analysis of 3689 patients enrolled in clinical trials. *Mayo Clin Proc* 83:679–686
14. De Keulenaer GW, Doggen K, Lemmens K (2010) The vulnerability of the heart as a pluricellular paracrine organ: lessons from unexpected triggers of heart failure in targeted ErbB2 anticancer

- therapy. *Circ Res* 106:35–46
15. Zhao YY, Sawyer DR, Baliga RR, Opel DJ, Han X et al (1998) Neuregulins promote survival and growth of cardiac myocytes. Persistence of ErbB2 and ErbB4 expression in neonatal and adult ventricular myocytes. *J Biol Chem* 273:10261–10269
 16. Sridharan V, Sharma SK, Moros EG, Corry PM, Tripathi P et al (2013) Effects of radiation on the epidermal growth factor receptor pathway in the heart. *Int J Radiat Biol* 89(7):539–547
 17. Seemann I, Gabriels K, Visser NL, Hoving S, te Poele JA et al (2012) Irradiation induced modest changes in murine cardiac function despite progressive structural damage to the myocardium and microvasculature. *Radiother Oncol* 103:143–150
 18. Mitri Z, Constantine T, O'Regan R (2012) The HER2 receptor in breast cancer: pathophysiology, clinical use, and new advances in therapy. *Chemother Res Pract* 2012:743193
 19. Slamon DJ, Leyland-Jones B, Shak S, Fuchs H, Paton V et al (2001) Use of chemotherapy plus a monoclonal antibody against HER2 for metastatic breast cancer that overexpresses HER2. *N Engl J Med* 344:783–792
 20. Halyard MY, Pisansky TM, Dueck AC, Suman V, Pierce L et al (2009) Radiotherapy and adjuvant trastuzumab in operable breast cancer: tolerability and adverse event data from the NCCTG Phase III Trial N9831. *J Clin Oncol* 27:2638–2644
 21. Tan-Chiu E, Yothers G, Romond E, Geyer CE Jr, Ewer M et al (2005) Assessment of cardiac dysfunction in a randomized trial comparing doxorubicin and cyclophosphamide followed by paclitaxel, with or without trastuzumab as adjuvant therapy in node-positive, human epidermal growth factor receptor 2-overexpressing breast cancer: NSABP B-31. *J Clin Oncol* 23:7811–7819
 22. Lemmens K, Doggen K, De Keulenaer GW (2007) Role of neuregulin-1/ErbB signaling in cardiovascular physiology and disease: implications for therapy of heart failure. *Circulation* 116:954–960
 23. Garcia-Rivello H, Taranda J, Said M, Cabeza-Meckert P, Vila-Petroff M et al (2005) Dilated cardiomyopathy in Erb-b4-deficient ventricular muscle. *Am J Physiol Heart Circ Physiol* 289:H1153–H1160
 24. Doroshow JH (1983) Effect of anthracycline antibiotics on oxygen radical formation in rat heart. *Cancer Res* 43:460–472
 25. Ewer MS, Vooletich MT, Durand JB, Woods ML, Davis JR et al (2005) Reversibility of trastuzumab-related cardiotoxicity: new insights based on clinical course and response to medical treatment. *J Clin Oncol* 23:7820–7826
 26. Garrett JT, Olivares MG, Rinehart C, Granja-Ingram ND, Sanchez V et al (2011) Transcriptional and posttranslational up-regulation of HER3 (ErbB3) compensates for inhibition of the HER2 tyrosine kinase. *Proc Natl Acad Sci USA* 108:5021–5026

27. Serra V, Scaltriti M, Prudkin L, Eichhorn PJ, Ibrahim YH et al (2011) PI3K inhibition results in enhanced HER signaling and acquired ERK dependency in HER2-overexpressing breast cancer. *Oncogene* 30:2547–2557
28. Kevil CG, Oshima T, Alexander B, Coe LL, Alexander JS (2000) H₂O₂-mediated permeability: role of MAPK and occludin. *Am J Physiol Cell Physiol* 279:C21–C30
29. Brush J, Lipnick SL, Phillips T, Sitko J, McDonald JT et al (2007) Molecular mechanisms of late normal tissue injury. *Semin Radiat Oncol* 17:121–130
30. Craig R, Larkin A, Mingo AM, Thuerlauf DJ, Andrews C et al (2000) p38 MAPK and NF-kappa B collaborate to induce interleukin-6 gene expression and release. Evidence for a cytoprotective autocrine signaling pathway in a cardiac myocyte model system. *J Biol Chem* 275:23814–23824
31. Meldrum, Dinarello CA, Cleveland JC, Cain BS, Shames BD et al (1998) Hydrogen peroxide induces tumor necrosis factor alpha-mediated cardiac injury by a P38 mitogen-activated protein kinase-dependent mechanism. *Surgery* 124:291–296 discussion 297
32. Swain SM (2008) Cardiovascular complications of breast cancer therapy. *Clin Adv Hematol Oncol* 6(247–248):282



Chapter 5

Endoglin haplo-insufficiency modifies the inflammatory response in irradiated mouse hearts without affecting structural and microvascular changes

I. Seemann, J. A.M. te Poele, S. J. Luikinga, S. Hoving, F. A. Stewart

PLoS One July 2013

Abstract

Background: It is now widely recognized that radiotherapy of thoracic and chest wall tumors increases the long-term risk of cardiovascular damage although the underlying mechanisms are not fully elucidated. There is increasing evidence that microvascular damage is involved. Endoglin, an accessory receptor for TGF- β 1, is highly expressed in damaged endothelial cells and may play a crucial role in cell proliferation and revascularization of damaged heart tissue. We have therefore specifically examined the role of endoglin in microvascular damage and repair in the irradiated heart.

Materials and Methods: A single dose of 16 Gy was delivered to the heart of adult Eng^{+/+} or Eng^{+/-} mice and damage was evaluated at 4, 20 and 40 weeks, relative to age-matched controls. Gated single photon emission computed tomography (gSPECT) was used to measure cardiac geometry and function, and related to histo-morphology, microvascular damage (detected using immuno- and enzyme-histochemistry) and gene expression (detected by microarray and real time PCR).

Results: Genes categorized according to known inflammatory and immunological related disease were less prominently regulated in irradiated Eng^{+/-} mice compared to Eng^{+/+} littermates. Fibrosis related genes, TGF- β 1, ALK 5 and PDGF, were only upregulated in Eng^{+/+} mice during the early phase of radiation-induced cardiac damage (4 weeks). In addition, only the Eng^{+/+} mice showed significant upregulation of collagen deposition in the early fibrotic phase (20 weeks) after irradiation. Despite these differences in gene expression, there was no reduction in inflammatory invasion (CD45+cells) of irradiated Eng^{+/-} hearts. Microvascular damage (microvascular density, alkaline phosphatase and von-Willebrand-Factor expression) was also similar in both strains.

Conclusion: Eng^{+/-} mice displayed impaired early inflammatory and fibrotic responses to high dose irradiation compared to Eng^{+/+} littermates. This did not result in significant differences in microvascular damage or cardiac function between the strains.

Introduction

Nearly 5 million long-term cancer survivors were registered in 2007 in the United States alone and at least half of these patients underwent radiotherapy as part of their cancer treatment. Although radiotherapy is an effective cancer treatment, it can contribute to late toxicity in surrounded normal tissue. Much work has been done to reduce the risk of late normal tissue toxicity induced by radiotherapy over the last decade, including modified fractionation schedules and conformal image-guided-radiotherapy (IGRT). Moreover, knowledge about the molecular mechanisms underlying the development of normal tissue toxicity after radiotherapy is increasing and this should eventually help in designing methods to prevent or treat normal tissue toxicity. Nevertheless, little is known of the underlying molecular mechanism of radiation-induced cardiac toxicity in thoracic cancer patients.

We and others (1,2,3) previously demonstrated that high dose cardiac irradiation induces microvascular damage and capillary loss, eventually leading to fibrosis. Radiation-induced fibrosis, defined by excessive fibroblast proliferation, myofibroblast differentiation and overproduction of extracellular matrix, is predominantly induced by activated Transforming Growth Factor- β 1 (TGF- β 1) (4). TGF- β 1 has been defined as the master switch in the fibrotic program and it acts on at least three different biological activities: regulation and inhibition of cell growth; immunosuppressive activities; and regulation of extracellular matrix component deposition (5). Numerous studies have shown correlations between increased severity in radiation-induced normal tissue toxicity and TGF- β 1 signal activation (6,7,8). For regulation of endothelial function by TGF- β 1, signaling of type I receptors ALK1 and ALK5 are the most important. Regulated (R-) Smads, phosphorylated by type I receptors, form heteromeric complexes and these accumulate in the nucleus where they regulate the transcription of specific target genes (9). Endoglin, a co-receptor for TGF- β 1, is highly expressed in proliferating endothelial cells and plays a crucial role in angiogenesis. Since endoglin has no kinase domain itself, it promotes TGF- β 1 signaling through ALK1 receptor to promote cell proliferation and migration (10,11,12). Mice that are deficient in endoglin die in mid-gestation due to vascular and cardiovascular defects. Moreover, mice carrying a single copy of the endoglin gene show a tendency to develop hereditary hemorrhagic telangiectasia (HHT) phenotype as they age, with extensive dilated and weak-walled vessels (13,14). Disease prevalence depends on the genetic background of the mice (7% in C57Bl/6 and 72% in Ola mice age 1 year). This phenotype is similar to radiation-induced microvascular damage, which raises the question of whether endoglin may also play a crucial role in radiation-induced cardiac injury. To explore this, we used a model of radiation-induced cardiac injury in Eng^{+/-} mice and compared this to damage in wild type littermates.

Materials and Methods

Mice and irradiation procedure

Eng^{+/-} C57BL/6 mice were originally obtained from H. Arthur (Institute of Human genetics, International Centre for Life, Newcastle upon Tyne, UK) and subsequently bred in the Netherlands Cancer Institute. Male Eng^{+/+} mice and Eng^{+/-} littermates aged 8-12 weeks were randomly allocated (after genotyping by PCR) to receive 16 Gy or 0 Gy to the heart. Mice were housed in a temperature-controlled room with 12 hour light-dark cycle. Standard mouse chow and water were provided *ad libitum*. Irradiation was performed with 250kV X-rays, operating at 12 mA and filtered with 0.6mm Copper. The dose rate was 0.94 Gy/min with a field size of 10.6x 15mm (including up to 30% lung volume) and the rest of the mouse was shielded with lead. Unanesthetized mice were immobilized in a prone position in acrylic perspex jigs. Separate cohorts of animals were included for analyses at 4, 20 and 40 weeks after irradiation, with age-matched controls (sham irradiated with 0 Gy). Each cohort typically comprised 10 to 15 mice (n=130 in total). This study was in agreement with the Dutch law on animal experiments and welfare by which the Animal Experiments Committee (AEC) of the Netherlands Cancer Institute has evaluated the set-up of the experiments and has given a positive recommendation (Permit number: 08008-1990) and in line with the international *Guide for the Care and Use of Laboratory Animals* (Eighth edition). No severe suffering was anticipated in this study. If mice appeared distressed, or lost >15% body weight, they were humanely sacrificed before the planned follow-up time. At termination of the experiment, mice were humanely sacrificed under lethal sodium pentobarbital anesthesia (18 mg per mouse, i.p).

Gene expression profiling and pathway analysis

Total RNA was isolated from frozen sections (30 sections of 30 µm per mouse and 4-7 mice per group) of the mid part of the heart using Trizol[®] Reagent (Invitrogen Corporation, Carlsbad, USA), according to the manufacturer's protocol. The quantity of total RNA was measured using a spectrophotometer (NanoDrop, Thermo scientific, Wilmington, USA) followed by a quality check measured by a Agilent 2100 Bioanalyzer with the RNA Integrity Number (RIN) (Agilent technologies, Santa Clara, USA). Samples with a RIN above 7 were used for DNase treatment and amplified (350 ng per sample) using Illumina Totalprep RNA Amplification kit (Ambion, Grand Island, USA). Before hybridization, individual RNA was pooled for each treatment group. Hybridization of aRNA to Illumina Expression Bead Chips Mouse Whole Genome (WG-6 vs. 2.0) and subsequent washing, blocking and detecting were performed

according to the manufacturer's protocol (Illumina, San Diego, USA). Samples were scanned on the IlluminaR BeadArray™ 500GX Reader using IlluminaR BeadScan image data acquisition software (version 2.3.0.13). MouseWG-6 vs. 2.0 BeadChip contains the full set of MouseRef-8 BeadChip probes with additional 11.603 probes from RIKEN FANTOM2, NCBI RefSeq as well from the MEEBO database.

Before analyzing, the database was normalized using robust spline normalization method within the microarray facility of the Netherlands Cancer Institute. Log² ratio between expression of genes from control mice and expression of genes from irradiated mice were calculated using Excel version 2003, as well as the sum of the expression of genes from both, control and irradiated mice. According to the sum of both expressions, genes with sums below 6 were discarded. The threshold for standard deviation (SD) was set to 3 and mean \pm nSD was calculated to identify genes that are above expression 6 and above threshold 3 of SD. These genes were further analyzed in Ingenuity Pathway Analysis (IPA) version September 2011 core analysis. IPA calculates a significant score for each associated network. This score indicates the likelihood that the assembly of a set of focus genes in a network could be explained by random chance alone. Networks with scores of 2 or higher have at least a 99% confidence of not being generated by random chance alone. For individual gene expression profiling, RNAs of each treatment group were individually transversely transcribed into cDNA. Expression of genes of interest was detected by qPCR with SYBR Green (Applied Biosystems, Carlsbad, USA). Changes in gene expression were analyzed with the comparative Δ Ct method and corrected for the expression of the housekeeping gene GAPDH. Primers used to detect changes in gene expression are listed in the Supplemental Table 1.

Tissue preparation for histology

At termination of the experiment, the heart was perfused via the aortic arch (retro-grade), under lethal sodium pentobarbital anesthesia (18 mg per mouse, i.p), with PBS (frozen sections) or PBS followed by 1% paraformaldehyde (paraffin sections). The heart was then quickly excised before freezing on dry ice or immersion in 1% paraformaldehyde.

Cross-sections were cut at the level of the mid-horizontal plane of the heart from fixed paraffin-embedded tissues (4 μ m) or frozen tissues (7 μ m).

Paraffin sections: Transverse sections were stained with hematoxylin and eosin (H&E) to measure the epicardial and myocardial thickness. To determine the extent of inflammation, sections were immuno-labeled with anti-CD45 antibody (1:400, Becton&Dickinson, Franklin lakes, USA). Perls'-staining was performed as indicator of previous hemorrhage. Based

on a Sirius red staining, interstitial collagen was determined in the subendocardium and myocardium of the left ventricle (LV). Within one follow-up time all sections were processed identically, at the same time with precisely the same incubation times for the primary and secondary antibody and diaminobenzidine (DAB) solution (Sigma, Zwijndrecht, the Netherlands). Therefore, all differences between the treatments are ultimately due to DAB identification of the relevant protein.

Photographs of the LV wall, excluding the septum, were taken using a 5x objective (Leica DFC320) and 12 measurements per heart were performed for the epicardial and myocardial thickness. The number of CD45+ cells per section was counted separately in the epicard and myocard to determine the extent of inflammation. Perls' stained sections were examined for evidence of iron-containing macrophages and this was recorded as positive or negative for each section. Interstitial collagen was quantified in five randomly selected areas of the subendocardium and myocardium of the LV (40x objective) and results were expressed as percentage tissue positive for Sirius red relative to myocardial area. Morphometric parameters were analyzed using a computerized morphometry system (Leica Qwin V3, Leica, Rijswijk, the Netherlands).

Frozen sections: An anti-CD31 antibody (1:50, Becton&Dickinson) was used to visualize cardiac vasculature of the central part of the heart. To determine functional changes in the microvasculature, a histochemical staining with Naphtol AS-MX / DMF and fast Blue BB salt was performed to detect endothelial cell alkaline phosphatase. Sections were also reacted with antibodies against von Willebrand Factor (vWF) (1:4000, Abcam, Cambridge, USA) as a marker of thrombotic changes. Within one time group all sections were processed identically, at the same time with precisely the same incubation times for the primary and secondary antibody and DAB solution. A double staining was performed to visualize the vasculature (anti-CD31) and the pericytes coverage (anti-NG2, 1:200, Chemicon, Temecula, CA). Primary antibodies were visualized with Alexa Fluor (AF) 633 (1:100, Invitrogen, Carlsbad, CA) and AF568 (1:250, Invitrogen).

For quantification of microvessels, five random fields (40x objective) from transverse sections of the subendocardium were photographed with a CCD 2 - Color Microscope system, including a Zeiss AxioCam color camera (AxioCam HRC, Zeiss, Göttingen, Germany), and a computerized morphometry system (Leica Qwin V3) was used to quantify the microvascular density (MVD). Vessels beneath a size of 1.5 or above 200 μm^2 were automatically excluded from the measurements. Photographs of whole sections stained for ALP and vWF were taken with an Aperio scanner (Scanscope-XT, Aperio technologies, Vista, USA) using 40x objective.

Analyses of the percentage myocardium, excluding endocardium, positive for each marker were done with a computerized morphometry system (Leica Qwin V3). Photographs of the fluorescent stainings were performed on a Leica SP5 system microscope (Leitz Wetzlar, Heidelberg, Germany); they were collected individually in the blue and red channels and merged thereafter. An average of 5 photographs were taken around the left ventricle and the pericyte coverage of microvessels was determined by counting NG2⁺/CD31⁺ vessels using a Image J computer analysis program.

Gated SPECT/CT

Gated single photon emission computed tomography (gSPECT) acquisitions were made with the dedicated small-animal NanoSPECT/CT (Bioscan Europe, Ltd., Paris, France). Animals were anesthetized with Hypnorm (Fentanyl 0.26 mg/kg/Fluanisone 8.33 mg/kg, VetaPharma, Ltd., Leeds, UK) and Dormicum (Midazolam, 4.17 mg/kg, Roche, Woerden, the Netherlands) via intraperitoneal (i.p.) injection (1:2:1 Hypnorm:H₂O:Dormicum; 120 µl/mouse). Serum Albumin (HSA) (Vasculosis, IBA Molecular, Gif-sur-Yvette, France) was labeled with 1-1.5 ml ^{99m}Tc-pertechnetate. The radiotracer (150 µl) was injected intravenously (i.v.), with a total activity of about 50 MBq per mouse. Three-lead electrodes (3M red Dot 2282E, 3M, St.Paul, USA) were attached to both hind paws and right front paw of the mouse, placed on the animal bed in the prone position and connected to the integrated electrocardiography (ECG) monitor to measure heart rate (HR). Once a stable HR was established, a short X-ray topogram was made to set the field of view (FOV) and so focus on the thorax to reduce scan time. After the FOV was set, gated SPECT acquisition was started using a quadruple-head gamma camera high precision gantry, equipped with 4 pyramid collimators and 9 pinhole apertures (diameter 1.2 mm). The axial FOV was 16 mm. A 20% window centered on the 140 keV photoelectric peak of ^{99m}Tc was used to acquire 20 projections with uniform angular sampling over a 360° radius into a 128 x 128 matrix Human X-ray topogram and SPECT acquisition were initiated directly after tracer administration. ECG-gated data were recorded in 8 time-bins per cardiac cycle. HiSPECT NG software (InVivoScope, Bioscan) was used to perform iterative reconstruction into 3D-datasets. Quantitative analysis of the reconstructed datasets was performed on a clinical e.soft (*syngo*-based) workstation (Siemens Medical Solutions, Siemens AG, Erlangen, Germany), using algorithms to automatically reconstruct a count based 3D model of the dimensions of the left ventricular (LV) end diastolic and systolic volumes (EDV, ESV). The ejection fraction (EF) was calculated based on the difference between EDV and ESV divided by EDV.

Statistics

Data are expressed as mean \pm SEM and groups were compared using non-parametric Mann–Whitney exact U-tests. Group differences were considered statistically significant at $p < 0.05$. Statistical analyses were performed using SPSS version 20.

Results

Mouse health

There were no significant differences between groups in mean body weight or health, based on genotype or treatment or time-point (Table S2), except a small decrease in heart/bodyweight ratio in irradiated $Eng^{+/-}$ mice after 20 weeks compared to age-matched controls. There was no obvious telangiectasia in external organs (ears, paws) of unirradiated $Eng^{+/-}$ mice at termination of the experiment (maximum follow-up 40 weeks, mice aged 1 year).

Impaired inflammatory response in irradiated hearts of $Eng^{+/-}$ mice at 4 weeks

In order to identify genes and pathways potentially involved in the cardiac response to irradiation in $Eng^{+/-}$ mice versus $Eng^{+/+}$ mice, microarray and pathway analyses were performed using the software program IPA (a full list of gene expression levels after cardiac irradiation of $Eng^{+/-}$ and $Eng^{+/+}$ mice can be found at <http://www.ebi.ac.uk/arrayexpress>). Known ingenuity functional and/or canonical pathway analysis was used to identify over-representation of radiation-correlated genes within known functional assignments (such as inflammatory response) and to generate hypotheses.

The most significantly altered network for $Eng^{+/+}$ mice at 4 weeks after 16 Gy was classed as “behavior/ nervous system development and function”. Immune response regulating genes interferon regulatory factor 7 (IRF7) and chemokine (C-X-C motif) ligand 10 (CXCL10) were identified as central molecules and were significantly upregulated within this top network (Figure 1A). “Inflammatory response” and “immunological disease” were the top functional pathways significantly regulated 4 weeks after cardiac irradiation of $Eng^{+/+}$ mice. This included 47 of the 115 molecules in these analyses (Table 1). The top upregulated genes were sarcolipin (SLN), myosin light chain 7 (MYL7) and myosin light chain 4 (MYL4), all of which are involved in maintaining cardiac contractility and function. Heat shock protein 70 (HSP70), involved in cardiomyocyte protection, was one of the top significantly down regulated genes (Table 2). In contrast, the most significantly altered network for $Eng^{+/-}$ mice at 4 weeks after 16 Gy was classed as “hematological system development and function”. Cell proliferation and cell death-regulating gene E2 transcription factor was the central molecule within this

top network (Figure 1B).

Inflammatory responses and immunological disease were much less prominent in Eng^{+/-} mice than Eng^{+/+} mice at 4 weeks after 16 Gy (Figure 2). Other upregulated functional pathways in Eng^{+/-} mice were “cell-to-cell signaling” and “cell death related pathways” (Table 1). These pathways include significant downregulation of genes related to binding of connective tissue cells and fibroblasts and significant upregulation of genes related to apoptosis of endothelial cells. Interestingly, cardiac function maintaining genes and cardiomyocyte protective genes (SLN, MYL7, MYL4, and HSP70) were oppositely regulated in these two mouse strains (Table 2)

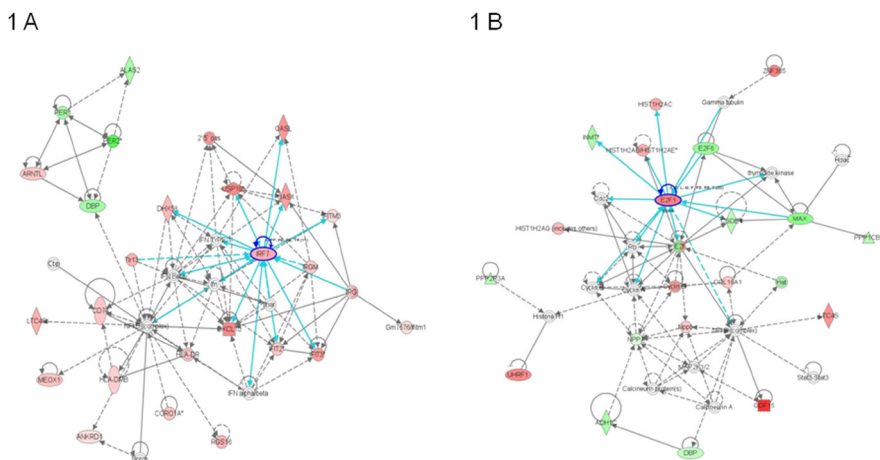


FIGURE 1 Graphical representation of the top networks of differentially regulated genes (4 weeks). Each network symbolizes the biological functions and/or diseases that were most significantly regulated 4 weeks after cardiac irradiation of Eng^{+/+} mice (n=5) (A) and Eng^{+/-} mice (n=4) (B). The genes marked in red represent the upregulated genes and in green the downregulated genes. The solid arrows represent direct interactions and the dotted arrows indirect interactions. Genes circled in dark blue represents central molecules and the light blue lines indicate interaction with other genes.

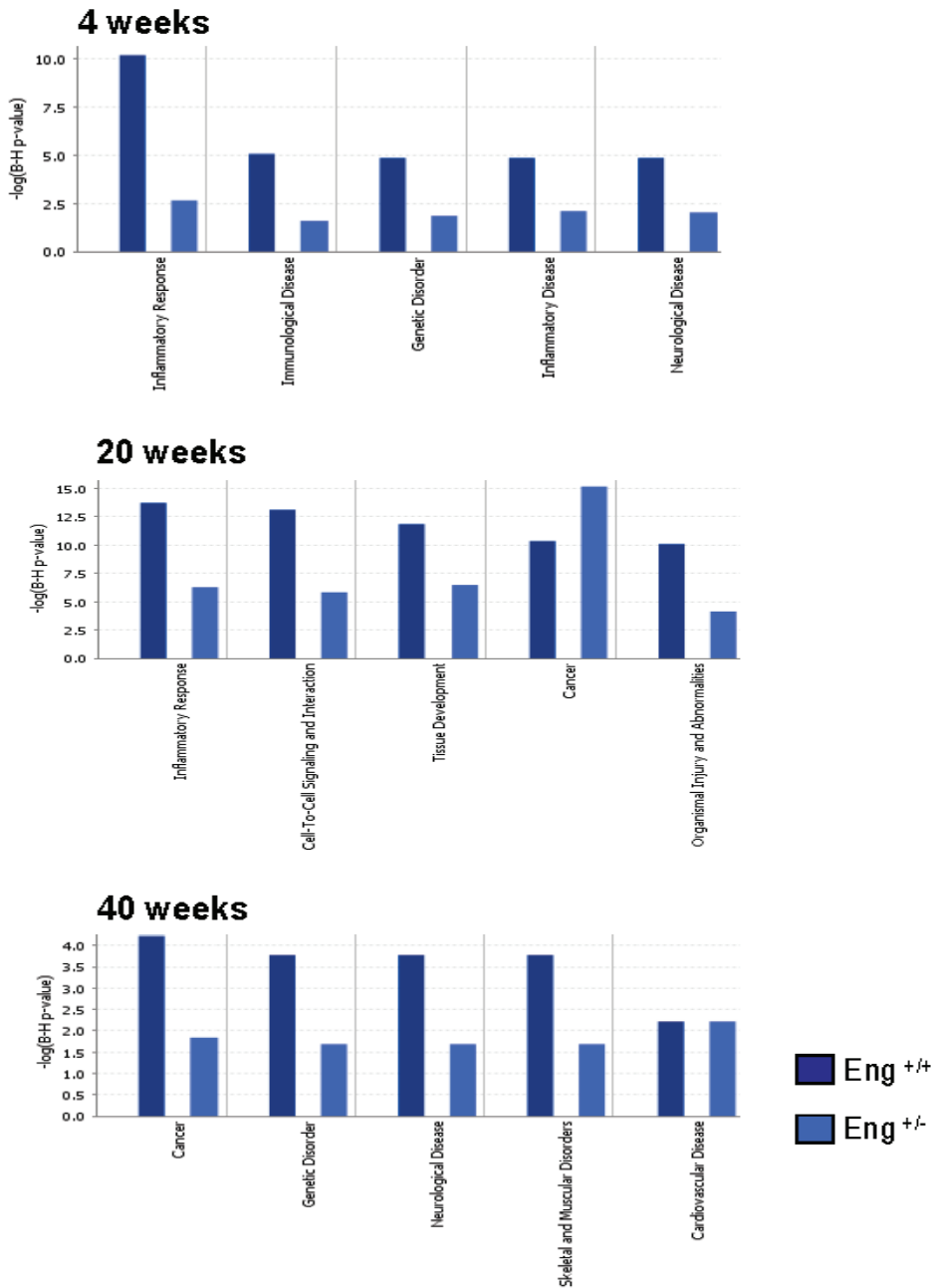


Figure 2 Comparison of top 5 functional pathways from Eng^{+/+} (dark blue) and Eng^{+/-} (light blue), generated by IPA analysis. Bars indicate top networks expressed and y-axis displays the – (log) significance. Taller bars are more significant than shorter bars. P-value display Benjamini-Hochberg multiple testing correction.

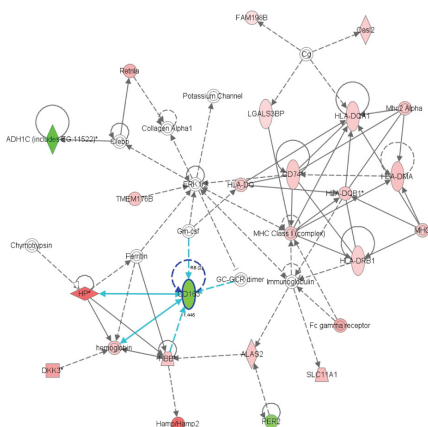
TABLE 1 Representation of the top network and functional pathways using IPA approach.

| | Eng^{+/+} 16 Gy | Eng^{+/-} 16 Gy | Eng^{+/+} 16 Gy | Eng^{+/-} 16 Gy |
|-----------------|--|--|---|--|
| | Network | Network | Functional pathway | Functional pathway |
| <i>4 weeks</i> | Nervous system development and function (51) | Hematological system development and function (36) | 1. Inflammatory response 2. Immunological disease | 1. Cell-to-cell signaling and interaction 2. Cell death |
| <i>20 weeks</i> | Inflammatory response (49) | Inflammatory response (40) | 1. Inflammatory response 2. Cell-to-cell signaling and interaction | 1. Cancer 2. Cardiovascular system development and function |
| <i>40 weeks</i> | Lipid metabolism, Molecular transport (49) | Cellular movement (36) | 1. Cancer 2. Genetic disorder | 1. Tissue development 2. Antigen presentation |

Top networks for 4, 20 and 40 weeks after 16 Gy irradiation of Eng^{+/+} and Eng^{+/-} mice. Numbers in brackets represent the network score, which is explained in material and methods. The first two functional pathways for 4, 20 and 40 weeks after 16 Gy irradiation of Eng^{+/+} and Eng^{+/-} mice are also shown.

The most significantly altered network for Eng^{+/+} mice at 20 weeks after 16 Gy was inflammatory response (Figure 2). Acute phase-regulated receptor and signal-inducing macrophage protein CD163 (downregulated) was one of many central molecules within this network (Figure 3A). As at 4 weeks, Eng^{+/+} mice still showed significant upregulation in inflammatory response, with 55/142 genes in this functional pathway analysis (Table 1). Both complement immune system related gene (CFD) and carbonic anhydrase III (CA3), which are related to cardiac myocyte damage, were significantly upregulated top genes (Table 2). Analysis of Eng^{+/-} hearts at 20 weeks after 16 Gy also indicated inflammatory response as the top network. However, the score of this network was lower than in Eng^{+/+} mice (Figure 2) and inflammation did not emerge as one of the top functional pathways (Table 1). Central molecules within this network were interferon regulatory factor 7 (IRF7), beta-2-microglobulin (B2M) and CHEMOKINE complex (Figure 3B). Top upregulated genes indicated endothelial disorder (endothelial cell-specific molecule 1 (ESM1)) (Table 2).

3 A



3 B

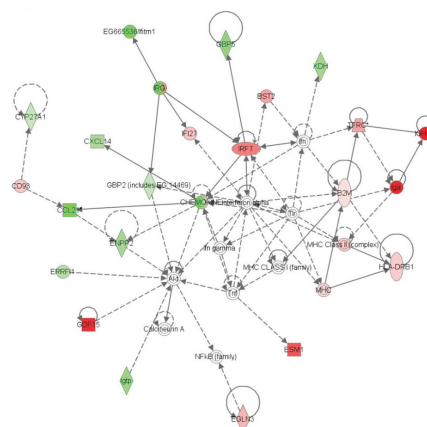
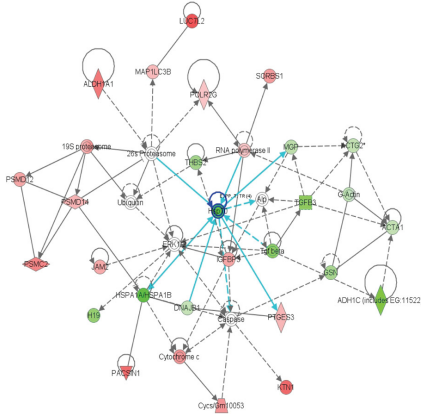


FIGURE 3 Graphical representation of the top network of differentially regulated genes (20 weeks). Each network symbolizes the biological functions and/or diseases that were most significantly regulated 20 weeks after cardiac irradiation of $Eng^{+/+}$ mice ($n=4-5$) (A) and $Eng^{-/-}$ mice ($n=5$) (B). The genes marked in red represent the upregulated genes and in green the downregulated genes. The solid arrows represent direct interactions and the dotted arrows indirect interactions. Genes circled in dark blue represents central molecules and the light blue lines direct interaction with other genes.

The most significantly altered network for $Eng^{+/+}$ mice at 40 weeks after 16 Gy was “lipid metabolism and molecular transport”, with cardiomyocyte protective gene HSP70 as the central molecule (Figure 4A). HSP70 was also one of the top downregulated genes, indicating a lack of cardiomyocyte protection (Table 2). “Neurological disorder” and “cardiovascular disease” were two of the top functional pathways (Figure 2), both containing adrenergic, beta-1, receptor (ADRB1). ADRB1, which stimulates smooth muscle contraction and promotes increased contractility and heart rate, was significantly upregulated (Table 1). Inflammatory response was no longer detected at 40 weeks after irradiation. Top network for $Eng^{+/-}$ mice at 40 weeks after 16 Gy was “cellular movement”. Two central molecules were involved within this network; myosin light chain (MLC) and chemokine (C-X-C motif) ligand 12 (CXCL12), and both were significantly upregulated (Figure 4B). Furthermore, many cardiac contractile stimulating genes were involved in this network (MYL7, MYL4, MYH6, tensin-1, titin and myosin). Again, the top upregulated genes were involved in cardiac contractility (SLN, MYL7) (Table 2). Inflammatory response and immunological disease were not within the top functional pathways at 40 weeks after 16 Gy but neurological disease, muscle disorder and cardiovascular disease were (Figure 2). Neurological disease and muscle disorder were

more pronounced in Eng^{+/+} mice than to Eng^{+/-} mice. Cardiovascular disease was equally upregulated within both strains (Figure 2).

4 A



4 B

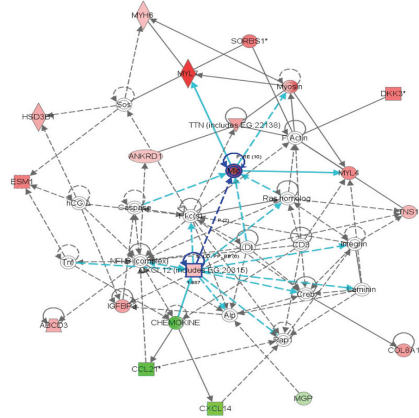


FIGURE 4 Graphical representation of the top network of differentially regulated genes (40 weeks). Each network symbolizes the biological functions and/or diseases that were most significantly regulated 40 weeks after cardiac irradiation of Eng^{+/+} mice (n=4-5) (A) and Eng^{+/-} mice (n=4-7) (B). The genes marked in red represent the upregulated genes and in green the downregulated genes. The solid arrows represent direct interactions and the dotted arrows indirect interactions. Genes circled in dark blue represents central molecules and the light blue lines direct interaction with other genes.

TABLE 2 Representation of differentially regulated genes after 16 Gy irradiation using IPA approach..

| | Eng ^{+/+} 16 Gy | | Eng ^{+/-} 16 Gy | | Eng ^{+/+} 16 Gy | | Eng ^{+/-} 16 Gy | |
|----------|--------------------------|-------|--------------------------|-------|--------------------------|--------|--------------------------|--------|
| | Top upregulated genes | | Top upregulated genes | | Top downregulated genes | | Top downregulated genes | |
| 4 weeks | SLN | (6.2) | GDF15 | (4.7) | C1orf51 | (-3.0) | Hamp/Hamp2 | (-4.9) |
| | MYL7 | (5.6) | Hsp70 | (3.4) | PER2 | (-2.3) | CA3 | (-3.3) |
| | MYL4 | (4.8) | MKI67 | (3.2) | CA4 | (-2.2) | TGFbRIII | (-3.3) |
| | GDF15 | (4.4) | PBK | (3.1) | Hsp70 | (-1.9) | Kcnp2 | (-3.3) |
| | Hamp/Hamp2 | (4.3) | IRF7 | (3.1) | COQ10B | (-1.8) | MYL7 | (-3.2) |
| 20 weeks | CA3 | (4.8) | IGHA | (3.7) | CHTOP | (-2.1) | CDO1 | (-3.5) |
| | CFD | (4.7) | GDF15 | (3.5) | CXCL14 | (-2.1) | Klra4 | (-3.3) |
| | HP | (3.4) | ESM1 | (2.9) | Klra4 | (-2.1) | Klk1b1 | (-3.3) |
| | Hamp/Hamp2 | (3.3) | HIST1H2AB | (2.7) | ADH1C | (-2.0) | INMT | (-3.2) |
| | IRF7 | (3.2) | PAC SIN1 | (2.6) | ALDOB | (-1.9) | GUCY | (-2.9) |

| | | | | | | | | |
|----------|---------|-------|--------|-------|--------|--------|--------|--------|
| 40 weeks | ESM1 | (3.9) | SLN | (6.2) | Hsp70 | (-4.3) | CCL21 | (-5.0) |
| | SRGN | (3.5) | MYL7 | (5.7) | CXCL14 | (-3.3) | INMT | (-4.3) |
| | HPRT1 | (3.3) | CLASP1 | (4.3) | ADH1C | (-3.0) | Mup1 | (-4.3) |
| | HOXB7 | (3.2) | DKK3 | (3.9) | TDRD3 | (-2.8) | ADH1C | (-4.2) |
| | C1orf52 | (3.2) | SORBS1 | (3.9) | CPXM1 | (-2.8) | Ifitm1 | (-3.7) |

The top 5 upregulated and downregulated genes per genotype are shown after 16 Gy at 4 weeks, 20 weeks and 40 weeks. Numbers in brackets show Log² ratio of sham treated mice versus 16 Gy irradiated mice.

Pro-fibrotic genes upregulated in Eng^{+/+} mice only at 4 weeks

Unirradiated Eng^{+/-} mice had reduced endoglin mRNA expression compared to Eng^{+/+} mice, as expected (Figure 5, top panels). Immunohistochemistry analysis confirmed that endoglin protein levels in hearts of Eng^{+/-} mice were also approximately half that of Eng^{+/+} mice (data not shown). By 40 weeks after irradiation, the mRNA levels of endoglin were decreased to < 50% of control values in both strains, although this did not reach statistical significance.

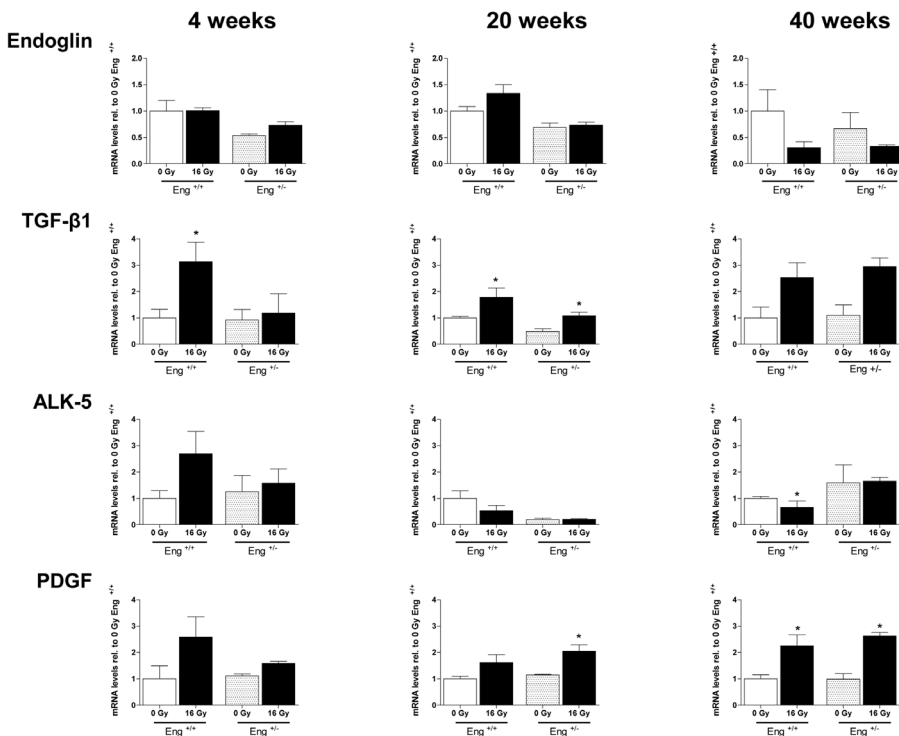


Figure 5 Expression of genes involved in TGFβ pathway measured by RT PCR. Each bar represents the average expression per group ± SEM. Values of sham-treated animals were set to 1. The graph show the fold-change in gene expression in irradiated mice relative to respective controls at 4 (n=4-5), 20 (n=4-5), and 40 (n=4-7) weeks after 16 Gy irradiation.

TGF- β 1 was significantly increased by 4 weeks after irradiation in Eng^{+/+} mice and in both strains at 20 weeks and 40 weeks (not significant) after irradiation. Irradiation did not alter the mRNA expression of fibrogenesis activator ALK5 in Eng^{+/+} mice but there was a non-significant increase in ALK5 in Eng^{+/+} mice at 4 weeks followed by significant decreased at 40 weeks after irradiation. PDGF showed a trend to increase in Eng^{+/+} mice at early times (4 weeks), with increases in both strains at later times (Figure 5). Profibrotic CTGF and PAI-1 were not altered significantly by radiation in either strain at 4, 20 or 40 weeks after irradiation (data not shown).

Microvascular damage in Eng^{+/+} and Eng^{+/-} mice

After demonstrating significant differences between Eng^{+/+} mice and Eng^{+/-} mice in

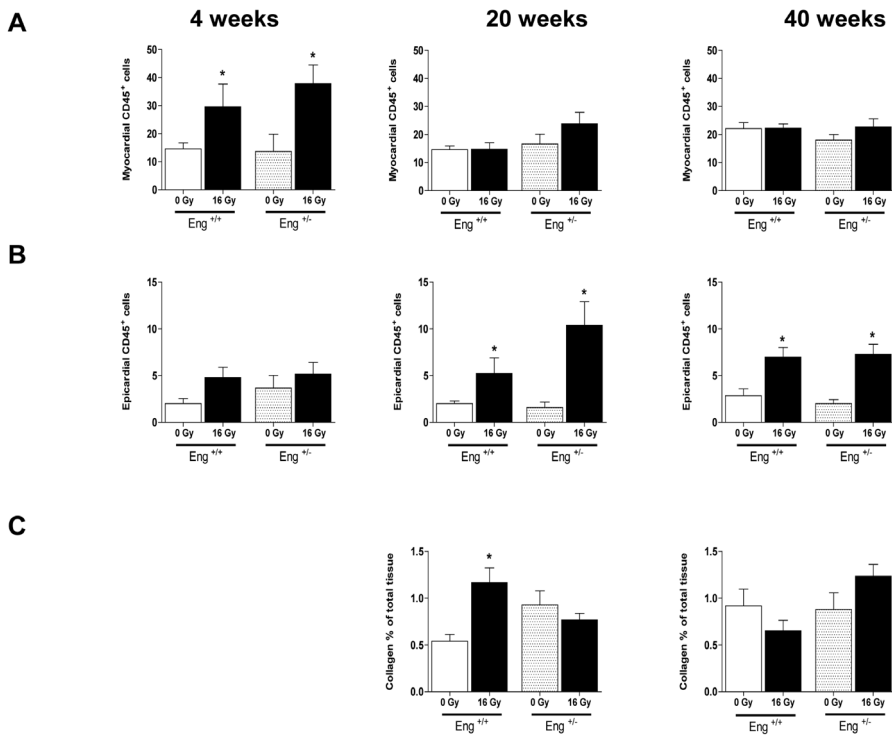


Figure 6 Inflammatory and fibrotic changes at 4, 20 and 40 weeks after irradiation or sham treatment. (A) Quantification of CD45+ cells per section in the myocardium and (B) epicardium. (C) Percentage interstitial collagen content of irradiated heart sections, relative to age-matched unirradiated controls. Values represent mean \pm SEM with 3-6 mice in the 4 weeks group, 4-5 mice in the 20 weeks group and 5-7 in the 40 weeks group, * $p < 0.05$ compared to age-matched unirradiated controls.

inflammatory, fibrogenic and survival pathway signaling in response to cardiac irradiation, we investigated this in more detail with respect to tissue morphology and function.

Epicardial thickness and myocardial thickness were not altered at any time-point after irradiation in either strain (data not shown). Irradiation led to a transient increase in CD45+ cells in the myocardium of both strains at 4 weeks and in the epicardium at 20 and 40 weeks. However, there were no differences in the inflammatory response noted between strains at the tissue level (Figure 6 A-B). Iron-containing macrophages, as an indicator of hemorrhage, were significantly increased in both myocardium and epicardium at 20 and 40 weeks after irradiation in both strains (data not shown). Collagen deposition in the myocardium was increased at 20 weeks after irradiation in Eng^{+/+} mice only, with no significant changes at 40 weeks in either strain (Figure 6 C).

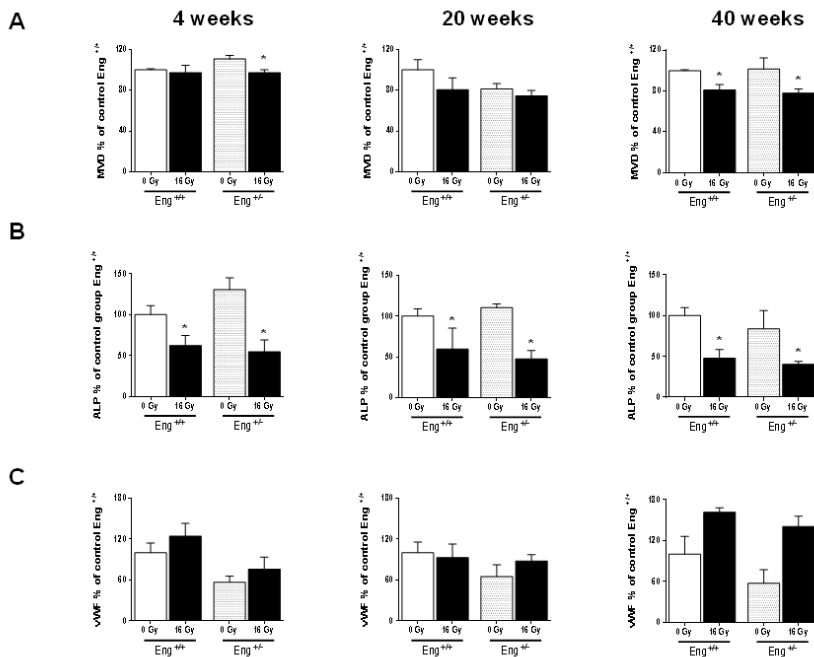


FIGURE 7 Microvascular alterations at 4, 20 or 40 weeks after irradiation or sham treatment. (A) MVD per unit area expressed as percentage of age-matched unirradiated control values. (B) ALP positive tissue areas as % of age-matched unirradiated controls. (C) vWF positive tissue areas as % of age-matched unirradiated controls. Values represents mean \pm SEM with 4-5 mice in the 4 and 20 weeks group and 4-7 mice in the 40 weeks group, * $p < 0.05$ compared to age-matched unirradiated controls.

Microvascular density (MVD) decreased significantly at 4 weeks after irradiation in $Eng^{+/-}$ mice and in both strains 40 weeks after irradiation (Figure 7 A). This was accompanied by endothelial damage, as shown by a marked decrease in ALP activity at 4, 20 and 40 weeks after irradiation, and increased expression of the thrombotic endothelial marker vWF (not significant) at 40 weeks in both strains (Figure 7 B-C).

Microvascular stability, assessed by pericyte coverage, was decreased in irradiated mice at 40 weeks (not significant) but there were no differences between strains (Figure 8).

Since $Eng^{+/-}$ mice are known to be susceptible to microvascular defects as they age (13,14), we also compared the microvascular density and functionality (pericyte coverage, ALP and vWF expression) in unirradiated $Eng^{+/-}$ and $Eng^{+/+}$ mice at 40 weeks follow-up. There were no significant differences in any of these parameters between the strains (Figures 7, 8).

Normalized cardiac function in $Eng^{+/-}$ mice at 40 weeks

Cardiac function, evaluated by gated SPECT (^{99m}Tc -HSA) showed modest decreases in EDV and ESV at 20 weeks after irradiation of $Eng^{+/-}$ mice only. SV decreased in both strains with no changes in EF (Figure 9). Almost all cardiac function parameters had normalized to control levels at 40 weeks after irradiation.

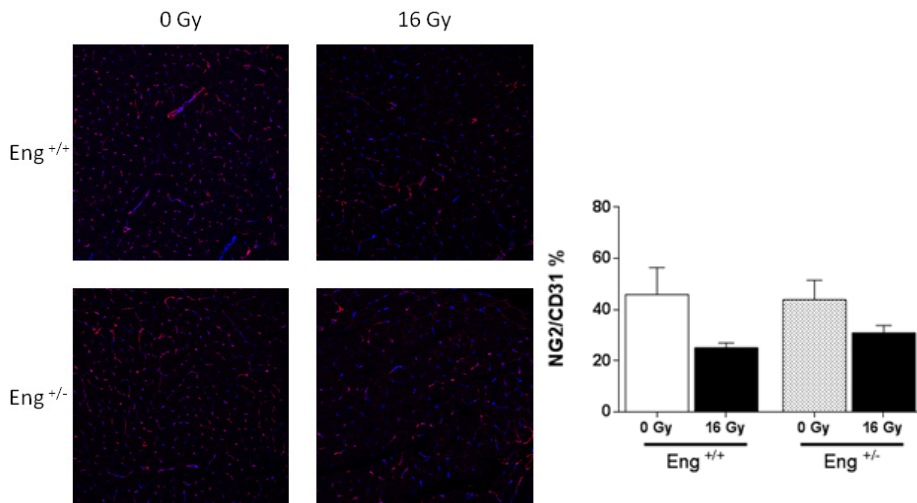


FIGURE 8 Pericyte coverage altered at 40 weeks after irradiation. Confocal imaging showing the effects of radiation on pericyte coverage (marked in red) on endothelial cells of the cardiac microvasculature (marked in blue). Graph displaying NG2/CD31 ratio as % of each individual treatment group and genotype. Values represents mean \pm SEM with 4-5 mice in the 4 and 20 weeks group and 4-7 mice in the 40 weeks group, * $p < 0.05$ compared to age-matched, unirradiated controls.

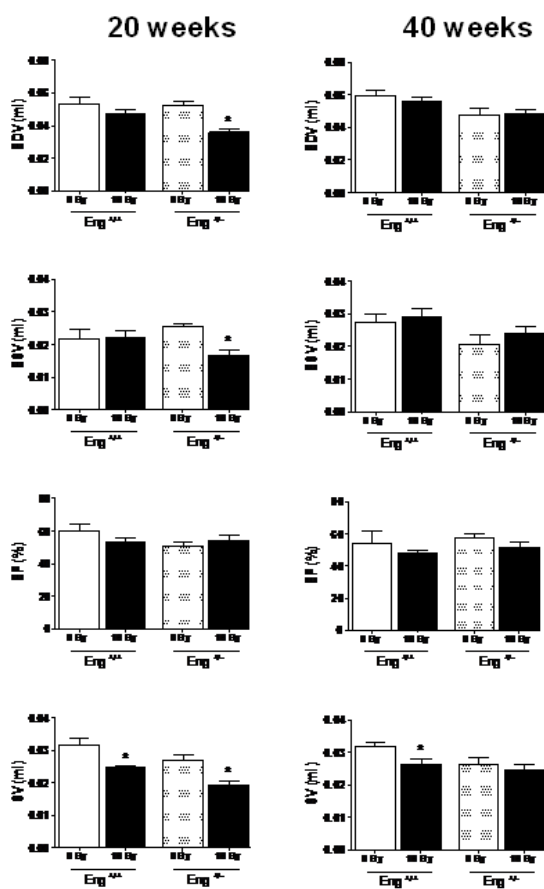


FIGURE 9 EDV, ESV, EF and SV measured by gated SPECT at 20 weeks or 40 weeks after irradiation or sham treatment. Values represent mean \pm SEM (7-14 mice in each irradiated group), * $p < 0.05$ compared to age-matched, unirradiated controls.

Discussion

Microvascular damage has been identified as a contributing factor in developing heart failure after high dose ionizing radiation (1,15,16,17). Endothelial cells are highly sensitive to radiation and aberrant signaling by damaged cells affects the pathological progression of radiation-induced tissue damage (18,19,20). Endoglin is a co-receptor for TGF- β 1; it is essential for angiogenesis and predominantly expressed in activated vascular endothelial cells (10,11,12,13,14,21,22). In vivo studies have demonstrated that a mutation or deficit in endoglin causes microvascular damage. Mice deficient in endoglin develop vascular and cardiovascular damage, leading to death of Eng^{-/-} embryos or to the HHT phenotype in Eng^{+/-} mice, including endothelial cell degeneration, defects in endothelial junctions and incomplete smooth muscle cell coating of the vessel (13,14,21,22). Several studies have shown that endoglin is upregulated in an inflammatory environment and plays a role in lymphocyte trafficking and migration. Furthermore, endoglin haplo-insufficient mice have been shown to have a reduced inflammatory response and limited cardiac fibrosis after inflammatory stimuli (23,24).

In this study gene expression analysis of irradiated hearts demonstrated a decreased inflammatory response in Eng^{+/-} mice compared to Eng^{+/+} mice. This was particularly evident during the early phase of radiation-induced normal tissue damage (4 weeks after 16 Gy). Genes involved in both inflammatory response and immunological related disease were less prominently regulated by radiation in Eng^{+/-} mice than in Eng^{+/+} mice. Similar results were previously obtained by Scharpfenecker et al. (25) in irradiated kidneys of Eng^{+/+} mice and Eng^{+/-} mice. In these studies the reduced endoglin levels in Eng^{+/-} mice were associated with both reduced expression of inflammatory cytokines (Ccr2, IL1b, IL6) and reduced inflammatory infiltration (CD45+ cells) in irradiated kidney (26). In our study the reduced inflammatory response indicated from gene expression analysis was not reflected in reduced inflammatory infiltration in irradiated heart tissue.

Radiation-induced cardiac inflammation often precedes a late fibrotic response. In our study, fibrosis related genes TGF- β 1, and to a lesser extent ALK5 and PDGF, were only upregulated in Eng^{+/+} mice during the early phase of radiation induced cardiac damage (4 weeks). Moreover, at 20 weeks after irradiation, immunohistochemical analysis showed significant collagen deposition in Eng^{+/+} mice only and not in Eng^{+/-} mice. Again, this is consistent with previous studies, in which endoglin haplo-insufficiency reduced fibrosis in irradiated kidneys and in a model of ischemic heart damage (23,26).

With increased follow-up, our results indicated a shift away from the inflammatory response, although profibrotic genes TGF- β 1 and PDGF were upregulated in both strains at 20 and 40

weeks follow up. This suggests that endoglin haplo-insufficiency only limits inflammation and fibrosis in the early phase of radiation-induced cardiac damage.

We had previously demonstrated that cardiac irradiation of wildtype C57BL/6 mice induced endothelial cell damage (3). Since endoglin is a co-receptor of TGF- β 1, and plays an important role in vascular morphogenesis, endothelial cell function and differentiation of pericytes and smooth muscle cells, one might expect increased endothelial cell damage and loosening of endothelial-pericyte interaction after irradiation in endoglin haplo-insufficient mice (13,14,27). Our results did indicate an early reduction of MVD in irradiated hearts of Eng^{+/-} mice but functional damage in remaining vessels, ALP, vWF expression and pericyte coverage, was not greater in Eng^{+/-} than Eng^{+/+} mice.

Changes in cardiac function were modest and non-progressive but significant decreases in ESV and EDV were seen at 20 weeks in endoglin haplo-insufficient mice and decreased SV in both strains. Upregulation in genes involved in cardiac contractility (top network 16 Gy 40 weeks) in irradiated Eng^{+/-} hearts may have contributed to a normalization of cardiac function at 40 weeks after irradiation.

In summary, high dose radiation induced endothelial cell damage in cardiac microvasculature, which progressed in time. This microvascular tissue damage was independent of endoglin expression levels. However, our data do demonstrate that endoglin haplo-insufficiency limited the early inflammatory response and fibrosis in our radiation-induced mouse model of cardiac damage. Another model of acute pressure overload heart failure (23) showed that reduced endoglin expression had a more pronounced effect on cardiac outcome, with attenuated fibrosis preserved left ventricular function and improved survival. However, radiation-induced heart damage does not result in acute or severe hypoxia but stimulates progressive endothelial dysfunction and capillary loss and leads to a delayed myocardial damage without severe hypoxia. The underlying mechanisms precipitating myocardial fibrosis and heart failure are therefore different and the importance of endoglin in these different pathologies probably varies.

Acknowledgment

The authors would like to thank Bert Pool, Department of Nuclear Medicine, The Netherlands Cancer Institute, for help with the NanoSPECT/CT and Dr. Jack Cleutjens, Department of Pathology, University of Maastricht, for help with the Leica Qwin morphometry system.

Moreover, we would like to thank Dr. Marion Scharpfenecker for fruitful and stimulating discussions on biological consequences of endoglin deficiency.

This research was funded by the European Atomic Energy Community's Seventh Framework Program, grant 211403 (Cardiorisk), and the Dutch Cancer Foundation, grant NKI 2008-3993.

There were no conflicts of interest.

Reference list

1. Boerma M, Kruse JJ, van Loenen M, Klein HR, Bart CI, et al. (2004) Increased deposition of von Willebrand factor in the rat heart after local ionizing irradiation. *Strahlenther Onkol* 180: 109-116.
2. Lauk S, Trott KR (1990) Endothelial cell proliferation in the rat heart following local heart irradiation. *Int J Radiat Biol* 57: 1017-1030.
3. Seemann I, Gabriels K, Visser NL, Hoving S, te Poele JA, et al. (2012) Irradiation induced modest changes in murine cardiac function despite progressive structural damage to the myocardium and microvasculature. *Radiother Oncol* 103: 143-150.
4. Andrianifahanana M, Wilkes MC, Repellin CE, Edens M, Kottom TJ, et al. (2010) ERBB receptor activation is required for profibrotic responses to transforming growth factor beta. *Cancer Res* 70: 7421-7430.
5. Martin M, Lefaix J, Delanian S (2000) TGF-beta1 and radiation fibrosis: a master switch and a specific therapeutic target? *Int J Radiat Oncol Biol Phys* 47: 277-290.
6. Anscher MS (2010) Targeting the TGF-beta1 pathway to prevent normal tissue injury after cancer therapy. *Oncologist* 15: 350-359.
7. Barcellos-Hoff MH, Derynck R, Tsang ML, Weatherbee JA (1994) Transforming growth factor-beta activation in irradiated murine mammary gland. *J Clin Invest* 93: 892-899.
8. Scharpfenecker M, Kruse JJ, Sprong D, Russell NS, Ten Dijke P, et al. (2009) Ionizing radiation shifts the PAI-1/ID-1 balance and activates notch signaling in endothelial cells. *Int J Radiat Oncol Biol Phys* 73: 506-513.
9. van Meeteren LA, Goumans MJ, ten Dijke P (2011) TGF-beta receptor signaling pathways in angiogenesis; emerging targets for anti-angiogenesis therapy. *Curr Pharm Biotechnol* 12: 2108-2120.
10. Gougos A, Letarte M (1988) Identification of a human endothelial cell antigen with monoclonal antibody 44G4 produced against a pre-B leukemic cell line. *J Immunol* 141: 1925-1933.
11. Lebrin F, Goumans MJ, Jonker L, Carvalho RL, Valdimarsdottir G, et al. (2004) Endoglin promotes endothelial cell proliferation and TGF-beta/ALK1 signal transduction. *EMBO J* 23: 4018-4028.
12. Li C, Hampson IN, Hampson L, Kumar P, Bernabeu C, et al. (2000) CD105 antagonizes the inhibitory signaling of transforming growth factor beta1 on human vascular endothelial cells. *FASEB J* 14: 55-64.
13. Arthur HM, Ure J, Smith AJ, Renforth G, Wilson DI, et al. (2000) Endoglin, an ancillary TGFbeta receptor, is required for extraembryonic angiogenesis and plays a key role in heart development. *Dev Biol* 217: 42-53.

14. Bourdeau A, Dumont DJ, Letarte M (1999) A murine model of hereditary hemorrhagic telangiectasia. *J Clin Invest* 104: 1343-1351.
15. Fajardo LF, Stewart JR (1971) Capillary injury preceding radiation-induced myocardial fibrosis. *Radiology* 101: 429-433.
16. Fajardo LF, Stewart JR (1973) Pathogenesis of radiation-induced myocardial fibrosis. *Lab Invest* 29: 244-257.
17. Lauk S, Kizsel Z, Buschmann J, Trott KR (1985) Radiation-induced heart disease in rats. *Int J Radiat Oncol Biol Phys* 11: 801-808.
18. Juncos LI, Cornejo JC, Gomes J, Baigorria S, Juncos LA (1997) Abnormal endothelium-dependent responses in early radiation nephropathy. *Hypertension* 30: 672-676.
19. Paris F, Fuks Z, Kang A, Capodiecì P, Juan G, et al. (2001) Endothelial apoptosis as the primary lesion initiating intestinal radiation damage in mice. *Science* 293: 293-297.
20. Ran XZ, Ran X, Zong ZW, Liu DQ, Xiang GM, et al. (2010) Protective effect of atorvastatin on radiation-induced vascular endothelial cell injury in vitro. *J Radiat Res* 51: 527-533.
21. Lopez-Novoa JM, Bernabeu C (2010) The physiological role of endoglin in the cardiovascular system. *Am J Physiol Heart Circ Physiol* 299: H959-974.
22. McAllister KA, Grogg KM, Johnson DW, Gallione CJ, Baldwin MA, et al. (1994) Endoglin, a TGF-beta binding protein of endothelial cells, is the gene for hereditary haemorrhagic telangiectasia type 1. *Nat Genet* 8: 345-351.
23. Kapur NK, Wilson S, Yunis AA, Qiao X, Mackey E, et al. (2012) Reduced endoglin activity limits cardiac fibrosis and improves survival in heart failure. *Circulation* 125: 2728-2738.
24. Rossi E, Sanz-Rodriguez F, Eleno N, Duwell A, Blanco FJ, et al. (2013) Endothelial endoglin is involved in inflammation: role in leukocyte adhesion and transmigration. *Blood* 121: 403-415.
25. Scharpfenecker M, Floot B, Russell NS, Stewart FA (2012) The TGF-beta co-receptor endoglin regulates macrophage infiltration and cytokine production in the irradiated mouse kidney. *Radiother Oncol* 105: 313-320.
26. Scharpfenecker M, Floot B, Russell NS, Ten Dijke P, Stewart FA (2009) Endoglin haploinsufficiency reduces radiation-induced fibrosis and telangiectasia formation in mouse kidneys. *Radiother Oncol* 92: 484-491.
27. Li DY, Sorensen LK, Brooke BS, Urness LD, Davis EC, et al. (1999) Defective angiogenesis in mice lacking endoglin. *Science* 284: 1534-1537.



Chapter 6

Thalidomide is not able to inhibit radiation-induced heart disease

S. Hoving, I. Seemann, N. L. Visser, J. A. te Poele, F.A. Stewart

Int. Journal of Radiation Biology September 2013

Abstract

Purpose: Radiotherapy to the thorax increases the risk of radiation-induced heart disease. We and others have shown that local irradiation to the murine heart results in inflammatory and fibrotic responses and decreased microvascular density. In the present study we tested whether thalidomide is able to inhibit radiation-induced heart disease.

Materials and Methods: Single doses of 16 Gy or 0 Gy (sham treatment) were delivered to the hearts of mice. At 16 weeks after irradiation the mice were allocated to receive a thalidomide-containing chow (100 mg/kg body weight/day) or control chow till the end of the experiment. At 40 weeks after irradiation, functional imaging was performed and the hearts were examined for histological damage.

Results: Irradiation led to an increase in epicardial thickness and infiltrating inflammatory cells in the epicardium as well as an increase in interstitial collagen content. The microvasculature had a decreased alkaline phosphatase activity and reduced pericyte coverage. Thalidomide had no protective role in any of these processes. There were no differences in heart function measured between the treatment groups.

Conclusions: Although others have shown protective effects of thalidomide in disease models involving inflammation, fibrosis and blood vessel maturation, thalidomide was not able to reduce radiation-induced heart damage.

Introduction

Radiotherapy to the thorax is performed widely for the treatment of breast cancer and Hodgkin lymphoma. However, these patients with a good long-term prognosis are at risk of developing treatment-related late normal tissue damage. Epidemiological studies have demonstrated increased risk for cardiac mortality and morbidity, which becomes significant 5-10 years after treatment and increases with time (1-4). The pathological consequences of radiation-induced heart disease are pericarditis, myocardial fibrosis, coronary artery disease, valvular disorders and conduction abnormalities (2, 5, 6). Regional cardiac perfusion defects have also been shown in breast cancer patients from 6 months after radiotherapy (7, 8) and preclinical studies have demonstrated considerable damage to endothelial cells after irradiation, including decreased microvessel density, increased epicardial thickness, the presence of inflammatory cells in epicardium and myocardium and fibrosis (9-14).

Thalidomide (α -(N-phthalidimido) glutarimide) was initially used as a sedative and anti-emetic drug for morning sickness. The drug was withdrawn from the market in 1961 when it became clear that the intake of thalidomide during pregnancy could lead to severe deformities in the embryo. Thalidomide is recently re-emerging as a treatment for inflammatory disease and cancers, including cutaneous lupus, Crohn's disease, rheumatoid arthritis, multiple myeloma and graft-versus-host disease, because of its anti-inflammatory and anti-angiogenic effects (15). Thalidomide inhibits the production of TNF- α (tumor necrosis factor-alpha), which regulates inflammatory cascades and inhibits the expression of vascular endothelial growth factor (VEGF) and interleukin-6 (IL-6), which play a role in angiogenesis (16-19). Recent studies also showed evidence of anti-fibrotic activity in various fibrosis-related diseases such as lung fibrosis (20, 21) and remodeling after myocardial infarction (22). Furthermore, thalidomide was found to induce vessel maturation by stimulating mural cell coverage and thereby rescuing vessel wall defects (23).

Since inflammatory and fibrotic events are dominant features in radiation-induced heart disease, we hypothesized that thalidomide might prevent or ameliorate radiation-induced heart disease. Therefore, we treated irradiated and unirradiated C57BL/6J mice with thalidomide-containing chow and compared cardiac damage with mice treated with control chow.

Materials and Methods

Experimental design and irradiation procedure

Endoglin heterozygous ($Eng^{+/-}$) mice on a C57BL/6J background were obtained from H. Arthur, Institute of Human Genetics, International Centre for Life, Newcastle upon Tyne, UK. These mice were crossed with C57BL/6J mice (from Charles River laboratories, France) and bred in isolator cages at the breeding facility of the Netherlands Cancer Institute. The $Eng^{+/+}$ wildtype offspring were used for the present studies and $Eng^{+/-}$ littermates were used in a parallel study. Standard mouse chow and water were provided ad libitum. At the age of 9-11 weeks, male mice were randomly allocated to different treatment groups and housed in a temperature-controlled room with 12 h light-dark cycle. Thirty mice received a single dose of 16 Gy to the heart using 250 kV X-rays, operating at 12 mA and filtered with 0.6 mm copper. The dose rate was 0.94 Gy/min and the irradiation field was 10.6 x 15.0 mm (including up to 30% lung volume). The rest of the body was shielded with a 3 mm thick lead plate. Twenty mice received sham irradiation. At 16 weeks after irradiation, half of the mice in both the 0 and 16 Gy groups received thalidomide containing chow (0.6667 g thalidomide per kg chow), until 1 week before sacrifice. The other half of the mice received control chow. Assuming the mice in our study consumed 4.5 g of feed per day (as measured in previous pilot studies), we estimated that the average 30 g mouse consumed 100 mg/kg body weight/day of thalidomide. The dose of thalidomide was based on published studies in mice and rats (22-24) and the start of drug administration was chosen to coincide with the onset of progressive vascular damage (14). At 40 weeks after irradiation, functional imaging was performed using gated Single-Photon Emission Computed Tomography (gated SPECT) and the mice were sacrificed to collect the heart. Experiments were in agreement with the Dutch law on animal experiments and welfare, and in line with the international Guide for the Care and Use of Laboratory Animals (Eighth edition).

Gated SPECT

The tracer tetrofosmin (Myoview, GE-healthcare, Hoevelaken, The Netherlands) was labeled with ^{99m}Tc -pertechnetate according to the manufacturer's protocol and injected i.v. (150 μ l) with a total activity of approximately 70 MBq per mouse. Three silver/silver-chloride coated plastic electrodes (3M red Dot 2282E; 3M, St. Paul, MN, USA) were attached to both hind paws and right front paw of the mouse and connected to the integrated electrocardiography (ECG) monitor to measure heart rate (HR). Acquisitions were started 1 h after injection of the tracer as described previously (14). HISPECT NG software (InVivoScope, Bioscan) was used to

perform iterative reconstruction into 3D-datasets. Quantitative analysis of the reconstructed datasets was performed on a clinical e.soft (*syngo*-based) workstation (Siemens Medical Solutions, Siemens AG, Erlangen, Germany), using algorithms to automatically reconstruct a count based 3D model of the dimensions of the left ventricle (LV) end diastolic and systolic volumes (EDV, ESV). The ejection fraction (EF) was calculated based on the difference between EDV and ESV divided by EDV.

Tissue handling and histology

Mice were anaesthetized with a lethal dose of sodium pentobarbital (18 mg i.p. per mouse). The heart was perfused via the aortic arch (retro-grade) with PBS (phosphate buffered saline) for frozen sections or PBS followed by 1% paraformaldehyde for paraffin sections. The heart and lungs were then quickly excised before freezing on dry ice or immersion in 1% paraformaldehyde. Cross sections of the heart were cut at the level of the mid-horizontal plane from fixed paraffin-embedded tissue (4 µm) or frozen sections (7 µm). Photographs were taken with a CCD 2 Color Microscope system, including a Zeiss AxioCam color camera (AxioCam HRc, Zeiss, Göttingen, Germany) or Aperio scanner (Scanscope-XT, Aperio technologies, Vista, USA) using a 40x objective. All analyses were performed in the left ventricle (LV) using a computerized morphometry system (Leica Qwin V3, Leica, The Netherlands).

Paraffin sections

Paraffin sections were stained with hematoxylin and eosin (H&E) to measure epicardial and myocardial thickness. Photographs of the LV wall (excluding the septum) were taken using a 5x objective and 12 measurements per heart were performed to measure the epicardial and myocardial thickness.

To determine the extent of inflammation, sections were stained with an anti-CD45 antibody (1:400, Becton & Dickinson, Franklin lakes, NJ, USA) to detect leukocytes. The total numbers of CD45+ cells in the epicardium were counted and in the LV myocardium five random photographs (40x objective) were analyzed. To quantify the number of macrophages, sections were stained with an anti-F4/80 antibody (1:400, Serotec, Kidlington, UK) and the numbers of macrophages were counted in the epicardium and LV myocardium (five random 40x photographs).

Perl's-staining was performed to investigate the presence of iron-containing macrophages (indicative of previous hemorrhage) and this was recorded in as positive or negative in epicardium and LV myocardium separately.

Interstitial collagen was quantified in five randomly selected areas of the LV myocardium (40x objective) based on a Sirius Red staining and the results were expressed as percentage tissue positive for Sirius Red, excluding perivascular collagen, relative to myocardial area.

Frozen sections

An anti-CD31 antibody (1:50, Becton & Dickinson) was used to visualize cardiac vasculature of the heart and to quantify microvascular density (MVD). Five random areas (40x objective) from the myocardium were photographed and analyzed. Vessels smaller than 1.5 or larger than 200 μm^2 were automatically excluded from the measurements, to ensure that only microvasculature was counted. To determine functional changes in the microvasculature, histochemical staining with Naphtol ASMX/DMF and fast Blue BB was performed to detect endothelial cell alkaline phosphatase (ALP) activity.

Sections were also stained using antibodies against von Willebrand Factor (vWF) (1:4000, Abcam), as a marker of thrombotic changes and vascular cell adhesion molecule 1 (VCAM-1) (1:200, Becton & Dickinson), as a marker of vascular inflammation.

Photographs of whole sections stained for ALP and vWF were taken with an Aperio scanner and analyses of the percentage myocardium positive for each marker were done with a computerized morphometry system (Leica Qwin V3). VCAM-1-stained sections were semi-quantitatively analyzed (without knowledge of treatment group) according to the criteria: No, mild, or strong expression.

All sections were processed identically, at the same time with precisely the same incubation times for the primary and secondary antibody and diaminobenzidine (DAB) solution (Sigma, Zwijndrecht, The Netherlands). Therefore, all differences between the treatments are ultimately due to DAB identification of the relevant protein.

A double staining was performed to visualize the vasculature and the pericytes covering the vessels. The primary antibodies used were CD31 (1:50, Becton & Dickinson) and NG2 (1:200, Chemicon, Temecula, CA, USA) and the primary antibodies were visualized with Alexa Fluor (AF) 633 (1:100, Invitrogen, Carlsbad, CA, USA) and AF568 (1:250, Invitrogen).

To visualize α -smooth muscle actin (α SMA) positive cells around blood vessels, a double staining was performed using the primary antibodies CD31 (1:50, Becton & Dickinson) and α SMA-Cy3 (1:200, Sigma). The primary antibody CD31 was visualized with AF633 (1:100, Invitrogen).

Photographs of the fluorescent stainings were taken with a confocal microscope (Leica). An average of five photographs were taken around the left ventricle and the pericyte coverage

of microvessels was determined by counting NG2⁺/CD31⁺ vessels using an ImageJ computer analysis program.

Statistics

Data are expressed as mean \pm SEM and groups were compared using non-parametric Mann–Whitney U tests or Fisher’s exact test. Group differences were considered statistically significant at $p < 0.05$. Statistical analyses were performed using SPSS version 20.

Results

Mouse survival and weight

The irradiated mice fed with control chow gained 7% less body weight than unirradiated mice on control chow and lungs of irradiated mice fed with control chow were 11% heavier than lungs of unirradiated mice treated with control chow, while there was no effect of irradiation on heart weight. Treatment with thalidomide had no effect on body, heart or lung weight in unirradiated or irradiated mice compared with mice treated with control chow (Table 1).

In total only six irradiated mice died during the experiment, two of which received thalidomide-containing chow.

Heart function

Gated-SPECT (^{99m}Tc-Myoview) was used to examine whether irradiation and/or thalidomide influenced cardiac function. There were no differences in end diastolic (EDV) and end systolic volume (ESV), ejection fraction (EF) and stroke volume (SV) between the treatment groups (data not shown).

Inflammation and fibrosis

Irradiation of the heart resulted in an increased epicardial thickness (Figure 1A), associated with the presence of CD45⁺ inflammatory cells (Figure 1B), F4/80⁺ macrophages (Figure 1C) and iron-containing macrophages (Table 2), indicative of previous hemorrhage. This irradiation effect was seen in mice treated with control chow and thalidomide-containing chow, with no differences between these two groups (Figure 1A, B and C). No differences were seen in inflammatory cells in the myocardium between the treatment groups (data not shown). The amount of interstitial collagen increased significantly after irradiation, but treatment with thalidomide did not result in a reduction of interstitial collagen (Figure 1D).

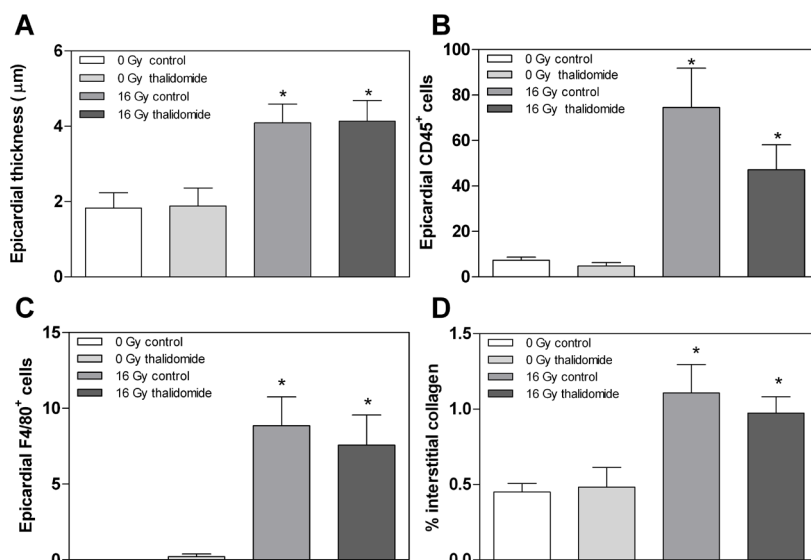


FIGURE 1 Inflammatory and fibrotic changes in hearts of unirradiator and irradiated mice treated with control chow or thalidomide-containing chow. (A) Epicardial thickness, (B) Number of CD45+ cells per section in the epicardium, (C) Number of F4/80+ cells per section in the epicardium, (D) Percentage interstitial collagen in the left ventricle. Values represent mean ± SEM (with 4-7 mice in each treatment group). *p<0.05 compared with unirradiator mice treated with the same chow.

TABLE 2 Incidence of mice showing iron-containing macrophages (Perl's staining) in epicardium and myocardium of unirradiator and irradiated mice treated with control or thalidomide-containing chow.

| Treatment | Epicardium | Myocardium |
|------------------------|------------|------------|
| 0 Gy control chow | 1/5 | 5/5 |
| 0 Gy thalidomide chow | 1/5 | 4/5 |
| 16 Gy control chow | 7/7 * | 6/7 |
| 16 Gy thalidomide chow | 6/7 * | 6/7 |

*p<0.05 compared to unirradiator mice with the same chow.

Microvascular density (MVD) and vascular function

Thalidomide did not significantly influence the number of microvessels in irradiated or unirradiator hearts (data not shown). Irradiation resulted in a non-significant decrease in MVD in animals fed control chow (7%) or thalidomide (23%). However, these decreases were smaller than the significant decreases (26-28%) seen in previous studies (8, 11). Despite

the lack of significant effect on microvascular density, the microvessels were damaged by irradiation as shown by the significant decrease in alkaline phosphatase (ALP) activity. However, thalidomide was not able to restore the ALP activity (Figure 2A). We saw an increased expression of the thrombotic marker vWF after irradiation, but once again thalidomide was not able to prevent this increase (Figure 2B).

Semi-quantitative analysis of VCAM-1 expression in endothelial cells of the left ventricle did not show an increased expression after irradiation and thalidomide had also no effect on the VCAM-1 expression (data not shown).

Although no differences were seen in the number of blood vessels after irradiation, clear differences were seen in the number of pericytes (identified by NG2 staining) around blood vessels (Figure 3A). In unirradiated hearts the pericytes were equally distributed over the myocardial tissue (Figure 3B), while in all irradiated hearts areas were seen with blood vessels but without pericytes (Figure 3C). Quantification confirmed a significant reduction in pericyte coverage in irradiated mice compared with unirradiated mice, but there were no differences between mice treated with thalidomide or control chow (Figure 3A).

α SMA staining was performed to investigate whether irradiation had an effect on the smooth muscle cell distribution, a (Figure 3D). Only the larger vessels were positive for α SMA and no differences were seen in the number of α SMA positive blood vessels between irradiated and unirradiated mice and between control and thalidomide chow treated mice (data not shown).

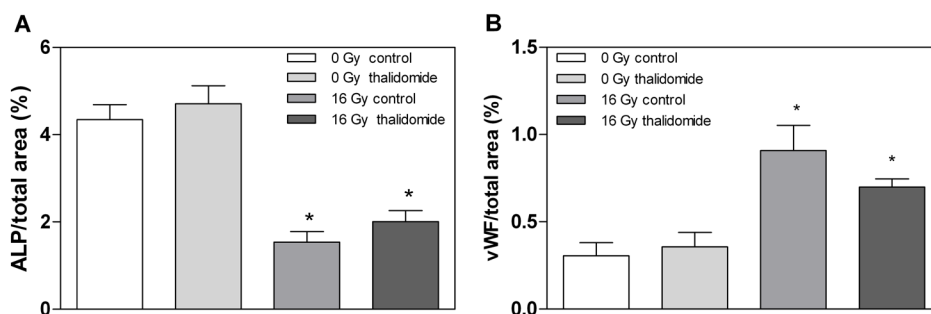


FIGURE 2 Microvascular alterations in hearts of unirradiated and irradiated mice treated with control chow or thalidomide-containing chow. (A) ALP-positive tissue per myocardial area, (B) vWF-positive tissue per myocardial area. Values represent mean \pm SEM (with 4-7 mice in each treatment group). * p <0.05 compared with unirradiated mice treated with the same chow.

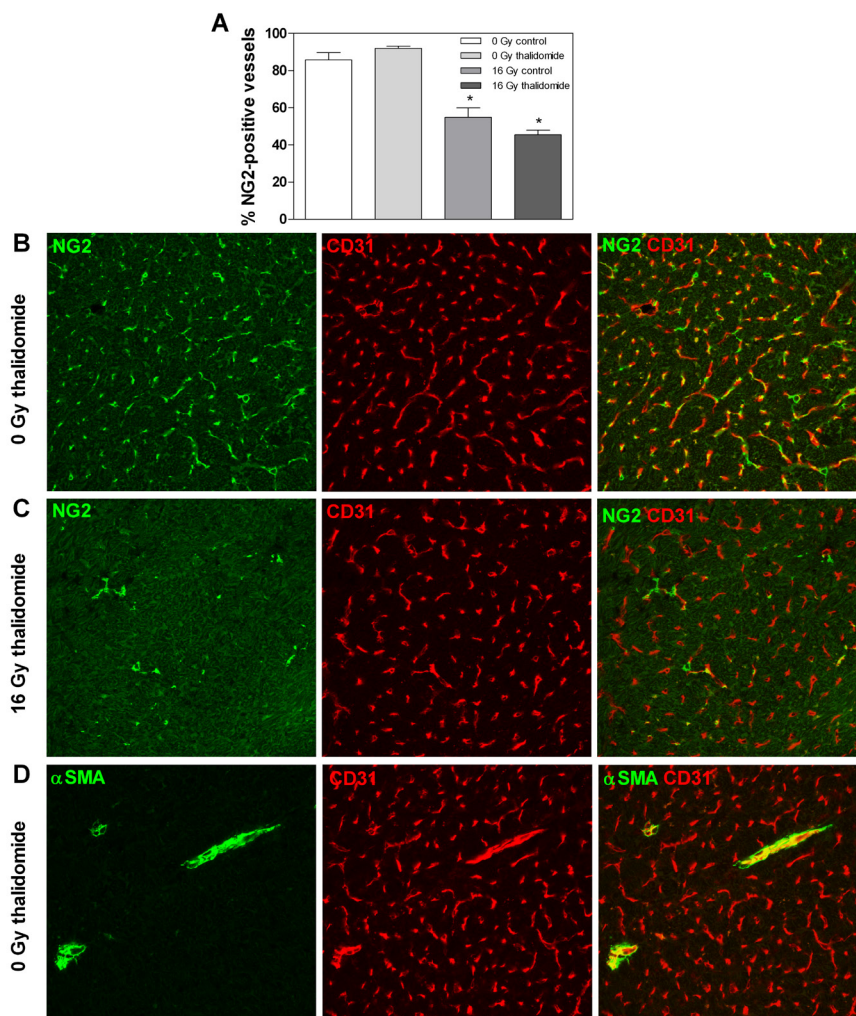


FIGURE 3 Pericyte and α SMA coverage of blood vessels in unirradiated and irradiated mice treated with control chow or thalidomide-containing chow. In unirradiated mice, most blood vessels were covered with pericytes, while in irradiated mice areas were present with blood vessels lacking pericytes. (A) Quantification of the percentage of pericyte-positive (NG2) blood vessels (CD31 positive). Values represent mean \pm SEM (with 4-7 mice in each treatment group). * $p < 0.05$ compared with unirradiated mice treated with the same chow. Representative pictures of pericyte positive (NG2, green) blood vessels (CD31, red) are shown of an unirradiated mouse (B) and an irradiated mouse (C) treated with thalidomide. (D) Representative pictures are shown of α SMA positive (green) blood vessels (red) of an unirradiated mouse treated with thalidomide. No differences were seen in α SMA staining between irradiated and unirradiated mice and between mice treated with thalidomide and control chow.

Discussion

We have previously shown that irradiation affects cardiac structure and microvascular function (11, 14). In the present study we confirmed that irradiation induced inflammation and fibrosis, and compromised microvascular function. Next, we tested whether thalidomide was able to affect these processes and thereby prevent radiation-induced heart disease, but no protective effect of thalidomide was seen in our mouse model.

Thalidomide has been shown to have anti-inflammatory properties and is currently used in the treatment of diseases like cutaneous lupus, Crohn's disease, rheumatoid arthritis, multiple myeloma and graft-versus-host disease (15). Several studies suggest that thalidomide may inhibit the production of inflammatory cytokines such as TNF- α , IL-1 β and IL-6, as well as enhance levels of anti-inflammatory cytokine IL-10 (17, 25). TNF- α has been shown to be elevated in patients with advanced heart failure. However, clinical studies analyzing the effect of thalidomide on plasma levels of TNF- α have shown discrepant results, demonstrating increased (26) or decreased plasma levels (27).

Irradiation has been shown to up-regulate expression of several inflammatory cytokines and chemokines, including TNF α and IL1 β , which has been associated with damage to both irradiated lung and brain (28, 29). We therefore hypothesized that thalidomide may be beneficial in radiation-induced heart disease, as inflammatory processes play an important role. We did not investigate the expression of specific inflammatory cytokines in this study, but thalidomide was not able to reduce the inflammatory cell recruitment (CD45+ and F4/80+ cells) into the irradiated heart. We also saw no decrease in VCAM-1 expression after thalidomide treatment in irradiated mice. This is in contrast with a study of Kim and colleagues, who found a significant decrease in VCAM-1 and ICAM-1 expression in rats with diabetic cardiomyopathy treated with thalidomide (100 mg/kg/day) compared with placebo treated rats (24).

Recent studies also showed evidence of anti-fibrotic activity of thalidomide in various fibrosis-related diseases such as lung fibrosis. IL-6 and TGF- β 1 play important roles in pulmonary fibrosis and reduced levels were found after thalidomide treatment leading to reduced collagen deposition (20, 21). Kim et al. showed reduced collagen levels in thalidomide treated rats suffering from diabetic cardiomyopathy (24) and thalidomide also attenuated the development of fibrosis during post-infarction myocardial remodeling in a rat model, although no effect on cardiac function was seen (22). Radiation is a known trigger of fibrosis in different organs, like lung, intestine and heart (9, 12, 30). In the present study an increase in collagen deposition was found in irradiated hearts, but thalidomide did not reduce this

fibrotic effect.

Irradiation to the heart causes damage to cardiac capillaries as is seen in a reduced microvascular density (11, 14). Several studies have also shown a reduced alkaline phosphatase activity and increased vWF in remaining capillaries of irradiated heart and this seems to precede the development of myocardial degeneration (9, 14, 31). Our study confirms these changes in irradiated cardiac microvasculature, but there was no protective effect of thalidomide. This is in contrast with a rat model of acute radiation proctitis, where thalidomide was able to attenuate the number of capillaries expressing vWF (32).

Perivascular cells, especially pericytes, contribute to blood vessel stability and maturation and help with the regulation of microvascular blood flow (33). Lebrin et al. showed, in an experimental mouse model of hereditary hemorrhagic telangiectasia, that thalidomide stimulated pericyte coverage and thereby rescued vessel wall defects (23). Thalidomide could therefore have a protective effect against microvascular damage, despite its known anti-angiogenic properties. In the present study we saw a decrease in pericyte coverage after irradiation, but thalidomide was not able to rescue this pericyte loss.

Although protective effects of thalidomide have been demonstrated in several disease models involving inflammation, fibrosis and blood vessel maturation, the drug was not effective in reducing radiation-induced heart damage. The dose of thalidomide used in our study was comparable with other studies, although the duration of our experiments was much longer (20, 22, 24). Previous experimental studies gave the drug by oral gavage over periods of 2 months. We incorporated the drug in the chow, fed to the mice for 24 weeks, leading to more sustained drug levels in the blood. From previous studies we know that incorporating drugs in the chow is a safe and reliable way of giving a drug for several months (34, 35). The timing of starting drug treatment could be a point of discussion. We chose to start thalidomide treatment from week 16, which is when cardiac damage starts to appear. However, we can not exclude that earlier treatment may have been more effective. Since thalidomide is used as an anti-cancer drug, it is not expected that thalidomide would negatively interfere with the radiotherapy itself.

In conclusion, we have shown that local irradiation to the heart induced an inflammatory, fibrotic response and microvascular damage and these effects could not be circumvented by thalidomide treatment. There are still patients at risk for developing radiation-induced heart disease and development of effective intervention strategies is needed. This study does not support the use of thalidomide to counteract radiation-induced cardiac damage, therefore alternative strategies need to be sought.

Acknowledgement

This work was supported by the Dutch Cancer Society (project number NKI 2005-3373). The authors thank Lisanne Ochse for her technical assistance.

There are no potential conflicts of interest, either financial or otherwise.

Legends

Reference list

1. Aleman BM, van den Belt-Dusebout AW, Klokman WJ, Van't Veer MB, Bartelink H, van Leeuwen FE. Long-term cause-specific mortality of patients treated for Hodgkin's disease. *Journal of clinical oncology : official journal of the American Society of Clinical Oncology*. 2003;21(18):3431-9.
2. Darby SC, Cutter DJ, Boerma M, Constine LS, Fajardo LF, Kodama K, et al. Radiation-related heart disease: current knowledge and future prospects. *International journal of radiation oncology, biology, physics*. 2010;76(3):656-65.
3. Galper SL, Yu JB, Mauch PM, Strasser JF, Silver B, Lacasce A, et al. Clinically significant cardiac disease in patients with Hodgkin lymphoma treated with mediastinal irradiation. *Blood*. 2011;117(2):412-8.
4. Gyenes G, Rutqvist LE, Liedberg A, Fornander T. Long-term cardiac morbidity and mortality in a randomized trial of pre- and postoperative radiation therapy versus surgery alone in primary breast cancer. *Radiotherapy and oncology : journal of the European Society for Therapeutic Radiology and Oncology*. 1998;48(2):185-90.
5. Andratschke N, Maurer J, Molls M, Trott KR. Late radiation-induced heart disease after radiotherapy. Clinical importance, radiobiological mechanisms and strategies of prevention. *Radiotherapy and oncology : journal of the European Society for Therapeutic Radiology and Oncology*. 2011;100(2):160-6.
6. Schultz-Hector S, Trott KR. Radiation-induced cardiovascular diseases: is the epidemiologic evidence compatible with the radiobiologic data? *International journal of radiation oncology, biology, physics*. 2007;67(1):10-8.
7. Marks LB, Yu X, Prosnitz RG, Zhou SM, Hardenbergh PH, Blazing M, et al. The incidence and functional consequences of RT-associated cardiac perfusion defects. *International journal of radiation oncology, biology, physics*. 2005;63(1):214-23.
8. Seddon B, Cook A, Gothard L, Salmon E, Latus K, Underwood SR, et al. Detection of defects in myocardial perfusion imaging in patients with early breast cancer treated with radiotherapy. *Radiotherapy and oncology : journal of the European Society for Therapeutic Radiology and Oncology*. 2002;64(1):53-63.
9. Boerma M, Kruse JJ, van Loenen M, Klein HR, Bart CI, Zurcher C, et al. Increased deposition of von Willebrand factor in the rat heart after local ionizing irradiation. *Strahlentherapie und Onkologie : Organ der Deutschen Rontgengesellschaft [et al]*. 2004;180(2):109-16.
10. Fajardo LF, Stewart JR. Pathogenesis of radiation-induced myocardial fibrosis. *Laboratory investigation; a journal of technical methods and pathology*. 1973;29(2):244-57.

11. Gabriels K, Hoving S, Seemann I, Visser NL, Gijbels MJ, Pol JF, et al. Local heart irradiation of ApoE^{-/-} mice induces microvascular and endocardial damage and accelerates coronary atherosclerosis. *Radiotherapy and oncology : journal of the European Society for Therapeutic Radiology and Oncology*. 2012;105(3):358-64.
12. Kruse JJ, Zurcher C, Strootman EG, Bart CI, Schlagwein N, Leer JW, et al. Structural changes in the auricles of the rat heart after local ionizing irradiation. *Radiotherapy and oncology : journal of the European Society for Therapeutic Radiology and Oncology*. 2001;58(3):303-11.
13. Lauk S, Kizsel Z, Buschmann J, Trott KR. Radiation-induced heart disease in rats. *International journal of radiation oncology, biology, physics*. 1985;11(4):801-8.
14. Seemann I, Gabriels K, Visser NL, Hoving S, te Poele JA, Pol JF, et al. Irradiation induced modest changes in murine cardiac function despite progressive structural damage to the myocardium and microvasculature. *Radiotherapy and oncology : journal of the European Society for Therapeutic Radiology and Oncology*. 2012;103(2):143-50.
15. Franks ME, Macpherson GR, Figg WD. Thalidomide. *Lancet*. 2004;363(9423):1802-11.
16. Gupta D, Treon SP, Shima Y, Hideshima T, Podar K, Tai YT, et al. Adherence of multiple myeloma cells to bone marrow stromal cells upregulates vascular endothelial growth factor secretion: therapeutic applications. *Leukemia*. 2001;15(12):1950-61.
17. Sampaio EP, Sarno EN, Galilly R, Cohn ZA, Kaplan G. Thalidomide selectively inhibits tumor necrosis factor alpha production by stimulated human monocytes. *The Journal of experimental medicine*. 1991;173(3):699-703.
18. Tamilarasan KP, Kolluru GK, Rajaram M, Indhumathy M, Saranya R, Chatterjee S. Thalidomide attenuates nitric oxide mediated angiogenesis by blocking migration of endothelial cells. *BMC cell biology*. 2006;7:17.
19. Maria de Souza C, Fonseca de Carvalho L, da Silva Vieira T, Candida Araujo ESA, Teresa Paz Lopes M, Alves Neves Diniz Ferreira M, et al. Thalidomide attenuates mammary cancer associated-inflammation, angiogenesis and tumor growth in mice. *Biomedicine & pharmacotherapy = Biomedecine & pharmacotherapie*. 2012;66(7):491-8.
20. Choe JY, Jung HJ, Park KY, Kum YS, Song GG, Hyun DS, et al. Anti-fibrotic effect of thalidomide through inhibiting TGF-beta-induced ERK1/2 pathways in bleomycin-induced lung fibrosis in mice. *Inflammation research : official journal of the European Histamine Research Society [et al]*. 2010;59(3):177-88.
21. Tabata C, Tabata R, Kadokawa Y, Hisamori S, Takahashi M, Mishima M, et al. Thalidomide prevents bleomycin-induced pulmonary fibrosis in mice. *Journal of immunology*.

- 2007;179(1):708-14.
22. Yndestad A, Vinge LE, Bjornerheim R, Ueland T, Wang JE, Froland SS, et al. Thalidomide attenuates the development of fibrosis during post-infarction myocardial remodelling in rats. *European journal of heart failure*. 2006;8(8):790-6.
 23. Lebrin F, Srun S, Raymond K, Martin S, van den Brink S, Freitas C, et al. Thalidomide stimulates vessel maturation and reduces epistaxis in individuals with hereditary hemorrhagic telangiectasia. *Nature medicine*. 2010;16(4):420-8.
 24. Kim DH, Kim YJ, Chang SA, Lee HW, Kim HN, Kim HK, et al. The protective effect of thalidomide on left ventricular function in a rat model of diabetic cardiomyopathy. *European journal of heart failure*. 2010;12(10):1051-60.
 25. Amirshahrokhi K, Ghazi-Khansari M. Thalidomide attenuates multiple low-dose streptozotocin-induced diabetes in mice by inhibition of proinflammatory cytokines. *Cytokine*. 2012;60(2):522-7.
 26. Gullestad L, Ueland T, Fjeld JG, Holt E, Gundersen T, Breivik K, et al. Effect of thalidomide on cardiac remodeling in chronic heart failure: results of a double-blind, placebo-controlled study. *Circulation*. 2005;112(22):3408-14.
 27. Gullestad L, Semb AG, Holt E, Skardal R, Ueland T, Yndestad A, et al. Effect of thalidomide in patients with chronic heart failure. *American heart journal*. 2002;144(5):847-50.
 28. Gallet P, Phulpin B, Merlin JL, Leroux A, Bravetti P, Mecellem H, et al. Long-term alterations of cytokines and growth factors expression in irradiated tissues and relation with histological severity scoring. *PloS one*. 2011;6(12):e29399.
 29. Hong JH, Chiang CS, Campbell IL, Sun JR, Withers HR, McBride WH. Induction of acute phase gene expression by brain irradiation. *International journal of radiation oncology, biology, physics*. 1995;33(3):619-26.
 30. Rodemann HP, Blaese MA. Responses of normal cells to ionizing radiation. *Seminars in radiation oncology*. 2007;17(2):81-8.
 31. Lauk S. Endothelial alkaline phosphatase activity loss as an early stage in the development of radiation-induced heart disease in rats. *Radiation research*. 1987;110(1):118-28.
 32. Kim KT, Chae HS, Kim JS, Kim HK, Cho YS, Choi W, et al. Thalidomide effect in endothelial cell of acute radiation proctitis. *World journal of gastroenterology : WJG*. 2008;14(30):4779-83.
 33. von Tell D, Armulik A, Betsholtz C. Pericytes and vascular stability. *Experimental cell research*. 2006;312(5):623-9.
 34. Hoving S, Heeneman S, Gijbels MJ, te Poele JA, Bolla M, Pol JF, et al. NO-donating

aspirin and aspirin partially inhibit age-related atherosclerosis but not radiation-induced atherosclerosis in ApoE null mice. PloS one. 2010;5(9):e12874.

35. Hoving S, Heeneman S, Gijbels MJ, te Poele JA, Pol JF, Gabriels K, et al. Anti-inflammatory and anti-thrombotic intervention strategies using atorvastatin, clopidogrel and knock-down of CD40L do not modify radiation-induced atherosclerosis in ApoE null mice. Radiotherapy and oncology : journal of the European Society for Therapeutic Radiology and Oncology. 2011;101(1):100-8.



Chapter 7

Mouse bone marrow-derived endothelial progenitor cells do not restore radiation-induced microvascular damage

I. Seemann, J. A.M. te Poele, S. Hoving, F. A. Stewart

ISRN Cardiology March 2014

Abstract

Background: Radiotherapy is commonly used to treat breast and thoracic cancers but it also causes delayed microvascular damage and increases the risk of cardiac mortality. Endothelial cell proliferation and revascularization are crucial to restore microvasculature damage and maintain function of the irradiated heart. We have therefore examined the potential of bone marrow-derived endothelial progenitor cells (BM-derived EPCs) for restoration of radiation-induced microvascular damage.

Materials and Methods: 16 Gy was delivered to the heart of adult C57BL/6 mice. Mice were injected with BM-derived EPCs, obtained from Eng^{+/+} or Eng^{+/-} mice, 16 weeks and 28 weeks after irradiation. Morphological damage was evaluated at 40 weeks in transplanted mice, relative to radiation only and age-matched controls.

Results: Cardiac irradiation decreased microvascular density and increased endothelial damage in surviving capillaries (decrease alkaline phosphatase expression and increased von Willebrand factor). Microvascular damage was not diminished by treatment with BM-derived EPCs. However, BM-derived EPCs from both Eng^{+/+} and Eng^{+/-} mice diminished radiation-induced collagen deposition.

Conclusion: Treatment with BM-derived EPCs did not restore radiation-induced microvascular damage but it did inhibit fibrosis. Endoglin deficiency did not impair this process.

Introduction

Radiotherapy is commonly used for treatment of thoracic and chest wall tumors. Although radiotherapy is effective against the cancer, it is also known to induce delayed damage in surrounded normal tissue, including cardiac damage (1-4). Nowadays, the volume of the heart exposed to radiation is kept as low as possible but for most left sided breast cancer patients the heart still receives a treatment dose of 1 to 5 Gy and this can eventually lead to ischemic heart disease (2,5-8).

Preclinical studies have demonstrated the involvement of radiation-induced microvascular damage in the development of cardiac injury. Radiation leads to endothelial cell loss, which results in a decrease in microvascular density. Radiation also activates thrombotic and inflammatory reactions in the remaining vessels and induces the development of fibrosis in the myocardium (9-12). Perfusion defects, measured with single photon emission computerized tomography (SPECT), have been identified in asymptomatic breast cancer patients 6 to 18 months after radiotherapy. The incidence of perfusion defects is much higher for patients with left sided cancer (71%), where radiation dose to the heart is higher, than for right sided cancer (17%) (13,14). Abnormalities in myocardial perfusion could eventually lead to symptomatic cardiac damage, although this has not been directly shown (14). Studies are ongoing to investigate strategies to overcome microvascular damage after irradiation and prevent delayed cardiac failure.

The development of new blood vessels, originating from precursor cells that differentiate into endothelial cells, is called vasculogenesis. Vasculogenesis is one of two processes, in addition to angiogenesis, by which new blood vessels are formed and which has been shown to be essential in tissue repair and remodeling during acute and chronic ischemic tissue damage (15-18). Vasculogenesis differs from angiogenesis, where preexisting and fully differentiated endothelial cells (ECs) respond to angiogenic growth factors (vascular endothelial growth factor (VEGF), fibroblast growth factor-1 (FGF-1), fibroblast growth factor-2 (FGF-2)) and form new blood vessels from pre-existing blood vessels. In animal models of ischemia, in vitro differentiated endothelial progenitor cells are incorporated into sites of active neovasculogenesis in ischemic tissue, leading to improved perfusion when transplanted after the induction of ischemia (19). Takahashi and colleagues demonstrated that circulating endothelial progenitor cells are also mobilized, as an endogenous response to tissue ischemia or exogenously in response to cytokine therapy, and thereby contribute to neovascularization of ischemic tissues (16). Further, myocardial infarct model has demonstrated the ability of EPCs to incorporate into blood vessels as a reparatory response to tissue ischemia (20).

Therapeutic neovasculogenesis is therefore a promising approach for treatment of ischemic cardiac damage, which could improve cardiac function by stimulating the formation of new vessels in regions of perfusion defects.

Several studies have confirmed the benefit of BM-derived EPCs to restore tissue vascularization after ischemia in the myocardium and other organs (15-19), although these approaches have not been tested after radiation injury.

Hereditary hemorrhagic telangiectasia (HHT) is a vascular disorder with a mutation in the transforming growth factor-beta (TGFbeta) signaling pathway. Patients suffer from dilated blood vessels, characterized by telangiectasis and epistaxis (21,22). HHT type 1 has a mutation in endoglin, an accessory TGFbeta receptor. Endoglin is highly expressed in proliferating endothelial cells and plays a crucial role in angiogenesis. Mice that are deficient in endoglin die in mid-gestation due to vascular and cardiovascular defects. Moreover, mice carrying a single copy of the endoglin gene show a tendency to develop HHT phenotype as they age (23,24). A previous study demonstrated that the recruitment of mononuclear cells (MNCs), which have the ability to stimulate myofibroblast proliferation and stimulate angiogenesis to sites of induced myocardial infarction, is impaired when using HHT1-derived MNCs compared to healthy MNCs (25,26).

In our study we investigate whether radiation-induced microvascular damage can be diminished by revascularization of BM-derived EPCs and whether endoglin plays a role in this process.

Materials and Methods

Mice and treatments groups

Eng^{+/-} C57BL/6 mice were originally obtained from H. Arthur (Institute of Human Genetics, International Centre for Life, Newcastle upon Tyne, UK) and subsequently bred in the Netherlands Cancer Institute. Male Eng^{+/+} mice age 8-12 weeks were randomly allocated (after genotyping by PCR) to receive 16 Gy or 0 Gy to the heart. Mice were housed in a temperature-controlled room with 12 hour light-dark cycle. Standard mouse chow and water were provided ad libitum. Irradiation was performed with 250 kV X-rays, operating at 12 mA and filtered with 0.6 mm Copper. The dose rate was 0.94 Gy/min with a field size of 10.6 x 15 mm (including the whole heart and up to 30% lung volume) and the rest of the mouse was shielded with lead. Mice were immobilized without anesthetics, in a prone position in acrylic perspex jigs. Four cohorts of animals were included for analyses at 40 weeks after

treatment: age-matched controls (sham irradiated with 0 Gy and no transplantations), 16 Gy irradiation alone, 16 Gy followed by transplantation with bone marrow-derived endothelial like progenitor cells (BM-derived EPCs) from either Eng^{+/+} or Eng^{+/-} mice (Figure 1). Animals in the transplantation cohorts were injected i.v., at 16 and 28 weeks after irradiation, with BM-derived EPCs from male Eng^{+/+} mice or Eng^{+/-} littermates age 8 -12 weeks (10⁶ cells per mouse per transplantation). Time points were chosen based on a previous study, where early microvascular damaged was detected by 20 weeks after cardiac irradiation with progression in time (11). A separate group of Eng^{+/+} mice age 8-12 weeks were injected with CellTracker Orange –labeled Eng^{+/+} BM-EPCs (n=10) or CellTracker Orange-labeled Eng^{+/-} BM-EPCs (n=10) 16 or 28 weeks after 16 Gy irradiation (10⁶ cells per mouse per transplantation). Each cohort typically comprised 10 to 15 mice (n=55 in total). This study was in agreement with the Dutch law on animal experiments and welfare, whereby the Animal Experiments Committee of the Netherlands Cancer Institute has evaluated the set-up of the experiments and has given a positive recommendation, in line with the international *Guide for the Care and Use of Laboratory Animals* (Eighth edition). No severe suffering was anticipated in this study. If mice appeared distressed, or lost >15% body weight, they were humanely sacrificed before the planned follow-up time. At termination of the experiment, mice were humanely sacrificed under lethal sodium pentobarbital anesthesia (18 mg per mouse, i.p).

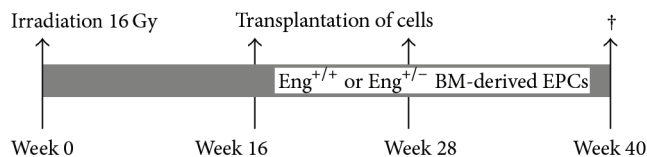


FIGURE 1 Schedule overview.

Schematic representation of Eng^{+/+} or Eng^{+/-} BM-derived EPCs transplantation at both 16 weeks and 28 weeks after 16 Gy heart irradiation.

BM-derived EPCs isolation

Donor male Eng^{+/+} mice or Eng^{+/-} littermates age 8-12 weeks were killed with an overdose of CO₂. Femurs, tibias and illia were surgically dissected, and the adhering tissues were completely removed. Both ends of the bones were excised, and bone marrow cells (BMCs) were harvested by flushing with Endothelial Cell Growth Medium2 (EGM-2), supplemented with fetal calf serum (0.02 ml/ml), VEGF (0.5 ng/ml), basic fibroblast growth factor, epidermal growth factor, insulin-like growth factor-1, ascorbic acid, heparin, hydrocortisone and

antibiotics, using a 25-gauge needle (Promocell, Huissen, the Netherlands). The BMCs were gently re-suspended with an 25-gauge needle in EGM-2 medium before culturing on 1% gelatine coated petridishes (Sigma G9391, bovine skin) at 5% CO₂ at 37°C. Adherent cells were gently washed with PBS at day 3 to remove unattached cells and fresh EGM-2 was added. This procedure was repeated every 2 days until day 14, at which time the BM-derived EPCs were identified by typical endothelial cell (EC) morphology. Petridishes were washed once with PBS and 1 ml trypsin/EDTA (Promocell) was added. The released cells were counted in a CASY Model TT system (Roche, Almere, the Netherlands) and then re-suspended at 10⁶ cells in 100 µl of PBS for transplantation.

BM-derived EPCs localization

Before injection, cells were washed with PBS and incubated with a fluorescent cell viability marker, CellTracker Orange CMTMR (5-(and-6)-(((4-Chloromethyl)Benzoyl)Amino)Tetramethylrhodamine) (Invitrogen, Breda, the Netherlands) for 30 minutes at 37°C. Incubation was at a concentration of 10 µM, which has previously been shown to have no effect on cellular differentiation, migration or proliferation (27). After a second washing step with PBS, cells were trypsinized and CellTracker Orange-labelled BM-EPCs (10⁶ cells per mouse) were injected i.v.. Mice were humanely sacrificed under lethal sodium pentobarbital anesthesia (18 mg per mouse, i.p) 3 days after injection of labeled CellTracker Orange BM-EPCs.

BM-derived EPCs characterization

Typical endothelial cell morphology was identified by cobblestone-like appearance (CCD - B/W Microscope system with a motorized Zeiss AxioObserver Z1 camera, Zeiss, Sliedrecht, the Netherlands).

In vitro tube formation assay

Phenol red-free Matrigel (Becton&Dickinson, Franklin lakes, USA) was added to a pre-chilled 24-well plate. The Matrigel was then solidified by incubation at 37°C for 1 hour. The BM-derived EPCs (200.000 cells/well) were suspended in 500 µl serum-free EGM-2 medium and seeded into each well. The formation of the tube-like network was photographed (CCD - Live Cell Microscope system with a Zeiss AxioCam Black and White camera (AxioCamMRm)), with temperature controlled live cell chamber (Zeiss, Sliedrecht, the Netherlands), every 20 minutes for 20 hours after seeding. Image processing was performed using Zeiss ZEN software (Zeiss).

Immunofluorescence staining

Cells were incubated overnight at 4°C with 2.5 µg/ml acetylated & Dil-labeled low-density lipoprotein (Dil-ac-LDL, Harbor Bio-Products, Heerhugowaard, the Netherlands) and fixed with 4% paraformaldehyde (PFA) before washing with PBS. For detection of lectin binding, cells were fixed in 4% PFA before incubation with Ulexeuropaeus agglutinin (UEA-1, Sigma, Zwijndrecht, the Netherlands) at 1:100 dilution overnight at 4°C. For immunostaining for anti-CD31, the cells were fixed with Zn-fix+0.1%TritonX-100 before being blocked with 3% BSA in TBS+0.1%Tween-20. Cells were incubated with primary antibody in block solution at 1:1000 dilution overnight at 4°C. Cells were washed with TBS/T before application of goat anti-rat alexafluor 568 secondary antibody (Invitrogen, Breda, the Netherlands) at 1:100 dilution.

Cells were further imaged to confirm incorporation of Dil-ac-LDL, binding of UEA-1 and staining for CD31 with CCD - B/W Microscope system with a motorized Zeiss AxioObserver Z1 camera (Zeiss). No fluorescence was observed when cells or tissues were stained with secondary antibody only (no primary antibody; negative control).

No differences in expression of specific endothelial markers were observed between BM-derived EPCs originated from Eng^{+/-} and Eng^{+/+}.

Tissue preparation for histology

At termination of the experiment, the heart was perfused via the aortic arch (retro-grade), under lethal sodium pentobarbital anesthesia (18 mg per mouse, i.p), with PBS (frozen sections) or PBS followed by 1% paraformaldehyde (paraffin sections). The heart was then quickly excised before freezing on dry ice or immersion in 1% paraformaldehyde.

Cross-sections were cut at the level of the mid-horizontal plane of the heart from fixed paraffin-embedded tissues (4 µm) or frozen tissues (7 µm). Frozen cross-sections for BM-EPCs localization were cut in 14 µm thickness.

Frozen sections: An anti-CD31 antibody (1:50, Becton&Dickinson) was used to visualize cardiac vasculature. To determine functional changes in the microvasculature, a histochemical staining with Naphtol AS-MX / DMF and fast Blue BB salt was performed to detect endothelial cell alkaline phosphatase (ALP). Sections were also incubated with antibodies against von Willebrand Factor (vWF) (1:4000, Abcam, Cambridge, USA), as a marker of thrombotic changes. Within one time group all sections were processed identically, at the same time, with precisely the same incubation times for the primary and secondary antibody and DAB solution.

For quantification of microvascular changes, five random fields (40x objective) from transverse sections cut at the mid-horizontal plane of the heart were photographed with a CCD 2 - Color

Microscope system, including a Zeiss AxioCam color camera (AxioCamHRc, Zeiss, Göttingen, Germany). A computerized morphometry system (Leica Qwin V3) was used to quantify the microvascular density (MVD) of CD31 positive structures. Vessels beneath a size of 1.5 or above 200 μm^2 were automatically excluded from the measurements. Photographs of whole sections stained for ALP and vWF were taken with an Aperio scanner (Scanscope-XT, Aperio technologies, Vista, USA) using 40x objective. Analyses of the percentage myocardium, excluding endocardium, positive for each marker were done with a computerized morphometry system (Leica Qwin V3, Leica, Rijswijk, the Netherlands).

Paraffin sections: Interstitial collagen was determined in the myocardium based on Sirius red staining. Photographs of the LV wall, excluding the septum, were taken using a 40x objective (Leica DFC320). Interstitial collagen was quantified in five randomly selected areas of the subendocardium and myocardium of the LV (40x objective) and results were expressed as percentage tissue positive for Sirius red relative to myocardial area. Morphometric parameters were analyzed using a computerized morphometry system (Leica Qwin V3, Leica, Rijswijk, the Netherlands).

Statistics

Data are expressed as mean \pm SEM and groups were compared using non-parametric Mann-Whitney exact U-tests. Group differences were considered statistically significant at $p < 0.05$. Statistical analyses were performed using SPSS version 20.

Results

BM-derived EPCs characterization

After 10-14 days in culture BM-derived EPCs from both Eng^{+/+} and Eng^{+/-} mice exhibited cobblestone morphology (Figure 2A). The endothelial phenotype was further confirmed by a Matrigel tube formation assay (Figure 2B-C). As shown in Figure 2B, BM-derived EPCs form vascular tube-like structures on Matrigel, although the network formation of Eng^{+/-} BM-derived EPCs was delayed compared to Eng^{+/+} BM-derived EPCs, and tube formation was less tight and organized (Figure 2B-C).

The BM-derived EPCs were then further examined for expression of endothelial cell markers using immunohistochemistry. Both Eng^{+/+} and Eng^{+/-} BM-derived EPCs expressed endothelial markers CD31 and bound to UEA-1 and took up Dil-ac-LDL (Figure 2D-F).

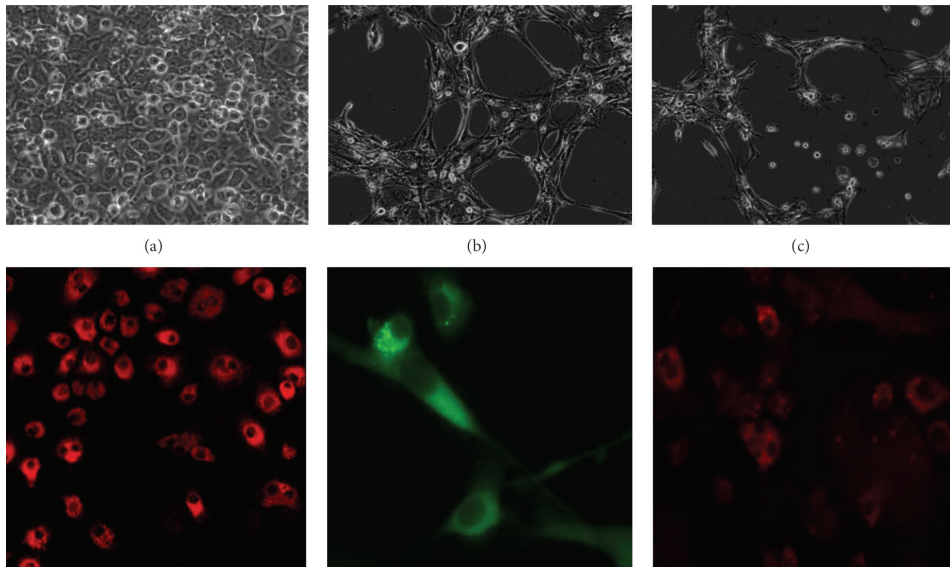


FIGURE 2 EPC characteristics by EPC culture assay and immunohistochemistry (A) Morphological features of confluent EPCs; EPCs after 14 days in culture demonstrating distinct flat, spread out, cobblestone morphology. (B) EPCs plated on Matrigel; EPCs originated from $Eng^{+/+}$ mice (C) and $Eng^{+/-}$ mice show initial capillary tube formation after 6 hours in Matrigel. (D) DiI-acLDL uptake in red and (E) binding of UEA-1 in EPCs (green) were analyzed by fluorescent microscope. Nearly all adherent cells bound UEA and internalized Ac-Dil-LDL. Original magnification 63. (F) Immunohistochemical staining with the endothelial marker CD31 (in red). Staining was analyzed by fluorescent microscopy. Original magnification 40x.

BM-derived EPCs localization

Analysis of frozen sections from mice transplanted with CellTracker Orange-labeled BM-EPCs revealed only a few BM-EPCs in the myocardium (data not shown). There were no differences between BM-EPCs transplantation of cells originated from either $Eng^{+/-}$ or $Eng^{+/+}$ mice.

Radiation-induced microvascular damage

Microvascular density (MVD) decreased significantly after 16 Gy irradiation alone and the decline was not restored by treatment with BM-derived EPCs from either $Eng^{+/+}$ mice or $Eng^{+/-}$ mice (Figure 3A). Radiation-induced changes in MVD were accompanied by endothelial damage, as shown by a marked decrease in ALP activity (Figure 3B) and an increased expression of the thrombotic endothelial marker vWF after irradiation alone (Figure 3C). Changes in ALP activity were not restored by treatment with BM-derived EPCs from $Eng^{+/+}$ mice or from $Eng^{+/-}$ mice (Figure 3B). Similarly, the treatment with BM-derived EPCs did not reduce the radiation-induced expression of vWF (Figure 3C).

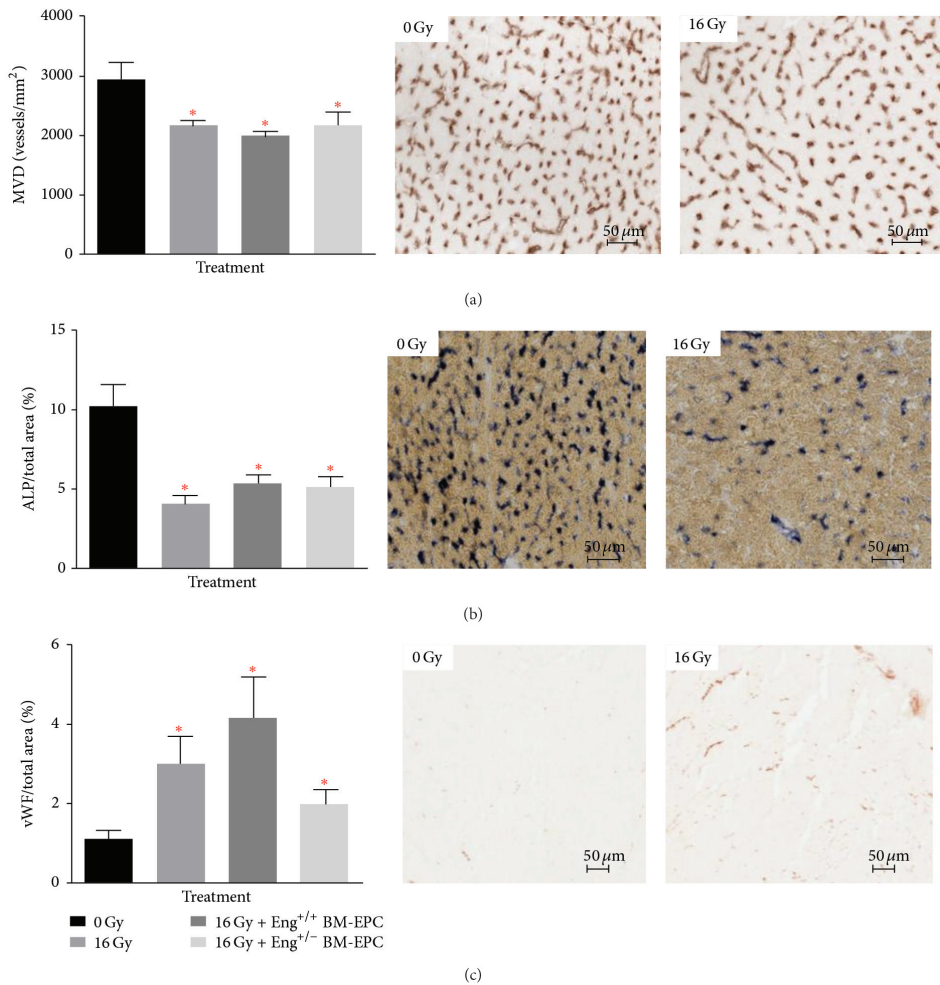


FIGURE 3 Microvascular alterations after irradiation alone or treatment with BM-derived EPCs (A) MVD per unit area expressed as number of microvessels per mm². (B) ALP positive tissue area as % of total tissue. (C) vWF positive tissue area as % of total tissue *p<0.05 compared to age-matched untreated (or do you mean sham treated) controls. Each bar represents the mean (\pm SEM) for at least 5 mice per group.

BM-derived EPCs inhibit the development of radiation-induced cardiac fibrosis

Cardiac fibrosis, established from the extent of collagen staining, was significantly increased after irradiation (Figure 4). BM-derived EPCs treatment (either derived from Eng^{+/+} or Eng^{+/-} mice) inhibited the fibrosis induced by irradiation. Strikingly, BM-derived EPCs from Eng^{+/-} mice were more effective in inhibition of collagen deposition than BM-derived EPCs from Eng^{+/+} mice (Figure 4).

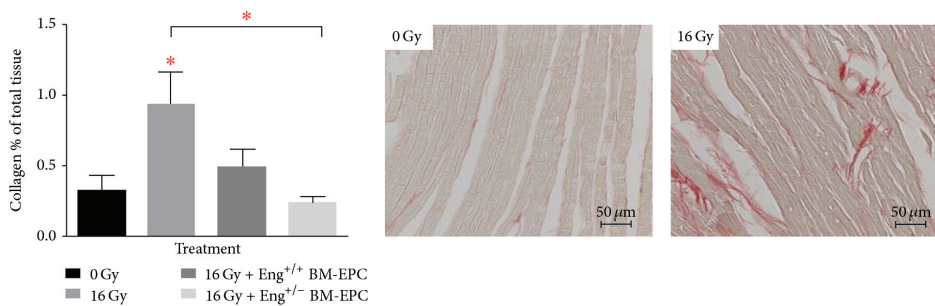


FIGURE 4 Fibrotic changes after irradiation alone or treatment with BM-derived EPCs Collagen positive tissue area as % of total tissue for animals treated with irradiation alone or with BM-derived EPCs * $p < 0.05$ compared to age-matched untreated (or do you mean sham treated) controls. Each bar represents the mean (\pm SEM) for minimal 5 mice per group.

Discussion

In this study we investigated whether endothelial progenitor cells, derived from bone marrow of Eng^{+/+} or Eng^{+/-} mice, can contribute to repair of radiation-induced microvascular injury. Our results indicate that microvascular damage was not improved by this approach but the development of radiation-induced fibrosis was inhibited by transplantation of BM-derived EPCs.

We demonstrated in a previous study that irradiation leads to microvascular damage, which progresses continuously over time, although cardiac function remained within normal ranges until sudden death of the mice. We hypothesized that compensatory mechanisms operate to maintain cardiac function until the extent of underlying damage overwhelmed these mechanisms (11). If severe microvascular damage could be prevented, this might avoid the subsequent cardiac failure. Previous studies using models of surgically induced ischemia to show BM-derived EPCs can stimulate neovascularization that eventually leads to revascularization of ischemic tissue (16,19,20). However, in our radiation model, damage occurs slowly and progressively, resulting in diffuse microvascular damage without the induction of strong ischemic foci. This might explain why no significant stimulation of revascularization took place and transplanted BM-derived EPCs were not able to reverse the progressive radiation-induced microvascular damage. Neither microvascular density nor ALP or vWF changes were influenced by BM-derived EPCs transplantation. On the other hand, transplantation of BM-derived EPCs decreased collagen deposition in the myocardium, thus reducing fibrosis development after irradiation. Cheng and colleagues investigated whether EPC transplantation enhanced cardiac function in a diabetic cardiomyopathy model. They

found, that EPCs reduced the expression of type I collagen, Bax, caspase-3 and p67phox, while increasing the expression of Bcl-2 and manganese superoxide dismutase (MnSOD), thereby improving cardiac function. They suggested that this was due to inhibition of cardiomyocyte apoptosis by EPCs transplantation (28). This might explain why we saw a decrease in collagen deposition after BM-derived EPC transplantation. We suspect, based on previous studies, that endoglin does not directly influence cardiomyocyte survival. Therefore it is not surprising that BM-derived EPCs from Eng^{+/-} mice were at least as competent as Eng^{+/+} cells at inhibition of collagen deposition.

Clinical studies have recently announced the safety of BM-EPCs transplantation, but their efficacy varies widely. This might be the result of uncertainties regarding the best method of administration, timing of administration or cell type utilized. In our pre-clinical studies, we might not have chosen the ideal timing of administration of BM-derived EPCs to restore radiation-induced microvascular damage, or the number of cells may have been insufficient. In our study we cultured the mononuclear fraction in a manner that usually results in EPCs (29,30) and our characterization tests indicated an endothelial-like phenotype. However, we cannot be certain that the cultured cells were true EPCs.

We conclude that radiation-induced endothelial cell damage and cell loss was not restored by transplantation of BM-derived EPCs. However, transplantation did reduce the amount of radiation-induced cardiac fibrosis. Endoglin deficiency in transplanted cells did not impair their ability to reduce fibrosis.

Acknowledgment

The authors would like to thank Dr. Jack Cleutjens, Department of Pathology, University of Maastricht, for help with the Leica Qwin morphometry system. Moreover, we would like to thank Prof.Dr. Christine L. Mummery, Department of Anatomy and Embryology, University of Leiden, and Dr. Marion Scharpfenecker, Department of Biological Stress Response, the Netherlands Cancer Institute, for their helpful discussions.

There were no conflicts of interest.

References

1. Aleman BM, van den Belt-Dusebout AW, De Bruin ML, van 't Veer MB, Baaijens MH, et al. (2007) Late cardiotoxicity after treatment for Hodgkin lymphoma. *Blood* 109: 1878-1886.
2. Darby SC, Ewertz M, Hall P (2013) Ischemic heart disease after breast cancer radiotherapy. *N Engl J Med* 368: 2527.
3. Gyenes G, Rutqvist LE, Liedberg A, Fornander T (1998) Long-term cardiac morbidity and mortality in a randomized trial of pre- and postoperative radiation therapy versus surgery alone in primary breast cancer. *Radiother Oncol* 48: 185-190.
4. McGale P, Darby SC, Hall P, Adorfsson J, Bengtsson NO, et al. (2011) Incidence of heart disease in 35,000 women treated with radiotherapy for breast cancer in Denmark and Sweden. *Radiother Oncol* 100: 167-175.
5. Aznar MC, Korreman SS, Pedersen AN, Persson GF, Josipovic M, et al. (2011) Evaluation of dose to cardiac structures during breast irradiation. *Br J Radiol* 84: 743-746.
6. Jaggi R, Moran J, Marsh R, Masi K, Griffith KA, et al. (2010) Evaluation of four techniques using intensity-modulated radiation therapy for comprehensive locoregional irradiation of breast cancer. *Int J Radiat Oncol Biol Phys* 78: 1594-1603.
7. Lohr F, El-Haddad M, Dobler B, Grau R, Wertz HJ, et al. (2009) Potential effect of robust and simple IMRT approach for left-sided breast cancer on cardiac mortality. *Int J Radiat Oncol Biol Phys* 74: 73-80.
8. Schubert LK, Gondi V, Sengbusch E, Westerly DC, Soisson ET, et al. (2011) Dosimetric comparison of left-sided whole breast irradiation with 3DCRT, forward-planned IMRT, inverse-planned IMRT, helical tomotherapy, and topotherapy. *Radiother Oncol* 100: 241-246.
9. Boerma M, Kruse JJ, van Loenen M, Klein HR, Bart CI, et al. (2004) Increased deposition of von Willebrand factor in the rat heart after local ionizing irradiation. *Strahlenther Onkol* 180: 109-116.
10. Gabriels K, Hoving S, Seemann I, Visser NL, Gijbels MJ, et al. (2012) Local heart irradiation of ApoE(-/-) mice induces microvascular and endocardial damage and accelerates coronary atherosclerosis. *Radiother Oncol* 105: 358-364.
11. Seemann I, Gabriels K, Visser NL, Hoving S, te Poele JA, et al. (2012) Irradiation induced modest changes in murine cardiac function despite progressive structural damage to the myocardium and microvasculature. *Radiother Oncol* 103: 143-150.
12. Schultz-Hector S, Balz K (1994) Radiation-induced loss of endothelial alkaline phosphatase activity and development of myocardial degeneration. An ultrastructural study. *Lab Invest* 71: 252-260.
13. Marks LB, Yu X, Prosnitz RG, Zhou SM, Hardenbergh PH, et al. (2005) The incidence and functional consequences of RT-associated cardiac perfusion defects. *Int J Radiat Oncol Biol Phys* 63: 214-223.

14. Seddon B, Cook A, Gothard L, Salmon E, Latus K, et al. (2002) Detection of defects in myocardial perfusion imaging in patients with early breast cancer treated with radiotherapy. *Radiother Oncol* 64: 53-63.
15. Isner JM, Asahara T (1999) Angiogenesis and vasculogenesis as therapeutic strategies for postnatal neovascularization. *J Clin Invest* 103: 1231-1236.
16. Takahashi T, Kalka C, Masuda H, Chen D, Silver M, et al. (1999) Ischemia- and cytokine-induced mobilization of bone marrow-derived endothelial progenitor cells for neovascularization. *Nat Med* 5: 434-438.
17. Vailhe B, Vittet D, Feige JJ (2001) In vitro models of vasculogenesis and angiogenesis. *Lab Invest* 81: 439-452.
18. Losordo DW, Dimmeler S (2004) Therapeutic angiogenesis and vasculogenesis for ischemic disease: part II: cell-based therapies. *Circulation* 109: 2692-2697.
19. Urbich C, Heeschen C, Aicher A, Dernbach E, Zeiher AM, et al. (2003) Relevance of monocytic features for neovascularization capacity of circulating endothelial progenitor cells. *Circulation* 108: 2511-2516.
20. Asahara T, Masuda H, Takahashi T, Kalka C, Pastore C, et al. (1999) Bone marrow origin of endothelial progenitor cells responsible for postnatal vasculogenesis in physiological and pathological neovascularization. *Circ Res* 85: 221-228.
21. Abdalla SA, Letarte M (2006) Hereditary haemorrhagic telangiectasia: current views on genetics and mechanisms of disease. *J Med Genet* 43: 97-110.
22. van den Driesche S, Mummery CL, Westermann CJ (2003) Hereditary hemorrhagic telangiectasia: an update on transforming growth factor beta signaling in vasculogenesis and angiogenesis. *Cardiovasc Res* 58: 20-31.
23. Arthur HM, Ure J, Smith AJ, Renforth G, Wilson DI, et al. (2000) Endoglin, an ancillary TGFbeta receptor, is required for extraembryonic angiogenesis and plays a key role in heart development. *Dev Biol* 217: 42-53.
24. Bourdeau A, Dumont DJ, Letarte M (1999) A murine model of hereditary hemorrhagic telangiectasia. *J Clin Invest* 104: 1343-1351.
25. Post S, Smits AM, van den Broek AJ, Sluijter JP, Hofer IE, et al. (2010) Impaired recruitment of HHT-1 mononuclear cells to the ischaemic heart is due to an altered CXCR4/CD26 balance. *Cardiovasc Res* 85: 494-502.
26. Lebrin F, Mummery CL (2008) Endoglin-mediated vascular remodeling: mechanisms underlying hereditary hemorrhagic telangiectasia. *Trends Cardiovasc Med* 18: 25-32.

27. Hinds KA, Hill JM, Shapiro EM, Laukkanen MO, Silva AC, et al. (2003) Highly efficient endosomal labeling of progenitor and stem cells with large magnetic particles allows magnetic resonance imaging of single cells. *Blood* 102: 867-872.
28. Cheng Y, Guo S, Liu G, Feng Y, Yan B, et al. (2012) Transplantation of bone marrow-derived endothelial progenitor cells attenuates myocardial interstitial fibrosis and cardiac dysfunction in streptozotocin-induced diabetic rats. *Int J Mol Med* 30: 870-876.
29. Sekiguchi H, li M, Jujo K, Yokoyama A, Hagiwara N, et al. (2011) Improved culture-based isolation of differentiating endothelial progenitor cells from mouse bone marrow mononuclear cells. *PLoS One* 6: e28639.
30. Wang QR, Wang BH, Huang YH, Dai G, Li WM, et al. (2008) Purification and growth of endothelial progenitor cells from murine bone marrow mononuclear cells. *J Cell Biochem* 103: 21-29.



Chapter 8

Discussion

The purpose of this thesis was to investigate the molecular players and pathways of late cardiac damage in cancer patients treated with radiotherapy and anthracycline chemotherapy. A better understanding of these mechanisms, and the role of the microvasculature in this process, should allow us to develop suitable intervention strategies.

Therefore, we first determined the dose and time dependency of the cardiac structural and microvascular dysfunction after single dose cardiac irradiation in wild-type mice (**chapter 2**). We next compared these findings to those from the same set up in time and dose, but using *ApoE^{-/-}* mice. This hypercholesterolemic model develops spontaneous atherosclerosis with aging (unlike wild type mice) and therefore mimics the effects of a western-type diet, which most citizens in the developed countries have chosen (**chapter 3**). We have also taken into account that many breast cancer patients receive anthracycline chemotherapy in addition to radiotherapy and, in some cases of HER overexpressed breast cancer, HER-inhibitors, like lapatinib. We investigated whether the additional chemotherapy treatment increased the existing radio-induced cardiac damage (**chapter 4**). To further understand the role of endothelial cell damage in radiation-induced cardiac damage, we focused on a specific gene (endoglin) that plays an important role in proliferating endothelial cells. Endothelial cells are highly sensitive to radiation and persistent damage after radiotherapy may inhibit restoration of organ function (**chapter 5**). Finally we explored two possible intervention strategies: treatment with thalidomide and bone marrow derived endothelial cells. While thalidomide acts as an anti-inflammatory agent and could further prevent organ failure by inhibiting tissue fibrosis, bone marrow derived endothelial cells may be able to restore cardiac microvasculature and therefore restore organ function (**chapter 6 & 7**).

Dose and time dependency of structural and functional cardiac damage

It is widely recognized that thoracic radiotherapy increases the risk of late cardiac damage, but little is known about the details of the pathogenesis of this damage.

We demonstrated in **chapter 2, 3 and 5** that local irradiation affects cardiac structure and microvascular function in a dose and time-dependent manner; with substantial damage after intermediate and high dose irradiation (8 and 16 Gy) and minor alterations after lower doses (2 Gy). Moreover, high doses induced changes at earlier time points and these effects progressed in time.

Endothelial injury and loss has been described as an early event in radiation-induced damage, associated with a pro-inflammatory, pro-thrombotic anti-fibrinolytic phenotype (1, 2). We found decreased amounts of endothelial cell ALP and increased vWF in irradiated hearts. ALP

is abundantly present in healthy cardiac microvasculature whereas loss of ALP is indicative of endothelial cell damage (3). ALP expression was significantly reduced at 20 weeks after doses of 8 or 16 Gy and after 2, 8 or 16 Gy at later time points. Increased deposition of vWF in irradiated rat hearts has been previously described as an indicator of thrombotic endothelial cell damage (4). In our studies, increases in vWF deposition were limited to hearts that received 8 or 16 Gy, with the largest increase at later times after the highest dose. Endothelial loss was measured after 16 Gy at 20 weeks and at 40–60 weeks after lower doses, which confirms earlier studies with rat hearts (3). However, this did not lead to a marked loss of vascular perfusion and no severe hypoxia was detected. A transient increase in MVD at 20 weeks after 2 and 8 Gy (**chapter 2**) was measured, presumably due to stimulated proliferation in response to damage, although this was insufficient to stimulate a granulomatous response (5).

Endothelial injury at 40 weeks after 8 and 16 Gy finally led to blood vessel rupture, indicated by strong extracellular albumin deposition. Albumin binds to amyloid-beta in blood plasma and may be the reason why albumin deposition correlates with myocardial amyloid deposition (6). A prominent clinical feature of cardiac amyloidosis is heart failure (7). The presence of amyloidosis (**chapter 2**) may therefore have contributed to the sudden death seen in 38% of mice between 30 and 40 weeks after 16 Gy. The amount of interstitial collagen in the myocardium indicated the development of fibrosis and this was significantly increased at 40 weeks after 8 to 16 Gy and 60 weeks after 2 to 8 Gy, although this was never more than 2-5% of the tissue area (**chapter 2**). Cardiac function remained largely unchanged despite the progressive deterioration of microvascular structure and function. The unchanged cardiac function, combined with progressive structural and functional microvascular damage and the sudden deaths of mice, without preceding loss of cardiac function, suggest that compensatory mechanisms maintain cardiomyocyte function until a certain threshold of damage is exceeded. Regardless of the initial nature of the events that cause cardiac damage, the cardiac pathology remains asymptomatic in the early stages due to compensatory mechanisms. The compensatory mechanism starts off with a decline in pumping capacity as illustrated by decreases in ESV and EDV, and activates the adrenergic nervous system, the renin angiotensin system, the cytokine system, and the IGF-1 receptor/PI3K/Akt signaling pathway. However, eventually the damaged hearts become overtly symptomatic and heart failure ensues (8-10).

Combining high-dose irradiation with hypercholesterolemia in *ApoE^{-/-}* mice accelerated the development of coronary atherosclerosis (**chapter 3**). The number of coronary atherosclerotic lesions in the mid part of the heart at 20 weeks after irradiation was increased and the

endocardium of the 16 Gy irradiated mice showed the appearance of foam cell accumulations at 20 weeks after irradiation, as well as erythrocyte accumulations, which was not observed after 0, 2 or 8 Gy. However, radiation-induced microvascular endothelial cell injury, as described in detail earlier, was not enhanced by hypercholesterolemia, although the baseline level of inflammation in unirradiated hearts was higher. Micro array analysis confirmed the early and pronounced onset of inflammatory response in this hypercholesterolemia model. The important role of *ApoE* in initiating immune/ inflammatory action has been well studied by Tenger et al. and explains the higher baseline level and pronounced inflammatory reaction in *ApoE*^{-/-} mice. Despite the observed blood vessel leakage in *ApoE*^{-/-} irradiated hearts, we could not detect any amyloid deposition. This can be explained by the fact that ApoE is a component of amyloidosis and a lack of ApoE therefore prevents its formation (11).

We have confirmed that endothelial cells are highly sensitive to radiation and aberrant signaling by damaged cells affects the pathological progression of radiation induced tissue damage, which has been described in earlier studies (12-14). Endoglin is co-receptor for TGF-β1 that is essential for angiogenesis and predominantly expressed in activated vascular endothelial cells (15-20).

In **chapter 5** we investigated whether dose- and time dependent cardiac damage after irradiation is influenced by endoglin, which may play a crucial role in endothelial cell proliferation and revascularization of damaged heart tissue. For these studies we used *Eng*^{+/-} and *Eng*^{+/+} mice to investigate the influence of endoglin in radiation-induced cardiac damage. Gene expression analysis demonstrated a decreased inflammatory response in *Eng*^{+/-} mice compared to *Eng*^{+/+} mice. Further, fibrosis related genes were only upregulated in *Eng*^{+/+} mice during the early phase of radiation induced cardiac damage (4 weeks), consistent with the finding that collagen deposition in the myocardium was increased at 20 weeks after irradiation in *Eng*^{+/+} mice only. Our observations are consistent with studies showing that endoglin is involved in inflammation, by playing a role in leucocyte adhesion and transmigration, as well as in reduced expression of inflammatory cytokines and reduced inflammatory infiltration (21, 22). No differences in inflammatory response or fibrotic response were detected between the strains at later time points. This suggests that endoglin haplo-insufficiency only limits inflammation and fibrosis in the early phase of radiation-induced cardiac damage. Further, endothelial damage in cardiac microvasculature was independent of endoglin expression.

Possible additional damage to cardiac microvasculature and cardiomyocyte when inhibiting EGFR signaling?

Breast cancer can be divided into two subtypes: Her2-positive and Her2-negative. Her2-positive breast cancers are prone to be highly aggressive, fast growing, highly invasive, resistant to CT and RT and characterized by epidermal growth factor receptor 2 (ErbB2) overexpression. Thus, Her2-inhibition became a common additional treatment in these breast cancers. Treatment of Her2-inhibitors in combination with adjuvant chemotherapy showed a reduction in the risk of relapse and death by 50% and 30% respectively (23-25). But the hallmark side effect of treatment with Her2-inhibitors is cardiac toxicity. Little is known about the detailed mechanism of cardiac toxicity after Her2-inhibitor treatment. However, ErbB2 signaling and the ligand Neuregulin-1 are known to play a crucial role in survival and growth of cardiac myocytes (26, 27). Moreover, a recent study demonstrated that irradiation inhibited ErbB2 signaling in rat hearts until the onset of fibrosis after 10 weeks. As fibrosis progressed, ErbB2 and the EGFR ligand neuregulin were significantly upregulated, presumably as an attempt to regenerate the myocardium (28). This raises the question whether delayed inhibition of ErbB2 after CT or RT could lead to increased cardiac toxicity. Therefore, in **chapter 4** we mimicked the clinical treatment schedule by either giving 20 weeks of the Her2-inhibitor lapatinib, directly with RT or CT or delayed until 20 weeks after RT or CT.

As described in detail in **chapter 2, 3 and 4**, RT induces dose- and time depended cardiac microvasculature damage without direct effect on the cardiomyocytes. None of these endothelial changes were more severe after combined treatments with lapatinib than after irradiation alone. However, clinical findings still remain controversial. The NCCTG Phase III Trial N9831 found that concurrent adjuvant RT and Her2-inhibitor trastuzumab for early-stage BC was not associated with increased acute cardiac adverse events at a median follow-up of 3.7 years (29). However, a prospective study of 106 patients treated by concurrent trastuzumab-radiotherapy for non-metastatic BC does show increased cardiac events (left ventricular systolic dysfunction) although these were characterized as tolerated, reversible and mild and occurred in 6 patients with preexisting risk factors like diabetes and age (30). In a clinical study where a total of 499 consecutive HER2-positive women were treated with adjuvant trastuzumab administered sequentially after RT and followed for 1 year, cardiac dysfunction occurred but again this was described as mild and asymptomatic in the majority of patients (31). However, most of these studies are missing long follow up or even missing a control group with Her2-inhibitor without radiotherapy and included patients with risk factors like smoking, diabetes, age, and hypertension.

Moreover, we found in **chapter 4**, that direct or delayed lapatinib decreased CD45+ and F4/80+ cells in the irradiated epicardium, compared to irradiation alone. Indicating, that blocking PI3K/Akt/mTOR signaling pathway decreases inflammatory response in normal tissue. Kinases play a crucial role in expression and activation of inflammatory mediators. PI3K/Akt pathway can function either as a positive or negative regulator of TLR signaling. (32). In a rat model it was shown that selective inhibition of PI3K/Akt/mTOR signaling pathway regulated macrophage autophagy and markedly affected atherosclerotic plaque inflammation, burden and vulnerability. These molecular and cellular effects translated into a successful prevention of plaque disruption, even in the presence of endothelial injury, hyperlipidemia and pharmacological triggering (33). Further, in a study with ovalbumin (OVA)-induced asthmatic mice, blocking the PI3K/Akt signaling pathway attenuated the early stages of airway remodeling induced by OVA, by regulating the abnormal process of epithelial-mesenchymal transition (34).

Our data do not indicate cardiac dysfunction after radiation alone or in combination with lapatinib, in contrast to the mild but significant changes in cardiac function after lapatinib alone. These data are consistent with the important role of ErbB signaling to maintain myocardium functionality and imply that that this compensatory mechanisms initiated by irradiation still operate in the presence of lapatinib. Compensatory mechanisms and pro-survival pathways might play a role in maintaining cardiomyocyte function in a damaged heart, at least until the extent of damage overwhelms the potential for stimulated survival. Sridharan et al. recently demonstrated upregulation of ErbB signaling in the irradiated rat heart in parallel with developing cardiac fibrosis, leading to the suggestion that ErbB signaling and pro-survival pathways are activated in an attempt to regenerate the myocardium (28). Moreover, inactivation of ErbB4 in ventricular muscle cells led to a severe dilated cardiomyopathy, demonstrating the important role of ErbB signaling in the myocardium (35). Kaplan-Meier estimates of overall survival in our studies indicated more unscheduled deaths of mice after treatment with Dox (27%), especially when combined with lapatinib (36 and 33 % deaths for direct and delayed lapatinib) compared to treatment with radiation alone (0%) or in combination with direct lapatinib (7%) and delayed lapatinib (12%) (**chapter 4**). Since the group analyses of morphological changes were done on material from surviving animals only, our results probably represents an underestimate of the total toxic effects of Dox. Changes in the microvasculature after Dox alone or with lapatinib were not seen. Nevertheless, fibrosis and degenerated cardiomyocytes (EM study) and 27–36% animal lethality, as well as decreased cell viability in vitro, do indicate doxorubicin-induced damage to the myocardium

via cardiomyocytes. Although anthracyclines induce acute damage, clinical symptoms are mostly detectable months or years after treatment (36). Therefore, besides acute myocardial damage, delayed and indirect microvascular damage may occur at later times.

Although our studies have shed some light on the mechanisms of development of radiation-induced cardiac damage, alone or in combination with anthracyclines or Her2-inhibitors, there are many unresolved questions that should be addressed in future studies.

How to overcome radiation-induced cardiac damage

Thalidomide is recently re-emerging as a treatment for inflammatory disease and cancers, including cutaneous lupus, Crohn's disease, rheumatoid arthritis, multiple myeloma and graft-versus-host disease, because of its anti-inflammatory and anti-angiogenic effects (37). Thalidomide inhibits the production of TNF- α (tumor necrosis factor-alpha), which regulates inflammatory cascades and inhibits the expression of vascular endothelial growth factor (VEGF) and interleukin-6 (IL-6), which play a role in angiogenesis (38-41).

Recent studies also showed evidence of anti-fibrotic activity in various fibrosis-related diseases such as lung fibrosis (42, 43) and remodeling after myocardial infarction (44). Furthermore, thalidomide was found to induce vessel maturation by stimulating mural cell coverage and thereby rescuing vessel wall defects (45).

In our previous studies (**chapter 2, 3, 4 and 5**) we have shown that local heart irradiation leads to cardiac damage by activating inflammatory response, which eventually led to fibrosis, decrease in microvasculature density and endothelial cell damage and mild but non-progressive changes in cardiac function. We hypothesized that by administering thalidomide daily to the mice we could inhibit the inflammatory response and therefore inhibit fibrosis development. In **chapter 6** we confirmed that irradiation induced inflammation and fibrosis and compromised microvascular function but no protective effect of thalidomide was seen. Therefore, we concluded that thalidomide is unable to inhibit radiation-induced inflammatory response and fibrosis after irradiation, at least in the doses we used.

Recent studies have shown evidence of anti-fibrotic activity of thalidomide in various, non-radiation related, fibrotic diseases such as lung fibrosis induced by bleomycin sulfate administration. IL-6 and TGF- β 1 play important roles in pulmonary fibrosis and reduced levels were found after thalidomide treatment leading to reduced collagen deposition (42, 43). Kim et al. showed reduced collagen levels in thalidomide treated rats suffering from diabetic cardiomyopathy (46). Thalidomide also attenuated the development of fibrosis during post-infarction myocardial remodeling in a rat model, although no effect on cardiac function was

seen (44). We can only hypothesize that our radiation-induced fibrotic model initiates less fibrosis compared to diabetic cardiomyopathy and myocardial infarction models, and therefore the effect of thalidomide is less visible. Also, we started thalidomide treatment at 16 weeks after irradiation, which is when radiation-induced cardiac fibrosis occurs, whereas other non-radiation cardiac models showing benefits of thalidomide started drug treatment at the same time as the fibrotic stimulus (47, 48). We cannot exclude that earlier treatment may have been more effective in our radiation model. A recently published study of Scharpfenecker et al. did show some beneficial effects from thalidomide in irradiated mouse kidneys (49). The inflammatory processes after kidney irradiation were inhibited, but thalidomide could not impede the development of fibrosis assessed at 40 weeks. In their study they suggest that CD45+ cells are not the main source of profibrotic cytokines in the irradiated kidney but that the observed reduction in the number of inflammatory cells may have slowed the progression of kidney fibrosis at time points beyond 40 weeks. Scharpfenecker et al. also mentioned that the delayed treatment with thalidomide, at week 16 after irradiation, might limit the impact of the reduced inflammatory response. Once more, one can hypothesize that the anti-inflammatory and anti-fibrotic effect of thalidomide is an organ-specific effect, which needs to be further studied.

We confirmed in our studies (**chapter 2, 3, 4 and 5**) the importance of endothelial cell proliferation and revascularization to restore microvasculature damage and maintain function of the irradiated heart. We have therefore examined the potential of bone marrow-derived endothelial progenitor cells (BM-derived EPCs) for restoration of radiation-induced microvascular damage. However, in this study we could not demonstrate that microvascular damage was improved by this approach, although the development of radiation-induced fibrosis was inhibited by transplantation of BM-derived EPCs. Previous studies using models of surgically induced cardiac infarct show that BM-derived EPCs can home to sites of ischemia and stimulate revascularization (50-52). However, in our radiation model, damage occurs slowly and progressively, resulting in diffuse microvascular damage without the induction of strong ischemic foci. This might explain why no significant stimulation of revascularization took place and transplanted BM-derived EPCs were not able to reverse the progressive radiation-induced microvascular damage. A recently published study investigated the antifibrotic effect of bone marrow-derived progenitor cells in a diabetic mouse model. Kishore et al. showed that several miRNAs, that have been implicated in the regulation of fibrosis, are overexpressed after MI. One of these miRNA, miR-155, is reduced in expression after BMPC administration and this could be the cause of the reduced the fibrosis response. Further, BMPC releases

hepatocyte growth factor (HGF), which inhibits miR-155-mediated profibrotic signaling (53). In studies of acute ischemic cardiac injury, BM-derived EPCs have been shown to contribute to recovery of the vascular system. Following mobilization into the circulation, EPCs are recruited to the traumatized or ischaemic tissues in response to secretion of stromal cell-derived factor-1 (54, 55), or vascular endothelial growth factor (56).

However, in a setting of radiation-induced vascular disease BM-derived EPCs did not restore dysfunctional endothelium and endothelial homeostasis (57). Perry et al. confirmed a lack of BM-derived endothelial cell incorporation into the lining of the dysfunctional endothelium, supporting findings of Hillebrands et al. and Aicher et al. (58, 59). In both studies the authors have shown that BM-derived EPCs do not contribute substantially to endothelial-cell replacement. Another study of Guthrie et al. showed evidence for positive effect of BM-derived EPCs after laser-induced retinal injury (60). One striking difference between these studies is that the laser treatment induced photoagglutination of the retinal vasculature and that may have produced an inflammatory or cytokine response leading to systemic endothelial cell damage and renewal. In the study of Perry et al, however, no injury was inflicted during the time interval between sub-lethal radiation, BM transplant, and tissue analysis (57).

Thus, it seems to be crucial whether BM-EPCs are administered during an acute phase of vascular injury or a chronic phase of injury. Related to our study, where we face a chronic phase of vascular injury, this could once more explain why we do not see a restore of endothelial cell damage after BM-EPCs administration.

Concluding remarks

With our studies, we show that radiation to the heart induces modest changes in cardiac function despite progressive structural (e.g. fibrosis) and microvascular damage. Further, the additional presence of hypercholesterolemia accelerated the development of coronary atherosclerosis. When combining radiation treatment with the cardiomyocyte pro-survival pathway inhibitor lapatinib, no enhanced radiation toxicity was detected. In our radiation mouse models, damage occurs slowly and progressively, resulting in diffuse microvascular damage without the induction of strong ischemic foci. This might explain why transplanted BM-derived EPCs were not able to reverse the progressive radiation-induced microvascular damage, nor did anti-fibrotic agent thalidomide inhibit the damage. Also, we have confirmed that the heart can compensate for a significant structural and microvascular damage until a certain threshold, before collapsing and leading to sudden death.

Future perspectives

Studies described in this thesis gave first insights in the underlying mechanisms of radiation and anthracycline induced cardiovascular damage but also raised new questions and hypothesizes for future research.

In our first study we described the phenomenon of sudden death in mice irradiated with 16 Gy. While structural and vascular damage were demonstrated, cardiac function remained within normal limits until sudden death. Further micro array analysis of irradiated hearts gave indications that one, or even more, compensatory mechanism may operate in damaged hearts. Future studies could investigate this further by first focusing on a group of interesting genes that were specifically upregulated in irradiated hearts. Proteomic analysis and immunohistochemistry may further indicate whether these genes play a role in protection of moderately damaged hearts, until the extent of damage becomes overwhelming. Mouse knock-out models could finally confirm the importance of these genes.

Cardiac function was mostly measured at 20 and 40 weeks after irradiation and demonstrated little or no changes in the left ventricle function. Further experiments, preferably with a small animal ultrasound device, with shorter intervals and starting at earlier time-points may be able to detect changes in the cardiac function prior to sudden death. Also the ultrasound, rather than the SPECT/CT, can detect myocardial perfusion abnormalities and may be more sensitive than the SPETC/CT.

In general, earlier time-points and shorter intervals after irradiation would give a broader insight of the late side effects in normal cardiac tissue.

References

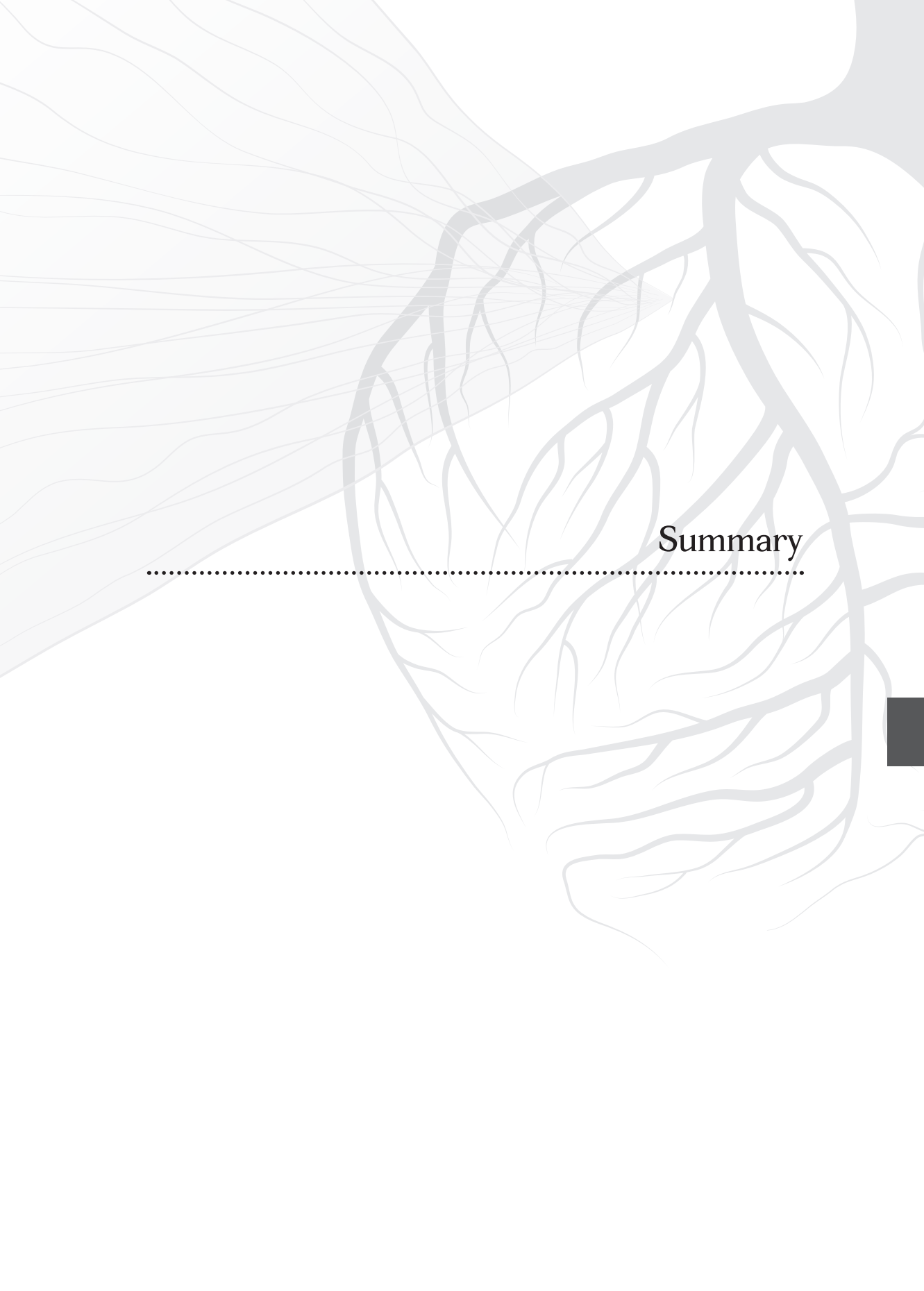
1. Bentzen SM. Preventing or reducing late side effects of radiation therapy: radiobiology meets molecular pathology. *Nature reviews Cancer*. 2006;6(9):702-13.
2. Wang J, Boerma M, Fu Q, Hauer-Jensen M. Significance of endothelial dysfunction in the pathogenesis of early and delayed radiation enteropathy. *World journal of gastroenterology : WJG*. 2007;13(22):3047-55.
3. Schultz-Hector S, Balz K. Radiation-induced loss of endothelial alkaline phosphatase activity and development of myocardial degeneration. An ultrastructural study. *Laboratory investigation; a journal of technical methods and pathology*. 1994;71(2):252-60.
4. Boerma M, Kruse JJ, van Loenen M, Klein HR, Bart CI, Zurcher C, et al. Increased deposition of von Willebrand factor in the rat heart after local ionizing irradiation. *Strahlentherapie und Onkologie : Organ der Deutschen Rontgengesellschaft [et al]*. 2004;180(2):109-16.
5. Lauk S, Trott KR. Endothelial cell proliferation in the rat heart following local heart irradiation. *International journal of radiation biology*. 1990;57(5):1017-30.
6. Stanyon HF, Viles JH. Human serum albumin can regulate amyloid-beta peptide fiber growth in the brain interstitium: implications for Alzheimer disease. *The Journal of biological chemistry*. 2012;287(33):28163-8.
7. McCarthy RE, 3rd, Kasper EK. A review of the amyloidoses that infiltrate the heart. *Clinical cardiology*. 1998;21(8):547-52.
8. Ceci M, Ross J, Jr., Condorelli G. Molecular determinants of the physiological adaptation to stress in the cardiomyocyte: a focus on AKT. *Journal of molecular and cellular cardiology*. 2004;37(5):905-12.
9. Hill SA, Balion CM, Santaguida P, McQueen MJ, Ismaila AS, Reichert SM, et al. Evidence for the use of B-type natriuretic peptides for screening asymptomatic populations and for diagnosis in primary care. *Clinical biochemistry*. 2008;41(4-5):240-9.
10. Mann DL, Bristow MR. Mechanisms and models in heart failure: the biomechanical model and beyond. *Circulation*. 2005;111(21):2837-49.
11. Guan J, Mishra S, Shi J, Plovie E, Qiu Y, Cao X, et al. Stanniocalcin1 is a key mediator of amyloidogenic light chain induced cardiotoxicity. *Basic research in cardiology*. 2013;108(5):378.
12. Juncos LI, Cornejo JC, Gomes J, Baigorria S, Juncos LA. Abnormal endothelium-dependent responses in early radiation nephropathy. *Hypertension*. 1997;30(3 Pt 2):672-6.
13. Paris F, Fuks Z, Kang A, Capodici P, Juan G, Ehleiter D, et al. Endothelial apoptosis as the primary lesion initiating intestinal radiation damage in mice. *Science*. 2001;293(5528):293-7.

14. Ran XZ, Ran X, Zong ZW, Liu DQ, Xiang GM, Su YP, et al. Protective effect of atorvastatin on radiation-induced vascular endothelial cell injury in vitro. *Journal of radiation research*. 2010;51(5):527-33.
15. Arthur HM, Ure J, Smith AJ, Renforth G, Wilson DI, Torsney E, et al. Endoglin, an ancillary TGFbeta receptor, is required for extraembryonic angiogenesis and plays a key role in heart development. *Developmental biology*. 2000;217(1):42-53.
16. Bourdeau A, Dumont DJ, Letarte M. A murine model of hereditary hemorrhagic telangiectasia. *The Journal of clinical investigation*. 1999;104(10):1343-51.
17. Lebrin F, Goumans MJ, Jonker L, Carvalho RL, Valdimarsdottir G, Thorikay M, et al. Endoglin promotes endothelial cell proliferation and TGF-beta/ALK1 signal transduction. *The EMBO journal*. 2004;23(20):4018-28.
18. Li C, Hampson IN, Hampson L, Kumar P, Bernabeu C, Kumar S. CD105 antagonizes the inhibitory signaling of transforming growth factor beta1 on human vascular endothelial cells. *FASEB journal : official publication of the Federation of American Societies for Experimental Biology*. 2000;14(1):55-64.
19. Lopez-Novoa JM, Bernabeu C. The physiological role of endoglin in the cardiovascular system. *American journal of physiology Heart and circulatory physiology*. 2010;299(4):H959-74.
20. McAllister KA, Grogg KM, Johnson DW, Gallione CJ, Baldwin MA, Jackson CE, et al. Endoglin, a TGF-beta binding protein of endothelial cells, is the gene for hereditary haemorrhagic telangiectasia type 1. *Nature genetics*. 1994;8(4):345-51.
21. Rossi E, Sanz-Rodriguez F, Eleno N, Duwell A, Blanco FJ, Langa C, et al. Endothelial endoglin is involved in inflammation: role in leukocyte adhesion and transmigration. *Blood*. 2013;121(2):403-15.
22. Scharpfenecker M, Froot B, Russell NS, Stewart FA. The TGF-beta co-receptor endoglin regulates macrophage infiltration and cytokine production in the irradiated mouse kidney. *Radiotherapy and oncology : journal of the European Society for Therapeutic Radiology and Oncology*. 2012;105(3):313-20.
23. Piccart-Gebhart MJ, Procter M, Leyland-Jones B, Goldhirsch A, Untch M, Smith I, et al. Trastuzumab after adjuvant chemotherapy in HER2-positive breast cancer. *The New England journal of medicine*. 2005;353(16):1659-72.
24. Romond EH, Perez EA, Bryant J, Suman VJ, Geyer CE, Jr., Davidson NE, et al. Trastuzumab plus adjuvant chemotherapy for operable HER2-positive breast cancer. *The New England journal of medicine*. 2005;353(16):1673-84.
25. Slamon DJ, Romond EH, Perez EA, Cme Consultants I. Advances in adjuvant therapy for breast cancer. *Clinical advances in hematology & oncology : H&O*. 2006;4(3 Suppl 7):suppl 1, 4-9; discussion suppl 10; quiz 2 p following suppl

26. De Keulenaer GW, Doggen K, Lemmens K. The vulnerability of the heart as a pluricellular paracrine organ: lessons from unexpected triggers of heart failure in targeted ErbB2 anticancer therapy. *Circulation research*. 2010;106(1):35-46.
27. Zhao YY, Sawyer DR, Baliga RR, Opel DJ, Han X, Marchionni MA, et al. Neuregulins promote survival and growth of cardiac myocytes. Persistence of ErbB2 and ErbB4 expression in neonatal and adult ventricular myocytes. *The Journal of biological chemistry*. 1998;273(17):10261-9.
28. Sridharan V, Sharma SK, Moros EG, Corry PM, Tripathi P, Lieblong BJ, et al. Effects of radiation on the epidermal growth factor receptor pathway in the heart. *International journal of radiation biology*. 2013;89(7):539-47.
29. Halyard MY, Pisansky TM, Dueck AC, Suman V, Pierce L, Solin L, et al. Radiotherapy and adjuvant trastuzumab in operable breast cancer: tolerability and adverse event data from the NCCTG Phase III Trial N9831. *Journal of clinical oncology : official journal of the American Society of Clinical Oncology*. 2009;27(16):2638-44.
30. Causa L, Kirova YM, Gault N, Pierga JY, Savignoni A, Campana F, et al. The acute skin and heart toxicity of a concurrent association of trastuzumab and locoregional breast radiotherapy including internal mammary chain: a single-institution study. *European journal of cancer*. 2011;47(1):65-73.
31. Tarantini L, Gori S, Faggiano P, Pulignano G, Simoncini E, Tuccia F, et al. Adjuvant trastuzumab cardiotoxicity in patients over 60 years of age with early breast cancer: a multicenter cohort analysis. *Annals of oncology : official journal of the European Society for Medical Oncology / ESMO*. 2012;23(12):3058-63.
32. Ozes ON, Mayo LD, Gustin JA, Pfeffer SR, Pfeffer LM, Donner DB. NF-kappaB activation by tumour necrosis factor requires the Akt serine-threonine kinase. *Nature*. 1999;401(6748):82-5.
33. Zhai C, Cheng J, Mujahid H, Wang H, Kong J, Yin Y, et al. Selective inhibition of PI3K/Akt/mTOR signaling pathway regulates autophagy of macrophage and vulnerability of atherosclerotic plaque. *PloS one*. 2014;9(3):e90563.
34. Wang J, Li F, Yang M, Wu J, Zhao J, Gong W, et al. FIZZ1 promotes airway remodeling through the PI3K/Akt signaling pathway in asthma. *Experimental and therapeutic medicine*. 2014;7(5):1265-70.
35. Garcia-Rivello H, Taranda J, Said M, Cabeza-Meckert P, Vila-Petroff M, Scaglione J, et al. Dilated cardiomyopathy in Erb-b4-deficient ventricular muscle. *American journal of physiology Heart and circulatory physiology*. 2005;289(3):H1153-60.
36. Swain SM. Cardiovascular complications of breast cancer therapy. *Clinical advances in hematology & oncology : H&O*. 2008;6(4):247-8, 82.
37. Franks ME, Macpherson GR, Figg WD. Thalidomide. *Lancet*. 2004;363(9423):1802-11.
38. Gupta D, Treon SP, Shima Y, Hideshima T, Podar K, Tai YT, et al. Adherence of multiple myeloma cells

- to bone marrow stromal cells upregulates vascular endothelial growth factor secretion: therapeutic applications. *Leukemia*. 2001;15(12):1950-61.
39. Maria de Souza C, Fonseca de Carvalho L, da Silva Vieira T, Candida Araujo ESA, Teresa Paz Lopes M, Alves Neves Diniz Ferreira M, et al. Thalidomide attenuates mammary cancer associated-inflammation, angiogenesis and tumor growth in mice. *Biomedicine & pharmacotherapy = Biomedecine & pharmacotherapie*. 2012;66(7):491-8.
 40. Sampaio EP, Sarno EN, Galilly R, Cohn ZA, Kaplan G. Thalidomide selectively inhibits tumor necrosis factor alpha production by stimulated human monocytes. *The Journal of experimental medicine*. 1991;173(3):699-703.
 41. Tamilarasan KP, Kolluru GK, Rajaram M, Indhumathy M, Saranya R, Chatterjee S. Thalidomide attenuates nitric oxide mediated angiogenesis by blocking migration of endothelial cells. *BMC cell biology*. 2006;7:17.
 42. Choe JY, Jung HJ, Park KY, Kum YS, Song GG, Hyun DS, et al. Anti-fibrotic effect of thalidomide through inhibiting TGF-beta-induced ERK1/2 pathways in bleomycin-induced lung fibrosis in mice. *Inflammation research : official journal of the European Histamine Research Society [et al]*. 2010;59(3):177-88.
 43. Tabata C, Tabata R, Kadokawa Y, Hisamori S, Takahashi M, Mishima M, et al. Thalidomide prevents bleomycin-induced pulmonary fibrosis in mice. *Journal of immunology*. 2007;179(1):708-14.
 44. Yndestad A, Vinge LE, Bjornerheim R, Ueland T, Wang JE, Froland SS, et al. Thalidomide attenuates the development of fibrosis during post-infarction myocardial remodelling in rats. *European journal of heart failure*. 2006;8(8):790-6.
 45. Lebrin F, Srun S, Raymond K, Martin S, van den Brink S, Freitas C, et al. Thalidomide stimulates vessel maturation and reduces epistaxis in individuals with hereditary hemorrhagic telangiectasia. *Nature medicine*. 2010;16(4):420-8.
 46. Kim DH, Kim YJ, Chang SA, Lee HW, Kim HN, Kim HK, et al. The protective effect of thalidomide on left ventricular function in a rat model of diabetic cardiomyopathy. *European journal of heart failure*. 2010;12(10):1051-60.
 47. Arai H, Furusu A, Nishino T, Obata Y, Nakazawa Y, Nakazawa M, et al. Thalidomide prevents the progression of peritoneal fibrosis in mice. *Acta histochemica et cytochemica*. 2011;44(2):51-60.
 48. Muriel P, Fernandez-Martinez E, Perez-Alvarez V, Lara-Ochoa F, Ponce S, Garcia J, et al. Thalidomide ameliorates carbon tetrachloride induced cirrhosis in the rat. *European journal of gastroenterology & hepatology*. 2003;15(9):951-7.
 49. Scharpfenecker M, Froot B, Russell NS, Coppes RP, Stewart FA. Thalidomide ameliorates inflammation

- and vascular injury but aggravates tubular damage in the irradiated mouse kidney. *International journal of radiation oncology, biology, physics*. 2014;89(3):599-606.
50. Asahara T, Masuda H, Takahashi T, Kalka C, Pastore C, Silver M, et al. Bone marrow origin of endothelial progenitor cells responsible for postnatal vasculogenesis in physiological and pathological neovascularization. *Circulation research*. 1999;85(3):221-8.
51. Takahashi T, Kalka C, Masuda H, Chen D, Silver M, Kearney M, et al. Ischemia- and cytokine-induced mobilization of bone marrow-derived endothelial progenitor cells for neovascularization. *Nature medicine*. 1999;5(4):434-8.
52. Urbich C, Heeschen C, Aicher A, Dernbach E, Zeiher AM, Dimmeler S. Relevance of monocytic features for neovascularization capacity of circulating endothelial progenitor cells. *Circulation*. 2003;108(20):2511-6.
53. Kishore R, Verma SK, Mackie AR, Vaughan EE, Abramova TV, Aiko I, et al. Bone marrow progenitor cell therapy-mediated paracrine regulation of cardiac miRNA-155 modulates fibrotic response in diabetic hearts. *PloS one*. 2013;8(4):e60161.
54. Askari AT, Unzek S, Popovic ZB, Goldman CK, Forudi F, Kiedrowski M, et al. Effect of stromal-cell-derived factor 1 on stem-cell homing and tissue regeneration in ischaemic cardiomyopathy. *Lancet*. 2003;362(9385):697-703.
55. Ceradini DJ, Kulkarni AR, Callaghan MJ, Tepper OM, Bastidas N, Kleinman ME, et al. Progenitor cell trafficking is regulated by hypoxic gradients through HIF-1 induction of SDF-1. *Nature medicine*. 2004;10(8):858-64.
56. Zentilin L, Tafuro S, Zacchigna S, Arsic N, Pattarini L, Sinigaglia M, et al. Bone marrow mononuclear cells are recruited to the sites of VEGF-induced neovascularization but are not incorporated into the newly formed vessels. *Blood*. 2006;107(9):3546-54.
57. Perry TE, Song M, Despres DJ, Kim SM, San H, Yu ZX, et al. Bone marrow-derived cells do not repair endothelium in a mouse model of chronic endothelial cell dysfunction. *Cardiovascular research*. 2009;84(2):317-25.
58. Aicher A, Heeschen C. Nonbone marrow-derived endothelial progenitor cells: what is their exact location? *Circulation research*. 2007;101(9):e102.
59. Hillebrands JL, Klatter FA, van Dijk WD, Rozing J. Bone marrow does not contribute substantially to endothelial-cell replacement in transplant arteriosclerosis. *Nature medicine*. 2002;8(3):194-5.
60. Guthrie SM, Curtis LM, Mames RN, Simon GG, Grant MB, Scott EW. The nitric oxide pathway modulates hemangioblast activity of adult hematopoietic stem cells. *Blood*. 2005;105(5):1916-22.



Summary



Radiotherapy is an effective treatment of cancer, although it contributes to late toxicity in surrounding normal (non-cancer) tissue. Little is known about the underlying mechanisms and the contribution of microvascular damage to late cardiac toxicity after radiotherapy alone or in combination with chemotherapy or tyrosine kinase receptor inhibitors. In this thesis we aim to shed light on the underlying mechanisms of radiation and anthracycline-induced cardiovascular damage.

In **chapter 2**, a mouse model was used to investigate the histological and functional effect of low, intermediate and high dose (2, 8, 16 Gy) single irradiation to the heart at early (20 weeks) and late (40 and 60 weeks) time points. With this study we demonstrated that irradiation affects cardiac structure and microvascular function in a dose and time-dependent manner, with substantial damage after intermediate and high dose irradiation (8-16 Gy) and minor alterations after lower doses (2 Gy).

High cholesterol level in the blood is linked to age-related atherosclerosis, an event that is also induced by irradiation in *ApoE^{-/-}* mice, which have elevated levels of cholesterol, similar to humans on western-type diet. We therefore treated *ApoE^{-/-}* mice in **chapter 3** with single irradiation to the heart of 2, 8 and 16 Gy, resulting in an early and pronounced inflammatory response and microvascular leakage in the hearts. These mice also developed atherosclerotic lesions in mid-sized coronary arteries.

The risk of cardiac toxicity after anthracyclines and radiotherapy is recognized, but little is known about the increased risk when these treatments are combined with inhibitors of epidermal growth factor receptor 2 (ErbB2). Thus, we investigated in **chapter 4** the effect of combined treatments on survival and growth of cardiomyocytes *in vitro*. We further studied histomorphology and microvascular damage of mice treated with radiation or anthracycline alone or in combination with ErbB2-inhibitor lapatinib. While radiation and anthracycline induced cardiac toxicity, we did not see any enhancement in structural and microvascular damage when blocking ErbB2.

Endothelial cells have been shown to be highly sensitive to radiation. Endoglin, co-receptor of TGF- β 1, is essential for angiogenesis and predominantly expressed in proliferating vascular endothelial cells and therefore may play a crucial role in cell proliferation and thus revascularization in damaged cardiac microvasculature. **Chapter 5** demonstrates that radiation-induced endothelial cell damage was independent of endoglin expression levels. However, lower endoglin expression levels limits the early inflammatory response and fibrosis in our radiation-induced mouse model of cardiac damage.

A better understanding of the underlying mechanisms of radiation-induced cardiac damage allows for the development of intervention strategies. In the second part of this thesis we focused on intervention and strategies to overcome radiation-induced cardiovascular damage. Since inflammatory and fibrotic events are dominant features in radiation-induced heart damage, we tested whether an anti-inflammatory and anti-fibrotic agent thalidomide could prevent further fibrotic progression after irradiation. In **chapter 6** we have shown that radiation leads to inflammatory and fibrotic response and that these events could not be reduced by thalidomide.

Radiation induces endothelial cell loss, which results in decreased microvascular density. Perfusion defects have been identified in asymptomatic breast cancer patients shortly after radiotherapy. Vaculogenesis, stimulated by precursor cells that differentiate into endothelial cells, has been shown to be essential in tissue repair and remodeling during acute and chronic ischemic tissue damage. In **chapter 7** we used bone-marrow derived endothelial cells from either endoglin haplo-insufficient or endoglin profficient mice and transplanted them into our radiation-induced mouse models. We demonstrated that bone-marrow derived endothelial cells did reduce the amount of radiation-induced cardiac fibrosis. However, these cells were unable to restore microvascular damage.

We believe that our data on cardiac microvascular damage induced by radiation, give new insights into the underlying mechanisms and provide some crucial aspects for finding new strategies to overcome radiation-induced cardiac damage.



Samenvatting

Radiotherapie is een effectieve behandelmodaliteit tegen kanker, maar draagt ook bij aan het ontstaan van late toxiciteit als gevolg van schade aan het omgevende normale weefsel, zoals het hart en bloedvaten. Er is echter weinig bekend over de onderliggende mechanismen en de relatieve bijdrage van beschadigde kleine bloedvaten op late hartschade na bestraling al of niet in combinatie met chemotherapie of tyrosine kinase remmers. In dit proefschrift trachten wij inzicht te geven in de oorzaken van hartschade na bestraling en anthracycline chemotherapie.

In hoofdstuk 2 beschrijven we de toepassing van een muizenmodel om acute (20 weken) en late (40 en 60 weken) histologische en functionele effecten van verschillende eenmalige bestralingsdoses (2, 8, 16 Gy) op het hart te onderzoeken. Met deze studie tonen wij aan dat bestraling de cardiale structuur en microvasculaire functie beïnvloedt in een dosis- en tijdafhankelijke manier, met substantiële schade na intermediaire en hoge dosis bestraling (8-16 Gy) en minder afwijkingen na een lage dosis (2 Gy).

Een hoge serum cholesterol spiegel is geassocieerd met ouderdom-gerelateerde atherosclerose, een aandoening die ook geïnduceerd wordt door bestraling in ApoE^{-/-} muizen die net als mensen met een Westers dieet, een hoge serum cholesterol spiegel hebben. In hoofdstuk 3 beschrijven we de resultaten van een behandeling van ApoE^{-/-} muizen met een eenmalig bestralingsdosis op het hart van 2, 8 en 16 Gy. Wij vonden een vroege en uitgesproken ontstekingsreactie en microvasculaire lekkage in het hart, en atherosclerotische veranderingen in middelgrote coronaire slagaders.

Het risico van cardiale schade na anthracycline en bestraling is eerder herkend, maar er is weinig bekend over het risico als deze behandelingen gecombineerd worden met remmers van de epidermale groei factor receptor 2 (ErbB2). Daarom onderzochten wij in hoofdstuk 4 het effect van deze gecombineerde behandelingen op groei en overleving van gekweekte cardiomyocyten. Daarnaast onderzochten wij de histomorfologie en microvasculaire schade bij muizen die behandeld werden met bestraling of anthracycline alleen of in combinatie met de ErbB2-remmer lapatinib. Terwijl bestraling en anthracycline hartschade veroorzaakten, vonden wij geen toename van schade als ErbB2 werd geblokkeerd.

Endotheelcellen die de binnenbekleding van bloedvaten vormen, zijn zeer stralengevoelig. Endoglin, een co-receptor van TGF- β 1 is essentieel voor angiogenese en komt voornamelijk tot expressie in prolifererende vasculaire endotheelcellen. Daarom zou endoglin een belangrijke rol kunnen spelen bij de re-vascularisatie van beschadigde cardiale bloedvaten.

Hoofdstuk 5 toont aan dat bestraling geïnduceerde endotheelschade onafhankelijk is van endoglin expressie. Echter, een laag niveau van endoglin expressie beperkt de vroege

ontstekingsreactie en fibrose in ons muizen model met bestraling geïnduceerd cardiale schade.

Het beter begrijpen van de onderliggende mechanismen van bestraling geïnduceerde hartschade kan leiden tot de ontwikkeling van interventiestrategieën.

In het tweede gedeelte van dit proefschrift richten wij ons op strategieën om bestraling geïnduceerd hartschade te voorkomen.

Aangezien ontstekingseffecten en fibrotische veranderingen overheersen in bestraling geïnduceerde cardiale schade, onderzochten wij of de ontstekingsremmer en anti-fibrotisch middel thalidomide dit proces kan voorkomen.

In hoofdstuk 6 laten wij zien dat bestraling leidt tot ontsteking en fibrose, en dat deze veranderingen niet konden worden verminderd door het toedienen van thalidomide.

Bestraling induceert endotheelcel verlies wat uiteindelijk leidt tot in afname in microvasculaire dichtheid. Perfusie defecten kunnen worden aangetoond bij asymptomatisch borstkanker patiënten vlak na radiotherapie. Vasculogenese, gestimuleerd door precursor cellen die gedifferentieerd zijn tot endotheelcellen, is essentieel voor weefselherstel en 'remodeling' tijdens de acute en chronische fase van ischemische weefselschade.

In hoofdstuk 7 gebruikten wij uit beenmerg afkomstige endotheelcellen van endoglin deficiënte en endoglin proficiënte muizen en transplanteerde wij deze in ons bestraling geïnduceerd muizenmodel.

Wij toonden aan dat deze uit het beenmerg afkomstige endotheelcellen in staat waren de door bestraling veroorzaakte fibrose te verminderen. Deze cellen konden echter niet de microvasculaire schade herstellen.

De in dit proefschrift beschreven studies dragen bij aan een beter inzicht in de onderliggende mechanismen van cardiale microvasculair schade geïnduceerd door bestraling, en bieden de mogelijkheid om nieuwe strategieën te ontwikkelen om bestraling geïnduceerde hartschade te verminderen of voorkomen.



List of abbreviations

List of abbreviations

| | |
|------------|--|
| αSMA | alpha-smooth muscle actin |
| ADRB1 | adrenergic, beta-1, receptor |
| AEC | animal experiments committee |
| AF | alexa fluor |
| ALK1 | activin receptor-like kinase 1 |
| ALK5 | activin receptor-like kinase 5 |
| ALP | alkaline phosphatase |
| ANGPT2 | angiopoietin 2 |
| ApoE | apolipoprotein E |
| ARNTL | aryl hydrocarbon receptor nuclear translocator like |
| | |
| B2M | beta-2-microglobulin |
| BMC | bone marrow cell |
| BMDC | bone marrow derived cells |
| BMEPC | bone marrow-derived endothelial progenitor cells |
| | |
| CA3 | carbonic anyhydrase III |
| CCK-8 | cell counting kit-8 |
| CCR | C-C chemokine receptor type |
| CDKN1A | cyclin dependent kinase inhibitor 1A |
| CFD | complement factor D |
| CT | chemotherapy |
| CTGF | connective tissue growth factor |
| CVD | cardiovascular disease |
| CXCL | chemokine motif ligand |
| | |
| DAB | diaminobenzidine |
| Dil-ac-LDL | Dil-labeled low-density lipoprotein |
| DNA | deoxyribonucleic acid |
| Dox | doxorubicin |
| | |
| EBCTCG | the Early Breast Cancer Trialists' Collaborative Group |
| EC | endothelial cell |
| ECG | electrocardiography |

List of abbreviations

| | |
|--------------------------|---------------------------------------|
| EDN1 | endothelin 1 |
| EDV | end diastolic volume |
| EF | ejection fraction |
| EGM-2 | endothelial cell growth medium-2 |
| EM | electron microscopy |
| <i>Eng^{+/-}</i> | endoglin heterozygous |
| <i>Eng^{+/+}</i> | endoglin homozygous |
| EPC | endothelial progenitor cell |
| ErbB | epidermal growth factor receptor |
| ERR | excess relative risk |
| ESM1 | endothelial cell-specific molecule 1 |
| ESV | end systolic volumes |
| | |
| FGF-2 | fibroblast growth factor-2 |
| FN1 | fibronectin 1 |
| FOV | field of view |
| F-type | flexible-type |
| FU | follow-up |
| | |
| Gy | gray |
| | |
| HCM | human cardiac myocytes |
| H&E | hematoxylin and eosin |
| HHT | hereditary hemorrhagic telangiectasia |
| HMOX1 | heme oxygenase 1 |
| HR | hazard rate (chapter 1) |
| HR | heart rate |
| HSA | human serum albumin |
| Hsp | heat shock protein |
| H-type | hierarchical-type |
| | |
| ICAM-1 | intercellular adhesion molecule-1 |
| IFRT | contemporary involved-field RT |
| IGRT | image-guided-radiotherapy |

List of abbreviations

| | |
|-------|--|
| IL | interleukin |
| IMRT | intensity modulated radiotherapy |
| INRT | involved-node RT |
| i.p. | intraperitoneal |
| IPA | ingenuity pathway analysis |
| IRF7 | interferon regulatory factor 7 |
| i.v. | intravenously |
| | |
| LADCA | left anterior descending coronary artery |
| LDL | low-density lipoprotein |
| LVEF | left ventricle ejection fraction |
| LV | left ventricular |
| | |
| MCP-1 | monocyte chemoattractant protein-1 |
| MMP2 | matrix metalloproteinase 2 |
| MNC | mononuclear cell |
| MnSOD | manganese superoxide dismutase |
| MVD | microvascular density |
| MYL | myosin light chain |
| | |
| PAI-1 | plasminogen activator inhibitor-1 |
| PBS | phosphate-buffered saline |
| PDGF | platelet-derived growth factor |
| PFA | paraformaldehyde |
| PFR | peak filling rate |
| PPAR | Peroxisome proliferator-activated receptor |
| PTX | Pentoxifylline |
| | |
| RIHD | Radiation-induced heart disease |
| RIN | RNA integrity number |
| ROS | reactive oxygen species |
| RR | relative risks |
| RT | radiotherapy |
| SD | standard deviation |

List of abbreviations

| | |
|----------|--|
| SERCA | sarcoplasmic reticulum Ca ²⁺ ATPase |
| SIR | standardised incidence ratios |
| SLN | sarcolipin |
| (g)SPECT | (gated) Single photon emission computed tomography |
| | |
| TGF-β1 | transforming growth factor β1 |
| TIMP1 | tissue inhibitor of metalloproteinase 1 |
| TM | thrombomodulin |
| TNF-α | tumor-necrosis factor-α |
| | |
| UEA-1 | <i>ulex europaeus</i> agglutinin-1 |
| | |
| VCAM-1 | vascular cell adhesion molecule-1 |
| VEGF | vascular endothelial growth factor |
| vWF | von Willebrand factor |



List of publications

List of publications (PhD project)

1. Mouse bone marrow-derived endothelial progenitor cells do not restore radiation-induced microvascular damage.

Seemann J, Te Poele JA, Hoving S, Stewart FA.

SRN Cardiol. 2014 Mar 27;2014:506348. doi: 10.1155/2014/506348. eCollection 2014.

2. Radiation-and anthracycline-induced cardiac toxicity and the influence of ErbB2 blocking agents.

Seemann J, te Poele JA, Song JY, Hoving S, Russell NS, Stewart FA.

Breast Cancer Res Treat. 2013 Oct;141(3):385-95. doi: 10.1007/s10549-013-2707-7. Epub 2013 Oct 4.

3. Endoglin haplo-insufficiency modifies the inflammatory response in irradiated mouse hearts without affecting structural and microvascular changes.

Seemann J, Te Poele JA, Luikinga SJ, Hoving S, Stewart FA.

PLoS One. 2013 Jul 24;8(7):e68922. doi: 10.1371/journal.pone.0068922. Print 2013.

4. Understanding radiation-induced cardiovascular damage and strategies for intervention.

Stewart FA, Seemann J, Hoving S, Russell NS.

Clin Oncol (R Coll Radiol). 2013 Oct;25(10):617-24. doi: 10.1016/j.clon.2013.06.012. Epub 2013 Jul 20. Review.

5. Thalidomide is not able to inhibit radiation-induced heart disease.

Hoving S, Seemann J, Visser NL, te Poele JA, Stewart FA.

Int J Radiat Biol. 2013 Sep;89(9):685-91. doi: 10.3109/09553002.2013.788797. Epub 2013 Apr 16.

6. Local heart irradiation of ApoE^{-/-} mice induces microvascular and endocardial damage and accelerates coronary atherosclerosis.

Gabriels K, Hoving S*, Seemann J, Visser NL, Gijbels MJ, Pol JF, Daemen MJ, Stewart FA, Heeneman S.*

Radiother Oncol. 2012 Dec;105(3):358-64. doi: 10.1016/j.radonc.2012.08.002. Epub 2012 Sep 5.

*These authors contribute equally

7. Irradiation induced modest changes in murine cardiac function despite progressive structural damage to the myocardium and microvasculature.

*Seemann J**, Gabriels K*, Visser NL, Hoving S, te Poele JA, Pol JF, Gijbels MJ, Janssen BJ, van Leeuwen FW, Daemen MJ, Heeneman S, Stewart FA.

Radiother Oncol. 2012 May;103(2):143-50. doi: 10.1016/j.radonc.2011.10.011. Epub 2011 Nov 21.

*These authors contribute equally

List of publications (master study)

1. Reducing glycosphingolipid content in adipose tissue of obese mice restores insulin sensitivity, adipogenesis and reduces inflammation.

van Eijk M, Aten J, Bijl N, Ottenhoff R, van Roomen CP, Dubbelhuis PF, *Seemann J*, Ghauharali-van der Vlugt K, Overkleef HS, Arbeeny C, Groen AK, Aerts JM.

PLoS One. 2009;4(3):e4723. doi: 10.1371/journal.pone.0004723. Epub 2009 Mar 23.

2. Regulation of direct transintestinal cholesterol excretion in mice.

van der Velde AE, Vrins CL, van den Oever K, *Seemann J*, Oude Elferink RP, van Eck M, Kuipers F, Groen AK. Am J Physiol Gastrointest Liver Physiol. 2008 Jul;295(1):G203-G208. doi: 10.1152/ajpgi.90231.2008.

Epub 2008 May 29.

List of publications (European project manager)

1. ANTIDotE: anti-tick vaccines to prevent tick-borne diseases in Europe.

Sprong H, Trentelman J, *Seemann J*, Grubhoffer L, Rego RO, Hajdušek O, Kopáček P, Šíma R, Nijhof AM, Anguita J, Winter P, Rotter B, Havlíková S, Klempa B, Schetters TP, Hovius JW.

Parasit Vectors. 2014 Feb 21;7:77. doi: 10.1186/1756-3305-7-77.



Acknowledgement

acknowledgment

Und dann ist es vollbracht, meine Doktorarbeit, my thesis, mijn proefschrift, liegt endlich in meinen Händen. Ein merkwürdiges Gefühl, etwas wo man Jahre lang intensiv an gearbeitet hat nimmt ein Ende. Ein Lebenstraum ist wahr geworden, denn seit ich denken kann wollte ich ein „Dr.“ werden. Und natürlich schafft man sowas nicht im Alleingang, und schon dafür bin ich euch sehr dankbar. Das ich eben auf eine Menge Menschen zurück fallen konnte, die mich unterstützt, motiviert, angetrieben haben um meinen Traum zu erfüllen. Es tut mir leid wenn ich hier nicht jeden nennen und schriftlich danken kann, das werde ich dann am 23.April nachholen. ;-)

Dear Fiona, thank you for all your support, encouragement, wise words, and high-level of education I was allowed to receive. Surely, it wasn't always going smoothly and we also had our disagreements, until I've noticed that it was in my hands to take your comments no longer as criticism but as an addition to my existing skills. In that way I could expand my skills in properties like patience, diplomacy, endurance and structured working (well, it still has my attention...). Fiona, obviously your way of supervising and guiding me was the key to 7 published articles!

Beste promotor, beste Marcel, jij hebt diepe indruk op mij gemaakt tijdens een congres op Maui. De mogelijkheid om voetbal uitslagen bij te houden en tegelijkertijd het praatje van de sessie te volgen, beoordelen en commentaar te geven vond ik buiten gewoon bijzonder. Dank je wel dat je op belangrijke momenten steun wist te bieden en dat ondanks je overvolle agenda jij altijd klaar stond voor mij.

Beste leden van de promotiecommissie, prof. dr. F. van Leeuwen, prof. dr. B. Slotman, dr. B. Aleman, prof. dr. H. te Riele en prof. dr. R. Coppes wil ik bedanken voor het beoordelen van mijn proefschrift en de bereidheid zitting te nemen in mijn promotiecommissie.

Liebe **Marion**, womit soll ich bloß anfangen? Absolut inspirierend und hilfreich auf dem wissenschaftlichem Bereich, brain storming, Data Analyse, kritische Sicht auf Artikel, Aussprachen und Resultaten... hab viel von dir gelernt. Schön war's mit dir ein bisschen Heimat im NKI zu haben ;-). Männer, allgemein Holländer, Wettkämpfe, Kollegen, ich muss zugeben am Ende waren es wohl eher die nicht-wissenschaftlichen Themen die ihren Vorrang kriegten bei uns im Zimmer. Marion, mir ist bewusst das das Dankeswort nicht ewig lang sein sollte und probiere ich mich hier auf die Highlights zu konzentrieren, merke aber das

acknowledgment

es grade die vielen kleinen Dingen waren, die dich so unschätzbar wertvoll gemacht haben. Daher bleibt mir nichts anders übrig um einfach Danke zu sagen, DANKE für so viele schöne, hilfreiche, unterstützende, witzige, lebensfrohe Momente.

Karin, wat is er eigenlijk van onze Duitse lessen geworden? Volgens mij zijn we geëindigd: "Das hab ich auch! Ist von Ikea, oder?". Ik ben ontzettend dankbaar jou als collega gehad te mogen hebben; fris, eerlijk, bijzonder, grappig...je was zeker een aanvulling voor onze groep. Jeetje, als ik terug kijk en mij herinner aan wat voor thema's onze gesprekken soms hadden... uiteraard heel blij dat er geen verstopte camera op onze kamer hing ;-). Ik hoop dat we nog heel vaak samen sushi gaan eten... Dank je wel voor al jouw steun, lieve Karin.

Lieve, lieve Stewart groep. Wat zijn wij een groepje mensen, verschillend had het niet kunnen zijn. ;-)

Saske, achteraf kan ik zeggen dat onze verschillende manieren van werken en denkwijze elkaar hebben aangevuld. Uiteraard heb ik van jou geleerd iets "gecontroleerder" te zijn en dus labjournaals, Excel sheets, externe harde schijf, mapjes voor resultaten, mapjes voor protocollen, mapjes voor ideeën, mapjes voor literatuur, mapjes voor studenten, mapjes voor to-do, mapjes voor te gebruiken. Dank je wel voor al de vele publicaties, samen hebben we een heleboel voor elkaar gekregen! Ik wens je het allerbeste toe!

Nicola, I would like to thank you for your input on all clinical aspects and your support and belief in this project.. I have deep respect for your enthusiasm on research and how you combine it with your clinical commitments. **Nils**, ondanks de eindeloze uren achter de analyse computer op NG en niet te vergeten in de "kelder" tijdens het imagen.... Is er dank jou een mooi boek uit gekomen. Dank je wel voor jou inzet!

Hans, wat hebben we veel tijd samen op de se(xy)ktiekamer doorgebracht.... En tot het laatst bleef ik bang voor de muizen! Wat had ik mazzel dat er zo'n "oude haas" op het lab rond liep die mij alle tips en tricks leerde over muizen en immuno's... en het schakelen op mijn racefiets. Samen zijn we over de finishlijn bij de Alpe d'HuZes gefietst en nu komen we samen over de finishlijn van mijn promotie traject, dank je wel Hans voor al jouw steun!

Ben, wat heb ik van jouw gezelschap in onze groep genoten. Je bent geen man van veel woorden maar van een heerlijk droge humor. Je bent loyaal en hebt principes, iets wat ik als heel aangenaam beschouw en waardeer. Heel veel plezier nog verder in het NKI, het gaat je goed.

Thea/Theachen. Dank je wel voor al jouw hulp bij uitzoekwerk, en het regelen waar ik geen

acknowledgment

zin in had. ;-) en natuurlijk het luisteren naar mijn gezeur over dit, dat, sus en zo... Hou je taai zonder jouw Stewart groep.

De Begg/Vens (Verheij)-groep; hoorden er toch ook bij en toch ook net niet.

Adrian, it brings a smile on my face when thinking of you. It 's the memory of 'floating-by-swimming pool-cocktail XXL- pineapple- conference- Maui'. Obviously, hiding a XXL cocktail in a plastic pineapple didn't do the trick believing the expression on your face... but this expression is it what still brings that smile on my face. ... Adrian, without your effort I wasn't able to publish my micro array data and that would have been a big mistake. You may have taken your body with you but your spirit lives on.

Caroline/Car, jij was er vanaf het begin aan en wat hebben we samen met Geert ons, af en toe, als de 3 musketiers gevoeld. Ons hoogtepunt was duidelijk Maui, een belevenis dat te bijzonder was om in woorden aan anderen uit te leggen. Ik bedoel, wie zal ooit de fun/lol begrijpen van een 3 uur foto-shoot aan het strand?? ;-)

Car, straks ben jij aan de beurt!!

Ingrid en Manon, het was altijd leuk even wat koekjes bij jullie te mogen pakken en een kort babbeltje te houden. En wat was ik boos dat Ingrid niet mee mocht verhuizen naar H3, grrchchch! En dan ging Manon ons ook nog verlaten... kwam op zich weer goed voor mij, hoor. ;-) **Monique**, ik wens je heel veel kracht in het afronden van jouw promotie traject, het zal goed komen! **Sari**, ons collegaschap was niet lang maar je hebt indruk op mij gemaakt en ik had gehoopt dat jouw uitspraak 'vanaf 30 wordt je rustiger' waar zou worden. Helaas.. ;-)

Conchita, ich hab viel Respekt vor deinem kritischen Blick auf Dinge und bin sehr dankbar für die ein oder andere Denkanstöße. Ich wünsch dir alles erdenklich Gute für die Zukunft.

Floor, ik wens je veel succes met jouw nieuwe carrière richting. Het was altijd gezellig met jou! **Burcu**, it's a shame we had to work that hard. Otherwise I would have liked to spent more time chatting with you ;-) I am so happy for you and Klaas, I wish you all the best for the future. **Damien**, oh wat hadden wij leuke mailwisselingen met elkaar. Toch, motzi??? ;-)

Dank voor al jouw tips en eerlijke opmerkingen. Ik hoop dan ook dat dit dankwoord niet al te teleurstellend is. ;) **David**, super geïnteresseerd, lieve, opmerkelijke collega met een groot hart. Je bent een mooi mens, David, veel succes met jouw geneeskunde studie. Zet hem op!

Albert, wij hadden wij een top lab uitje georganiseerd! Ik wens je veel succes in jouw nieuwe carrièreontwikkeling. **Shureila**, ik vond het altijd spannend hoe je journalistiek en labwerk met elkaar kunt combineren (en kids!). Dank je wel voor al die leuke en hulpvolle praatjes en steun.

acknowledgment

De Schellens-groep dank voor de gezelligheid en de borrels; **Maarten, Lot, Bart, Dick en Stuurman. Ruud**, Texel-retraite-kamergenootje, het was een top tijd met jou. Binnen 4 jaar PC Hoofdstraat...ben benieuwd waar je over 10 jaar bent!?

Arthur, altijd moeilijk en altijd leuk! Heerlijk dat er iemand bestaat die ook zo lekker veel kan zeuren. Hou je directheid en hou jouw glimlach, het maakt je zo speciaal. **Geerti!!!** C2 was onze tijd, wat was ik blij jouw vrolijke gezicht mijn kantoor langs zien te verschijnen. Gelukkig was mijn kantoor op weg naar de printer die jij regelmatig opzocht. ;-) Ik ben je heel dankbaar voor alle cola-sessies in Tiffanies en jouw niet ophoudend blijmoedigheid die mij elke keer opnieuw uit mijn dip heeft kunnen halen. Je hebt mede bijgedragen dat dit stukje van mijn leven een heel bijzonder stukje is geworden.

H6, B8, C2 en H3 (dat noem je dan behoorlijk vaak verhuisd)-collega's. Allemaal erg bedankt voor jullie steun, inzet, babbels, koekies, hugs en noem maar op. **Linde, Lennard, Richard, die twee Petra's, Annegien, Esther, Kim, Lorenza**, dank jullie wel allemaal! Het was een gezellig tijd met jullie en wat fijn dat ik altijd mocht aanschuiven met mijn probleempjes (niet altijd van wetenschappelijke natuur).

Heel veel dank voor al de professionele hulp, input en probleemoplossingen gaat naar de ondersteunende faciliteiten binnen het NKI-AvL; Micro-array, biostatistiek, digitale microscopie, en in het bijzonder de proefdier pathologie met **Ji-Ying, Ellen en Joost** en de rest van het clubje. Jullie waren al die jaren fantastisch! Ook de mannen (en vrouw) in het proefdierenhuis, **Maaïke, Henk, Sjaak en Sido**, zonder jullie inzet en goede zorg was er sowieso geen boek van gekomen. Het was altijd heerlijk gezellig bij jullie in de kelder, dank ook hiervoor. Ik wens jullie het beste toe! Bjorn en Tanja op G2 jullie waren alert, gemotiveerd, nauwkeurig... bij jullie waren mijn muizen in goede handen. Dank!

Ik had het geluk aan een framework 7 project mee te mogen werken, Cardiorisk. Hierbij hoorde ook de groep uit Maastricht met **Sylvia, Mat, Marion en Karen**. Van deze samenwerking zijn er twee hoofdstukken tot stand gekomen en heb ik mijn wetenschappelijke horizon mogen uitbreiden door jullie kennis. Karen, dank voor de gezelligheid tijdens het schrijven van ons eerste hoofdstuk, wat is Maastricht mooi. ;-) En eindelijk dan straks samen feesten in Amsterdam! Heel veel moois voor jouw toekomst toegewenst.

En dan zijn er nog mensen die mij eerst zo ver hebben gekregen om als PhD te willen

acknowledgment

beginnen; **Alex**, door jou ben ik überhaupt in aanraking gekomen met medische biologie! Ik ben spontaan naar Amsterdam gevlogen en langs de UvA gegaan om even uit te leggen dat ik een stage plek nodig had. Dat is dus dan ook gelukt, dankzij jou. Wat was dat wennen voor mij, een eigen supervisor, hele dag op het lab, alles in het Engels... beetje anders dan wat ik in Berlijn gewend was. Alex, jij hebt bij mij het enthousiasme voor onderzoek opgewekt en duidelijk gemaakt dat geneeskunde en biologie wel te combineren valt. Dank!

Daarna had ik het geluk bij **Astrid** en **Carlos** mijn master stage te mogen uitvoeren. Met maar liefs twee tassen bij me vloog ik (weer spontaan) in april naar Amsterdam om uit te vinden dat een master studie pas in september begint. Wat te doen? Gelukkig mocht ik toch meteen bij het 'Liver Centre (AMC)' aan de slag en wat had ik geluk met deze twee tegenovergestelde supervisors! Carlos, jij wist om te gaan met mijn onzekerheid en hebt mij het gevoel gegeven dat ik op mezelf kan vertrouwen. Dank je wel voor deze mooie les, het heeft mij het zelfvertrouwen gegeven om te solliciteren voor een PhD plek! Astrid, jouw nauwkeurigheid, jouw geduld bij uitleg achter de computer (presentaties, pubmed etc.) heeft mij getraind in de theorie van de wetenschap, iets waar ik weinig geduld voor had in mijn enthousiasme. Dank voor al jou steun ook veel jaren na deze stage bij het zoeken voor nieuwe carrière mogelijkheden!

Mike, je zult het niet geloven maar je hebt me met al jouw goede toespraken; privé-lessen in kweken; kalmeren op de AMC parkeerplaats als er weer eens een experiment mislukt was; eindverslag corrigeren; presentaties oefenen ... wel door mijn Master studie geslept. Ik weet niet of ik het zonder jouw steun wel had gehaald. Dat je dan uiteindelijk de PhD "onzin" vond heeft me alleen nog meer gestimuleerd om hem af te maken ;-)

MaPa, "Flügel gibt man seinen Kindern, aber fliegen müssen sie selber", trifft absolut auf euch zu. Schnell habt ihr mich selbstständig erzogen mit dem Gefühl, das falls ich falle mir 4 starke Arme zur Hilfe eilen um mir wieder auf die Beine zu helfen (absolut grandioses Beispiel ist die Reise nach Canada...mit dem Perso und dem rasenden Papa hinterm Steuer). Das hat mir die nötige Stärke gegeben um meinen Weg zu gehen und dafür bin ich unglaublich dankbar. Egal wie meine Pläne auch aussahen, ihr habt sie immer unterstützt (außer als ich Ballett und Fußball lernen wollte), solange ich mit guten Argumenten kam (sogar ein Tattoo mit 17! Ihr habt echt nen Knall ;-)). Ich dank euch von ganzen Herzen das ihr mir die Freiheit gebt meine Träume zu träumen und das Vertrauen und die Sicherheit meine Träume zu leben.





Curriculum Vitae

Curriculum Vitae

Ingar Seemann was born on October 5th 1981 in Hentstedt-Ulzburg in the north of Germany. After completing school, Ingar moved to Berlin in autumn 2001 to study Biology at the Free University (FU) of Berlin. During her bachelor in biology she attended the Amsterdam marathon in 2004 and was impressed by the beauty of the city. Thus, she applied for an 3-months internship at the University of Amsterdam titled: *"Stress responses in Bacillus subtilis – How do bacteria get stressed?"* under supervision of Dr. Alex ter Beek. Back in Berlin, Ingar obtained her bachelor in Biology and left Berlin to follow a Master in biomedical Science at the University of Amsterdam in spring 2006.

During her master study Ingar performed two internships: the first entitled *"Finding a new pathway for cholesterol excretion"* at the Liver center of the Academic Medical Center (AMC) under supervision of Dr. Astrid van der Velde and Dr. Carlos Vrans. The second internship was entitled *"The role of glycosphingolipids in regulation CD163"* and performed at the AMC under supervision of Dr. Marco van Eijk. Ingar finished her Master study with the master thesis *"Efficient monitoring of immune response to monoclonal antibodies"* under supervision of Prof.dr. Lucien Aarden at Sanquin.

After finishing her masters in summer 2008, she started with her PhD training at the Netherlands Cancer Institute at the department of Experimental Therapy (later became: Biological Stress Response) under the supervision of Dr. Fiona A. Stewart and promoter Prof. Marcel Verheij. She also gave birth the same year to her funny, cute, smart and wonderful daughter Emma Pippi.

Ingar now works as a project manager for EU-funded research projects at the AMC.



